VOL. 26 NO. 1 JUNE 1970
PUBLISHED MONTHLY

JOURNAL OF

ELECTROANALYTICAL CHEMISTRY

AND INTERFACIAL ELECTROCHEMISTRY

International Journal devoted to all Aspects of Electroanalytical Chemistry, Double Layer Studies, Electrokinetics, Colloid Stability, and Electrode Kinetics.

ELSEVIER SEQUOIA S.A.
LAUSANNE

GENERAL INFORMATION

Detailed *Suggestions and Instructions to Authors* were published in the June 1969 issue of the journal, *J. Electroanal. Chem.*, 21 (1969) 565–572. A free reprint can be obtained by application to the publisher.

Types of contributions

(a) Original research work not previously published in other periodicals (regular papers). (b) Reviews on recent developments in various fields. (c) Short communications. (d) Preliminary notes.

A Preliminary Note is a brief report of work which has progressed to the stage when it is considered that the science of chemistry would be advanced if the results were made available as soon as possible to others working on the same subject. Preliminary Notes can in general be published within 4–8 weeks of their acceptance by the editor although this implies that proofs cannot be sent to the author(s). The publisher will attend to correction of the proof but it should be remembered that errors in the manuscript will also appear in the published Note. Preliminary Notes, clearly marked as such, must be sent to Dr. R. Parsons (address given below).

Submission of papers

Papers should be sent to one of the following Editors:

Dr. R. PARSONS, Department of Chemistry, The University, Bristol BS8 1TS, England.

Dr. R. DE LEVIE, Department of Chemistry, Georgetown University, Washington, D.C. 20007, U.S.A.

Dr. R. H. OTTEWILL, Department of Chemistry, The University, Bristol BS8 1TS, England.

For rapid handling papers originating from the American continent should be sent to Dr. DE LEVIE, those of colloid interest to Dr. OTTEWILL, and all others to Dr. PARSONS.

Authors should preferably submit two copies in double-spaced typing on pages of uniform size. Legends for figures should be typed on a separate page. The figures should be in a form suitable for reproduction, drawn in Indian ink on drawing paper or tracing paper, with lettering etc. in thin pencil. The sheets of drawing or tracing paper should preferably be of the same dimensions as those on which the article is typed. Photographs should be submitted as clear black and white prints on glossy paper. Standard symbols should be used in line drawings, the following are available to the printers:

▼ ▽ ■ □ ● ◎ ▪ ◘ ⊷ ▣ ▪ + ×

All references should be given at the end of the paper. They should be numbered and the numbers should appear in the text at the appropriate places.

A summary of 50 to 200 words should be included.

Authors are recommended to use wherever possible the "Système International d'Unités" (SI Units) approved by the Conférence Générale des Poids et Mesures in 1960. If units are used which are not SI units, authors should provide a conversion factor to SI units. Axes of graphs and headings for tables should always be given clearly with the units of the quantities concerned. It is recommended that this should be done in the form consistent with "Quantity calculus", *e.g.* time as t/min or e.m.f. as E/mV, or capacity per unit area as $C/\mathrm{F\,m^{-2}}$.

Reprints

Fifty reprints will be supplied free of charge. Additional reprints (minimum 100) can be ordered at quoted prices. They must be ordered on order forms which are sent together with the proofs.

Publication

The *Journal of Electroanalytical Chemistry and Interfacial Electrochemistry* appears monthly. For 1970, each volume has 3 issues and 4 volumes will appear.

Subscription price: Sfr. 318.75 (U.S. $ 75.--) per year incl. postage. Additional cost for copies by air mail available on request. For subscribers in the U.S.A. and Canada, 2nd class postage paid at New York, N.Y. For advertising rates apply to the publishers.

Subscriptions should be sent to:

ELSEVIER SEQUOIA S.A., P.O. Box 851, 1001 Lausanne 1, Switzerland

Unprecedented Computer Power for the Lab

The new PAR™ Model 131 Instrument/Computer Interface System brings the full power of interactive time-sharing computers to the laboratory. So you can take advantage of the problem-solving capabilities of large-scale computers, no matter how complex – or simple – your experiment may be. And use easy-to-program languages such as BASIC or FORTRAN, to save more time and add to efficiency.

You can use the Model 131 to process analog or digital data from 1 to as many as 90 similar or different instruments. Data is sent over the telephone to a remote time-sharing computer while the experiment is running. The computer interacts immediately to reduce, correlate, or interpret the data in accordance to programs and data bases previously stored in its memory.

With the Model 131, the time-sharing computer can operate in the Question/Response mode. In answer to the computer's requests, you can input varying parameters for the experiment to obtain new test results from the same set of data. You can also use the time-sharing computer to monitor and control experiments. And it can even amplify the power and capabilities of certain laboratory instruments.

The Modularized Model 131 System is easily expanded as your instrumentation and data processing requirements grow. Price of a typical system consisting of an analog multiplexer, analog to digital converter, a system interface, and teleprinter is less than $6,200.

For more information, ask for P.A.R. Bulletin T-206A. Write Princeton Applied Research Corporation, Box 565, Princeton, New Jersey 08540, or call (609) 924-6835.

PRINCETON APPLIED RESEARCH CORPORATION

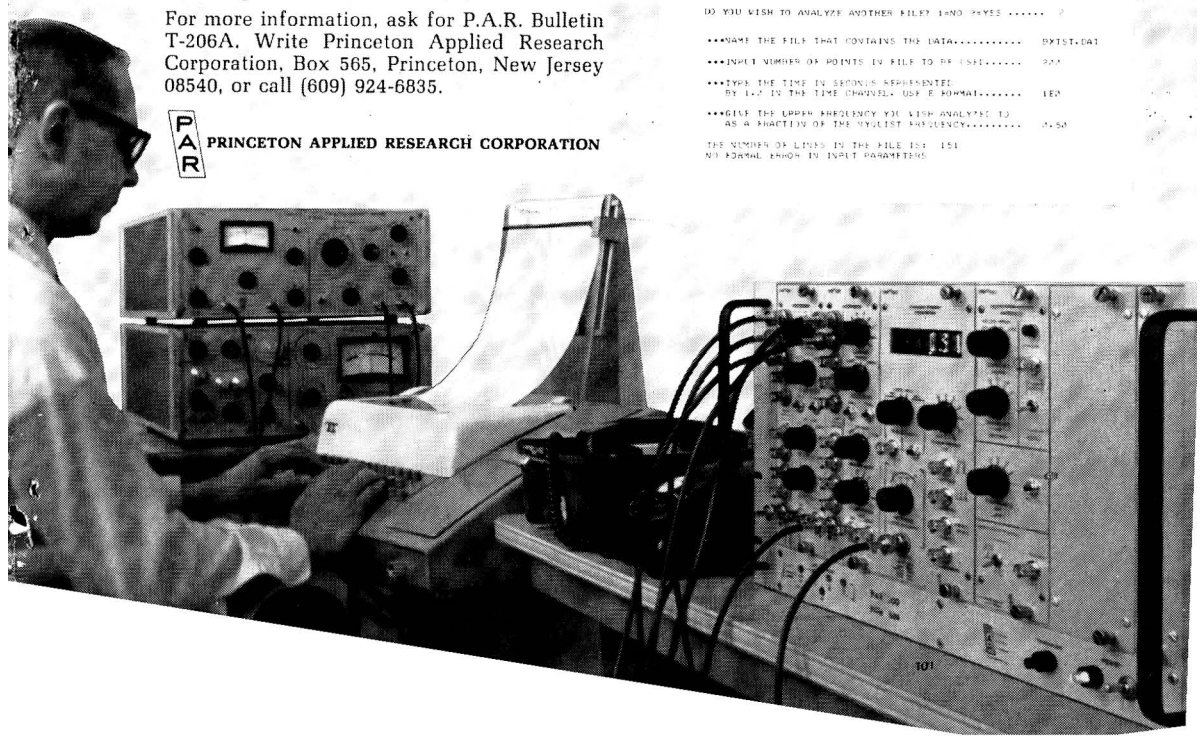

Detect one part per billion!

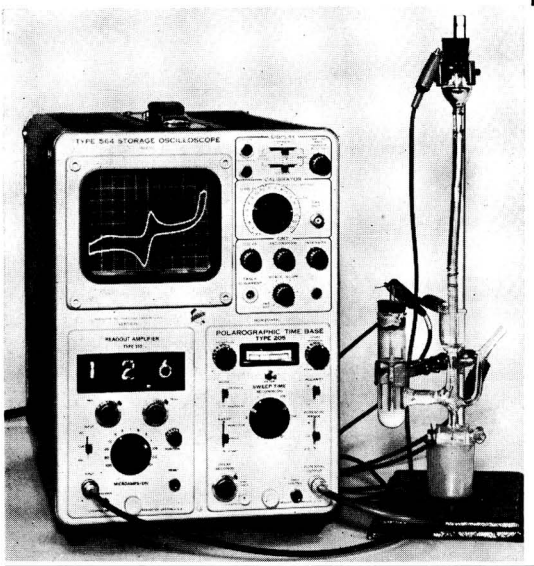

by Anodic Stripping Polarography

Anodic Stripping Polarography with Chemtrix Single-Sweep Polarographic Analyzers is capable of detecting many elements and compounds in amounts of one ppb and less. This high sensitivity is due to a combination of factors: the concentrating effect of stripping technique, characteristics of the mercury film electrode, and the fast scan capabilities of the Chemtrix Instruments. If you have a detection problem with trace elements or contaminants, anodic stripping may well be the solution.

free-new booklet

The complete story of ANODIC STRIPPING POLAROGRAPHY with detailed experiments and many references.

simple procedure for detection

1. Use wax impregnated graphite electrode coated with a thin layer of mercury.
2. Immerse electrode in cell with electrolyte.
3. Electrolyze at 1.00 volt for 10 minutes with controlled stirring.
4. Stop stirring and scan anodically to zero volts. (Leave peaks stored on oscilloscope screen as blank).
5. Add sample and repeat steps 3 and 4. Note change in peaks and relate to trace metal calibration curves.

rapid simultaneous detections

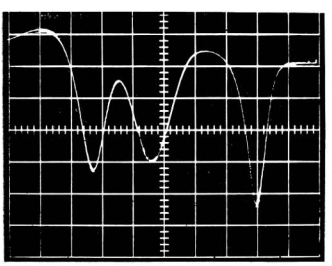

Anodic peaks in illustration are Zinc, Cadmium, and Lead at approximately 50 ppb in 1 molar KC1, stored on screen with single anodic scan.

some typical applications for anodic stripping polarography

- Trace impurities in reagents
- Trace metals in biological systems
- Water pollutants
- Lead in air (tetraethyl)
- Semiconductor trace metals

U.S. SALES PRICES F.O.B. FACTORY

CHEMTRIX polarographic analyzers

for Single-Sweep and Anodic Stripping Polarography

Model SSP-2 Three-Electrode Polarographic Analyzer . . . $3070.00

Model SSP-5 Differential System with Dual DME 3785.00

Illustrated Above:

Model SSP-3 Digital Readout Polarographic Analyzer . . . 3510.00

NEW—TYPE 804—$495 Potentiostatic Waveform Source

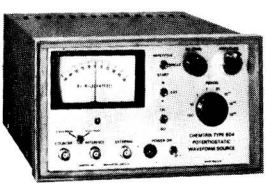

This versatile instrument is a waveform source for triangle and square waveforms, single or repetitive, with ±5 volt dc offset and up to 5 volt amplitude. It is also a potentiostat which can accept an external input and combine it with an internal dc level to provide controlled-potential output. It is both a waveform source and a potentiostat, providing controlled-potential output of its internally generated waveforms. In addition, it is

■ A Power Supply, ±5 v dc at 100 ma ■ A Controlled Potential Coulometer ■ An Integrator for Coulometric Titrations ■ An Integrator for External Signals ■ A Supply for Controlled-Current Titrations

CHEMTRIX, INC.

Instrumentation for Science

P. O. Box 725 Beaverton, Oregon 97005 (503) 648-1434

JOURNAL OF ELECTROANALYTICAL CHEMISTRY AND INTERFACIAL ELECTROCHEMISTRY

VOL. 26 (1970)

JOURNAL
of
ELECTROANALYTICAL CHEMISTRY
and
INTERFACIAL ELECTROCHEMISTRY

AN INTERNATIONAL JOURNAL DEVOTED TO ALL ASPECTS OF ELECTROANALYTICAL CHEMISTRY, DOUBLE LAYER STUDIES, ELECTROKINETICS, COLLOID STABILITY AND ELECTRODE KINETICS

VOL. 26 1970

ELSEVIER SEQUOIA S.A.

LAUSANNE

PRINTED IN THE NETHERLANDS

ELECTROANALYTICAL CHEMISTRY AND INTERFACIAL ELECTROCHEMISTRY
Elsevier Sequoia S.A., Lausanne – Printed in The Netherlands

THE OXIDATION OF HYDRAZINE IN ALKALINE SOLUTION AT PLATINUM AND MERCURY

J. A. HARRISON AND Z. A. KHAN

Electrochemistry Research Laboratories, Department of Physical Chemistry, University of Newcastle upon Tyne, Newcastle upon Tyne, NE1 7RU (England)

(Received December 18th, 1969)

INTRODUCTION

The oxidation of hydrazine in alkaline solution is the basis of a fuel cell. The mechanism has been investigated by a number of authors who come to different conclusions. The overall reaction involves four electrons

$$N_2H_4 + 4OH^- \rightarrow N_2 + 4\,H_2O + 4e; \quad E_0 = -1160\ \text{mV} \tag{1}$$

A platinum electrode in alkaline hydrazine solution attains a potential in which eqn. (1) is balanced by

$$H_2O + e \rightarrow \tfrac{1}{2}H_2 + OH^-; \quad E_0 = -826\ \text{mV} \tag{2}$$

or

$$N_2H_4 + 2e + 4\,H_2O \rightarrow 2\,NH_4OH + 2\,OH^-; \quad E^0 = +80\ \text{mV} \tag{3}$$

On platinum only reaction (2) is thought to occur at an appreciable rate, especially at low concentrations of hydrazine[1]. Reaction (3) is more pronounced on platinised carbon[2,3]. Gutjahr and Vielstich[4] conclude

$$\begin{aligned} &N_2H_4 \rightarrow N_2 + 4\,H^{\cdot}_{ads} \\ &4\,H^{\cdot}_{ads} \rightarrow 2\,H_2 \\ &4\,H^{\cdot}_{ads} + 4\,OH^- \rightarrow 4\,H_2O + 4e \end{aligned} \tag{4}$$

mainly on observed gas volumes at a stationary electrode.

The reaction orders have been measured[5] on a platinised platinum rotating disc and suggest

$$\begin{aligned} &N_2H_{4ads} + OH^-_{ads} \xrightarrow{\text{slow}} N_2H^{\cdot}_{3ads} + H_2O + e \\ &N_2H^{\cdot}_{3ads} + 3OH^- \xrightarrow{\text{fast}} N_2 + 3\,H_2O + 3e \end{aligned} \tag{5}$$

This differs from Szpak *et al.*[6] who use the shift of equilibrium potential with concentration and assume

$$N_2H_{4ads} \rightarrow X^{2+} + ZH^{\cdot} + Ze \tag{6}$$

where the mechanism is not further specified.

Other metals which have been attempted are nickel[7], gold[8] and silver[8]. Measurements have also been reported in dimethylsulphoxide platinum[9].

The mechanism of oxidation of hydrazine on mercury has been investigated polarographically[8,10].

It is the purpose of the present work to investigate the mechanism on platinum and to compare it with mercury.

EXPERIMENTAL

The experiments on Hg were carried out on a drop formed on an upturned syringe of usual type. The counter electrode was a platinum spiral surrounding the drop. An Hg/HgO reference electrode system containing the same concentration of NaOH as in the cell served to control the potential *via* a thick walled and tapered Luggin capillary.

The experiments on platinum used a small flawless Pt sphere produced in an H_2/O_2 flame. The electrode was mounted horizontally in a sliding joint and separated from the Pt gauze counter electrode by a glass frit.

The rotating platinum disc comprised a disc of 0.184 cm^2 area, which was polished to 0.1 μ with diamond paste (Stuess, Copenhagen, D. P. Polishing Machine). The disc was set in Teflon.

The reference electrode was Hg/HgO, NaOH. The particular concentration of NaOH is given in the legends. Glassware was cleaned in chromic–sulphuric acid. Reagent grade NaOH, recrystallised $N_2H_4 \cdot H_2SO_4$ and KNO_3 were used to make up solutions in triply distilled water. For the work on Hg, all solutions were made to a total of 1.5 *M* with KNO_3.

Pre-electrolysis of NaOH (40 mA for 48 h) improved the measurements at platinum. The NaOH solutions were stood over purified charcoal.

Drop areas were estimated for Hg by differential capacity measurements in 1 *M* NaOH (at 1.0 V w.r.t. Hg/HgO/1 *M* NaOH, the capacity = 16.14 $\mu F\ cm^{-2}$).

The area of platinum electrode given in the legends is geometric area. The roughness factor found from hydrogen adsorption peaks for the sphere (observed at 1 V s^{-1} and assuming the charge to correspond to a complete monolayer in 0.5 *M* H_2SO_4) was about 1.4.

Transistor potentiostat TR 70/2A and wave form generator RBI (Chemical Electronics) controlled the potential profile given to the working electrode.

Transients were recorded on a Tektronix 503 oscilloscope photographically.

Hydrazine on mercury

(*a*) *Potentiostatic pulses.* Single shot pulses (few ms in length) on the Hg drop showed typical electrochemical control. The current–time transients at low potentials are flat and at higher potentials show increasing effect of diffusion. The value of initial current, measured directly after the double layer charging is plotted against potential. The currents at higher potentials, where diffusion is appreciable, are not included in these plots. The curves in Fig. 1 correspond to fixed 0.5 *M* NaOH and varied hydrazine (10^{-2}–10^{-1} *M*). Currents at fixed potential are plotted in Fig. 2, and show the order of reaction for hydrazine to be unity. The deviation at large N_2H_4 is probably due to transport of OH^- at higher reaction rate.

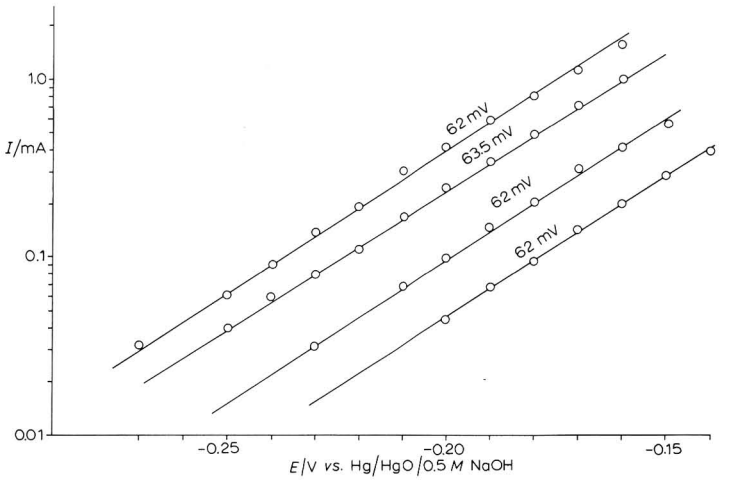

Fig. 1. Current–potential plots from potentiostatic pulse experiments. 0.5 *M* NaOH + (a) 0.01, (b) 0.02, (c) 0.05, (d) 0.1 *M* N_2H_4. Working electrode Hg 0.057 cm^2.

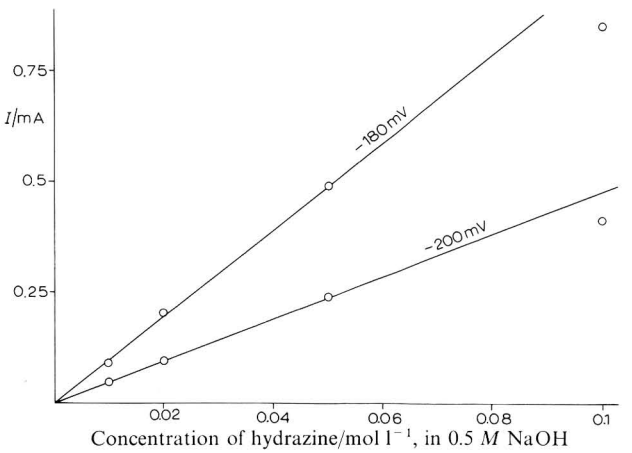

Fig. 2. Current *vs.* concn. of N_2H_4 at fixed potential w.r.t. Hg/HgO/0.5 *M* NaOH from Fig. 1.

The result of varying NaOH is shown in Fig. 3. Figure 4 shows the dependence of current on NaOH concentration at fixed potential, keeping the hydrazine concentration constant. The measurements were made with the same concentration of NaOH in the reference electrode as in the cell, and the potentials converted to one concentration of NaOH. The reaction order with respect to OH^- is also unity (Fig. 4).

The total number of electrons involved could not be measured by pulsing to complete diffusion control because too positive a potential was necessary. The total number of electrons was, however, derived from sweep measurements as in the next section.

(*b*) *Potential sweeps.* There were no detectable intermediates. Capacity curves measured at high sweep rates show that hydrazine is not adsorbed on Hg. Similar

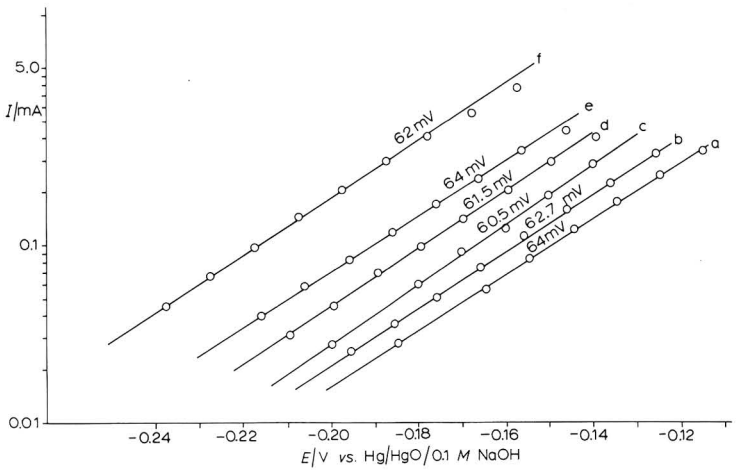

Fig. 3. Current–potential plots from potentiostatic pulse experiments. 0.01 M N_2H_4 + (a) 0.05, (b) 0.08, (c) 0.1, (d) 0.15, (e) 0.2, (f) 0.5 M NaOH. Working electrode Hg 0.057 cm^2.

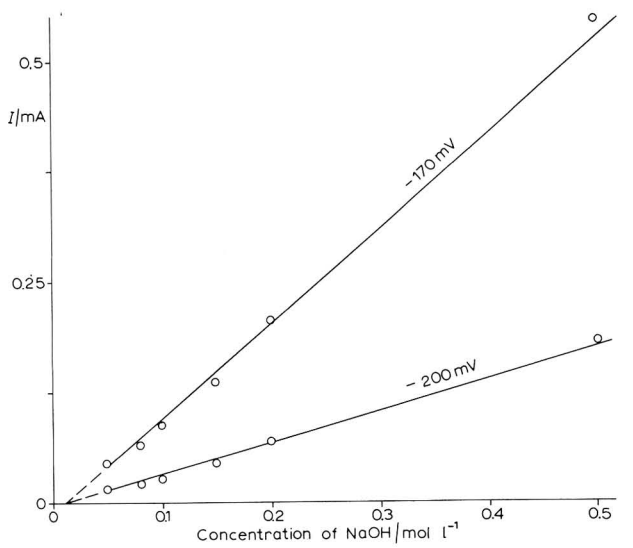

Fig. 4. Current *vs.* concn. of NaOH at fixed potential w.r.t. Hg/HgO/0.1 M NaOH from Fig. 3.

results were obtained by measuring the differential capacity with Lissajous figures observed by feeding a low amplitude 1 kHz sine wave to the cell by means of the potentiostat.

Peaks were obtained on sweeping for solutions containing 10^{-3} M and 10^{-2} M hydrazine. Analysis was effected in the usual way by measuring the change in peak current (I_p) and the shift of peak potential (E_p) with sweep rate (ω_s). Figure 5 shows I_p. The charging current in the absence of hydrazine was negligible, so no correction was applied to I_p. Figure 5 is a straight line. There is some deviation at high sweep rates, where the peak of hydrazine oxidation enters the Hg dissolution region.

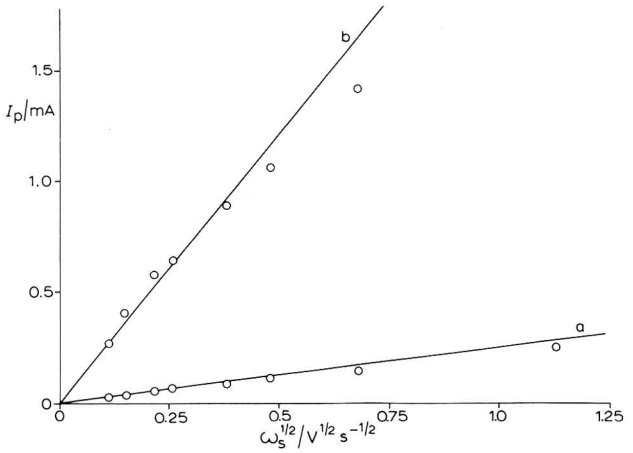

Fig. 5. Dependence of peak current on sweep rate. (a) 1 m*M* N_2H_4 + 0.1 *M* NaOH, (b) 10 m*M* N_2H_4 + 0.5 *M* NaOH. Working electrode Hg 0.057 cm^2.

Two explanations seem possible: that the $Hg(OH)_2$ which is formed[11] 100 mV negative to HgO slows down the oxidation of hydrazine, or hydrazine is prevented from reaching the electrode by the same $Hg(OH)_2$ species.

In agreement with the potentiostatic pulse measurements, the dependence of E_p on ω_s corresponds to an irreversible electron transfer with $(dE_p/d \log \omega_s) = 34 \pm 1$ mV for 10^{-2} *M* and 10^{-3} *M* (Fig. 6) solutions of hydrazine in 0.5 *M* NaOH and 0.1 *M* NaOH, respectively.

This suggests immediately that $\alpha n_a = 0.88$ independently of *n* from the equation

$$dE_p/d \log \omega_s = b/2 \tag{7}$$

where n_a is the number of electrons in the rate determining step, α is the charge

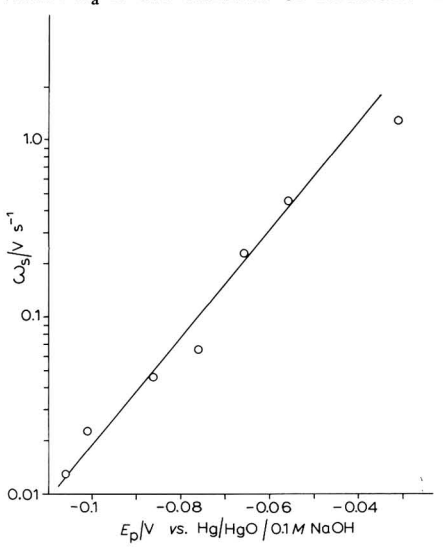

Fig. 6. Peak potential *vs.* sweep rate, 1 m*M* N_2H_4 + 0.1 *M* NaOH for electrode of Fig. 5.

transfer coefficient, and b is the Tafel slope given by $b = 2.303\ RT/\alpha n_a F$ when the rate determining electron transfer precedes other electron transfers. When fast electron transfer steps precede the rate determining step, $b = 2.303\ RT/[\alpha n_a + (n - n_a)]F$.

The value of αn_a can also be calculated from the slope of Fig. 5 by the equation

$$I_p = 0.496\ nFACD^{\frac{1}{2}}\ (2.303\ \omega_s/b)^{\frac{1}{2}} \tag{8}$$

Here n is four and D (diffusion coefficient) was taken as 1.39×10^{-5} cm^2 s^{-1}. αn_a could also be calculated[12], independently of n, A and C by the relation

$$I_p/\theta_p = 1.109\ \omega_s/b \tag{9}$$

where θ_p is the charge of the peak (from initial to peak potential) measured from experimental curves.

αn_a, assuming $n = 4$, from eqn. (8) is 0.89 ± 0.01. The same value is obtained from eqn. (9). αn_a from the potentiostatic pulse measurements (Figs. 1 and 3) is 0.92 ± 0.02. The best value of α is 0.46 ± 0.01, if $n_a = 2$ is chosen so that α is close to 0.5.

Mechanism

As two electrons, one hydroxyl ion and one hydrazine molecule are involved in the rate determining step, two alternative formal slow steps[10] are:

$$\left.\begin{aligned} &N_2H_4 \rightleftharpoons N_2H_3^- + H^+ \\ &N_2H_3^- \xrightarrow{\text{slow}} N_2H_3^+ + 2e \end{aligned}\right\} \tag{10}$$

$$N_2H_4 + OH^- \xrightarrow{\text{slow}} N_2H_3^+ + H_2O + 2e \tag{11}$$

with the following common fast reaction

$$3\ OH^- + N_2H_3^+ \longrightarrow N_2 + 3\ H_2O + 2e \tag{12}$$

The experimental evidence will clearly not distinguish between (10) and (11); however, we prefer (11) which can be understood by a kinetic process as follows.

When hydrazine is in a favoured position in the outer Helmholtz plane for electron transfer it is in the neighbourhood of an OH^- ion. Two electrons are then removed from the molecule. The simultaneous removal of two electrons is probably due to the symmetrical structure of the molecule. Once $2e$ and an H^+ leave the molecule the $N_2H_3^+$ must collide further with OH^- ions and the further steps are rapid.

The α value of 0.46 in conjunction with $2e$ suggests that the electrons are transferred simultaneously.

Hydrazine on platinum

(*a*) *Potential sweep.* It is well known that the platinum is easily poisoned and must be activated before each measurement[13]. Reproducible results were obtained by cycling a few times before each measurement between -879 mV and $+600 - 650$ mV (*vs.* Hg/HgO/1 *M* NaOH) in 1 *M* NaOH, hydrazine solutions, and similar potentials in other solutions. Sweeps with and without hydrazine are shown in Figs. 7 and 8. In Fig. 7 the small peak labelled **a** before the H$^\bullet$ desorption peaks is due to the oxidation of molecular hydrogen. When platinum is swept from -879 mV, however, this is not present.

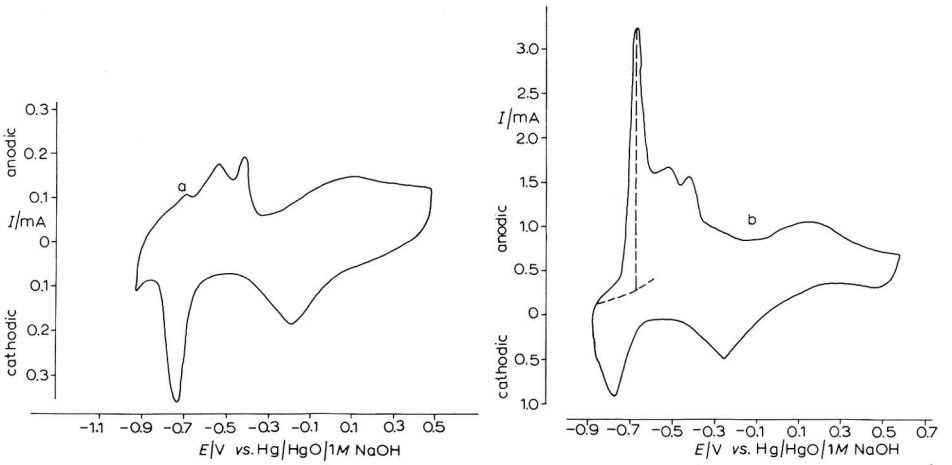

Fig. 7. Single anodic going sweep in 1 M NaOH at a Pt sphere. $\omega_s = 4.5$ V s^{-1}. Electrode area 0.033 cm^2.

Fig. 8. Single anodic going sweep for 5 mM $N_2H_4 + 1.0$ M NaOH at a Pt sphere. $\omega_s = 13$ V s^{-1}. Electrode area 0.033 cm^2.

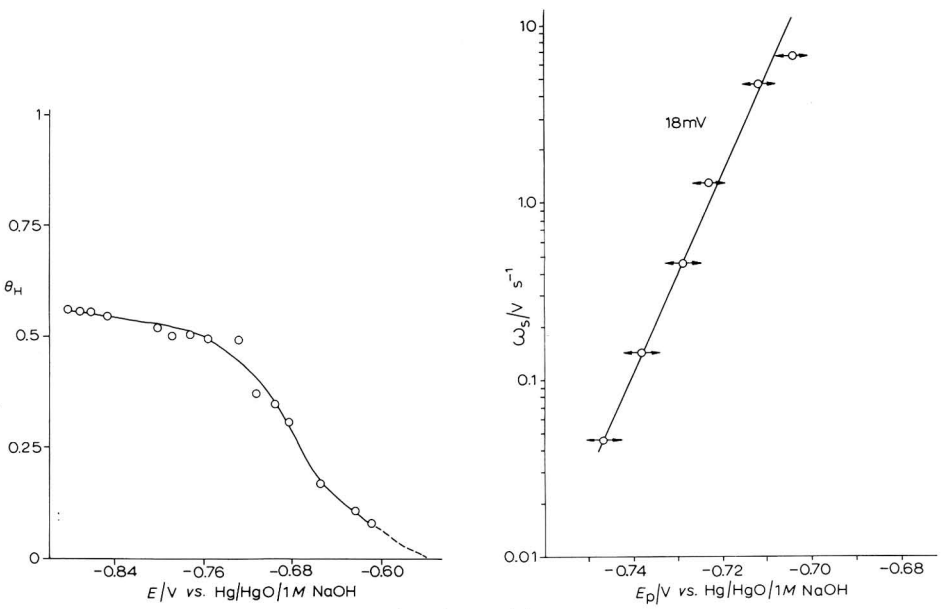

Fig. 9. Coverage, θ_H, of Pt with H$^\cdot$ as a function of potential.

Fig. 10. Peak potential *vs.* sweep rate for 5 mM $N_2H_4 + 1.0$ M NaOH at a Pt sphere. Electrode area 0.033 cm^2.

In the absence of hydrazine the two H$^\cdot$ desorption peaks are similar to those observed in acid solution. Adsorption of H$^\cdot$ is however more irreversible than in acid solution and occurs in one peak. The equilibrium coverage of platinum with H$^\cdot$, θ_H, as a function of potential is shown in Fig. 9. The measurement was made by

polarising until equilibrium at the appropriate potential after activation of platinum, and then measuring the H$^{\cdot}$ desorption charge in a fast sweep. When hydrazine is added to the solution a peak is observed before H$^{\cdot}$ desorption peaks. The peak shift in potential ($dE_p/d \log\omega_s$) = 18 mV is shown in Fig. 10.

The peak current, Fig. 11, is first order in hydrazine which is expected for a maximum determined by diffusion. Analysis by eqns. (7) and (8) shows that the reaction behaves as 4*e* overall with a 4*e* rate determining step. This analysis is not strictly correct for a surface reaction but as shown in the rotating disc experiment is almost valid. This rather strange result becomes clear in the rotating disc experiments in the next section.

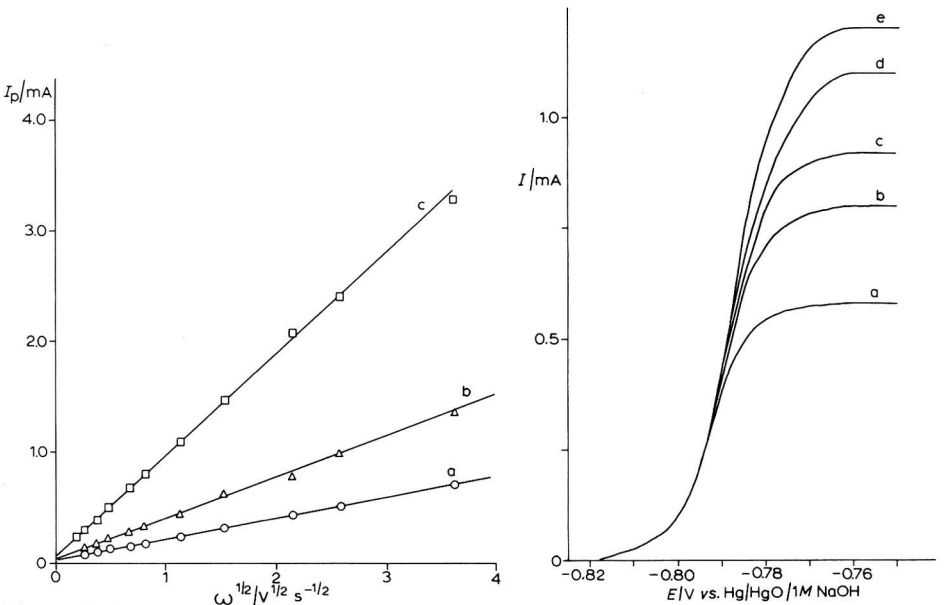

Fig. 11. Peak current *vs.* sweep rate for 1.0 *M* NaOH + (a) 1, (b) 2, (c) 5 m*M* N_2H_4 at a Pt sphere. Electrode area 0.033 cm^2.

Fig. 12. Current–potential curves at a platinum rotating disc for 1.0 *M* NaOH + approx. 2 m*M* N_2H_4. Rotations s^{-1} = (a) 10.5, (b) 19.5, (c) 25, (d) 32.2, (e) 39.

(*b*) *Rotating disc.* Stationary current–voltage curves were measured as a function of rotation speed, the concentration of N_2H_4 and OH^-. The electrode was activated at potential and the current measured immediately. A typical set is shown in Fig. 12. At high potential the limiting current (I_l) is completely diffusion controlled and the slope of I_l *vs.* $\omega^{\frac{1}{2}}$ (Fig. 13) gives the correct concentration of hydrazine checked by titration (provided OH^- is in excess). At low potentials the curves have all the characteristics of an irreversible reaction and are independent of rotation speed. The Tafel slope shown in Fig. 14 was derived from the rotation independent region in Fig. 12 and also by extrapolation in the usual way, namely plotting $1/i$ *vs.* $1/\omega^{\frac{1}{2}}$ at fixed potential and reading off the intercept. As the diffusion current is approached a slight curvature of the plots $1/i$ *vs.* $1/\omega^{\frac{1}{2}}$ at slow rotation speeds is seen due to N_2 gas

evolution. The Tafel slope is 17.3 mV. Also shown in Fig. 14 is the OH^- dependence. The OH^- dependence was measured with a fixed concentration of NaOH in the reference electrode and the curves adjusted by the calculated junction potential (Henderson equation). A more satisfactory procedure was also tried in which the curves were measured against the same concentration of NaOH in the reference electrode. The curves then shifted to bring them on the same scale. In both cases the current is proportional to $[OH^-]^4$. The current–voltage curve at the foot of the wave is independent of hydrazine concentration (Fig. 14) in the measured range 1–6 m*M*.

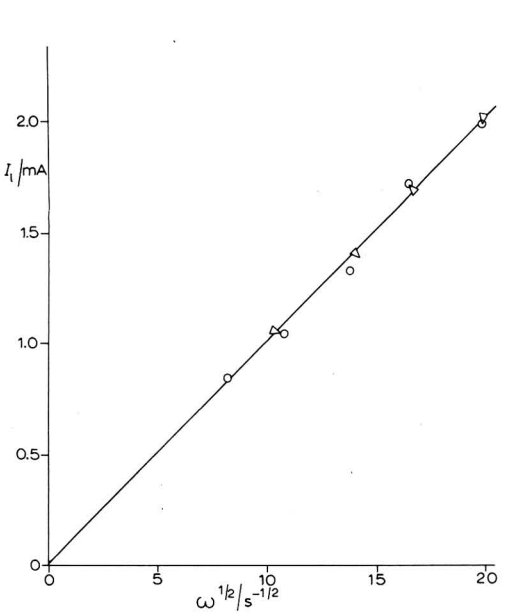

Fig. 13. Limiting current, I_l, *vs.* rotation speed for a Pt rotating disc, (○) 2 m*M* N_2H_4 + 1.0 *M* NaOH, (△) 2 m*M* N_2H_4 + 0.1 *M* NaOH.

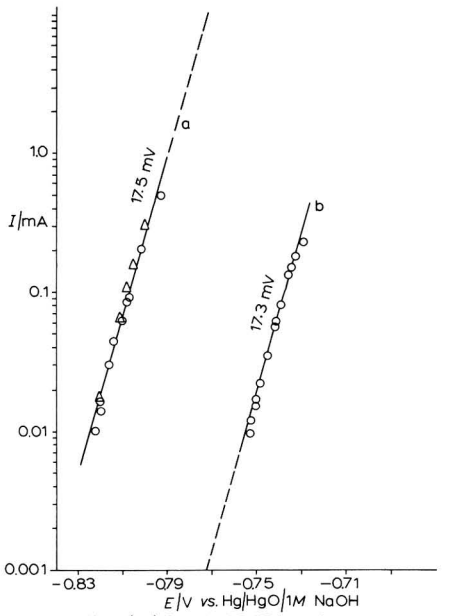

Fig. 14. Tafel plot for Pt rotating disc at the foot of the wave. (a): (○) 2 m*M* N_2H_4 + 1.0 *M* NaOH, (△) 6 m*M* N_2H_4 + 1.0 NaOH; (b): (○) 2 m*M* N_2H_4 + 0.1 *M* NaOH.

Mechanism

Reaction rate is independent of hydrazine conc. in the electrochemical region and hydrazine itself is clearly adsorbed, which is also indicated by the intercept in Fig. 11. Capacity measurements with and without hydrazine were not possible due to proximity of hydrogen evolution. The rate determining reaction involves 4*e* and is a surface process. The last statement is based on the experimental result that hydrazine is much more easily oxidized on platinum than mercury. According to Parsons[14] electrochemical reactions in which there is a strong interaction between reactant and metal should depend strongly on the nature of the substrate metal.

In principle, a surface reaction involving a number of electron exchange steps would have the form shown below. The intermediates are written as radicals although it is not possible to specify exactly their nature.

$$N_2H_{4(soln.)} \rightleftharpoons N_2H_{4ads} \tag{13}$$

$$\theta_1\colon\ N_2H_{4(ads)} + OH^- \underset{k_B}{\overset{k_A}{\rightleftharpoons}} N_2H_3^{\cdot} + H_2O + e \tag{14}$$

$$\theta_2\colon\ N_2H_3^{\cdot} + OH^- \underset{k_D}{\overset{k_C}{\rightleftharpoons}} N_2H_2^{\cdot} + H_2O + e \tag{15}$$

$$\theta_3\colon\ N_2H_2^{\cdot} + OH^- \underset{k_F}{\overset{k_E}{\rightleftharpoons}} N_2H^{\cdot} + H_2O + e \tag{16}$$

$$\theta_4\colon\ N_2H^{\cdot} + OH^- \xrightarrow{k_G} N_2 + H_2O + e \tag{17}$$

The last step must be irreversible as N_2 is not reducible under these conditions. The θ on the l.h.s. of the above equations is the stationary coverage with the nitrogen containing radicals.

The expression for current

$$i = k_G\, \theta_4 [OH^-] \exp(\alpha FE/RT) \tag{18}$$

becomes by simple calculation (assuming coverage by intermediates is small)

$$i = \theta_1 [OH^-]^4 (k_A k_C k_E k_G / k_B k_D k_F) \exp\{(3+\alpha) FE/RT\} \tag{19}$$

Figure (9) shows the H$^{\cdot}$ coverage θ_H to be constant at about 0.5 in the region of the hydrazine oxidation curve, so θ_1 is constant at about $(1-\theta_H)$. Hydrazine adsorption probably does not displace H$^{\cdot}$ as the desorption curves are not suppressed when hydrazine reacts for example in Fig. 8. The observed curves have the characteristics of eqn. (19), namely the experimental slope 17.3 mV is close to theoretical of 16.6 mV with $\alpha = 0.5$ and an $[OH^-]^4$ dependence. This definitely rules out a slow step further along the chain as both the OH^- dependence and the Tafel slope would be seriously changed.

ACKNOWLEDGEMENT

One of us (Z.A.K.) wishes to thank the British Council for financial support. We are also indebted to Dr. R. D. Armstrong and Professor H. R. Thirsk for their interest in the problem.

SUMMARY

The mechanism of hydrazine oxidation in alkaline solution has been investigated at platinum and mercury. The rate determining step on mercury takes place at the outer Helmholtz plane and involves simultaneous transfer of two electrons and one hydroxyl ion. On platinum the oxidation is a surface process involving a fast three electron transfer preceding a one electron rate determining step. The reaction is fourth order in OH^-.

REFERENCES

1 G. SUSBIELLES AND O. BLOCH, *Compt. Rend.*, 256 (1962) 685.
2 V. S. DANIEL-BEK AND G. V. VITVITSKAYA, *Sov. J. Electrochem.*, 3 (1967) 5.
3 V. S. DANIEL-BEK AND T. N. GLAZAMOVA, *Sov. J. Electrochem.*, 2 (1966) 1279.
4 M. GUTJAHR AND W. VIELSTICH, *Chem. Ing.-Tech.*, 40 (1968) 180.
5 G. V. VITVITSKAYA AND V. S. DANIEL-BEK, *Sov. J. Electrochem.*, 3 (1967) 863.
6 S. SZPAK, P. STONEHART AND T. KATAN, *Electrochim. Acta*, 10 (1965) 563.
7 B. P. NESTEROV AND N. V. KOROVIN, *Sov. J. Electrochem.*, 2 (1966) 1184.
8 K. KORINEK, J. KORYTA AND M. MUSILOVA, *J. Electroanal. Chem.*, 21 (1969) 319.
9 M. MICHLMAYR AND D. T. SAWYER, *J. Electroanal. Chem.*, 23 (1969) 375.
10 S. KARP AND L. MEITES, *J. Am. Chem. Soc.*, 84 (1962) 906.
11 R. D. ARMSTRONG, M. FLEISCHMANN AND H. R. THIRSK, *J. Electroanal. Chem.*, 11 (1966) 208.
12 J. H. CHRISTIE, G. LAUER AND R. A. OSTERYOUNG, *J. Electrochem. Soc.*, 111 (1964) 1420.
13 S. GILMAN, *J. Phys. Chem.*, 67 (1963) 78.
14 R. PARSONS, *Surface Science*, 2 (1964) 418.

ELECTROANALYTICAL CHEMISTRY AND INTERFACIAL ELECTROCHEMISTRY
Elsevier Sequoia S.A., Lausanne – Printed in The Netherlands

THE ELECTROREDUCTION OF MOLTEN PHOSPHATES

E. FRANKS* AND D. INMAN

Nuffield Research Group in Extraction Metallurgy, Department of Metallurgy, Imperial College, London, S.W.7. (England)

(Received 6th, December 1969)

INTRODUCTION

Molten phosphates are effective solvents for metal oxides and have been widely used in studies of electrode processes and reactions. By examining the products arising from the electrolysis of molten sodium metaphosphate, it has been confirmed that the overall products are phosphorus and trisodium orthophosphate at the cathode, and oxygen together with branched phosphates at the anode[1,2]. These results are consistent with the cationic conduction of the metaphosphate[3] and the reduction of the phosphate oxy-anion at a potential more anodic than that required to reduce the sodium ion.

Results for the cathode reactions have shown some inconsistency. Whereas Yocom[1] and Caton and Freund[2] were not able to proceed beyond a first decomposition potential of approximately -1 V against a platinum non-polarisable anode, both Andreeva[4] and Francis *et al.*[5] obtained two decomposition potentials. The first decomposition corresponded to the evolution of phosphorus, and it was assumed by Andreeva that sodium was formed at the second decomposition potential.

In order to clarify the position, it was decided to investigate the following:

1. the occurrence of a limiting current,
2. the species reacting at the cathode,
3. the mechanisms of the cathode process.

EXPERIMENTAL

Apparatus

The electrolysis was carried out in an atmosphere of dried argon using a dense graphite pot as a container and a non-polarisable anode as shown in Fig. 1. The working electrode was either a 3 mm diameter impermeable graphite rod enclosed in boron nitride or a 1 mm diameter tungsten rod insulated with alumina or Supremax glass.

Constant currents were obtained from a Farnell 350 V stabilised voltage supply in series with a Cambridge variable resistance box of 10,000 Ω maximum. The voltage between the micro-electrode and the anode was determined by a Radiometer pH meter; it was also displayed on a Tektronix 545B oscilloscope.

* Present address: Department of Science, Hendon College of Technology, London, N.W.4.

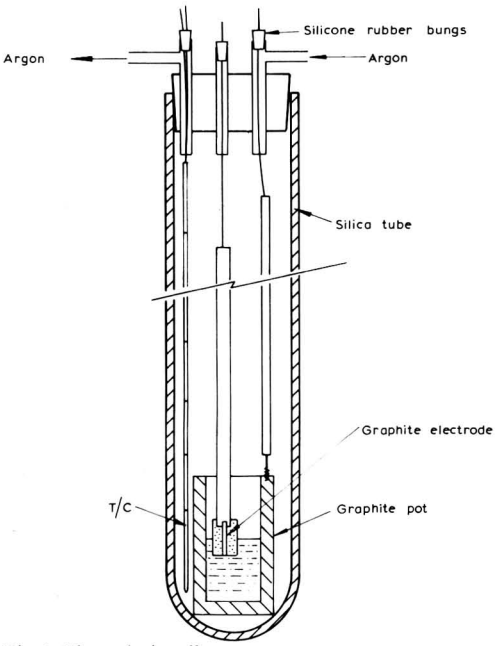

Fig. 1. Electrolysis cell.

The electrolysis cell was heated in a Camlab vertical furnace. This incorporated a Sunvic controller and temperature indicator; thermocouple readings showed that the temperature was constant within $\pm 5^{\circ}$C over the bottom four inches of the cell.

Materials

Sodium metaphosphate. This was supplied as pure anhydrous trimetaphosphate by Albright and Wilson, Oldbury.

Sodium orthophosphate. Since pure orthophosphate could not be obtained, an equimolar mixture of AnalaR sodium peroxide and AnalaR sodium pyrophosphate was used (sodium peroxide was similarly used by Shams El Din and Gerges[12] in place of sodium oxide which tends to absorb moisture more readily). The mixture was ground and dried for 12 h at 120°C.

Sodium pyrophosphate. The AnalaR reagent was used.

Sodium tripolyphosphate. This was prepared from a mixture of the metaphosphate and pyrophosphate in the ratio of 1 : 2 molar, respectively.

Lithium chloride–potassium chloride. The AnalaR reagents were mixed and purified by preelectrolysis under vacuum, followed by filtration.

Sodium chloride–potassium chloride. Equimolar quantities of AnalaR reagents were mixed and heated for 12 h at 120°C under vacuum. All materials were stored in a desiccator over magnesium perchlorate.

RESULTS AND DISCUSSION

Molten sodium metaphosphate

(*a*) *Voltammetry.* In establishing a limiting current for the electrolysis of

$NaPO_3$ at 820°C, Francis *et al.*[5] had employed increasing current densities up to a value of 3 A cm^{-2} whereas Yocom[1] and Caton and Freund[2] used maximum current densities of about 0.3 A cm^{-2}.

In the present work, the cathodic reaction in molten metaphosphate was initially examined at 700°C using the 3 mm diameter graphite electrode; potentials were measured *versus* the graphite pot. The steady-state potentials were determined as the applied currents were increased; electrode potentials were allowed to decay to the initial rest potential between each reading. The rising part of the *E vs. I* curve occurred from about 3 mA, *i.e.* 0.07 A cm^{-2}; this corresponds to the current density at which phosphorus is evolved. On increasing the current to 20 mA, at which stage the cathode potential was about −1.2 V, cyclic variations of 0.2–0.3 V occurred. These cyclic variations of potential continued over the applied current range 20–30 mA and a mean value was taken. At 35 mA the electrode potential rose to above −2 V and remained steady. Further increase of current led to a steady increase in the steady-state potential, as shown on the oscilloscope. A similar pattern was shown for a new melt at a temperature of 730°C; the second process occurred at 65 mA instead of about 35 mA in this case.

To avoid high currents, the 3 mm diameter graphite electrode was replaced by a 1 mm diameter tungsten rod, which was allowed just to touch the melt surface. Polarograms for melt temperatures of 660°–810°C are shown in Fig. 2. These results

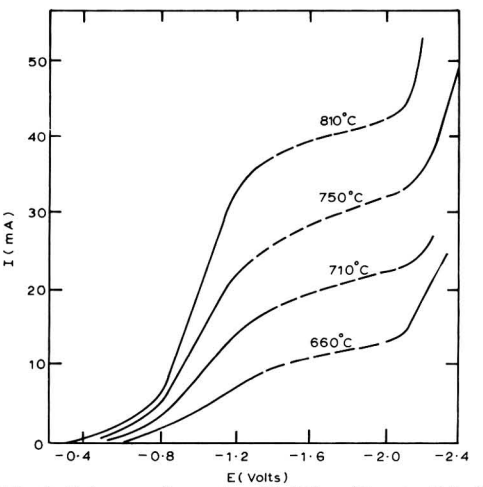

Fig. 2. *E–I* curves for molten $NaPO_3$. (*E*, potential of tungsten cathode *vs.* graphite pot).

confirm the existence of a limiting current; its magnitude increases with increase of temperature. The two decomposition potentials occurred at about −0.7 V and −2.1 V *versus* the graphite pot.

It would appear that the concentration of the reducible ion, which gives phosphorus as the overall product, increases with temperature. However, as a first approximation the diffusion current i_d is related to the concentration of the reducible species by the equation:

$$i_d = nFCD/\delta \qquad (1)$$

where i_d = diffusion current density (A cm^{-2}), n = number of electrons involved in the unit electrode reaction, F = Faraday (96,487 C), C = concentration of reducible species (mol cm^{-3}), δ = thickness of diffusion layer (cm).

Since D increases with increase of temperature and δ might be expected to decrease, there is no direct relationship between i_d and C over a range of temperatures. Further evidence for the presence of reducible species in the molten metaphosphate was obtained by chronopotentiometry, the results of which are more amenable to quantitative interpretation than are polarographic results when solid electrodes are used.

(*b*) *Decay curves.* The potential reached by an electrode for any charging current I is made up of the reversible electrode potential E_0, overpotential arising from the ohmic resistance of the melt and the activation and diffusion overpotentials for the electrode processes. In this system, the ohmic overpotential or IR drop makes the largest contribution. Hickling[18] showed that if the measurement of potential could be made very quickly after switching off the polarising current, a value for E_0 could be obtained. Francis *et al.*[5] used this method to determine decomposition potentials in molten phosphates.

Using the oscilloscope as a voltmeter, it was possible to examine the decay of electrode potential, at different charging currents, when the current was switched off. Typical open circuit curves are shown in Fig. 3 for currents above and below the i_d

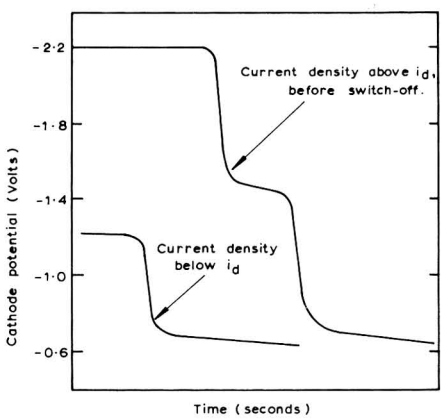

Fig. 3. Decay curves for molten $NaPO_3$ at 730°C.

values. When values of current larger than i_d were used, two processes could be detected at about 0.8 V apart. The lower one corresponded to the first decomposition potential but the more cathodic one did not correspond to the -2 V previously determined for the second decomposition potential from the E–I curves. However, as was shown above, the steady-state potentials between -1.2 V and -1.8 V were subject to cyclic variations. It would seem that the process occurring at -1.6 V had been obscured by these variations in voltage.

(*c*) *Chronopotentiometry.* For these experiments the alumina insulation on the tungsten wire as used for voltammetry was replaced by a high alumina Supremax glass sleeve. A glass bead of the same material was formed at the end of the tungsten by

wiping the heated wire with the glass. The glass sleeve was then sealed onto the Supremax bead and the end of the electrode was ground flat and polished on a diamond pad. Adherent phosphate glass tended to crack the bead due to thermal expansion; this was avoided by lifting the electrode from the melt after each run. When cracking did occur, the glass sleeve was removed, the bead was reformed and the sleeve resealed onto it.

Using a similar arrangement to that employed in voltammetry, the current density was increased to beyond that corresponding to limiting current conditions and the charging curve was displayed on a Tektronix storage oscilloscope 564. At an electrode potential of *ca.* -1 V, a first transition appeared. On further increasing the current density, such that the electrode potential reached -2 V, a second transition occurred. The transitions were examined over the temperature range 660°–800°C; a charging curve for the high current densities is shown in Fig. 4. This shows similar cyclic variations to those that had been noticed in voltammetry. The potentials at which the two processes occur are approximately -0.7 V and -1.5 V.

Typical results for the first transition are shown in Table 1.

Similar results were obtained at other temperatures as can be seen in Fig. 5. This decrease in the $i\tau^{\frac{1}{2}}$ value with increase of current density has been considered by Delahay and Berzins[6]; it indicates that a chemical reaction occurs prior to the electroreduction. Using the Sand relationship for the linear diffusion of electroactive species under a constant electrolysis current i A cm^{-2} (results obtained in horizontal regions of $i\tau^{\frac{1}{2}}$ *vs.* i plots), the transition time is related to the concentration of reducible species by

$$i\tau^{\frac{1}{2}} = \tfrac{1}{2}\pi^{\frac{1}{2}} nFD^{\frac{1}{2}} C \qquad (2)$$

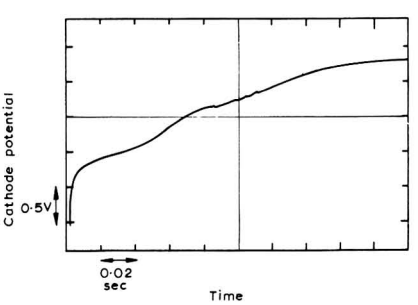

Fig. 4. Chronopotentiogram for molten $NaPO_3$.

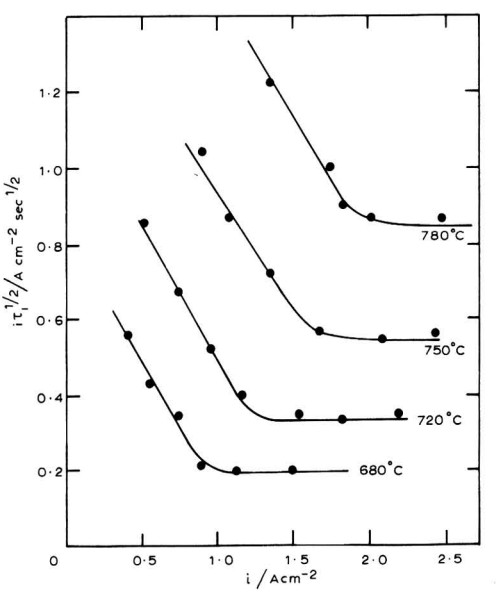

Fig. 5. Plots of $i\tau_1^{\frac{1}{2}}$ *vs.* i.

TABLE 1

TRANSITION TIMES IN MOLTEN SODIUM METAPHOSPHATE AT 710°C

$i/A\ cm^{-2}$	$\tau/s.$	$i\tau^{\frac{1}{2}}/A\ cm^{-2}\ s^{\frac{1}{2}}$
0.64	1.4	0.77
0.72	0.8	0.68
0.84	0.38	0.42
0.96	0.19	0.42
1.20	0.09	0.36
1.80	0.038	0.34
2.40	0.024	0.36

Again the temperature of the melt affects D but the increase of $i\tau^{\frac{1}{2}}$ with increase of temperature appears to be greater than that expected on the basis of a $D^{\frac{1}{2}}\alpha T$ relationship. Thus an increase of C with temperature appears likely. A chemical reaction which might lead to increasing concentrations of reducible species with increase of temperature is the formation of lower polymers in the highly polymerised metaphosphate melt. This reaction could also couple to the electrode reaction proper.

(*d*) *Composition of molten phosphates.* Phosphates can be considered as condensation products of metal oxides and phosphorus pentoxide based on phosphorus with an sp^3 bond structure. Van Wazer[7] discusses the combinations possible using the following structural units:

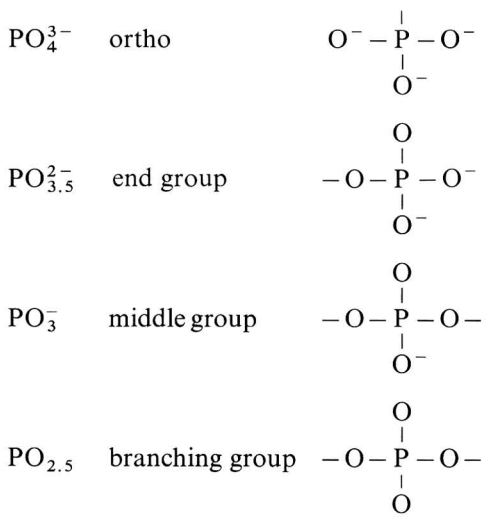

Two end groups form the pyro ion $P_2O_7^{4-}$ and unreacted oxide gives oxide ion O^{2-}. Depending upon the ratio R of M_2O/P_2O_5, alkali metal phosphates form two main types of polymeric structure. Chain phosphates made up of a middle group and two end groups have the general formula $M_{n+2}P_nO_{3n+1}$. For $R=1$, ring phosphates are obtained with the general formula $M_nP_nO_{3n}$. As n increases, the polymeric oxyanions for chain and ring structures tend to become similar. This equilibrium mixture is found in trimetaphosphate melts; it can be considered as a mixture of chain polymers

with an average n value ($\bar{n}$) of above fifty. The average chain length for linear polymers can be estimated from the formula

$$\bar{n} = 2/(R-1) \tag{3}$$

The distribution of polymers in phosphate glass has been followed by hydrolysis and paper chromatography[8-10] and the suggested depolymerisation reaction is:

$$2(P_nO_{3n+1})^{-n-2} = (P_{n-1}O_{3n-2})^{-n-1} + (P_{n+1}O_{3n+4})^{-n-3} \tag{4}$$

This could produce the monomer PO_4^{3-} from a series of reactions of which the last step is

$$2P_2O_7^{4-} = PO_4^{3-} + P_3O_{10}^{5-} \tag{5}$$

The depolymerisation is known to be endothermic[10] and increase of temperature could produce increased quantities of the lower oxyanions.

Since the metaphosphate melt is a very complex polymeric mixture it was decided to examine the behaviour of lower polymers, the ortho, pyro and tripolyphosphates in halide melts. In this way the concentrations of phosphate anions could be better defined.

Solutions of phosphates in molten halides: chronopotentiometry

(*a*) *LiCl–KCl*

Laitinen and Lucas[11] used lithium chloride–potassium chloride eutectic over the temperature range 450°–700°C as a solvent for sodium metaphosphate. Voltammetry gave ill-defined curves with two processes occurring at −0.80 V and −1.55 V with respect to a Pt(II)/Pt reference. A number of chronopotentiometric experiments were carried out and at least two transitions were noted. However no efforts were made to determine the relationship between the transition times.

At 450°C the orthophosphate in LiCl–KCl prepared as above gave only one transition and the $i\tau^{\frac{1}{2}}$ value was constant. The pyrophosphate gave two transitions, the second occurring at a potential 0.4 V more cathodic than the first.

It was found that lithium chloride led to difficulties in handling, due to its hygroscopic nature. The graphite crucibles were not readily cleaned and there was evidence of penetration by the melt. It was therefore decided to use a sodium chloride–potassium chloride mixture for further experiments. The experimental temperature range available is comparable to the temperatures used for the molten metaphosphate.

(*b*) *NaCl–KCl*

(*i*) Na_3PO_4. Sodium orthophosphate prepared as described above was added to the chloride mixture. Only one transition was obtained with an $E_{\tau/4}$ value approximately −0.7 V referred to the graphite anode over the temperature range 670°–780°C. The $i\tau^{\frac{1}{2}}$ values were constant; typical results at 780°C are shown in Table 2.

The effect of varying the concentration of orthophosphate at 780°C is shown in Fig. 6. These results indicate that Sand's behaviour is obeyed over the concentration range used. In order to determine the type of reduction reaction occurring and the number of electrons transferred, the electrode potential over the rising part of the curve was examined. Reinmuth[13] has considered the interpretation of chronopotentiometric potential–time curves and proposed diagnostic criteria for various kinetic schemes.

TABLE 2

TRANSITION TIMES FOR SODIUM ORTHOPHOSPHATE IN NaCl–KCl AT 780°C
$C = 5.8 \times 10^{-5}$ mol cm^{-3}

i/mA cm^{-2}	τ/s.	$i\tau^{\frac{1}{2}}$/mA cm^{-2} s$^{\frac{1}{2}}$
20.7	2.1	30.0
27.1	1.4	31.8
32.5	0.8	29.1
43.0	0.45	28.8
53.6	0.32	30.8
65.0	0.21	29.8
71.3	0.16	28.6
94.5	0.11	31.2
		30.0 ± 1.2

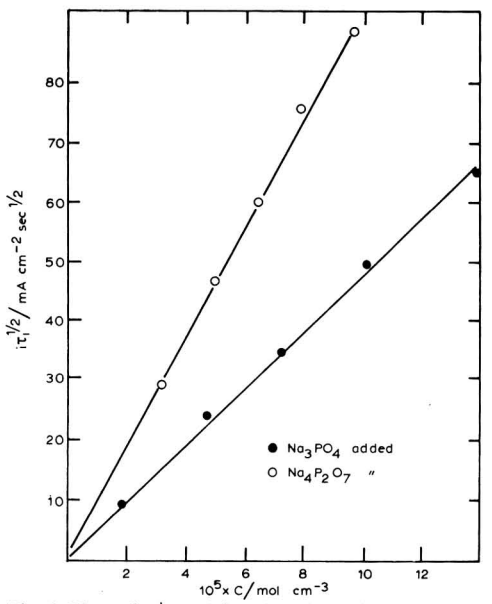

Fig. 6. Plots of $i\tau_i^{\frac{1}{2}}$ *vs.* C for phosphates in NaCl–KCl at 780°C.

Plots of electrode potential against log $(\tau^{\frac{1}{2}} - t^{\frac{1}{2}})$ and log $(\tau^{\frac{1}{2}} - t^{\frac{1}{2}})/t^{\frac{1}{2}}$ are shown in Fig. 7. The straight line plot of E *vs.* log $(\tau^{\frac{1}{2}} - t^{\frac{1}{2}})/t^{\frac{1}{2}}$ suggests a reversible reaction with soluble reactants and products. From the slope of this curve the number of electrons transferred is two, which corresponds to the value determined by Laitinen and Lucas[11] for sodium metaphosphate in lithium chloride–potassium chloride eutectic when carrying out controlled potential coulometry at -1.0 V with regard to a Pt(II)/Pt reference electrode.

If the reduction of the orthophosphate occurs with the transfer of two electrons, the pentavalent phosphorus is reduced to the trivalent state. However, it is

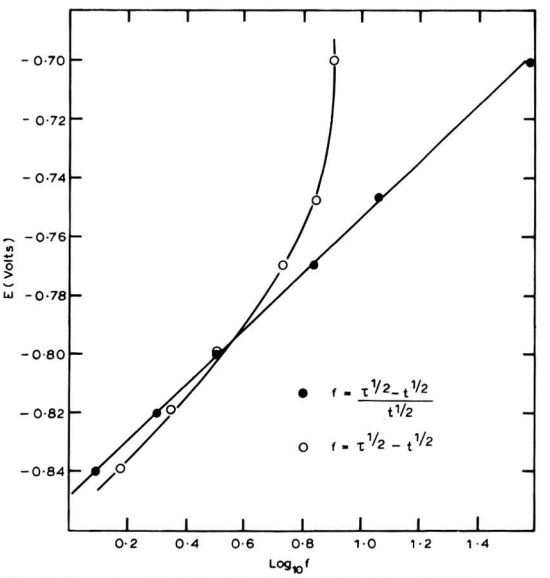

Fig. 7. E *vs.* $\log f$ for Na_3PO_4 in NaCl–KCl at 780°C.

known that phosphorus is the overall product; therefore a further chemical reaction must occur to produce the phosphorus.

The following mechanism is suggested:

(1) $PO_4^{3-} + 2\,e \rightarrow PO_2^- + 2\,O^{2-}$

(2) $5\,PO_2^- + 2\,O^{2-} \rightarrow 3\,PO_4^{3-} + 2\,P$

Eliminating the "hypo-phosphite" ion PO_2^-, the overall reaction becomes

(3) $2\,PO_4^{3-} + 10\,e \rightarrow 2\,P + 8\,O^{2-}$

or

$$PO_4^{3-} + 5\,e \rightarrow P + 4\,O^{2-} \qquad (6)$$

This corresponds to the overall reduction process used as the basis of coulometry in transport measurements[3].

Using the value $n=2$ in the Sand equation the diffusion coefficient at 780°C can be determined from the $i\tau^{\frac{1}{2}}$ *vs.* C curve in Fig. 6. The diffusion coefficient of the orthophosphate ion in NaCl–KCl has a value of 8.2×10^{-6} cm^2 s^{-1}.

(*ii*) $Na_4P_2O_7$. When sodium pyrophosphate was added to the sodium chloride–potassium chloride mixture at 670°C and the solution electrolysed, two transitions occurred; this result was similar to that obtained in lithium chloride–potassium chloride eutectic at 450°C. As the temperature of the melt was increased, the ratio of the first to second transition times increased. At 750°C the second transition had disappeared.

Two steps in a potential–time curve can be obtained when either (*a*) a single electroactive ion is reduced in two stages or (*b*) there are two ions present which are reduced at different cathodic potentials.

(*a*) *Single ion**. It can be shown that the two transition times τ_1 and τ_2 are given by:

$$\tau_1 = (\pi F^2 C^2 D n_1^2)/4 i^2$$

and

$$\tau_2 = [\pi F^2 C^2 D(2n_1 n_2 + n_2^2)]/4 i^2$$

or

$$\tau_2/\tau_1 = 2(n_2/n_1) + (n_2/n_1)^2 \quad (7)$$

where n_1 and n_2 are the numbers of electrons transferred in the reduction processes.

(*b*) *Mixture of ions.* In this case after the potential of the electrode becomes more cathodic than that at which the first process occurs; simultaneous reduction of the two ions occurs. The transition times are given by:

$$\tau_1 = \pi F^2 C_1^2 D_1 n_1^2/4\ i^2$$

$$\tau_2 = (\pi F^2/4\ i^2)\ (2n_1 n_2 D_1^{\frac{1}{2}} D_2^{\frac{1}{2}} C_1 C_2 + n_2^2 D_2 C_2^2)$$

Assuming $D_1 = D_2$

$$\tau_2/\tau_1 = 2(n_2/n_1)(C_2/C_1) + (n_2/n_1)^2 (C_2/C_1)^2 \quad (8)$$

Comparing the two cases, for the same n_1 and n_2 values, one would expect a constant τ_2/τ_1 for (a) and a ratio dependent on C_2/C_1 for (b). The variation in τ_2/τ_1 for pyrophosphate indicates that the melt contains at least two different ionic species and that at 750°C the C_2 values have decreased to zero.

The first transition corresponds to the reduction of the orthophosphate ion and it is probable that the second transition corresponds to the reduction of the pyrophosphate ion. Beyond 750°C only the orthophosphate is noted and in order to compare the behaviour with that observed in the previous experiments, varying concentrations of pyrophosphate were electrolysed at 780°C. These results are shown together with those for the orthophosphate in Fig. 6. For the same concentrations the pyrophosphate gives twice the $i\tau_1^{\frac{1}{2}}$ value, indicating that two moles of orthophosphate are produced for each mole of pyrophosphate added.

The pyrophosphate might be expected to give orthophosphate from the depolymerisation reaction shown in eqn. (5) above. However this would give one mole of orthophosphate from two moles of pyrophosphate for complete dissociation. The correct molar relationship can be obtained from the reaction

$$P_2O_7^{4-} + O^{2-} \rightleftarrows 2\ PO_4^{3-} \quad (9)$$

It has been shown by Shams El Din *et al.*[14] that the equilibrium is displaced well over to the orthophosphate side in chloride melts. Mitchell[15], investigating the equilibrium in molten potassium bromide, obtained a K value of 81 at 1000°K. The chlorides used contained oxide to the equivalent of 0.1×10^{-5} mol cm^{-3}; this would facilitate the formation of orthophosphate. In addition, reduction of the orthophosphate at the electrode releases 4 moles of oxide per mol of orthophosphate reduced (eqn. (6)). These oxide ions can react with the pyrophosphate ions diffusing up to the electrode.

* For a concise review of chronopotentiometry, see ref. 17.

(*iii*) Na_3PO_4–$Na_4P_2O_7$ *mixtures.* Owing to the dissociation of the pyrophosphate even at the lowest temperature that can be used for sodium chloride–potassium chloride melts, the concentration of pyrophosphate cannot be measured directly. However one can estimate the concentration of the respective ions from the transition times.

If τ_1 = transition time for orthophosphate, τ_2 = second transition time measured from τ_1, $i\tau_1^{\frac{1}{2}} = \frac{1}{2}\pi^{\frac{1}{2}} FD_1^{\frac{1}{2}} n_1 C_1$ for orthophosphate and $i[(\tau_1+\tau_2)^{\frac{1}{2}} - \tau_1^{\frac{1}{2}}] = \frac{1}{2}\pi^2 FD_2^{\frac{1}{2}} n_2 C_2$ for pyrophosphate, putting $(\tau_2')^{\frac{1}{2}} = (\tau_1+\tau_2)^{\frac{1}{2}} - \tau_1^{\frac{1}{2}}$ and assuming $D_1 = D_2$

$$\frac{i\tau_1^{\frac{1}{2}}}{i(\tau_2')^{\frac{1}{2}}} = \frac{n_1 C_1}{n_2 C_2}$$

If it is assumed that the concentrations of an orthopyrophosphate mixture remain unchanged in the melt, the value of n_2 can be determined from the ratios (r) of $i\tau_1^{\frac{1}{2}}$ and $i(\tau_2')^{\frac{1}{2}}$ (see Table 3).

Starting with an excess of orthophosphate and keeping the temperature as low as possible, increasing amounts of pyrophosphate were added and the transition times determined.

TABLE 3

ORTHOPHOSPHATE–PYROPHOSPHATE MIXTURES IN NaCl–KCl AT 670°C ($n_1 = 2$)

C_1/C_2	r	*Calcd.* n_2
5.9	2.0	5.9
3.4	1.5	4.6
2.4	1.3	3.7
1.8	0.9	4.0

These results would seem to indicate that as C_1/C_2 approaches the value two, an equilibrium is set up and the added concentrations remain unchanged. For those conditions n_2 becomes equal to four, which corresponds to the reduction of phosphorus valency in the pyrophosphate ion from five to three.

(*iv*) $Na_5P_3O_{10}$. Sodium tripolyphosphate was added to the melt and on electrolysis at 750°C three transitions were obtained. The first and second transitions were comparable to those found in the pyrophosphate-containing melt and the third could arise from the reduction of the tripolyphosphate ion. The processes occurred at approximately −0.7, −1.1 and −1.5 V which correspond to the quarter-wave potentials of −0.4, −0.85 and −1.19 V reported by Senderoff *et al.*[16] for trimetaphosphate dissolved in LiCl–KCl at 500°C.

For three transitions at times from commencement of electrolysis of τ_1, $\tau_2+\tau_2$ and $\tau_1+\tau_2+\tau_3$,

$$i\tau_1^{\frac{1}{2}} = \tfrac{1}{2}\pi^{\frac{1}{2}} F n_1 C_1 D_1^{\frac{1}{2}}$$
$$i[(\tau_1+\tau_2)^{\frac{1}{2}} - \tau_1^{\frac{1}{2}}] = i(\tau_2')^{\frac{1}{2}} = \tfrac{1}{2}\pi^{\frac{1}{2}} F n_2 C_2 D_2^{\frac{1}{2}}$$
$$i[(\tau_1+\tau_2+\tau_3)^{\frac{1}{2}} - (\tau_1+\tau_2)^{\frac{1}{2}}] = i(\tau_3')^{\frac{1}{2}} = \tfrac{1}{2}\pi^{\frac{1}{2}} F n_3 C_3 D_3^{\frac{1}{2}}.$$

The results are shown in Table 4.

TABLE 4

TRANSITION TIMES FOR $Na_3P_5O_{10}$ IN NaCl–KCl AT 750°C
$C = 9.0 \times 10^{-5}$ mol cm^{-3}

$i/mA\ cm^{-2}$	$(\tau_1+\tau_2+\tau_3)/s$	$(\tau_1+\tau_2)/s$	τ_1/s	$i\tau_1^{\frac{1}{2}}/$ $mA\ cm^{-2}\ s^{\frac{1}{2}}$	$i(\tau_2')^{\frac{1}{2}}/$ $mA\ cm^{-2}\ s^{\frac{1}{2}}$	$i(\tau_3')^{\frac{1}{2}}/$ $mA\ cm^{-2}\ s^{\frac{1}{2}}$
37.4	–	5.5	3.0	64.6	22.8	–
50.0	5.5	2.8	1.5	61.7	21.9	35.0
57.4	4.6	2.4	1.2	63.8	26.0	34.8
70.0	3.2	1.6	0.9	66.2	22.2	36.6
87.2	1.9	1.0	0.5	61.0	21.7	37.5
102.5	1.4	0.7	0.4	66.0	22.5	35.6
150.0	0.8	0.4	0.2	67.0	28.2	39.0

The results support the idea that three reducible ions are present in the melt and that these are reduced at progressively more cathodic potentials.

(*v*) $Na_3P_3O_9$. Transition times were examined in the temperature range 680°–780°C for sodium trimetaphosphate in sodium chloride–potassium chloride melts. Again three transitions were obtained and the respective potentials for the processes were similar to those found for the tripolyphosphate. As the temperature increased the ratios of the appropriate $i\tau^{\frac{1}{2}}$ values indicated an increasing proportion of the orthophosphate ion.

Oscilloscope traces for the ortho, pyro, tripoly and metaphosphates are shown in Figs. 8–11, respectively. Francis *et al.*[5] had shown that a decay curve obtained after switching off the current gave a good indication of the potentials at which the electrode processes occurred; the high ohmic over-potential of the melt was thereby eliminated. Figure 10 shows a charging and decay curve for tripolyphosphate and the decay section clearly indicates the potential differences between the three processes.

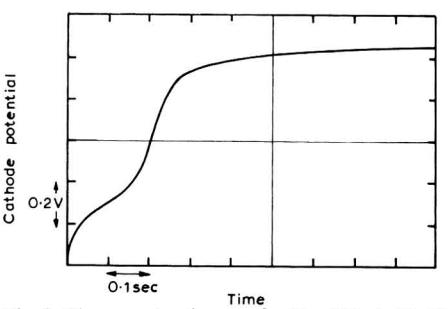

Fig. 8. Chronopotentiogram for Na_3PO_4 in NaCl–KCl.

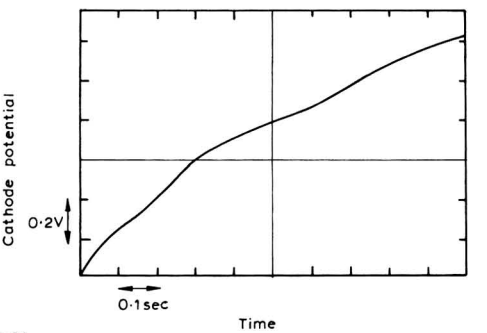

Fig. 9. Chronopotentiogram for $Na_4P_2O_7$ in NaCl–KCl.

GENERAL DISCUSSION

It would appear that in the highly polymerised sodium metaphosphate melt only the lower polymer phosphate ions are reduced at the cathode. Chronopotentio-

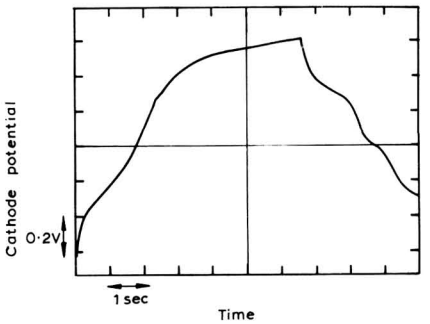

Fig. 10. Chronopotentiogram for $Na_5P_3O_{10}$ in NaCl–KCl.

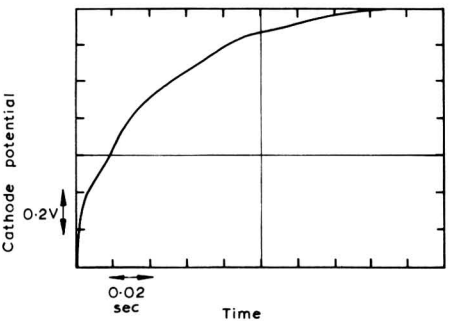

Fig. 11. Chronopotentiogram for $Na_3P_3O_9$ in NaCl–KCl.

metry indicates that a chemical reaction, probably depolymerisation, precedes the reduction process. The extent of depolymerisation increases with temperature and the availability of lower polymers is affected by the current density. At low current densities, as used by Yocom[1] and Caton and Freund[2], there is sufficient time for the prior depolymerisation to occur. Thus only the decomposition of the orthophosphate is observed giving phosphorus evolution. At high current densities there is insufficient time for complete depolymerisation and polymers higher than the monomer can be reduced. This gives rise to the limiting current observed by Andreeva[4] and Francis *et al.*[5].

The two-electron transfer observed by Laitinen and Lucas[11] for the first reduction process was confirmed. This indicates that in the electroreduction of phosphate ions the pentavalent phosphorus is reduced to trivalent phosphorus. Thus the final electrode products probably result from further chemical reactions, *cf.* the production of phosphorus occurring in the reduction of the orthophosphate ion.

SUMMARY

The electroreduction of phosphates has been examined by voltammetry and chronopotentiometry in molten sodium trimetaphosphates and as solutions in sodium chloride–potassium chloride over the temperature range 400°–800°C. Three electroactive species, reducing at potentials more anodic than the solvent, were found by chronopotentiometry; these were identified as the ortho, pyro and tripoly-phosphate ions. The electroreduction appears to be that of pentavalent to trivalent phosphorus; the overall products probably result from further chemical reactions.

REFERENCES

1 P. N. Yocom, Ph. D. thesis, University of Illinois, 1958.
2 R. D. Caton and H. Freund, *Anal. Chem.*, 35 (1963) 2103.
3 E. Franks and D. Inman, *Trans. Inst. Mining Met.*, Section C (1967) 76.
4 V. N. Andreeva, *Ukr. Khim. Zh.*, 21 (1955) 569.
5 P. Francis, A. S. McKie and N. E. Topp, National Chemical Laboratory (U.K.) N.C.L./Dep., 11 (1965).
6 P. Delahay and T. Berzins, *J. Am. Chem. Soc.*, 75 (1953) 2486.

7 J. R. VAN WAZER, *Phosphorus and its Compounds, Vol. I*, Interscience, New York, N.Y.
8 A. E. R. WESTMAN AND J. CROWTHER, *J. Am. Ceram. Soc.*, 37 (1954) 420.
9 A. E. R. WESTMAN AND P. A. GARTAGANIS, *J. Am. Ceram. Soc.*, 40 (1957) 293.
10 T. R. MEADOWCROFT AND F. D. RICHARDSON, *Trans. Faraday Soc.*, 59 (1963) 1564.
11 H. A. LAITINEN AND K. R. LUCAS, *J. Electroanal. Chem.*, 12 (1966) 553.
12 A. M. SHAMS EL DIN AND A. A. GERGES, *Electrochim. Acta*, 9 (1961) 123.
13 W. REINMUTH, *Anal. Chem.*, 11 (1960) 1515.
14 A. M. SHAMS EL DIN, A. A. EL HOSARY AND A. A. A. GERGES, *J. Electroanal. Chem.*, 6 (1963) 131.
15 A. MITCHELL, *Trans. Faraday Soc.*, 62 (1960) 5470.
16 S. SENDEROFF, E. M. KLOPP AND M. L. KRONENBERG, *8th and 9th Technical Progress Reports*, Contract Nord, 18240, 1960.
17 M. PAUNOVIC, *J. Electroanal. Chem.*, 14 (1967) 447.
18 A. HICKLING, *Trans. Faraday Soc.*, 33 (1937) 1540.

ELECTROANALYTICAL CHEMISTRY AND INTERFACIAL ELECTROCHEMISTRY
Elsevier Sequoia S.A., Lausanne – Printed in The Netherlands

A NOTE ON THE ORIGIN OF THE FIRST DOUBLET WAVE IN THE POLAROGRAPHY OF Bi(III) FROM ACID PERCHLORATE MEDIA

E. D. MOORHEAD* AND S. LIPCSEY
School of Chemistry, Rutgers University, New Brunswick, New Jersey 08903 (U.S.A.)

(Received November 3rd, 1969)

The polarographic behavior of Bi(III) in a variety of acid complexing media is well established[1-7]. Nonetheless, a recent survey of the literature has shown, that a great variety of opinion still exists regarding interpretation of the current–voltage behavior of bismuth in indifferent, or "non-complexing" solutions such as nitrate or perchlorate. The origin of this difficulty seems to be a lack of agreement as to which of the various possible hydrolyzed forms of the metal is actually responsible for the reduction process.

Exact identification of the electroactive species is complicated because the acidity of the triply-charged Bi(III) leads to coupled equilibria which can involve higher polynuclear forms of the metal. The formation of such species was originally suggested in 1947 by Granér and Sillén[8] who proposed that Bi hydrolysis leads to formation of a continuous series of polycentric cations. However, the formation of a single polynuclear moiety—thought to be $Bi_4(OH)_8^{4+}$—was subsequently favored in a report by Souchay and Peschanski[9]. Good proof for the existence at sufficiently high pH of a stoichiometrically identifiable "hexamer", $Bi_6(OH)_{12}^{6+}$, has been obtained from the results of more modern investigations using ultracentrifugation[10], solution X-ray scattering[11], light scattering[12], and Raman spectroscopy[13].

From a careful potentiometric investigation, Olin[14] reported values for the formation constants of a hexamer and also the monohydroxy Bi(III) species. His findings obtained at 25°C using 3.0 *M* (Na, H)ClO_4 as electrolyte were consistent with the following two equilibria:

$$Bi_{aquo}^{3+} = Bi(OH)^{2+} + H^+ \; ; \quad \log \beta = -1.58 \pm 0.02 \qquad (1)$$

$$6\, Bi_{aquo}^{3+} = Bi_6(OH)_{12}^{6+} + 12\, H^+ \; ; \quad \log \beta_{12,6} = 0.330 \pm 0.005 \qquad (2)$$

Olin pointed out that the dihydroxy $Bi(OH)_2^+$ cation [*i.e.*, the so-called "bismuthyl ion", BiO^+] was undetectable as a separate species in solution within the error of his experimental measurements. Tobias and Tyree in their later titrimetric study[15] using 1.0 *M* (Na, H)ClO_4 chose to avoid including $Bi(OH)^{2+}$ in their calculations. Instead, they fitted their experimental data to eqn. (2) and reported $\log \beta_{12,6} = -0.53$ (25°C). On this basis their recalculation of Olin's results yielded a considerably different value, *viz.*, $\log \beta_{12,6} = +0.03$ for 3.0 *M* perchlorate (25°C).

In assessing the polarography of Bi in nitrate and perchlorate, Goward[16]

* Department of Chemical Engineering, University of Kentucky, Lexington, Kentucky, 40506; author to whom reprint requests should addressed.

noticed that the Bi singlet wave in strong acid solution split into a doublet on raising the pH from 0 to 2. The two waves above pH 1.4, separated by more than 100 mV, were believed by Goward to come from separate reduction of $Bi(NO_3)_3$ and $Bi(OH)(NO_3)_2$ in nitrate, and to $Bi(OH)^{2+}$ and $Bi(OH)_2^+$ in perchlorate medium. His study did not yield reliable half-wave potentials, however, as both waves were obscured by severe maxima, and Goward dismissed observed shifts in $E_{\frac{1}{2}}$ with changing pH as probably the result of a variation in junction potential. The same doublet wave was subsequently found by Losev and Gorodetskii[17] in their polarization studies using the Bi(Hg) pool electrode, and they ascribed the two steps to sequential reduction of $Bi(OH)^{2+}$ and $Bi_6(OH)_{12}^{6+}$. Levine[7] recently concluded that only the Bi^{3+}_{aquo} cation is responsible for the first polarographic wave, and also asserted that the reduction process is free of detectable kinetic or catalytic complications. Presumably because reduction of the aquo ion should be free of pH effects, he attributed small $E_{\frac{1}{2}}$ variations with acidity to a combination of solution viscosity changes and activity effects.

In the face of the uncertainty regarding the assignment of species, we felt that it might be a desirable step to examine more closely both the $E_{\frac{1}{2}}$ and limiting current dependence of Bi(III) on the pH distribution of the metal as a prelude to investigating bismuth reduction at much higher salt concentrations. We wish to report here a number of preliminary observations which, when they are cast in the light of Olin's earlier conclusions, seem to provide a basis for viewing the origin of the first bismuth singlet wave in terms of two participating electroactive species, *viz.*, Bi^{3+}_{aquo} and $Bi(OH)^{2+}$, with possible assignment of the second wave to reduction of $Bi(OH)_2^+$, as suggested by Goward.

EXPERIMENTAL

Apparatus

A custom-built polarograph[18,19] of conventional operational amplifier design was used for both the a.c. and d.c. measurements together with a Metrohm three-electrode cell (EA-874-876) to minimize *IR*-drop through the solution. The a.c. results were obtained by superposing a 50 Hz, 5.0 mV r.m.s. signal on the d.c. potential applied to the DME and recording the first harmonic signal.

The saturated calomel electrode (SCE) was adopted as the reference for all potentials, although actual potentials were measured with a Metrohm (EA-425) Ag/AgCl electrode. To avoid contaminating the test cell with chloride, the Metrohm Ag/AgCl reference electrode was isolated from the solution using a saturated $NaNO_3$ salt bridge fitted with a fritted disc and agar plug. Because of the concentration range of supporting electrolyte used, the reference salt-bridge combination was corrected for the junction potential only in the measured $E_{\frac{1}{2}}$ for Tl(I) reduction from 0.1 *M* $NaNO_3$ assumed equal to -0.460 V *vs.* SCE[20]. As nitrate also acted as a contaminant, the salt bridge was not placed in contact with the test solution until immediately before recording a polarogram; frequent renewal of the bridge reservoir solution helped to avoid the small amount of Cl^- diffusing from the reference electrode compartment.

Test solutions were degassed with Matheson high-purity argon, then thermostatted to $30.0 \pm 0.02°$ C rather than 25° C which proved difficult to maintain in practice. All pH measurements were made with an Orion Model 801 meter. It should be em-

phasized that so-called pH measurements refer in this study to p_cH derived by calibration of the meter reading using solutions of known hydrogen ion concentration. The $E_{\frac{1}{2}}$ data in Fig. 8 were analysed by a least-squares fit using a Hewlett–Packard 9100-A desk computer.

Reagents

Stock bismuth solutions were prepared with G. F. Smith reagent $BiOClO_4 \cdot H_2O$ and standardized by direct titration with EDTA using pyrocatechol violet as indicator[21]. British Drug House ("Low Chloride") $NaClO_4$ was used throughout, while all other chemicals were domestic reagent grade.

All solutions used were prepared with triple distilled water.

Capillary characteristics

The dropping mercury electrode (DME) displayed the following capillary characteristics at $E_{applied} = 0.00$ V *vs.* SCE in argon-saturated 1.0 *M* $HClO_4$ at 30.0°C and 60.0 cm Hg head: $m = 2.28$ mg s^{-1}; $t = 3.59$ s. These flow characteristics were checked periodically.

RESULTS AND DISCUSSION

Effect of pH on d.c. current

In strongly acid solution (1.0 *M* $HClO_4$) one well-defined wave was obtained at about -0.01 V *vs.* SCE for reduction of 1.0 m*M* Bi(III) at 30°C. As shown by Goward, increasing the pH beyond 1.2 causes this wave to split into a doublet with the two steps separated by about 120–140 mV (we found no evidence in any of our work of the interferring maxima reported by Goward, and both waves were well-defined at all times). Further elevation of the pH decreased the first wave height and enhanced the second. Oscilloscope tracings of the current–time (i–t) curves for individual drops at this temperature indicated a mixture of kinetic and diffusion control for the first wave in the region $1.2 \leqq pH \leqq 2.0$, but complete diffusion control (essentially a $t^{\frac{1}{6}}$ profile over most of the drop) for the second; however, when the second wave was not present ($pH < 1.2$) the first wave exhibited diffusion control also.

A solution of $pH > 1$ which produced a ratio of the second wave height to the first of about 3:2 was polarographed at 50°, 39°, 30°, 9°, and 0°C to determine the temperature coefficient of the two limiting currents. The results indicated that the charge transfer process corresponding to the first of the two waves displayed increasingly more diffusion control on going to lower temperatures, while the second appeared controlled by diffusion over the entire range of temperature investigated.

In a separate study carried out at 0°C, solutions containing 1.0 m*M* Bi(III) dissolved in 1.0 *M* (H, Na)ClO_4 produced i–t curves characteristic of diffusion control for both waves from pH 0 to 2. To simplify comparison of these results, plots of the fractional change in the d.c. limiting currents with change in acidity are shown as Curves C and D of Fig. 1. Beyond pH 2 the current of wave I continued to diminish, and was eventually followed by precipitation which began about pH 3. Because even at 0°C loss of diffusion control became evident about pH 2, measurements were confined to $0 \leqslant pH \leqslant 2$. Table 1 lists the corresponding corrected experimental currents, and it is clear that the sum of the two waves gradually diminishes, declining to

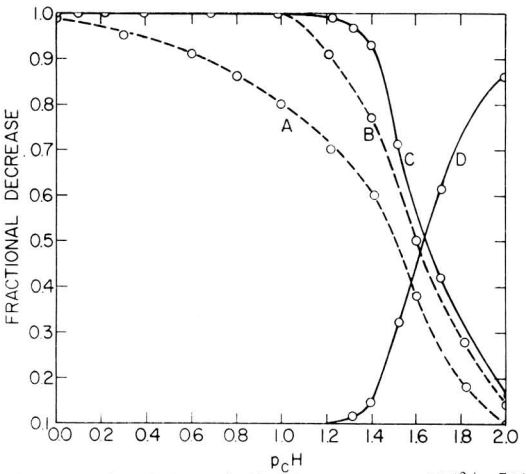

Fig. 1. Fractional change in limiting currents and Bi^{3+}_{aquo}, $[Bi^{3+}_{aquo} + BiOH^{2+}]$ as a function of pH (total Bi = 1.0 m*M*, 1.0 *M* (Na, H)ClO_4, $T = 0°C$): (A) fraction of total Bi as Bi^{3+}_{aquo}, calcd. from Olin[14], (B) fraction of total Bi as $[Bi^{3+}_{aquo} + BiOH^{2+}]$, calcd. from Olin[14], (C) fractional decrease in limiting current of Wave I, (D) fractional increase in limiting current of Wave II.

TABLE 1

POLAROGRAPHIC D.C. CURRENTS *vs.* pH FOR REDUCTION OF 1.0 m*M* Bi(III) IN 1.0 *M* (Na,H)ClO_4 ($T = 0° \pm 0.2°C$)

pH	$i_{corrected}/\mu A$ *d.c., (wave I)*	$i_{corrected}/\mu A$ *d.c., (wave II)*
0	7.93	0.00
0.1	7.86	0.00
0.22	7.85	0.00
0.39	7.83	0.00
0.70	7.85	0.00
0.99	7.82	0.00
1.23	7.76	0.00
1.32	7.64	0.11
1.40	7.30	0.60
1.52	5.55	2.02
1.71	3.26	3.86
2.01	1.26	5.39

approximately 80% of its original value at pH 2.5.

Curves A and B of Fig. 1 are plots of $[Bi^3_{aquo}]$ and $[Bi^3_{aquo}] + [Bi(OH)^2]$ *vs.* pH which were constructed from Olin's 25° data for 1.0 m*M* metal. Despite the slight difference in temperature (25°C *vs.* 30°C), Curves B and C were found to track each other closely, except for some deviation between pH 1 and 1.4. This parallelism is viewed as a strong indication that the first wave reflects mixed reduction of *both* the aquo and the monohydroxy Bi(III). That the two curves are not exactly superimposed probably reflects combined errors in the current–voltage and/or potentiometric results, as well as the temperature difference. Above pH 1 these two monomeric ions

exist in equilibrium with the hexamer, which in their study Losev and Gorodetskii[17] assigned to the second wave.

A clue to the coupled involvement of the hexamer above pH 1 lay in the asymmetry of the reaction given in eqn. (2). A shift of the equilibrium species distribution along the pH axis is predicted if the total solution metal ion concentration, C_M, is changed. For the overall equilibrium

$$n\mathrm{M}^{3+} + 2\,n\mathrm{H_2O} = \mathrm{M}_n(\mathrm{OH})_{2n}^{n+} + 2\,n\mathrm{H}^+ \tag{3}$$

where M^{3+} designates the sum of all monomeric Bi(III) species, it is easily shown that

$$2n\ \mathrm{pH} = -\log K + \log [\mathrm{M}_n(\mathrm{OH})_{2n}^{n+}] - n \log [\mathrm{M}^{3+}]. \tag{4}$$

Since,

$$[\mathrm{M}_n(\mathrm{OH})_{2n}^{n+}] = [\mathrm{M}^{3+}], \quad \text{when} \quad [\mathrm{M}^{3+}] = \frac{1}{(n+1)} \cdot C_M \tag{5}$$

then,

$$\mathrm{pH} = \frac{1}{2n} \log K + \frac{(n-1)}{2n} \log (n+1) + \frac{(n-1)}{2n} \log C_M\ ; \tag{6}$$

and for two values of C_M,

$$\Delta\mathrm{pH} = -\frac{(n-1)}{2n} \log \frac{C_{M(2)}}{C_{M(1)}} \tag{7}$$

For a ten-fold increase in C_M, the calculated equilibrium distribution at $[\mathrm{M}^{3+}] = (n+1)^{-1}$. C_M for the system $[\mathrm{M}^{3+}] - [\mathrm{M}_n(\mathrm{OH})_{2n}^{n+}]$ *vs.* pH will be displaced by -0.43, -0.42, -0.38, -0.33 pH units for $n = 7$, 6, 5, and 4. Figure 2 shows the

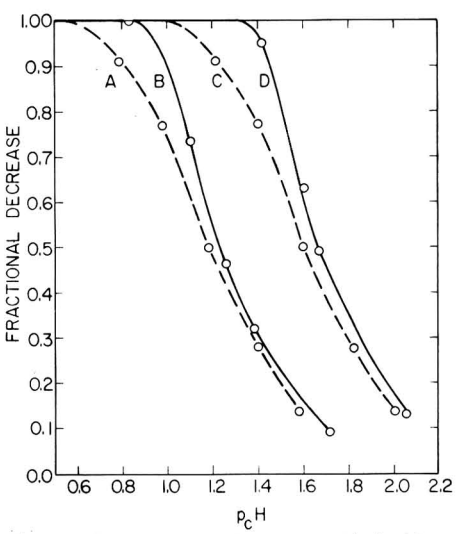

Fig. 2. Shift in pH plots of polarographic limiting currents and $[\mathrm{Bi}^{3+}_{aquo} + \mathrm{BiOH}^{2+}]$ for ten-fold decrease in total bismuth concn. (1.0 *M* (Na, H)$\mathrm{ClO_4}$, $T = 0°\mathrm{C}$): (A) decrease of $[\mathrm{Bi}^{3+}_{aquo} + \mathrm{BiOH}^{2+}]$ from Olin[14] ($C_{Bi} = 10.0$ m*M*), (B) decrease of first-wave current ($C_{Bi} = 10.0$ m*M*), (C) decrease of $[\mathrm{Bi}^{3+}_{aquo} + \mathrm{BiOH}^{2+}]$ from Olin[14] ($C_{Bi} = 1.0$ m*M*), (D) decrease of first-wave current ($C_{Bi} = 1.0$ m*M*).

effect of raising the pH on the quantity $[M^{3+}] = [Bi^{3+}_{aquo}] + [Bi(OH)^{2+}]$ as calculated from the Olin data for 1.0 m*M* and 10.0 m*M* total bismuth, as well as the corresponding effect on the limiting current of the first polarographic wave in 1.0 *M* $(Na,H)ClO_4$ over identical limits of total bismuth concentration. The agreement of the measured shift, -0.42 ± 0.02 pH, with the calculated value for $n=6$ is good.

Assuming that the first wave is a function of the bulk concentration sum of the aquo and monohydroxy Bi(III), the question arose as to whether the charge transfer actually occurs *via* one species in rapid equilibrium with the other, or by two species reduced at potentials not sufficiently separated to be resolved into two steps. Also with regard to the second wave, it seemed extremely doubtful to assume, as did Losev and Gorodetskii, that the hexamer is directly responsible for the second step, as this would require the improbable, virtually simultaneous transfer of 18 electrons. A more acceptable proposal from a mechanistic standpoint would implicate a structually simpler, easily reduced species in rapid equilibrium with the hexameric ion.

Effect of pH on the bromide-catalyzed a.c. polarographic reduction of Bi(III)

It has been known for some time that bismuth reduction at the DME is quite sensitive to acceleration by halides present in solution[20]. The effect of bromide which is shown in Figs. 3 and 4 was used in the present study as an aid to interpreting the

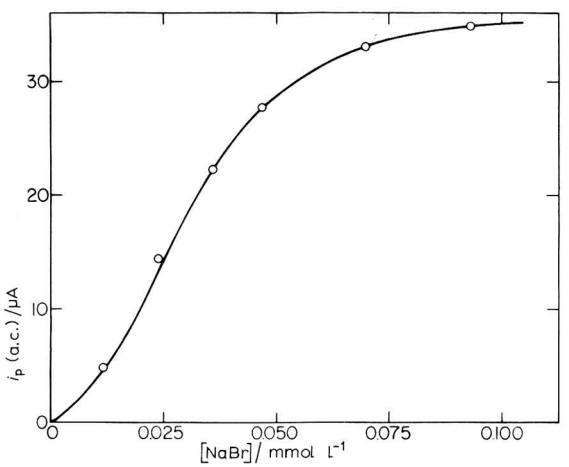

Fig. 3. Variation of a.c. peak current with bromide concn. for reduction of 1.0 m*M* Bi(III) in 1.0 *M* (Na, H)-ClO_4; $T=30°C$. a.c. signal: 5.0 mV (r.m.s.) at 50 Hz.

behavior of the first wave. Alternating current polarography was employed, as this technique is well known to be responsive only to fast or "reversible" charge transfer processes. Figure 3 records the rate-sensitive a.c. current produced by addition of varying small (micromolar) amounts of Br^- to a *constant* 1.0 m*M* concentration of Bi(III) in 1.0 *M* $HClO_4$ (30°C), while the a.c. currents which resulted from varying the Bi(III) concentration at 0°C in 1.0 *M* $HClO_4$ containing *constant* 0.16 m*M* Br^- are summarized in Fig. 4, along with the corresponding d.c. current–concentration plot.

In the following experiments in which *i* (a.c.) and *i* (d.c.) are correlated to bulk

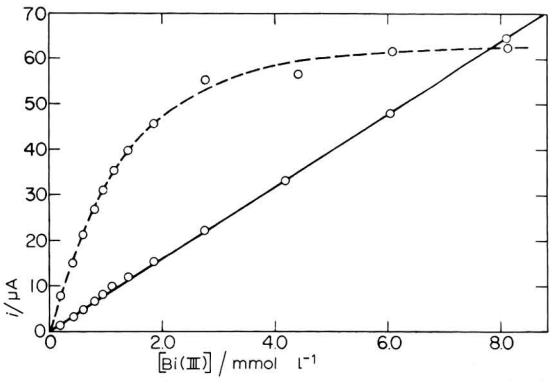

Fig. 4. Variation of a.c. and d.c. current with increase in Bi(III) concn. at constant 0.16 m*M* NaBr and 1.0 *M* (Na, H)ClO_4; $T = 0°C$. (- - -) a.c. current, (———) d.c. current .

Bi(III) concentration it was desirable to avoid as much as possible a shift toward bulk metal–halide complexation, and for this reason solution conditions were chosen for maximum bismuth and minimum bromide concentrations.

A series of polarograms were recorded for solutions containing 1.0 m*M* metal at various adjusted pH values. After recording the d.c. polarogram, the solution was adjusted to 0.06 m*M* in NaBr and the run repeated; an a.c. polarogram was then recorded immediately thereafter. Because the experiments were done at 0°C and 30°C, at both 1.0 *M* and 3.0 *M* perchlorate, it was necessary as a precautionary measure to construct a working *i vs.* [Bi(III)] calibration curve for each individual set of conditions in order to relate the experimental a.c. or d.c. current to the actual known total concentration of the electroactive species. Slight curvature was noted in the *i* (a.c.) *vs.* [Bi(III)] plot, but the degree of curvature was found to be independent of changes in either electrolyte concentration or temperature, and it was also verified that the curvature did not arise from a nonlinear instrument response. The fractional decrease in concentration of the electroactive species with increasing pH was then determined from these calibration curves. The observed currents for these runs are listed in Table 2. It may be seen by comparing the limiting d.c. current in the presence and absence of Br^- that the halide appears to have an essentially negligible effect. However, the substantial positive shift in $E_{\frac{1}{2}}$ and improved reversibility ($n = 3$ electrons) which occurred for the first wave in bromide are significant. This effect was pronounced in the a.c. behavior, with a well-defined a.c. peak appearing in the presence of Br^- while none at all was observed in the absence of this anion. Table 3 lists both the d.c. half-wave potentials and corresponding $E_{\frac{3}{4}} - E_{\frac{1}{4}}$ ("ΔE") values for each set of conditions.

The effect of raising the pH on both the d.c. step and a.c. peak height for the Br^- catalyzed reduction is depicted in Fig. 5. These results were obtained at 30°C in 3.0 *M* perchlorate media at constant 0.16 m*M* Br^- to enable some comparison with the Olin data taken at 25°C at the same perchlorate concentration. Olin's findings are reflected in plots of $[Bi^{3+}]$ and $[Bi^{3+}] + [Bi(OH)^{2+}]$, also shown in Fig. 5. Comparison of the polarographic data with these calculated values indicated that the a.c. current (Fig. 5, Curve A) produced in the presence of bromide arose from catalysis of the Bi^{3+}_{aquo} reduction process only. There thus appeared the prospect of obtaining

TABLE 2

VARIATION OF D.C. DIFFUSION CURRENT WITH pH AT 0° AND 30°C (REDUCTION OF 1.0 m*M* Bi(III) IN 3.0 *M* (Na,H)ClO_4 CONTAINING 0.06 m*M* Br^-)

T	*pH*	*Wave I*		*Wave II*	
		$i_d(no\ Br^-)/\mu A$	$i_d(Br^-)/\mu A$	$i_d(no\ Br^-)/\mu A$	$i_d(Br^-)/\mu A$
0°C	0.0	7.08	7.10	0.0	0.0
	0.08	7.08	7.08	0.0	0.0
	0.21	7.04	7.04	0.0	0.0
	0.38	7.04	7.06	0.0	0.0
	0.99	7.00	6.90	0.0	0.0
	1.08	6.97	6.90	0.0	0.0
	1.21	6.85	6.80	0.0	0.0
	1.38	5.53	5.64	1.24	1.04
	1.51	3.91	4.11	2.56	2.40
	1.69	2.13	2.31	3.91	3.75
	1.99	0.91	1.02	4.73	4.66
30°C	0.0	11.7	11.7	0.0	0.0
	0.11	11.7	11.6	0.0	0.0
	0.23	11.7	11.6	0.0	0.0
	0.41	11.7	11.6	0.0	0.0
	0.71	11.7	11.6	0.0	0.0
	1.01	11.7	11.6	0.0	0.0
	1.14	11.8	11.7	0.0	0.0
	1.27	10.8	10.9	0.72	0.50
	1.47	8.82	9.10	2.02	1.26
	1.75	5.13	5.50	4.95	4.41
	2.02	2.61	2.92	7.30	6.65

TABLE 3

pH VARIATION OF $E_{\frac{1}{2}}$ AND ΔE FOR REDUCTION OF 1.0 m*M* Bi(III) CATALYZED BY 0.16 m*M* Br^-

pH	1.0 *M* (*Na,H*)ClO_4				3.0 *M* (*Na,H*)ClO_4			
	$T=0°C$		$T=30°C$		$T=0°C$		$T=30°C$	
	$E_{\frac{1}{2}}/V$	$\Delta E/mV$	$E_{\frac{1}{2}}/V$	$\Delta E/mV$	$E_{\frac{1}{2}}/V$	$\Delta E/mV$	$E_{\frac{1}{2}}/V$	$\Delta E/mV$
0.0	−.060	−54	−.010	−53	−.021	−41	+.036	−40
0.25	−.056	−52	−.006	−52	−.020	−43	+.036	−41
0.50	−.050	−47	−.001	−49	−.020	−41	+.036	−41
0.75	−.046	−43	+.003	−45	−.024	−43	+.031	−43
1.0	−.039	−40	+.007	−42	−.020	−42	+.033	−40
1.2	−.039	−37	+.002	−40	−.024	−39	+.028	−42
1.4	−.035	−37	−.002	−43	−.019	−38	+.022	−43
1.6	−.031	−34	−.004	−42	−.016	−36	+.019	−43
1.8	−.029	−37	−.007	−42	−.016	−37	+.009	−43
2.0	−.027	−37	−.011	−42	−.016	−37	+.003	−42

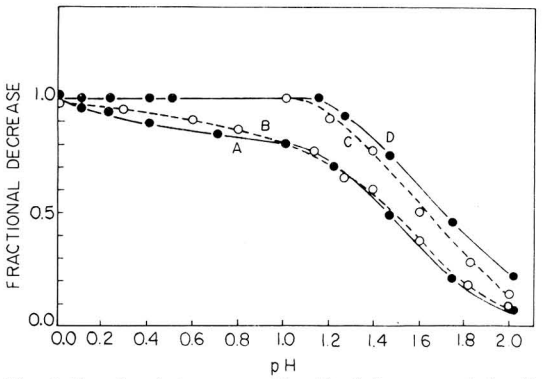

Fig. 5. Fractional decrease with pH of the a.c. and d.c. Br^--catalyzed currents at 30°C together with decrease in Bi^{3+}_{aquo} and $[Bi^{3+}_{aquo} + BiOH^{2+}]$ (from Olin[14]) (1.0 m*M* Bi(III), 3.0 *M* (Na,H)ClO_4, 0.16 m*M* NaBr): (A) a.c. peak current, (B) fraction of total bismuth as Bi^{3+}_{aquo}, (C) fraction of total bismuth as $[Bi^{3+}_{aquo} + BiOH^{2+}]$, (D) d.c. current of first wave.

an indirect experimental estimate of the equilibrium concentration of $Bi(OH)^{2+}$ from the differences in the calibrated d.c. data which yield $[Bi^{3+}_{aquo}] + [Bi(OH)^{2+}]$, and the calibrated a.c. currents which were taken to be proportional to $[Bi^{3+}_{aquo}]$ only. This would require that the rate of interconversion between the aquo and monohydroxy bismuth species must be slower than the Br^--catalyzed rate of Bi^{3+}_{aquo} reduction at the electrode surface.

Kinetic nature of the first d.c. wave

In the pH range corresponding to development of the second wave, the concentration of $Bi(OH)^{2+}$ obtained from the difference between plots of the catalyzed a.c. and d.c. data taken at 30°C (Fig. 5) is considerably larger than Olin's figures would predict. Subsequent data taken at 0°C in 3.0 *M* (Na,H)ClO_4 (see Fig. 6) gave currents which were entirely diffusion controlled, and under these conditions the difference between the a.c. and d.c. plots (fractional concentration of $BiOH^{2+}$) is much smaller; upon lowering the temperature from 30°C to 0°C the a.c. currents

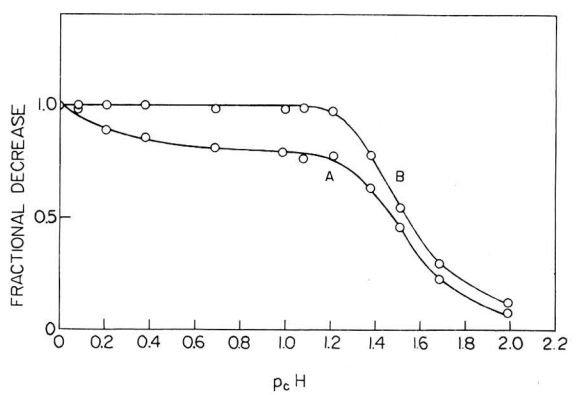

Fig. 6. Fractional decrease with pH of the a.c. and d.c. Br^--catalyzed currents at 0°C [1.0 m*M* Bi(III), 3.0 *M* (Na, H)ClO_4, 0.16 m*M* NaBr]: (A) a.c. peak current, (B) d.c. current of first wave.

remained relatively unchanged, while the d.c. values were significantly lowered. Exactly the same behavior was found using solutions adjusted to one molar in total perchlorate.

Using the differences between the pairs of a.c.–d.c. current plots of both Figs. 5 and 6 and normalizing these *via* the corresponding calibration curves (*vide supra*) to correspond to fractional concentration of Bi(III) present as kinetically reduced $Bi(OH)^{2+}$, a profile of the current *differences* was constructed which appears as Curve B in Fig. 7. As $Bi(OH)^{2+}$ at the electrode surface is depleted in concentration during

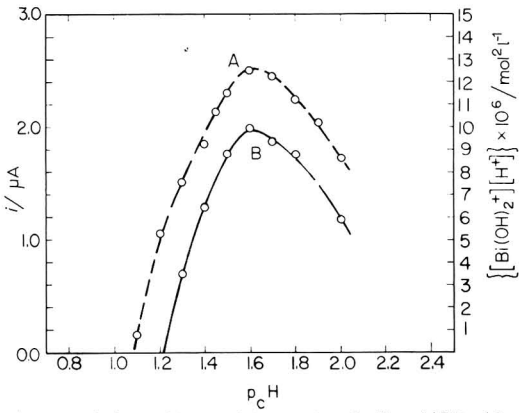

Fig. 7. Variation with pH of the product $[Bi(OH)_2^+][H^+]$ calcd. from Olin[14] (Curve A), together with variation in the kinetic current contribution to the first wave at 30°C calcd. from differences in the a.c.–d.c. data of Figs. 5 and 6 (Curve B).

the course of reduction, more may be formed from either of two possible precursor reactions:

$$Bi_6(OH)_{12}^{6+} + 6\,H^+ \rightarrow 6\,BiOH^{2+} + H_2O \tag{8}$$

$$Bi(OH)_2^+ + H^+ \rightarrow BiOH^{2+} + H_2O \tag{9}$$

The calculated product $[Bi(OH)_2^+][H^+]$ which should be proportional to the formation rate of $BiOH^{2+}$ (eqn. (9)) is depicted as Curve A in Fig. 7. While Curve B should be viewed with caution due to the built-in uncertainty of taking differences of differences, the excellent variational agreement of the polarographic data with variation in $[Bi(OH)_2^+][H^+]$ rather than with the monotonically decreasing product $[Bi_6(OH)_{12}^{6+}][H^+]^6$ predicted from eqn. (8) indicates that, at 30°C, the $BiOH^{2+}$ kinetic current contribution to Wave I above pH 1.0 arises from a rate controlling slow dissociation of intermediate $Bi(OH)_2^+$ at the electrode surface. This would require that interconversion between the monohydroxy Bi(III) and the dihydroxy species be of the order of the reduction rate of $BiOH^{2+}$ itself.

The presence of intermediate $Bi(OH)_2^+$ which is directly implied by the Fig. 7 plot is interesting from another standpoint, as it strengthens Goward's original suggestion that the second wave of the doublet probably originates from direct charge transfer to $Bi(OH)_2^+$, in rapid exchange with the larger hexameric cation, rather than direct charge transfer to the hexamer itself as postulated by Losev and Gorodetskii[17].

The effect of pH on $E_{\frac{1}{2}}$

The sensitivity of the bismuth $E_{\frac{1}{2}}$ to variation in electrolyte composition is quite pronounced. This has led to the appearance in the literature of numerous, often conflicting $E_{\frac{1}{2}}$ values for reduction from non-complexing media, including perchlorates. Our desire at this stage was to obtain a preliminary but accurate picture of the pH dependence of $E_{\frac{1}{2}}$ at different levels of inert salt concentration and at several different temperatures. Initial results obtained at 0°C and 30°C using 1.0 *M* and 3.0 *M* mixtures of $HClO_4$–$NaClO_4$ are plotted in Fig. 8. The measured $E_{\frac{1}{2}}$'s and corresponding ΔE values appear in Table 3.

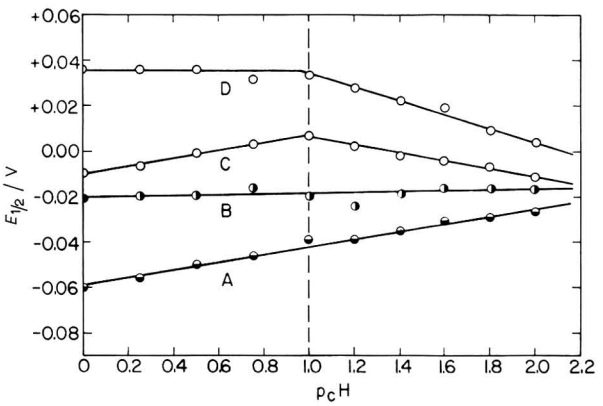

Fig. 8. pH Variation of $E_{\frac{1}{2}}$ for the first bismuth wave in (Na, H)ClO_4. 1.0 m*M* Bi(III) + (A) 1.0 *M* (Na,H)-ClO_4, $T=0°C$; (B) 3.0 *M* (Na,H)ClO_4, $T=0°C$; (C) 1.0 *M* (Na,H)ClO_4, $T=30°C$; (D) 3.0 *M* (Na,H)ClO_4, $T=30°C$.

A prominent feature which is common to all four curves in Fig. 8 is the uniform linear change of $E_{\frac{1}{2}}$ with pH, which displays either positive, zero, or negative slope depending on the particular set of experimental conditions.

At 0°C the change in $E_{\frac{1}{2}}$ is linear over the entire pH range studied. In 1.0 *M* (Na,H)ClO_4 the linear shift is toward a more positive potential with a slope of +17 mV/pH unit, while at 3.0 *M* (Na,H)ClO_4, $E_{\frac{1}{2}}$ remains virtually constant and Curve B displays zero slope (actually 1 mV/pH unit from a least-squares fit).

At 30°C, on the other hand, the trend in results is more complex. Aside from the fact that reduction in this case occurs at generally more positive potentials, a sharp change in slope is observed for both curves at pH 1. Up to this pH log ($[BiOH^{2+}]/[Bi^{3+}_{aquo}]$) increases linearly. For the metal concentration used in these experiments (1×10^{-3} *M*), the sharp break in Curves C and D exactly coincides with an abrupt leveling off in log ($[BiOH^{2+}]/[Bi^{3+}_{aquo}]$) from pH 1 to 2. The invariance of the log ratio in this range is probably due to a "buffering" of these two species during formation of the highly ordered hexamer.

The 17 mV/pH positive shift for the 1.0 *M* perchlorate curves in the range $0 \leqq pH \leqq 1$ at both temperatures is puzzling, as ordinarily no shift would be expected for reduction of Bi^{3+}_{aquo}, which is predicted to be the predominant species at low pH

(at pH 1.0, $BiOH^{2+}$ reaches 20%, remains constant to pH 1.6, then rises to 35% of C_M at pH 2.0); and the effect is opposite the negative trend which one would associate with direct reduction of, for example, a hydroxylated ion such as $BiOH^{2+}$. Significantly, the factors which promote the positive trend at 1.0 *M* $HClO_4$ appear inoperative in the 3.0 *M* electrolyte range, as evidenced by the zero slopes of Curves B and D in the region $0 \leqq pH \leqq 1.0$. Alternatively, if one directs attention to the pair of 3.0 *M* lines (Curves B and D), then a step reduction in ionic strength to 1.0 *M* perchlorate generates a corresponding pair of curves displaced approximately 50 mV negative in potential and rotated counter-clockwise through an angle $\theta = \tan^{-1} 0.017 = 0.97$ degrees. Upon accounting for this angular displacement, the resulting slope of Curve C beyond pH 1 closely agrees with the -29 mV/pH slope of Curve D, and the morphology of the two pairs of curves (AC and BD) in the range $0 \leqq pH \leqq 2$ is then essentially the same.

Figure 8 and the corresponding numerical data of Table 3 conclusively establish that the bismuth $E_{\frac{1}{2}}$ is indeed dependent upon the pH of the solution and serve to invalidate earlier contentions that observed slight variations of this potential with acidity are inconsequential and primarily attributable to combined changes in such factors as junction potential, activity coefficients, or viscosity—though it is recognized that these may exert a second-order effect.

Our results thus far are too preliminary to explain with any satisfaction the positive shift of $E_{\frac{1}{2}}$ within the range $0 \leqq pH \leqq 1$. The same can be said for the effect of salt in diminishing the overpotential. However, in the latter case both theory and experience[12] would suggest that, since cationic Bi(III) reduces quite positive to the potential of zero charge, a contributing factor toward increasing the overall charge transfer rate (decreased overpotential) could be the negative shift in the value of the outer Helmholtz plane potential, ϕ_2, due to a normal double layer salt effect coupled with adsorption of perchlorate.

Additional work is in progress on the reduction of bismuth the results of which will appear in a separate paper.

ACKNOWLEDGEMENT

This research was supported in part by The National Science Foundation (Grant No. GP-7255) and the Research Corporation.

SUMMARY

A preliminary study has been made of the pH dependence of the polarographic limiting current and half-wave potential for reduction of Bi(III) from constant 1.0 *M* and 3.0 *M* perchlorate media at both 0°C and 30°C. Interpretation of these results in the light of Olin's earlier potentiometric study of bismuth hydrolysis strongly suggests that, at intermediate acid pH the first wave of the Bi(III) doublet probably arises from mixed reduction of Bi^{3+}_{aquo} and $BiOH^{2+}$. The results further show that the Bi(III) reduction overpotential is decreased by about 57 mV on increasing the ionic strength to 3.0 *M* $(Na, H)ClO_4$ and that the change in $E_{\frac{1}{2}}$ with acidity is linear with pH and not primarily attributable to secondary changes in viscosity, junction potentials or activity effects as suggested by several previous authors.

REFERENCES

1 J. J. LINGANE, *Ind. Eng. Chem., Anal. Ed.*, 15 (1943) 583.
2 A. A. MOUSSA AND H. M. SAMMOUR, *J. Chem. Soc.*, (1960) 2151.
3 J. E. B. RANDLES AND K. W. SOMERTON, *Trans. Faraday Soc.*, 48 (1952) 951.
4 B. BREYER, F. GUTMAN AND S. HACOBIAN, *Australian J. Sci. Res.*, A4 (1951) 595.
5 B. BREYER, F. GUTMAN AND S. HACOBIAN, *Australian J. Sci. Res.*, A3 (1950) 567.
6 H. H. BAUER AND P. J. ELVING, *Electrochim. Acta*, 2 (1960) 240.
7 R. LEVINE, Ph.D. Thesis, Syracuse University, 1964.
8 F. GRANÉR AND L. G. SILLÉN, *Acta Chem. Scand.*, 1 (1947) 631.
9 P. SOUCHAY AND D. PESCHANSKI, *Bull. Soc. Chim. France*, (1948) 439.
10 R. W. HOLMBERG, K. A. KRAUS AND J. S. JOHNSON, *J. Am. Chem. Soc.*, 78 (1956) 5506.
11 M. D. DONFORTH, H. A. LEVY AND P. A. AGRON, *J. Chem. Phys.*, 31 (1959) 1458.
12 R. S. TOBIAS, *J. Am. Chem. Soc.*, 82 (1960) 1070.
13 V. MARONI AND T. G. SPIRO, *J. Am. Chem. Soc.*, 88 (1966) 1410.
14 A. OLIN, *Acta Chem. Scand.*, 11 (1957) 1445.
15 R. S. TOBIAS AND S. Y. TYREE, JR., *J. Am. Chem. Soc.*, 82 (1960) 3244.
16 G. W. GOWARD, Ph.D. Thesis, Princeton University, 1954.
17 V. V. LOSEV AND V. V. GORODETSKII, *Zh. Fiz. Khim.*, 37 (1963) 842.
18 E. D. MOORHEAD, *J. Am. Chem. Soc.*, 87 (1965) 2503.
19 E. D. MOORHEAD AND G. M. FRAME II, *Anal. Chem.*, 37 (1965) 203.
20 I. M. KOLTHOFF AND J. J. LINGANE, *Polarography*, Vol. 2, Interscience, New York, 1952.
21 F. J. WELCHER, *The Analytical Uses of Ethylenediaminetetraacetic Acid*, D. Von Nostrand Co., Inc., Princeton, N.J. p. 207.
22 P. DELAHAY, *Double Layer and Electrode Kinetics*, Interscience, New York, 1965, p. 42.

ELECTROANALYTICAL CHEMISTRY AND INTERFACIAL ELECTROCHEMISTRY
Elsevier Sequoia S.A., Lausanne – Printed in The Netherlands

POLAROGRAPHISCHES VERHALTEN VON ALIZARIN UND ALIZARIN S UND DIE BILDUNG VON AL-KOMPLEXEN IN METHANOLISCHER LÖSUNG

J. M. ABD EL KADER*, A. M. SHAMS EL DIN*, B. KASTENING** UND L. HOLLECK
Chemisches Institut der Hochschule Bamberg (Deutschland)
(Eingegangen am 9. Juli 1969; revisioniert am 2. Januar 1970)

Kürzlich haben wir über das polarographische Verhalten von Solochrom-Violett RS und dessen Komplexbildung mit Aluminium in wasserfreiem Methanol berichtet[1]. Ein Mechanismus für die Reduktion des Farbstoffes und für seine Komplexbildung mit Aluminium wurde vorgeschlagen und die geeigneten Bedingungen für die hierauf beruhende Möglichkeit der analytischen Bestimmung von Al^{3+} in Methanol angegeben.

Da auch Alizarin (1,2-Dihydroxyanthrachinon) (AZ) und seine Derivate, z.B. Alizarin S (1,2-Dihydroxyanthrachinon-3-sulfonsäure-Natriumsalz) (AZS), mit Al^{3+} gefärbte stabile Komplexe bilden, schien es von Interesse, das Verhalten dieser Verbindungen in Methanol und ihre Eignung als Reagenzien für die polarographische Bestimmung von Al^{3+} in diesem Medium zu untersuchen. Weiterhin erhob sich die Frage nach der Struktur des violett-roten Aluminium–AZ- (bzw. AZS)-Reaktionsproduktes, über das in der Literatur unterschiedliche Ansichten vertreten werden. Einer Auffassung zufolge beruht die Farbe auf einer Adsorptionsverbindung zwischen $Al(OH)_3$ und dem Farbstoff (Alizarin-Lack)[2]. Andere Autoren sind hingegen der Meinung, dass die Färbung durch die Bildung eines regulären Wernerschen Komplexes verursacht wird; unter den Vertretern dieser Ansicht besteht jedoch keine Übereinstimmung in bezug auf die Zusammensetzung des Aluminium–AZ-Komplexes, für die die Verhältnisse $1:1$[3], $1:2$[4,5] und $1:3$[6–8] vorgeschlagen wurden. Über AZ, AZS und ihre Al-Komplexe in Methanol liegen bislang keine Arbeiten vor.

EXPERIMENTELLES

Für die Herstellung von Stammlösungen in absolutem Methanol (E. Merck, p.a.) wurden AZ und AZS (E. Merck, p.a.) ohne weitere Reinigung verwendet. Die Depolarisatoren wurden mit einer Konzentration von 10^{-3} *M* angewendet. Als Leitelektrolyt diente 0.1 *M* LiCl.

Als Protonendonator bzw. -akzeptor wurden Benzoesäure bzw. Tetraäthylammonium-Hydroxid, als Protonenüberträger N,N-Dimethyl-*p*-phenylendiamin verwendet. Eine Stammlösung von 2×10^{-3} *M* $AlCl_3$ wurde durch Auflösen des

* jetzt: National Research Centre, Dokki-Cairo, U.A.R.
** jetzt: Forschungsabteilung Angewandte Elektrochemie, Kernforschungsanlage Jülich G.m.b.H., 517 Jülich.

wasserfreien Salzes in Methanol hergestellt.

Die Arbeitsweise bei Aufnahme der polarographischen Stromspannungskurven wurde in einer vorhergehenden Arbeit beschrieben[1]. Entlüftung der Lösungen erfolgte durch 10-minütiges Durchleiten von reinem Stickstoff. Die Untersuchungen wurden bei Raumtemperatur von 18 bis 21°C durchgeführt; Potentialangaben beziehen sich auf die (wässrige) gesättigte Kalomelelektrode (GKE).

ERGEBNISSE UND DISKUSSION

A. Verhalten von Alizarin

Die polarographische Reduktion von AZ in wasserfreiem Methanol erfolgt in zwei Stufen mit $E_{\frac{1}{2}} = -0.63$ bzw. -0.84 V (GKE), wobei die erste Stufe etwas höher ist als die zweite, vergl. Kurve 0 in Abb. 1. Nach der Abhängigkeit der Stufenhöhen von der effektiven Hg-Niveauhöhe sind beide Stufen diffusionsbestimmt. Die Gesamthöhe ist nahezu gleich der Hälfte derjenigen einer gleich konzentrierten Lösung von Azoxybenzol[9] oder Solochrom-Violett RS[1] unter ähnlichen Bedingungen Bei Annahme vergleichbarer Diffusionskoeffizienten für alle Verbindungen ergibt sich hieraus, dass die Zahl der bei der Reduktion von AZ übertragenen Elektronen halb so gross ist wie für die zum Vergleich herangezogenen Verbindungen, d.h. $z = 2$.

Wie aus dem weiter unten geschilderten polarographischen Verhalten der Aluminium-Komplexe gefolgert werden kann, führt die Reduktion von AZ (und ebenso bei AZS) nicht, wie in wässrigen Lösungen angenommen wird, zum Anthrachinol (I)[10,11], sondern zum entsprechenden Oxanthron (II)[12]. Dass die Carbonylgruppe in letzterem keiner weiteren Reduktion unterliegt, ist auf die Wasserstoff-Brückenbindung mit der benachbarten α-Hydroxy-Gruppe zurückzuführen (vgl. ref. 13).

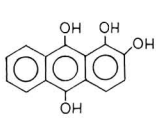

(I)

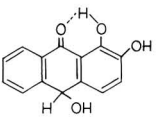

(II)

Nimmt man an, dass die Reduktion auch beim Potential der ersten Stufe über zwei Elektronen erfolgt, so erklärt sich die beschränkte Höhe der ersten Stufe am einfachsten dadurch, dass nur ein Teil der Moleküle der Reduktion unterliegt, während der andere Teil hierfür lediglich Protonen aus den Hydroxy-Gruppen zur Verfügung stellt und damit selbst bei diesem Potential inaktiv wird:

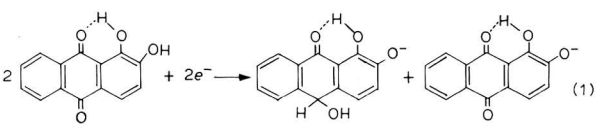

(1)

Die Vorverlagerung eines Teils der Reduktionsstufen durch die Wirkung von im Depolarisatormolekül selbst enthaltenen saueren Gruppen wurde mit anderen

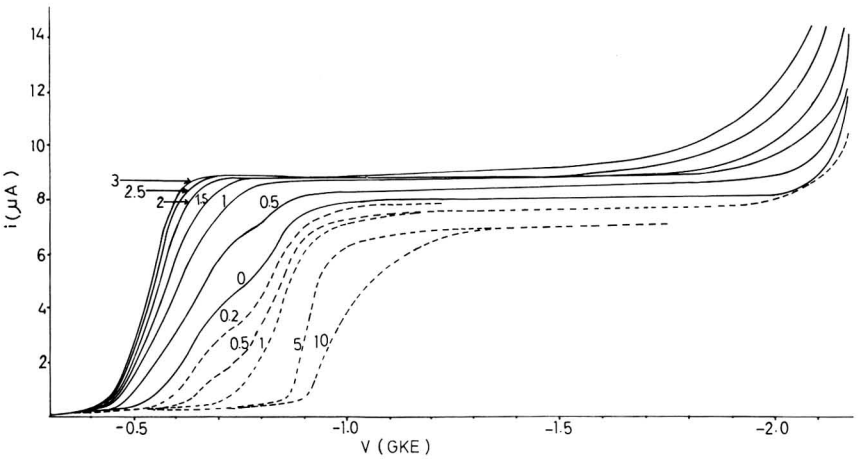

Abb. 1. Polarographische Kurven von Alizarin (10^{-3} *M*) in wasserfreiem Methanol mit 0.1 *M* LiCl als Leitelektrolyt. Zahlen an den Kurven geben den Gehalt an Benzoesäure (———) bzw. $N(C_2H_5)_4OH$ (----) in 10^{-3} *M* an.

Depolarisatoren in Methanol auch früher schon beobachtet[14,15]. Das in Reaktion (1) gebildete Anion des Depolarisators wird dann erst in der zweiten Stufe reduziert, sei es unter Reduktion der Gesamtheit der antransportierten Moleküle zum Dianion (wobei wegen Aufhebung der Wasserstoffbrückenbindung der zweiten CO-Gruppe dann auch Reduktion zum Anthrachinol denkbar ist), sei es unter Beteiligung von Protonen des Lösungsmittels, die weniger leicht verfügbar sind als diejenigen der OH-Gruppen des Depolarisators.

Dass die erste Stufe etwas höher ist als die Hälfte der Gesamtstufe, mag darauf beruhen, dass auch hier schon eine kinetisch begrenzte Bereitstellung von Solvens-Protonen erfolgt; der kinetische Charakter dieses Anteils kommt in der Hg-Niveau-Abhängigkeit nicht zum Ausdruck, da er nur einen Bruchteil der gesamten Höhe der ersten Stufe ausmacht.

Im Einklang mit dieser Vorstellung steht die Auffüllung der Höhe der ersten Stufe bei Zusatz von Benzoesäure (Abb. 1): bei einem Äquivalent Benzoesäure erfolgt die Gesamtreduktion in einer Stufe etwa im Bereich des Potentials der vorher ersten Stufe:

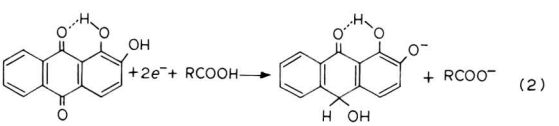

(2)

Dass diese Stufe überwiegend etwas positiver liegt als die ursprünglich erste Stufe, dürfte auf der grösseren Acidität von Benzoesäure gegenüber dem bei Reaktion (1) als Protonendonator wirksamen Depolarisator beruhen; die weitere Vorverlagerung bei höherer Benzoesäure-Konzentration kann auf die dann mögliche Bildung des undissoziierten Reduktionsprodukts bei Mitwirkung von zwei Molekülen Benzoesäure zurückgeführt werden.

Auch das Verhalten beim Zusatz einer Base(Tetraäthylammonium-Hydroxid;

gestrichelte Kurven der Abb. 1) steht mit den genannten Annahmen im Einklang. Zusatz eines Äquivalents Base überführt den Depolarisator in sein Anion und die Reduktion erfolgt daher praktisch vollkommen beim Potential der ursprünglich zweiten Stufe. Die weitere Verschiebung der Gesamtreduktion zu negativeren Potentialen bei höherer Basekonzentration kann auf dadurch erzwungener weiterer Dissoziation des Depolarisators zum Dianion beruhen.

Eine andere Erklärung für das Auftreten zweier Stufen in Abwesenheit von Säure und Base, nämlich die teilweise Dissoziation des Depolarisators, kann ausgeschlossen werden. Zum einen ist ein so stark sauerer Charakter der OH-Gruppen, dass er in Methanol zu merklicher Dissoziation führt, kaum wahrscheinlich. Zum zweiten würde das Auftreten diffusionsbestimmter Stufen mit der Reduktion des undissoziierten Moleküls in der ersten, des Anions in der zweiten Stufe ein vollkommen immobiles Dissoziations-Gleichgewicht voraussetzen. Zum dritten entstünde bei der Dissoziation eine entsprechende Menge solvatisierter Protonen H^+_{solv}, unter deren Wirkung der undissoziierte Anteil jedoch—wie bei Zusatz von HCl—bei erheblich positiveren Potentialen reduziert werden müsste.

N,N-Dimethyl-*p*-phenylendiamin (DMPD), das sich bei früheren Untersuchungen als wirksamer Katalysator für Protonentransferprozesse erwiesen hatte, hat weder in Abwesenheit noch in Gegenwart von Benzoesäure einen Einfluss auf die Reduktionsstufen von AZ.Hingegen verursacht DMPD in Lösungen mit mehr als einem Äquivalent Säure pro Mol AZ das Auftreten einer katalytischen Wasserstoff-Entwicklung bei -1.4 V (GKE) aus dem Säureüberschuss[16]. Die Höhe der Wasserstoff-Stufe ist proportional der über ein Äquivalent pro Mol AZ hinausgehenden Säurekonzentration; die katalysierte Wasserstoff-Entwicklung ist demnach gegenüber einer über ein Äquivalent hinausgehenden Beteiligung der Säure an der Depolarisator-Reduktion nach Gl. (2) begünstigt.

B. Verhalten von Alizarin S

Das polarographische Verhalten von AZS ist demjenigen von AZ sehr ähnlich. In Abwesenheit von Zusatzstoffen treten jedoch drei Stufen auf. Dies mag auf die Aktivierung auch der zweiten Hydroxylgruppe als Protonendonator infolge der Wirkung der SO_3^--Gruppe in 3-Stellung zurückzuführen sein, durch die Protonenaustausch auch anderer Stöchiometrie als in Gl. (1) möglich wird. Zufolge der Hg-Niveauhöhen-Abhängigkeit erscheinen auch diese drei Stufen diffusionsbestimmt und sind der Lösungskonzentration des Depolarisators proportional. Die Gesamthöhe der AZS-Stufen ist erheblich geringer als diejenige der AZ-Stufen; dies muss auf einen geringeren Diffusionskoeffizienten—vermutlich infolge Solvatation an der Sulfogruppe— zurückgeführt werden. In Gegenwart von einem Äquivalent eines Protonendonators (Benzoesäure) bzw. Protonenakzeptors (Tetraäthylammoniumhydroxid) erfolgt wiederum Reduktion in einer einzelnen Stufe bei positiverem bzw. negativerem Potential. Die Wirkung von DMPD-Zusatz ist wie bei AZ.

C. Die Bildung von Aluminium-Komplexen

Bei Zusatz von Al^{3+} zu AZ- bzw. AZS-Lösungen in Methanol schlägt die Gelb-Orange-Färbung der Lösung sofort in tiefrot um. Die Polarogramme dieser Lösungen, wenige Minuten nach dem Vermischen registriert, bleiben über einen Zeitraum von 24 Stunden unverändert. Es erfolgt demnach sofortige Komplexbildung.

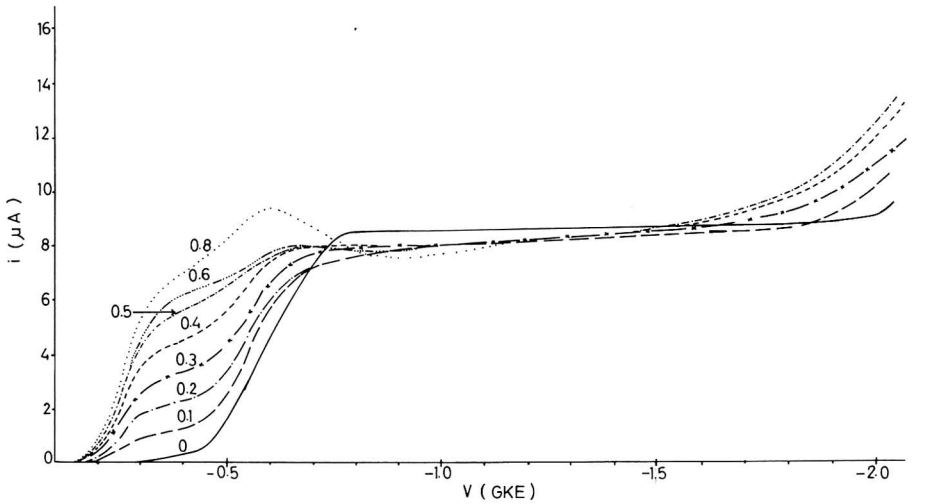

Abb. 2. Polarographische Kurven von 10^{-3} *M* Alizarin ($+10^{-3}$ *M* Benzoesäure) in Methanol bei Gegenwart von Al^{3+} (Zahlen an den Kurven geben den Gehalt an Al^{3+} in 10^{-3} *M* an).

Um die Polarogramme übersichtlicher zu gestalten, wurde bei den folgenden Untersuchungen im allgemeinen ein Äquivalent Benzoesäure pro Mol AZ (bzw. AZS) zugesetzt, sodass für den Komplexbildner nur eine einzelne Reduktionsstufe vorliegt. Zusatz von Al^{3+} verursacht die Ausbildung einer Vorstufe bei um etwa 250 bis 300 mV positiveren Potentialen gegenüber der Hauptstufe des Komplexbildners. Die Gesamthöhe von Vor- und Hauptstufe ist geringfügig niedriger als die Stufe von AZ allein (Abb. 2); die Verringerung ist vermutlich der Verminderung des Diffusionskoeffizienten durch die Komplexbildung zuzuschreiben. Die Ursache der Vorstufe ist offensichtlich die Freisetzung von Protonen bei der Komplexbildung:

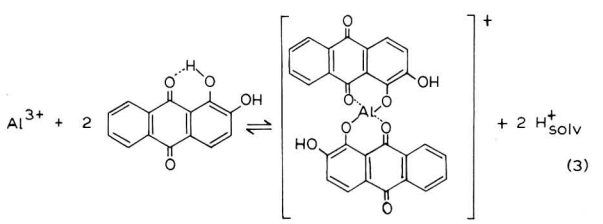

(Zur Begründung für die Formulierung als $AlAZ_2$-Komplex vergl. unten.) Beim gleichen Potential bildet sich eine Vorstufe nämlich auch dann aus, wenn anstelle von Al^{3+} der Lösung HCl zugesetzt wird (Abb. 3). Bis zu gewissen Maximalwerten der Konzentration an Al^{3+} bzw. H^+_{solv} sind die Vorstufenhöhen diesen Konzentrationen proportional, und zwar beträgt die Stufenhöhe in diesem Bereich 5.4 μA/m*M* H^+_{solv} bzw. 10.8 μA/m*M* Al^{3+} (vergl. Abb. 4). Aus diesem Ergebnis kann die Bildung von 2 H^+_{solv} pro komplex gebundenem Al^{3+} und damit Komplexbildung nach Gl. (3) gefolgert werden. Da die Höhe der Vorstufe schliesslich die Höhe der AZ-Stufe allein erreicht und die Gesamthöhe der Reduktionsstufen auch stets diesen Wert besitzt, erfolgt beim Potential der Vorstufe offenbar gleichzeitig die durch Mitwirkung von

H^+_{solv} erleichterte Reduktion sowohl des freien als auch des komplex gebundenen AZ gemäss:

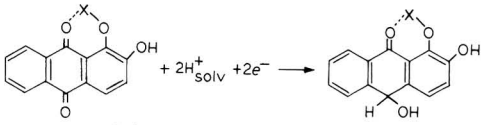

(X = H oder Al)

Da H^+_{solv} eine viel stärkere Säure ist als die OH-Gruppen von AZ bzw. seinem Reduktionsprodukt, wird alles H^+_{solv} aufgezehrt, bevor sich die Protonen der OH-Gruppen an der Reduktion beteiligen könnten. Infolgedessen wird die Höhe der Vorstufe durch die Diffusion von H^+_{solv} bestimmt.

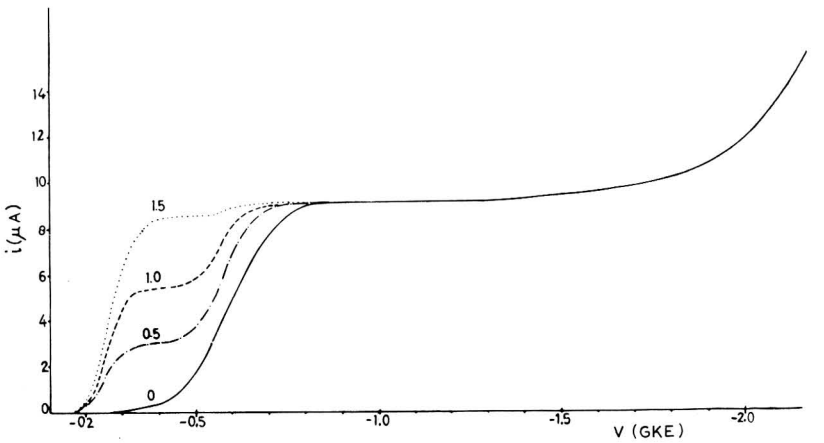

Abb. 3. Polarographische Kurven von 10^{-3} *M* Alizarin ($+10^{-3}$ *M* Benzoesäure) in Methanol bei Zusatz von HCl (Zahlen an den Kurven geben den Gehalt an HCl in 10^{-3} *M* an).

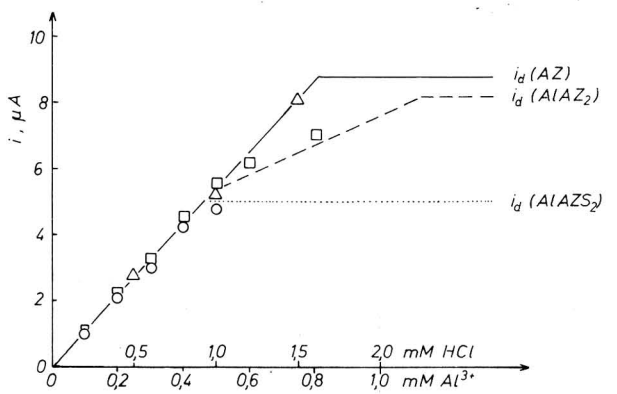

Abb. 4. Grenzstromstärke der Vorstufe von AZ und AZS in Abhängigkeit vom Zusatz von Al^{3+} bzw. HCl. (△) AZ + HCl, (□) AZ + Al^{3+}, (○) AZS + Al^{3+}. Nach dem Text theoretisch erwarteter Verlauf: (———) AZ + HCl, (- - - -) AZ + Al^{3+}, (. . . .) AZS + Al^{3+}.

Während die Höhe der Vorstufe bei Zusatz von HCl nach diesen Vorstellungen ohne weiteres bis zur Gesamthöhe der AZ-Stufe anwachsen kann (danach wird sie durch die Diffusion von AZ bestimmt, bleibt also konstant), sollte sie bei Zusatz von Al^{3+} und Annahme einer ausschliesslichen Bildung des 1:2-Komplexes auch in Gegenwart von überschüssigem Al^{3+} nur bis zur Höhe von 5.4 μA anwachsen können, weil nach Gl. (3) pro Mol AZ maximal 1 Mol H^+_{solv} gebildet werden kann. (Gleiches gilt übrigens auch für die wahrscheinlichste Formulierung der Bildung eines 1:1-Komplexes, so dass dessen Bildung auch bei Überschuss von Al^{3+} das weitere Anwachsen der Vorstufe nicht zu erklären vermag.) Eine plausible Erklärung für das weitere Anwachsen der Vorstufe bei Überschuss von Al^{3+} ist der saure Charakter des nicht komplex gebundenen Al^{3+} gemäss:

$$Al(MeOH)_x^{3+} \rightleftharpoons Al(MeOH)_{x-1}(MeO)^{2+} + H^+_{solv} \tag{5}$$

Unabhängig von der Lage dieses Gleichgewichts ergibt sich die Bereitschaft des freien Al^{3+}-Ions zur Abspaltung eines Protons aus dem Auftreten einer katalytischen Wasserstoff-Stufe in methanolischen Lösungen von Al^{3+} allein, insbesondere bei Gegenwart von DMPD als Katalysator. Aus der Höhe dieser katalytischen Stufe ergibt sich eine Diffusionsstromkonstante von 4.5 μA/mM Al^{3+}; sie ist deutlich niedriger als der Wert von 5.4 μA/mM H^+_{solv}, so dass das Gleichgewicht (5) weitgehend auf der linken Seite liegt. Immerhin vermag die Bereitstellung von Protonen aus dem Gleichgewicht (5) (bzw. eine unmittelbare Protonendonatorwirkung von Al^{3+}) eine Erhöhung der Vorstufe über die infolge Freisetzung von Protonen bei der Komplexbildung erreichte Höhe hinaus zu bewirken. Die Höhe der Vorstufe sollte sich diesen Annahmen zufolge bei überschüssigem Al^{3+} (d.h. für $c_{Al^{3+}} > \frac{1}{2} c_{AZ}$) aus den Anteilen durch freie Protonen und durch freies Al^{3+} zusammensetzen:

$$i_{Vorstufe} = 5.4\, c_{AZ} + 4.5\,(c_{Al} - 0.5\, c_{AZ})\,\mu A \tag{6}$$

(c_{AZ} und c_{Al} in mM).

Abbildung 4 lässt erkennen, dass die Vorstufenhöhe dieser Beziehung für $c_{Al^{3+}} > 0.5\, c_{AZ}$ tatsächlich folgt.

Das Verhalten von AZS in Gegenwart von Al^{3+} entspricht vollkommen demjenigen von AZ. Da hier jedoch der Diffusions-Grenzstrom von AZS nur etwa 5.5 μA/mM AZS beträgt, kann sich eine Mitwirkung von freiem Al^{3+} als Protonendonator nicht auswirken.

In Gegenwart einer hinreichenden Konzentration von DMPD verschwindet sowohl die durch HCl als auch die durch Al^{3+} hervorgerufene Vorstufe vollständig. Die ursprüngliche AZ-Stufe bleibt unverändert. Bei etwa -1.4 V entsteht eine neue Stufe, deren Höhe der Al^{3+}-Konzentration proportional ist und die der katalytischen Wasserstoffentwicklung aus den bei Komplexbildung freigesetzten Protonen entspricht. Bei Verringerung der DMPD-Konzentration bzw. Erhöhung derjenigen von Al^{3+} (oder HCl), wenn als $c_{H_{solv}} > c_{DMPD}$, tritt die Vorstufe wieder in Erscheinung, wobei ihre Höhe gerade so gross ist, als wäre die Protonen-Konzentration gleich ($c_{H_{solv}} - c_{DMPD}$), wobei jeweils anstelle von $c_{H_{solv}}$ auch 0.5 $c_{Al^{3+}}$ gesetzt werden kann (Abb. 5). Hieraus kann geschlossen werden, dass die Verringerung bzw. Eliminierung der Vorstufe nicht auf einem Inhibitionseffekt von DMPD beruht, sondern darauf, dass DMPD als hinreichend starke Base in einer Lösungsreaktion jeweils ein Proton bindet und dass das gebildete Kation $(DMPD\text{-}H)^+$ zur erleichterten Reduktion von

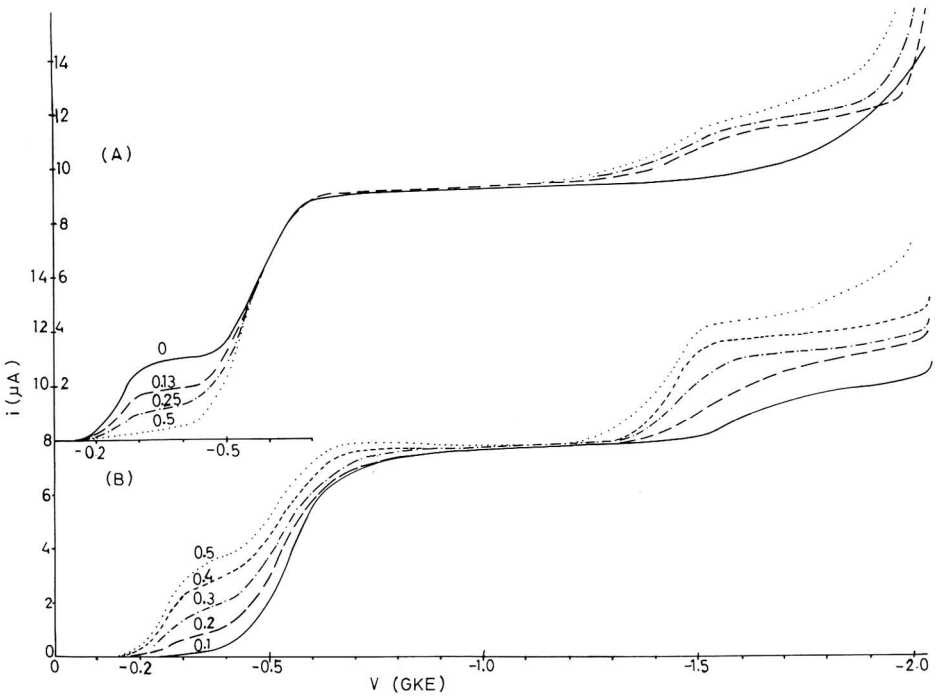

Abb. 5. Polarographische Kurven von 10^{-3} *M* Alizarin ($+10^{-3}$ *M* Benzoesäure) in Gegenwart von DMPD und HCl bzw. Al^{3+}.
(A) 0.5×10^{-3} *M* HCl + DMPD (Konzentration in 10^{-3} *M* an den Kurven), (B) 0.25×10^{-3} *M* DMPD $+Al^{3+}$ (Konzentration in 10^{-3} *M* an den Kurven).

AZ beim Vorstufenpotential nicht beitragen kann, wohl aber eine katalytische Wasserstoffentwicklung verursacht.

Das Verhalten von AZS–Al-Lösungen in Gegenwart von DMPD ist demjenigen bei AZ völlig analog.

SCHLUSSBETRACHTUNG

Aufgrund der Proportionalität zwischen Vorstufenhöhe und Konzentration an Al^{3+} kann eine analytische Bestimmung von Al^{3+} in methanolischen Lösungen in Gegenwart von AZ oder AZS durchgeführt werden. Um hierbei sicher im Bereich der Proportionalität zu bleiben, sollte der Komplexbildner wenigstens in dreifachem Überschuss vorliegen; die Aufnahme einer Eichkurve scheint angezeigt. Ausserdem sollte die Lösung weder starke Säuren (die selbst eine Vorstufe hervorrufen) noch starke Basen (die durch Bindung von Protonen die Vorstufenhöhe vermindern) zugegen sein.

Das polarographische Verhalten von Al-Komplexen mit AZ und AZS unterscheidet sich von demjenigen der Komplexe mit Solochromviolett RS in zwei wesent-

lichen Punkten. Erstens erfolgt die Reduktion dieser Komplexe nicht in einer besonderen, eigenen Stufe, sondern gemeinsam mit dem überschüssigen Farbstoff in einer zusammenhängenden Stufe. Abgesehen von einer geringfügigen Verminderung des Grenzstromes wegen des verringerten Diffusionskoeffizienten des Komplexes gegenüber dem freien Farbstoff bleibt die Gesamtstufenhöhe dementsprechend konstant und unabhängig vom Al-Gehalt der Lösung. Zweitens wurde im Falle von Solochromviolett RS eine dritte Stufe beobachtet, die denen des freien Farbstoffes und seines Al-Komplexes folgte[1]. Dies wurde der Reduktion des beim Bruch der N=N-Bindung des Komplexbildners freigesetzten Al^{3+} zugeschrieben. Eine solche Stufe wird jedoch im Falle des Al–AZ-Komplexes nicht beobachtet. Dies ist eine wichtige Stütze für die Schlussfolgerung, dass Al nach der Reduktion des Farbstoffes an diesen gebunden bleibt.

Da die Komplexbildung mit α-Hydroxy-Anthrachinonen unter kovalenter Bindung mit der Carbonylgruppe in Nachbarschaft zur OH-Gruppe erfolgt, ist es naheliegend anzunehmen, dass die Reduktion des Komplexes an der zweiten, freien Carbonylgruppe erfolgt. Aus der Analogie im Stufenverlauf für Mischungen von freiem und komplex-gebundenem Farbstoff kann geschlossen werden, dass die Reduktion in beiden Fällen zur Bildung von Oxanthron-Derivaten führt. Da trotz Komplexbildung praktisch keine Verlagerung der Reduktionsstufen erfolgt, ist die Reduzierbarkeit des freien Farbstoffes und des Komplexes vergleichbar.

Dem Bundesministerium für Wirtschaft wird für die materielle Unterstützung der Arbeit gedankt, ebenso der Alexander-von-Humboldt-Stiftung für die Gewährung eines Forschungsstipendiums (A.M.S.).

ZUSAMMENFASSUNG

Alizarin (AZ) und Alizarin S (AZS) werden in Methanol polarographisch in zwei bzw. drei Stufen 2-elektronig zum entsprechenden Oxanthron reduziert; die Mehrstufigkeit wird auf die Mitwirkung der sauren OH-Gruppen des Moleküls zurückgeführt. Bei Zusatz von Protonendonatoren (wie Benzoesäure), die anstelle der OH-Gruppen treten, oder von Protonenakzeptoren (wie $N(C_2H_5)_4OH$), die Protonen von den OH-Gruppen abziehen, erfolgt die Reduktion in einer einzigen Stufe bei positiverem bzw. negativerem Potential.

In Gegenwart von Al^{3+} entsteht bei beträchtlich positiverem Potential eine Vorstufe, deren Höhe der Al-Konzentration proportional ist, solange letztere klein genug ist. Die Vorstufe wird auf die Reduktion von AZ (AZS) unter Mitwirkung von bei der Komplexbildung freigesetzten Protonen zurückgeführt. (Eine ganz entsprechende Vorstufe entsteht auch bei Zusatz von HCl). Aufgrund der stöchiometrischen Verhältnisse wird geschlossen, dass ein Komplex $Al(AZ)_2$ bzw. $Al(AZS)_2$ gebildet wird. Übersteigt die Al-Konzentration die im Komplex gebundene Menge, so kann die Vorstufe auch Anteile enthalten, die auf der Protonendonatorwirkung freier Al^{3+}-Ionen beruht. Bei dem Potential der ursprünglichen AZ-Stufe steigt die Stromstärke stets auf den Wert für den Diffusionsstrom der Gesamtmenge von AZ an. Hieraus folgt, dass freies und ungebundenes AZ (bzw. AZS) beim gleichen Potential reduziert werden; eine besondere Stufe für bei der Reduktion des Komplexbildners in Freiheit gesetztes Al^{3+} ist nicht vorhanden. Daraus folgt, dass die von den OH-

Gruppen entfernte CO-Gruppe im freien Farbstoff und im Komplex praktisch die gleiche Neigung zur Reduktion aufweist und dass die komplexe Bindung von Al^{3+} auch nach der Reduktion—nun mit dem gebildeten Oxanthron—erhalten bleibt.

Ein Zusatz von N,N-Dimethyl-*p*-phenylendiamin (DMPD) zu den Lösungen der Komplexe (und ebenso zu den Lösungen mit HCl) führt zu teilweiser oder vollständiger Eliminierung der Vorstufen. Aus den stöchiometrischen Verhältnissen folgt, dass dies auf der Bindung der freigesetzten Protonen durch das als Base (nicht als Inhibitor) wirkende DMPD beruht. Bei -1.4 V (GKE) ruft DMPD eine katalytische Wasserstoff-Entwicklung hervor.

Aufgrund der Proportionalität zwischen Vorstufen-Höhe und Al^{3+}-Konzentration bei hinreichendem Farbstoff-Überschuss ergibt sich die Möglichkeit einer quantitativen Bestimmung von Al^{3+}.

SUMMARY

Alizarin (AZ) and Alizarin S (AZS) in methanol are polarographically reduced in two and three waves, respectively, with the transfer of two electrons/molecule to give the corresponding oxanthrons. The occurrence of more than one wave is explained by the participation of the acid OH-groups of the depolarizer in the electrode reaction. In presence of proton donors (such as benzoic acid) supplying protons instead of the OH-groups and/or the solvent, as well as in presence of proton acceptors (*e.g.*, $(C_2H_5)_4NOH$) depriving the molecules of their acidic protons, reduction proceeds in a single wave at more positive or more negative potentials, respectively.

In presence of Al^{3+}, a prewave is observed at rather positive potentials, the height of which is proportional to the Al content when the latter is small enough. The prewave is due to the facile reduction of AZ in the presence of free (solvated) protons set free during complexation. A quite analogous prewave develops in the presence of HCl. On the basis of stoichiometric relations, it is concluded that $Al(AZ)_2$ or $Al(AZS)_2$ complexes are formed. If the Al^{3+} content exceeds the 1 : 2 ratio, the prewave increases in height due to the proton donating character of free Al-ion. At the potential of the original AZ wave, the current in each case rises to the diffusion current of the total amount of AZ. Hence, both free and complexed AZ (or AZS) are reduced at the same potential. In contrast to the Al-complexes of Solochrome-violet RS, no separate wave is recorded due to the reduction of Al^{3+} set free in the course of reduction of the complexing agent. It is concluded that the free CO group has approximately equal reducibilities in the dye and in its complex, and that Al^{3+} remains attached—after reduction—to the oxanthron derivative.

The prewave can be partly or totally eliminated on addition of N,N-dimethyl-*p*-phenylendiamine (DMPD) to the complex solutions (and, similarly, to solutions with HCl). From stoichiometric considerations, this is related to the basic character of DMPD. At -1.4 V (SCE), DMPD causes the development of a catalytic hydrogen wave.

The proportionality between the height of the prewave and the concentration of Al^{3+} at sufficient excess of the dye offers the possiblity of the quantitative determination of Al^{3+} in nonaqueous methanolic solutions.

LITERATUR

1 L. HOLLECK, J. M. ABD EL KADER UND A. M. SHAMS EL DIN, *J. Electroanal. Chem.*, 20 (1969) 287.
2 F. FEIGL, *Tüpfelanalyse*, Akad. Verlagsges., Frankfurt/Main, 1960, S. 190.
3 A. K. BABKO UND T. N. NAZARCHUK, *Akad. Nauk. Ukr. SSR*, 2 (1959) 199, zitiert in H. BAUMANN UND H. R. HENSEL, *Fortschritte der Chemischen Forschung*, Bd. 7, *Metallkomplex-Farbstoffe*, Springer-Verlag, Berlin, 1967, S. 732.
4 Y. DORTA-SCHAEPPI, H. HÜRZELER UND W. D. TREADWELL, *Helv. Chim. Acta*, 34 (1951) 797.
5 E. G. KIEL UND P. M. HEERTJES, *J. Soc. Dyers Colourists*, 79 (1963) 186.
6 F. FEIGL UND R. STERN, *Z. Anal. Chem.*, 60 (1921) 9.
7 F. W. ATACK, *J. Soc. Chem. Ind.*, 34 (1935) 936.
8 K. HELLER UND P. KRUMHOLZ, *Mikrochemie*, 7 (1929) 221.
9 L. HOLLECK UND A. M. SHAMS EL DIN. *Electrochim. Acta*, 13 (1968) 199.
10 R. GILL UND H. I. STONEHILL, *J. Chem. Soc.*, (1952) 1845.
11 N. H. FURMAN UND K. G. STONE, *J. Am. Chem. Soc.*, 70 (1948) 3055.
12 L. A. WILES, *J. Chem. Soc.*, (1952) 1358.
13 L. HOLLECK, H. MARSEN UND H. J. EXNER, *Z. Naturforsch.*, 9b (1954) 274.
14 L. HOLLECK, D. JANNAKOUDAKIS UND A. WILDENAU, *Electrochim. Acta*, 12 (1967) 1523.
15 D. JANNAKOUDAKIS UND A. WILDENAU, *Z. Naturforsch.*, 22b (1967) 118.
16 D. JANNAKOUDAKIS, A. WILDENAU UND L. HOLLECK, *J. Electroanal. Chem.*, 15 (1967) 83.

ELECTROANALYTICAL CHEMISTRY AND INTERFACIAL ELECTROCHEMISTRY
Elsevier Sequoia S.A., Lausanne – Printed in The Netherlands

THE MAXIMUM WAVE IN A.C. POLAROGRAPHY AS EVIDENCED BY USING THE MAGNETIC FIELD EFFECT

SHIZUO FUJIWARA, HIROYUKI KOJIMA, YOSHIO UMEZAWA AND TERUHIKO KUGO
Department of Chemistry, Faculty of Science, The University of Tokyo, Hongo, Tokyo (Japan)
(Received June 2nd, 1969; in revised form January 5th, 1970)

INTRODUCTION

The effect of magnetic field in d.c. polarography has recently been observed and shown to be useful for the clarification of electrode processes in polarography[1,2]. This paper concerns the investigation of this effect in a.c. polarography. To aid further discussion, the results which have been obtained in d.c. polarography will be briefly summarized first[2].

When a static magnetic field is applied perpendicularly to a polarographic cell, the intensities of the maximum currents of the first and of the second kinds are decreased compared to those measured in the absence of magnetic field. However, the diffusion current, residual current and half-wave potential are in most cases not affected by the application of magnetic field. It has also been confirmed that the magnetic field does not influence the drop time and the flow rate of mercury. This effect of magnetic field on the maximum currents has been interpreted in terms of retardation by magnetic field of the tangential motion at the surface of the dropping mercury electrode.

According to the *Faradaic Impedance Theory* developed by Grahame[3], the maximum wave is not expected to appear in a.c. polarography. In this paper, the magnetic field effect is used to prove the existence of the maximum wave in a.c. polarography. This maximum wave will be discussed with respect to the reversibility of electrode reactions.

EXPERIMENTAL

Apparatus

A.c. and d.c. polarograms were taken with the use of a Yanagimoto Polarograph Model PA-102. A.c. polarograms were obtained by the superposition of an alternating voltage of 15 mV and 50 Hz. A static magnetic field of 7050 Oersted was applied perpendicularly to the dropping mercury electrode. The electro-magnet used in this experiment is the same one as that used in the former experiment[2]. The drop time of mercury (τ) is about 3–4 s/drop at a mercury column height of 70 cm.

Chemicals

Chemical reagents used in this experiment were of analytical reagent grade. In order to remove surface active impurities completely, sample solutions were passed through a charcoal filter bed before measurements.

Measurements of the magnetic field effect

The effect of magnetic field is expressed in terms of ΔH, which is defined as

$$\Delta H = (I_{ac}^{0} - I_{ac}^{H})/I_{ac}^{0} \times 100\ (\%) \quad (1)$$

where I_{ac}^{H} and I_{ac}^{0} are the peak current intensities obtained with and without magnetic field, respectively, I_{ac}^{H} were measured under the same conditions as I_{ac}^{0} except for the application of magnetic field. The value of ΔH is accurate to within $\pm 1\%$. All measurements were performed at $23.5 \pm 0.5°C$.

RESULTS AND DISCUSSION

(I) Evidence of the maximum wave in a.c. polarography

Figure 1 shows the presence of magnetic field effect in the a.c. polarogram as well as in the d.c. polarogram for 1.0 m*M* Mn(II) ion in 1.0 *M* KCl solution. The maximum wave of the d.c. polarogram of this system is classified as the second kind of maxima (*Spüleffekt*)[4]. It has been established in the previous paper that the magnetic

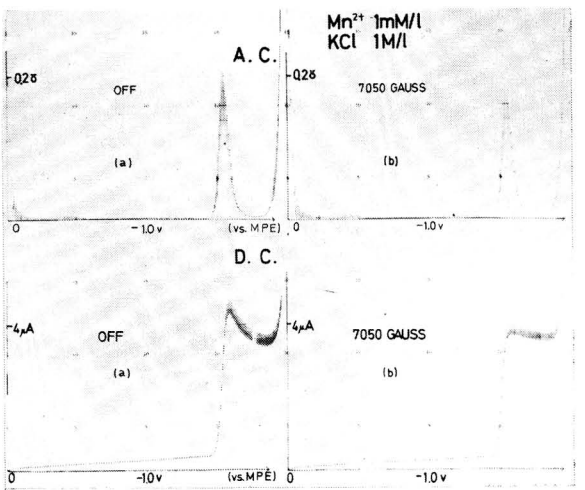

Fig. 1. Magnetic field effect in a.c. (above) and d.c. (below) polarography (a) in the absence and (b) in the presence of magnetic field in the system 1 m*M* $MnCl_2$ and 1 *M* KCl. The mercury pool electrode (MPE) is used as an anode.

field effect on the second kind of maxima of d.c. polarograms always appears as the reduction of the maximum wave currents[2]. It can be seen in Fig. 1 that the peak current intensity of the a.c. polarogram is reduced with the application of magnetic field and this implies that the peak current intensity of the a.c. polarogram contains, as a part of it, the current which is the same as that of the second kind of maxima of the d.c. polarogram. This is interpretable in terms of the nature of the a.c. wave, that is, in a.c. polarography the mean concentrations of the depolarizer at the surface of the mercury drop are determined by the d.c. polarographic current which flows under a.c. polarographic conditions[1,3]. This suggests that the maximum wave in the d.c. process contributes to the a.c. wave as a result of the increase in the surface concentration. Partial suppression of the maximum wave by magnetic field implies

that this effect appears in the a.c. wave *via* the d.c. profile. The experimental evidence for this discussion will be given later using the system 1.0 m*M* Mn(II) ion in 1.0 *M* KCl.

The dependence of the magnetic field effect on the drop time τ is shown in Fig. 2. The magnitude of the magnetic field effect ΔH, is increased with decrease in τ until it reaches an equilibrium value of about 3 s. This implies that the *Spüleffekt* increases with the reduction of τ, which results in the increase of the maximum wave in the d.c. process, and this results in an increase in ΔH.

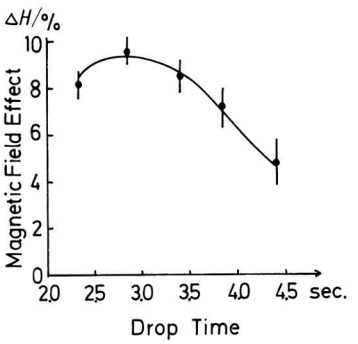

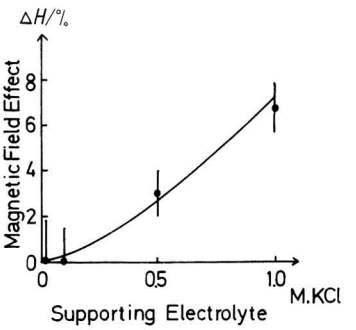

Fig. 2. Dependence of the magnetic field effect on the drop time in the system 1 m*M* $MnCl_2$ and 1 *M* KCl.

Fig. 3. Dependence of the magnetic field effect on the concn. of supporting electrolyte in the systems 1 m*M* $MnCl_2$ and 0.01–1.0 *M* KCl.

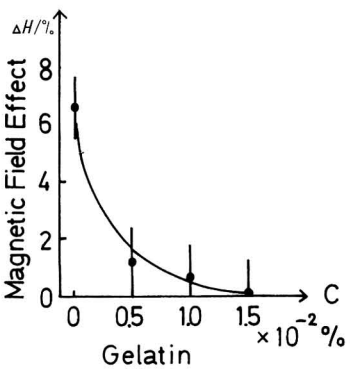

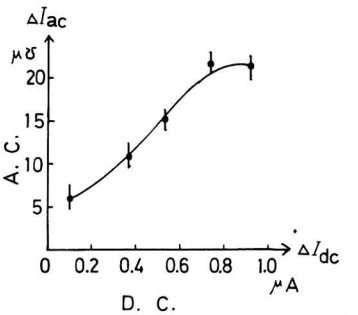

Fig. 4. Dependence of the magnetic field effect on the concn. of gelatin in the system 1 m*M* $MnCl_2$ and 1 *M* KCl.

Fig. 5. Comparison of the magnetic field effect between d.c. and a.c. polarography in the system 1 m*M* $MnCl_2$ and 1 *M* KCl.

The magnetic field effect is dependent upon the concentration of supporting electrolyte as shown in Fig. 3. The *Spüleffekt* becomes smaller with decrease in concentration of the supporting electrolyte[5], which results in a decrease in ΔH.

Figure 4 shows that the magnitude of the magnetic field effect is reduced with increase in the concentration of surface active substances. When 1.5×10^{-2}% of

TABLE 1

COMPARISON OF THE MAGNETIC FIELD EFFECT IN A.C. AND D.C. POLAROGRAPHY

Depolarizer	*Supporting electrolyte*	*Magnetic field effect*		$(E_p - E_{\frac{1}{2}})/V$
		a.c.	*d.c.*	
$MnCl_2$, 1 m*M*	LiCl, 1 *M*	○	○	−0.02
	KCl, 1 *M*	○	○	−0.02
	CsCl, 1 *M*	○	○	−0.02
$Co(NH_3)_6Cl_3$, 1 m*M*[a]	KCl, 1 *M*	○	○	−0.03
$NiCl_2$, 0.5 m*M*	KCl, 0.2 *M*	○	○	−0.03
$CoCl_2$, 1 m*M*	KCl, 1 *M*	○	○	−0.03
TlCl, 0.5 m*M*	LiCl, 1 *M*	×	○	0.00
	KCl, 1 *M*	×	○	0.00
	CsCl, 1 *M*	×	○	0.00
$CuCl_2$, 1 m*M*[b]	LiCl, 1 *M*	×	○	0.00
	KCl, 1 *M*	×	○	0.00
	CsCl, 1 *M*	×	○	0.00
$ZnCl_2$, 1 m*M*	KI, 1 *M*	×	○	0.00
$CdCl_2$, 1 m*M*	KCl, 1 *M*	×	○	0.00
$PbCl_2$, 1 m*M*	KCl, 1 *M*	×	×	0.00
$Bi(NO_3)_3$, 0.1 m*M*	H_2SO_4, 3.6 *N*	×	×	0.00

[a] $Co(NH_3)_6^{3+}$ (II→0).
[b] 1 *N* HCl soln.
(○) The magnetic field effect is clearly observed.
(×) The magnetic field effect is almost negligible.

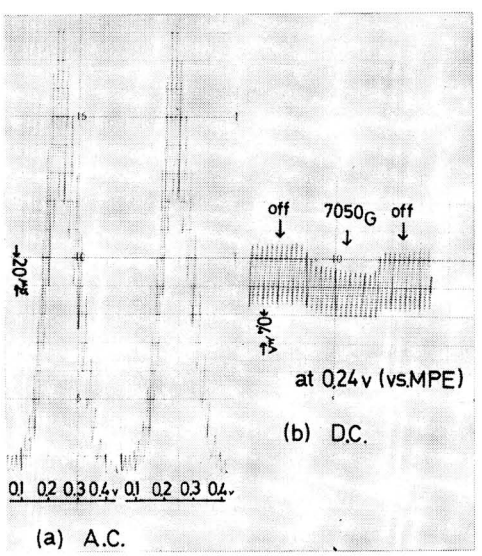

Fig. 6. Comparison of the magnetic field effect between (a) a.c. and (b) d.c. polarography in the system 1 m*M* $CuCl_2$ and 1 *M* KCl, 1 *N* HCl. In the d.c. polarogram, the applied voltage is fixed at the peak potential of the a.c. polarogram. In Fig. 6(a), right: in magnetic field; left: without magnetic field.

gelatin is added to the solution, the magnetic field effect becomes unobservable. This can be interpreted in terms of the suppression of the *Spüleffekt* by the addition of gelatin.

As shown above, the magnitude of ΔH depends on the contribution of the maximum wave of the d.c. process under a.c. polarographic conditions. In Fig. 5, the magnetic field effect in a.c. polarography is compared to that in d.c. polarography. The decrease in a.c. and d.c. polarographic currents, ΔI_{ac} and ΔI_{dc} are defined as

$$\Delta I_{ac} = I_{ac}^{0} - I_{ac}^{H} \tag{2}$$

$$\Delta I_{dc} = I_{dc}^{0} - I_{dc}^{H} \tag{3}$$

respectively, where I_{dc}^{H} and I_{dc}^{0} denote the maximum values of d.c. polarographic currents observed with and without magnetic field, respectively. When ΔI_{ac} is plotted as a function of ΔI_{dc}, ΔI_{ac} changes almost linearly with ΔI_{dc} as shown in Fig. 5, where ΔI_{ac} and ΔI_{dc} are varied by controlling the mercury column height. This proves that the magnetic field effect in a.c. polarography is due to the maximum wave in the d.c. process.

The system 1.0 m*M* $Co(NH_3)_6^{3+}$ ion in 1.0 *M* KCl shows results similar to those shown in former Figs. 2–5.

In conclusion, the existence of the magnetic field effect in a.c. polarography clearly shows that there is an appreciable contribution of the maximum wave to the observed a.c. wave. These results can be taken as the first examples to prove the presence of the maximum wave in a.c. polarography.

In the above discussion, the effect of the magnetic field on an a.c. process which involves the a.c. polarization of the surface concentration, was not considered. Since the magnetic field effect was not observed when the maximum wave is suppressed in the d.c. process (see Fig. 4), this effect need not be considered.

(II) Magnetic field effect and the reversibility of electrode reactions

The exptl. results of the magnetic field effect on a.c. polarography for some metal ions are summarized in Table 1. All experiments were performed with a column height of 70 cm, and the results are compared to those obtained in d.c. polarography using the same column height of mercury. Among the ions listed in Table 1, several show the maximum waves in d.c. polarography; $Tl^{+}(I \rightarrow 0)$ and $Cu^{2+}(I \rightarrow 0)$* show maxima of the first kind, and $Mn^{2+}(II \rightarrow 0)$, $Cd^{2+}(II \rightarrow 0)$, $Co(NH_3)_6^{3+}(II \rightarrow 0)$, $Ni^{2+}(II \rightarrow 0)$, $Zn^{2+}(II \rightarrow 0)$ and $Co^{2+}(II \rightarrow 0)$ show those of the second kind. The other two ions, $Pb^{2+}(II \rightarrow 0)$ and $Bi^{3+}(III \rightarrow 0)$ do not show maxima in d.c. polarography[1]. In this Table, $E_p - E_{\frac{1}{2}}$ represents the difference between the peak potential of the a.c. polarogram and the half-wave potential of the d.c. polarogram. This may be used as a measure of the degree of irreversibility of electrode reactions[6]. In Table 1, the Tl^{+}, Cu^{2+}, Cd^{2+} and Zn^{2+} systems have been classified as those which give *reversible reactions* at the electrode surface[7]. These systems clearly show the magnetic field effect in d.c. polarography. However, the magnetic field effect in a.c. polarography is almost negligible. Figure 6 presents the result of Cu^{2+} ion as a typical example.

In Table 1, Mn^{2+}, $Co(NH_3)_6^{3+}$, Ni^{2+} and Co^{2+} systems are classified as those

* There is probably superposition of the maxima of the second kind.

which undergo *less reversible reactions* at the electrode surface[7]. These systems clearly exhibit the magnetic field effect both in d.c. and a.c. polarography. This suggests that the a.c. polarographic waves of *less reversible ions* contain the contribution of maximum waves; on the other hand, the contribution of maximum waves is not contained in the a.c. polarographic waves of *reversible ions.*

Both the first and the second kind of maxima are known to be due to the convectional motion of electrolyte solutions at the mercury surface[5]. Consequently, the above results suggest that convection significantly influences the a.c. polarographic waves of *less reversible ions.* However, this is apparently inconsistent with the statement of Grahame who proposed the so-called *Faradaic Impedance Theory*[3]. According to his statement, the a.c. components of the current of electrode reactions are not affected by the convection which occurs on and/or near the surface of the electrode. However, as we have seen in the above mentioned results, this is not the case for *less reversible ions.* It should be noted here, furthermore, that the present results are inconsistent with those of Tanaka and his coworkers, who concluded that the *Spüleffekt* is negligible in a.c. polarography[8,9]. We point out that this statement is not always the case, and holds good only with *reversible ions* such as Cd^{2+} and Pb^{2+}. In fact, they only used the *reversible ions* mentioned above.

The difference between the *reversible* and *less reversible ions* may be interpreted as follows. The a.c. polarographic wave is responsible for the sum of the surface concentrations of the oxidized and reduced forms, and the d.c. polarographic wave for the difference between them. In other words, the reduced form of the depolarizer contributes as an increase to the a.c. wave, but as a decrease to the d.c. wave. Consequently, as the convectional motion of the solution brings excess ions of the oxidized form to the electrode surface, the change in the total a.c. wave which is produced by convection should be much smaller than that in the d.c. wave. Such a situation can occur in the case of *reversible ions*, where the reduced form sufficiently contributes to the total a.c. wave, whereas in the case of *less reversible ions*, the influence of convection directly affects the a.c. wave, because the contribution of the reduced form to the a.c. wave is almost negligible compared to that of *reversible ions.*

In the cases of Tl^{+}, Cd^{2+}, Cu^{2+} and Zn^{2+}, the a.c. waves are slightly increased with increase in the drop time. This suggests that the contribution of the reduced form to the a.c. wave is sufficiently large, although account is taken of the fact that the surface area is increased with the drop time[10].

Delmastro and Smith discussed the influence of spherical diffusion on the a.c. wave equation[11,12]. The number of ions of the oxidized form which are brought to the electrode surface is slightly larger in the case of spherical diffusion than in the case of planar diffusion. In this sense, the influence of spherical diffusion on the a.c. wave is analogous to that of the convection on the a.c. wave. Delmastro and Smith predict that spherical diffusion significantly contributes to the observed a.c. wave only for *less reversible ions, i.e.* for *reversible ions* excess ions brought by spherical diffusion do not increase the a.c. wave. Results obtained in the present work are qualitatively in agreement with their prediction.

SUMMARY

The presence of the maximum wave in a.c. polarography has been confirmed

using the magnetic field effect. It has been concluded that the maximum wave contributes to the a.c. polarographic wave *via* the d.c. process under a.c. polarographic conditions. This contribution is important for *less reversible ions*, while it is almost negligible for *reversible ions*. This result has been interpreted in terms of the difference in magnitude of the contribution from the reduced form to the a.c. wave.

ACKNOWLEDGEMENT

The authors express their thanks to the Yanagimoto Manufacturing Company for the use of the apparatus. We are also grateful to Dr. Hiroaki Matsuda of the Government Chemical Industrial Research Institute, Tokyo and to Dr. Yoji Arata of our Department for valuable discussions.

REFERENCES

1 S. FUJIWARA, H. HARAGUCHI AND Y. UMEZAWA, *Anal. Chem.*, 40 (1968) 249.
2 S. FUJIWARA, Y. UMEZAWA AND T. KUGO, *Anal. Chem.*, 40 (1968) 2186.
3 D. C. GRAHAME, *J. Electrochem. Soc.*, 99 (1952) 370c.
4 J. HEYROVSKÝ, *Principles of Polarography*, Academic Press, New York and London, 1966.
5 See for example, M. VON STACKELBERG, *Fortschr. Chem. Forsch.*, 2 (1951) 229.
6 H. MATSUDA, *Z. Elektrochem.*, 62 (1958) 977.
7 N. TANAKA AND R. TAMAMUSHI, *Electrochim. Acta*, 9 (1964) 963.
8 N. TANAKA, T. KOIZUMI, T. MURAYAMA, M. KODAMA AND Y. SAKUMA, *Anal. Chim. Acta*, 18 (1958) 97.
9 N. TANAKA, R. TAMAMUSHI AND M. KODAMA, *Anal. Chim. Acta*, 20 (1959) 573.
10 G. H. AYLWARD AND J. W. HAYES, *J. Electroanal. Chem.*, 8 (1964) 442.
11 J. R. DELMASTRO AND D. E. SMITH, *J. Electroanal. Chem.*, 9 (1965) 192.
12 J. R. DELMASTRO AND D. E. SMITH, *Anal. Chem.*, 39 (1967) 1050.
13 H. L. HUNG AND D. E. SMITH, *Anal. Chem.*, 36 (1964) 922.

ELECTROANALYTICAL CHEMISTRY AND INTERFACIAL ELECTROCHEMISTRY
Elsevier Sequoia S.A., Lausanne – Printed in The Netherlands

SECOND HARMONIC A.C. POLAROGRAPHY: THEORETICAL PREDICTIONS FOR SYSTEMS WITH FIRST-ORDER CHEMICAL REACTIONS PRECEDING THE CHARGE TRANSFER STEP*

THOMAS G. McCORD** AND DONALD E. SMITH***
Department of Chemistry, Northwestern University, Evanston, Illinois 60201 (U.S.A.)
(Received October 17th, 1969)

INTRODUCTION

The electrode reaction mechanism involving a first-order homogeneous chemical reaction preceding the heterogeneous charge transfer step

$$Y \underset{k_2}{\overset{k_1}{\rightleftharpoons}} O + ne \overset{k_s, \alpha}{\rightleftharpoons} R \qquad \text{(R1)}$$

is of fundamental importance in electrochemical kinetics. This frequently-encountered pathway is discussed prominently in numerous textbooks and review articles[1-6]. Earlier theoretical work[7-13] has contributed significantly to the understanding of the linear faradaic a.c. response to applied sinusoidal potentials of small amplitude. However, for this mechanism, little attention has been given to the theory associated with non-linear aspects of the faradaic response to small amplitude sinusoidal perturbations, such as the second harmonic[11,14-21] and intermodulation[16] currents. Paynter[16] briefly considered intermodulation polarography with mechanism R1, confining his treatment to the special case in which the d.c. process is controlled by diffusion only. Second harmonic a.c. polarography was briefly considered by Smith[11] for mechanism R1, utilizing the rather approximate stationary plane model.

Recently, a general theory was presented for the second harmonic a.c. polarographic behavior of systems involving rate control by diffusion, a single heterogeneous charge transfer step and any number or type of coupled first-order homogeneous chemical reactions[22]. The theory was developed within the framework of the reasonably precise expanding plane model of the dropping mercury electrode[23] and involves only minor restrictions on magnitudes of relevant rate parameters. It provides the theoretical expressions for mechanism R1 as a special case. Our concern with the applicability of second harmonic a.c. polarography to detecting and quantitatively characterizing electrode processes involving coupled chemical reactions gave origin to a detailed study of the predictions of this theory for the case in question. The results of this effort are presented here.

---

* Work supported by National Science Foundation Grants GP5778 and GP7985.
** NIH Graduate Fellow, 1966–68: present address, General Electric Corp., Materials and Processes Laboratory, Schenectady, New York, 12305.
*** To whom correspondence should be addressed.

NOTATION

C_T^* = total initial concentration of species O and Y ($C_T^* = C_O^* + C_Y^*$).
C_O^* = initial concentration of oxidized form.
D_i = diffusion coefficient of species i.
f_i = activity coefficient of species i.
$E_{d.c.}$ = d.c. component of applied potential.
E^0 = standard redox potential in European convention.
ΔE = amplitude of applied alternating potential.
$E_{\frac{1}{2}}^r$ = reversible d.c. polarographic half-wave potential (planar diffusion theory).
$E_{\frac{1}{2}}^{rc}$ = d.c. polarographic half-wave potential with chemical equilibrium preceding nernstian charge transfer.
$(E_{d.c.})_{min}$ = d.c. potential at minimum of second harmonic current amplitude polarogram.
$I(2\omega t)$ = second harmonic faradaic alternating current.
ϕ_2 = second harmonic current phase angle.
ω = applied angular frequency (rad. s^{-1}).
t = time (s).
A = electrode area.
F = Faraday's constant.
T = absolute temperature.
R = ideal gas constant.
n = number of electrons transferred in heterogeneous charge transfer step.
k_s = heterogeneous charge transfer rate constant at E^0 (cm s^{-1}).
α = charge transfer coefficient.
k_1 = forward first-order rate constant for chemical reaction preceding charge transfer (s^{-1}).
k_2 = backward first-order rate constant for chemical reaction preceding charge transfer (s^{-1}).
K = equilibrium constant for chemical reaction preceding charge transfer ($=k_1/k_2$).
Γ = Euler gamma function.
i_a = second harmonic anodic peak current amplitude.
i_c = second harmonic cathodic peak current amplitude.
$i_{d,a}$ = second harmonic anodic peak current amplitude with diffusion-controlled process.
$i_{d,c}$ = second harmonic cathodic peak current amplitude with diffusion-controlled process.

THEORY

Adaptation of the general theory for the second harmonic a.c. polarographic response[22] to the special case of mechanism R1 yields the following result (notation definitions are given above):

$$I(2\omega t) = Z(2\omega)\,W(\omega)\sin(2\omega t + \phi_2) \tag{1}$$

$$Z(2\omega) = \frac{n^2F^2AC_O^*(2\omega D_O)^{\frac{1}{2}}\Delta E}{4RT\cosh^2(\frac{1}{2}j)}\,F(t)G(2\omega) \tag{2}$$

$$G(2\omega) = \left[\frac{2}{V_2^2+U_2^2}\right]^{\frac{1}{2}} \tag{3}$$

$$W(\omega) = (nF\Delta E/4RT)(P^2+L^2)^{\frac{1}{2}} \tag{4}$$

$$\phi_2 = \cot^{-1}\left(\frac{LV_2+PU_2}{LU_2-PV_2}\right) \tag{5}$$

$$F(t) = \frac{1+M_p}{M_p}\left\{1+\left[\alpha\left(1+\frac{Ke^{-j}}{1+K}\right)-\gamma_p\right]\frac{\psi(\xi)}{\gamma_p}\right\} \tag{6}$$

$$U_2 = \frac{1}{1+e^j}\left\{\frac{1}{1+K}\left[\frac{(1+h^2)^{\frac{1}{2}}-h}{1+h^2}\right]^{\frac{1}{2}}+e^j+\frac{K}{1+K}\right\} \tag{7}$$

$$V_2 = \frac{2\omega^{\frac{1}{2}}}{\lambda}+\frac{1}{1+e^j}\left\{\frac{1}{1+K}\left[\frac{(1+h^2)^{\frac{1}{2}}+h}{1+h^2}\right]^{\frac{1}{2}}+e^j+\frac{K}{1+K}\right\} \tag{8}$$

$$\psi(\xi) = 1+\sum_{p=1}^{\infty}(-1)^p\prod_{l=1}^{l=p}\frac{\Gamma(3l+7)/14}{\Gamma(3l+14)/14}\left(\sqrt{\tfrac{3}{7}}\xi\right)^p \tag{9}$$

$$L = \frac{2}{V^2+U^2}\left(\frac{U-V}{1+e^{-j}}+\alpha U\frac{(2\omega)^{\frac{1}{2}}}{\lambda}\right) \tag{10}$$

$$P = \frac{2}{V^2+U^2}\left(\alpha\frac{(2\omega)^{\frac{1}{2}}}{\lambda}V+\frac{V+U}{1+e^{-j}}\right)+\frac{\alpha\beta(1+e^{-j})\psi(\xi)}{\gamma_p F(t)}-1 \tag{11}$$

$$V = \frac{(2\omega)^{\frac{1}{2}}}{\lambda}+\frac{1}{(1+e^j)}\left\{\frac{1}{1+K}\left[\frac{(1+g^2)^{\frac{1}{2}}+g}{1+g^2}\right]^{\frac{1}{2}}+e^j+\frac{K}{1+K}\right\} \tag{12}$$

$$U = \frac{1}{(1+e^j)}\left\{\frac{1}{1+K}\left[\frac{(1+g^2)^{\frac{1}{2}}-g}{1+g^2}\right]^{\frac{1}{2}}+e^j+\frac{K}{1+K}\right\} \tag{13}$$

$$\gamma_p = 1+\lambda/k^{\frac{1}{2}}(1+K)(1+e^j) \tag{14}$$

$$M_p = K+e^j(1+K) \tag{15}$$

$$\xi = \lambda_p t^{\frac{1}{2}}/\gamma_p \tag{16}$$

$$\lambda_p = k_s f D^{-\frac{1}{2}}\left(\frac{Ke^{-\alpha j}}{1+K}+e^{\beta j}\right) \tag{17}$$

$$\lambda = k_s f D^{-\frac{1}{2}}(e^{-\alpha j}+e^{\beta j}) \tag{18}$$

$$g = 2h = k/\omega \tag{19}$$

$$k = k_1+k_2 \tag{20}$$

$$K = k_1/k_2 \tag{21}$$

$$j = (nF/RT)(E_{d.c.}-E^r_{\frac{1}{2}}) \tag{22}$$

$$E^r_{\frac{1}{2}} = E^0-\frac{RT}{nF}\ln\left(\frac{f_R}{f_O}\right)\left(\frac{D_O}{D_R}\right)^{\frac{1}{2}} \tag{23}$$

$$D = D_O^{\beta}D_R^{\alpha} \tag{24}$$

$$f = f_O^{\beta} f_R^{\alpha} \tag{25}$$

$$\beta = 1-\alpha \tag{26}$$

The potential-dependent parameter employed in the above relationships, j, refers the applied d.c. potential, $E_{d.c.}$, to the quantity $E_{\frac{1}{2}}^{r}$ which is the reversible (diffusion-controlled) d.c. polarographic half-wave potential and a.c. polarographic (fundamental harmonic) peak potential in *absence* of the preceding chemical reaction. As has been pointed out previously[13], $E_{\frac{1}{2}}^{r}$ is often not the most rational choice of reference potential. Frequently it is preferable to utilize as the reference the quantity $E_{\frac{1}{2}}^{rc}$, where[13]

$$E_{\frac{1}{2}}^{rc} = E_{\frac{1}{2}}^{r} + (RT/nF)\ln\{K/(1+K)\} \tag{27}$$

That is, one employs as the reference potential in the theoretical formulation the reversible d.c. polarographic half-wave potential in the presence of a chemical equilibrium preceding charge transfer. In this framework one replaces the parameter j with

$$J = (nF/RT)[E_{d.c.} - E_{\frac{1}{2}}^{r} - (RT/nF)\ln\{(1+K)/K\}] \tag{28}$$

using the transformation

$$e^{j} = \{(1+K)/K\}\, e^{J} \tag{29}$$

The reformulation of the foregoing theoretical expressions (eqns. 1–26) in terms of the parameter J may be written:

$$I(2\omega t) = Z_J(2\omega)\, W_J(\omega) \sin(2\omega t + \phi_{2,J}) \tag{30}$$

$$Z_J(2\omega) = \frac{n^2F^2AC_T^*(\omega D_O)^{\frac{1}{2}}\Delta E}{4RT\cosh^2(\frac{1}{2}J)}\, F_J(t)\, G_J(2\omega) \tag{31}$$

$$W_J(\omega) = (nF\Delta E/4RT)\,(P_J^2 + L_J^2)^{\frac{1}{2}} \tag{32}$$

$$\phi_{2,J} = \cot^{-1}\left(\frac{L_J V_{2,J} + P_J U_{2,J}}{L_J U_{2,J} - P_J V_{2,J}}\right) \tag{33}$$

$$G_J(2\omega) = \sqrt{2}[V_{2,J}^2 + U_{2,J}^2]^{-\frac{1}{2}} \tag{34}$$

$$F_J(t) = 1 + [\alpha(1+e^{-J}) - \gamma_p]\,\psi(\xi)/\gamma_p \tag{35}$$

$$U_{2,J} = \frac{K^{-1}}{(1+e^{J})}\left[\frac{(1+h^2)^{\frac{1}{2}} - h}{1+h^2}\right]^{\frac{1}{2}} + 1 \tag{36}$$

$$V_{2,J} = \frac{2\omega^{\frac{1}{2}}}{\lambda_p} + \frac{K^{-1}}{(1+e^{J})}\left[\frac{(1+h^2)^{\frac{1}{2}} + h}{1+h^2}\right]^{\frac{1}{2}} + 1 \tag{37}$$

$$L_J = \frac{2}{V_J^2 + U_J^2}\left(\frac{\alpha U_J\sqrt{2\omega}}{\lambda_p} + \frac{U_J - V_J}{1+e^{-J}}\right) \tag{38}$$

$$P_J = \frac{2}{V_J^2 + U_J^2}\left(\frac{\alpha V_J\sqrt{2\omega}}{\lambda_p} + \frac{V_J + U_J}{1+e^{-J}}\right) + \frac{\alpha\beta}{\lambda_p}(1+e^{-J})\frac{\psi(\xi)}{F_J(t)} - 1 \tag{39}$$

$$V_J = \frac{\sqrt{2\omega}}{\lambda_p} + \frac{K^{-1}}{(1+e^J)}\left[\frac{(1+g^2)^{\frac{1}{2}}+g}{1+g^2}\right]^{\frac{1}{2}} + 1 \quad (40)$$

$$U_J = \frac{K^{-1}}{(1+e^J)}\left[\frac{(1+g^2)^{\frac{1}{2}}-g}{1+g^2}\right]^{\frac{1}{2}} + 1 \quad (41)$$

$$\lambda_p = k_s f K^{\beta}(1+K)^{-\beta}(e^{-\alpha J}+e^{\beta J}) \quad (42)$$

$$\gamma_p = 1+\lambda_p/(1+e^J)Kk^{\frac{1}{2}} \quad (43)$$

All other quantities remain unchanged by the transformation.

Both foregoing theoretical formulations are valid for $kt \geqq 10$ and $D_Y = D_O$. The kinetic status of the preceding chemical reaction determines which formulation is preferred, as has been discussed previously[13].

The above general theoretical expression for the second harmonic response is rather cumbersome since it incorporates the possibility of simultaneous rate control by three rate processes, diffusion, heterogeneous charge transfer and the coupled preceding chemical reaction. However, notable simplification of this general solution is possible in a number of special cases. It already has been pointed out that when the homogeneous chemical reaction is thermodynamically inoperative ($K \gg 1$) and/or kinetically inoperative ($k \rightarrow 0$), the theoretical expression reduces to one associated with the simple quasi-reversible case[22] (rate control by diffusion and heterogeneous charge transfer only). Table 1 compiles additional special situations, together with the relevant mathematical conditions, which allow one to simplify the general theory. With the aid of the mathematical relationships of Table 1 and algebraic manipulation, the above general theory may be reduced to simplified formulations appropriate to each special situation. Most of these special cases were considered in some detail for the fundamental harmonic case[13] and the reader is referred to ref. 13 for additional discussion relevant to Table 1.

RESULTS AND DISCUSSION

A detailed examination of the predictions of the above theoretical relationships was carried out with the aid of a Control Data Corporation Model 3400 digital computer. Computer readout was provided in an analog form with the aid of a Calcomp Model 565 digital incremental plotter, as well as in the usual digital form. All calculations were based on the general theory defined by eqns. (1)–(26). The Fortran program used for this purpose is available on request.

Figures 1–13 illustrate some of the most noteworthy aspects of the predicted second harmonic response for mechanism R1. The plots represented in these figures include three different forms of experimentally accessible [11,25,26] second harmonic a.c. "polarograms": total current amplitude *versus* d.c. potential (conventional second harmonic a.c. polarogram), phase angle *versus* d.c. potential (second harmonic phase angle polarogram) and the complex plane response *versus* d.c. potential (second harmonic complex plane polarogram). The magnitude of the independent variable, $E_{d.c.}$, is indicated by markers in the complex plane polarograms which simultaneously represent changes in three variables. Implicit in the complex plane polarograms are still other types of experimentally feasible forms of data readout—*e.g.*, plots of the

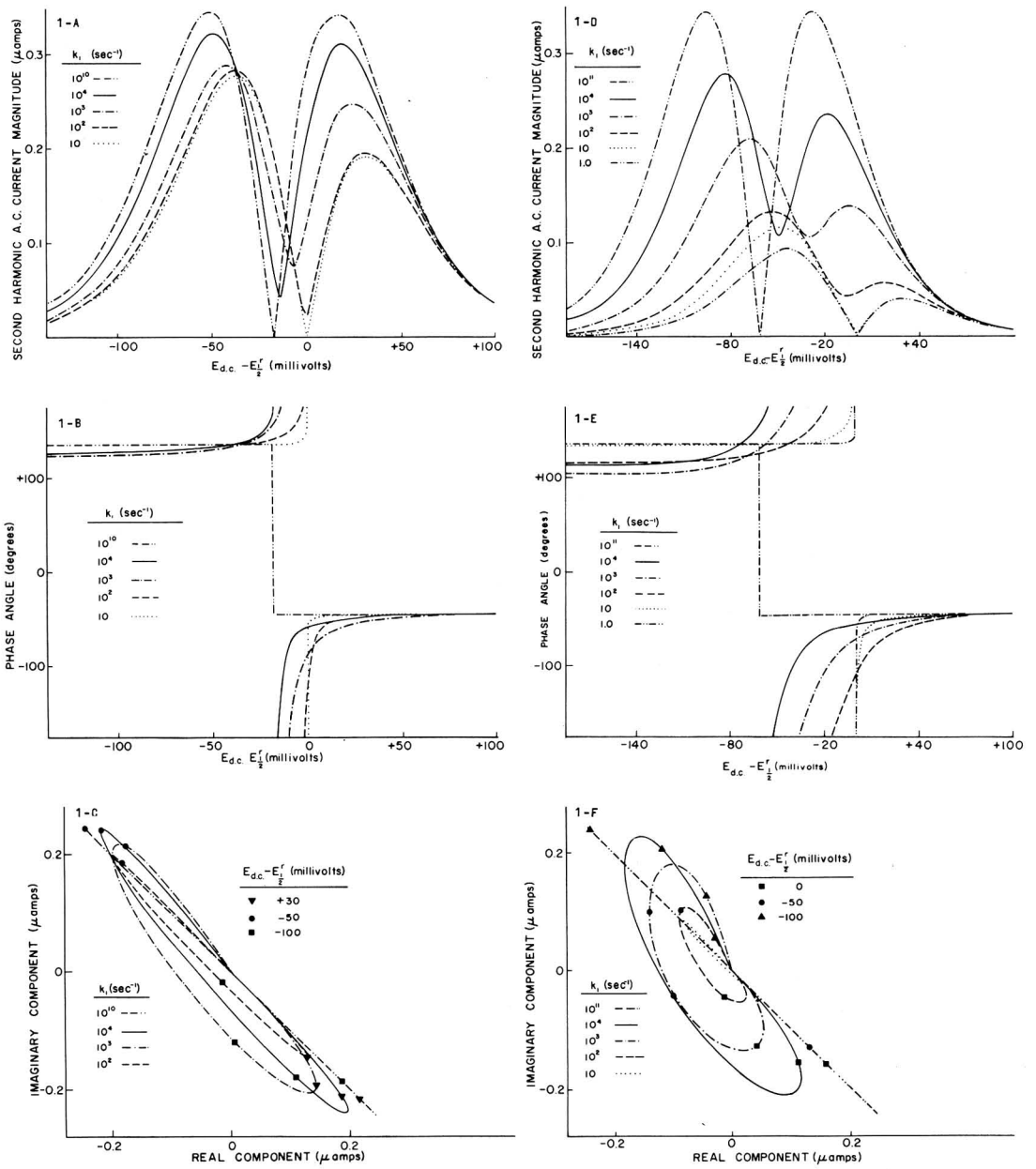

Fig. 1. Second harmonic a.c. polarographic response *vs.* d.c. potential with nernstian system. (A,D) Conventional second harmonic a.c. polarograms, (B,E) second harmonic phase angle polarograms, (C,F) second harmonic complex plane polarograms.
Parameter values: $n=1$, $T=298°\mathrm{K}$, $A=0.035\ \mathrm{cm}^2$, $\Delta E=5.00\ \mathrm{mV}$, $C_{\frac{1}{2}}^{*}=1.00\times10^{-3}\ M$, $D_O=D_R=1.00\times10^{-5}\ \mathrm{cm}^2\ \mathrm{s}^{-1}$, $k_s=\infty$, $\omega=6.28\times10^2\ \mathrm{s}^{-1}$, $f=1$, k_1 values shown in figure $[k=k_1(K^{-1}+1)]$; (A, B, C) $K=1.00$, $t=12.0\ \mathrm{s}$; (D, E, F) $K=0.100$, $t=6.0\ \mathrm{s}$.

TABLE 1

COMPILATION OF IMPORTANT SPECIAL CASES

Special case	*Mathematical condition*	
1. Chemical equilibrium exists in the d.c. sense	$\frac{\lambda_p}{(1+e^J)Kk^{\frac{1}{2}}} \ll 1$	(1A)
2. Chemical equilibrium exists in the a.c. sense	$\frac{K^{-1}}{(1+e^J)}\left[\frac{(1+h^2)^{\frac{1}{2}}\pm h}{1+h^2}\right]^2 \ll 1$	(1B)
3. Nernstian conditions (equilibrium with respect to the heterogeneous charge transfer step) prevail in the d.c. sense	$\frac{\lambda_p}{(1+e^J)Kk^{\frac{1}{2}}} \gg 1$	(1C)
4. Nernstian conditions prevail in the a.c. sense	$\frac{2\omega^{\frac{1}{2}}}{\lambda_p} \ll 1 + \frac{K^{-1}}{(1+e^J)}\left[\frac{(1+h^2)^{\frac{1}{2}}+h}{1+h^2}\right]^{\frac{1}{2}}$	(1D)
5. Chemical reaction rate constant greatly exceeds angular frequency of applied alternating potential—*i.e.* $k \gg \omega$	$\left[\frac{(1+h^2)^{\frac{1}{2}}-h}{1+h^2}\right]^{\frac{1}{2}} = \left[\frac{(1+g^2)^{\frac{1}{2}}-g}{1+g^2}\right]^{\frac{1}{2}} \cong 0$	(1E)
	and $\left[\frac{(1+h^2)^{\frac{1}{2}}+h}{1+h^2}\right]^{\frac{1}{2}} \cong \left(\frac{2}{h}\right)^{\frac{1}{2}}$	(1F)
	and $\left[\frac{(1+g^2)^{\frac{1}{2}}+g}{1+g^2}\right]^{\frac{1}{2}} \cong \left(\frac{2}{g}\right)^{\frac{1}{2}}$	(1G)
7. Chemical reaction rate is much smaller than the applied angular frequency so that the chemical reaction is kinetically inoperative in the a.c. sense—*i.e.* $k \ll \omega$	$\left[\frac{(1+h^2)^{\frac{1}{2}}\pm h}{1+h^2}\right]^{\frac{1}{2}} = \left[\frac{(1+g^2)^{\frac{1}{2}}\pm g}{1+g^2}\right]^{\frac{1}{2}} \cong 1$	(1H)

real or imaginary second harmonic current components *versus* d.c. potential (phase-selective second harmonic a.c. polarograms[25]).

A. Nernstian conditions

Results for the case where k_s is sufficiently large that nernstian conditions prevail in the a.c. and d.c. sense will be surveyed first. It represents a special case which is likely to be encountered frequently in experimental work at low and intermediate frequencies. In addition, a pedagogical advantage attends the examination of predictions for the nernstian case because the effects of the preceding chemical reaction are readily demonstrated without the obscuring influence of charge transfer kinetic effects.

Various manifestations of a preceding chemical reaction on the second harmonic response are illustrated in Figs. 1 and 2. The curves show the effect of chemical reaction rate on current amplitude, phase angle and complex plane polarograms for three values of the equilibrium constant K ($K=1$, 10^{-1}, 10^{-2}). All other parameters are held constant and are of typical magnitude. The frequency employed, 100 Hz, is at least two orders of magnitude below the upper limit at which second harmonic measurements can be made with modern instrumentation[27]. Thus, the frequency considered in Figs. 1 and 2 is on the low side of the accessible frequency spectrum.

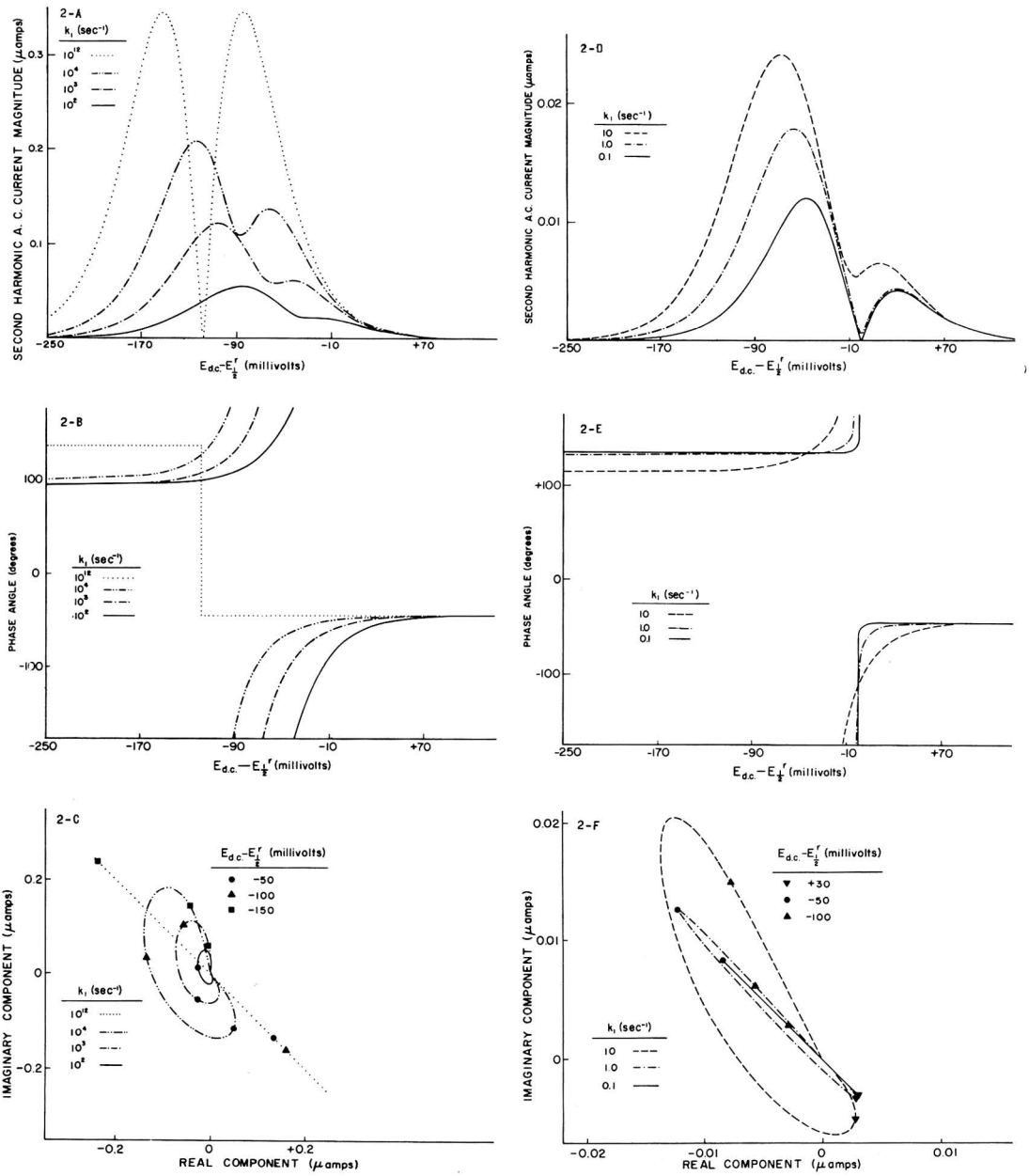

Fig. 2. Second harmonic a.c. polarographic response *vs.* d.c. potential with nernstian system: all parameters and notation same as Fig. 1, except $K = 1.00 \times 10^{-2}$, $t = 6.00$ s, and k values given in figure.

An important frame of reference to apply in evaluating these results is the well-known second harmonic response with a strictly diffusion-controlled process. In this limiting case the current amplitude polarogram is characterized by two symmetrical peaks separated by a zero-current minimum. The phase angle polarogram is a step function where the phase angle jumps discontinuously from $-45°$ (anodic potentials) to $+135°$ (cathodic potentials) at the $E_{d.c.}$ value where the current amplitude becomes zero. The diffusion-controlled complex plane polarogram is a straight line of -1 slope. For the nernstian case under consideration, diffusion-controlled conditions arise either when the preceding reaction is reversible and sufficiently rapid that chemical equilibrium exists in the d.c. and a.c. sense ($k \rightarrow \infty$), or when the chemical reaction is effectively inoperative ($k \rightarrow 0$ or $K \gg 1$). Polarograms for the largest k-value in each of the three sets of curves ($K = 1, 10^{-1}, 10^{-2}$) in Figs. 1 and 2 correspond to the former diffusion-controlled situation (chemical equilibrium). In this case the current amplitude becomes zero and the phase angle transition occurs at the potential $E_{d.c.} = E^{rc}_{\frac{1}{2}}$ (see eqn. 28). The diffusion-controlled responses for an inoperative chemical reaction are not shown, but are identical to the polarograms for the chemical equilibrium case except that: (1) they are centered about the potential $E_{d.c.} = E^{r}_{\frac{1}{2}}$, rather than $E_{d.c.} = E^{rc}_{\frac{1}{2}}$ and (2) the current magnitudes are proportional to C^*_O, rather than the sum $C^*_O + C^*_Y$.

Between these two extremes, the influences of the preceding chemical reaction on the second harmonic behavior are profound, as the data of Figs. 1 and 2 attest. Analogs of some of the effects shown are found in the fundamental harmonic response. For example, the current amplitude decreases monotonically with decreasing k value, while the whole wave shifts anodically, the minimum moving from $E^{rc}_{\frac{1}{2}}$ to $E^{r}_{\frac{1}{2}}$. Also, smaller equilibrium constants accentuate chemical kinetic effects, a phenomenon common to all voltammetric techniques. For $K \leqq 0.01$, the second harmonic response shows sensitivity to k_2 values characteristic of collision controlled processes ($k_2 = 10^{11}$–10^{12} s^{-1}) with experimentally accessible frequencies (*e.g.* $\omega = 10^5$ s^{-1})[24].

Other aspects of the second harmonic response shown in Figs. 1 and 2, such as the symmetry of the current amplitude polarogram, the shapes of the phase angle and complex plane polarograms, etc., also are illustrative of the substantial effects of the preceding chemical reaction. The loss of the current amplitude polarogram's symmetry as the chemical kinetic contribution becomes more important is one of the more obvious and useful diagnostic tools. Although kinetic influence of the preceding chemical reaction suppresses both peaks of the current amplitude polarogram, the anodic peak is attenuated significantly more than the cathodic peak. Grossly unsymmetrical polarograms result. With sufficiently small K values, the anodic peak can be suppressed to the point that it becomes merely a shoulder on the larger cathodic peak (*e.g.* Fig. 2A for $k_1 = 10^2$ s^{-1}). The qualitative observation of such asymmetric second harmonic current amplitude polarograms is indicative of a homogeneous chemical reaction preceding the charge transfer step, although more careful, quantitative data analysis is required to establish that the simple, single-step, first-order chemical reaction (mechanism R1) is operative. Higher-order or multi-step preceding chemical reactions also are expected to produce qualitatively similar results. The fact that the anodic peak is more sensitive to chemical kinetic effects clearly suggests that the best estimates of the chemical kinetic parameters from current measurements usually will result from measurements of the anodic peak current. It

should be recalled that with a chemical reaction *following* the charge transfer step, a similar current amplitude polarogram asymmetry arises, but of opposite direction—*i.e.* the anodic peak is larger[28].

The fact that second harmonic currents are more sensitive to effects of the preceding chemical reaction at anodic potentials is somewhat unusual and interesting, considering the fact that with many voltammetric responses (*e.g.* d.c. polarographic currents, fundamental harmonic a.c. polarographic currents and phase angles), greater sensitivity to such chemical kinetic effects is found on the cathodic side of the wave. In fact even the second harmonic phase angle exhibits the "normal" type of behavior—*i.e.* phase angle deviations from the diffusion-controlled limit induced by the preceding chemical reaction are greater at the cathodic extremity of the wave. The explanation of this unusual behavior of the current amplitude response is analogous to that advanced for the case of the following reaction[28] where a similar "backwards" result is obtained for the effect of $E_{d.c.}$ on the chemical reaction's contribution to the current amplitude.

One of the most interesting and important features of the predicted second harmonic current amplitude polarogram with nernstian systems is the behavior of the minimum between the peaks. Figures 1 and 2 show that under many conditions the current magnitude at the minimum is zero or nearly zero. Furthermore, whenever it is characterized by a null current signal, the minimum occurs either at $E_{d.c.} = E^{r}_{\frac{1}{2}}$ or $E_{d.c.} = E^{rc}_{\frac{1}{2}}$. The former ($E_{d.c.} = E^{r}_{\frac{1}{2}}$) corresponds to the high frequency limit where $k/\omega \ll 1$ and is usually associated with an asymmetric current amplitude polarogram (see Figs. 1 and 2—smallest k values). At the low frequency limit ($k/\omega \gg 1$), $E_{d.c.} = E^{rc}_{\frac{1}{2}}$ and a symmetrical second harmonic polarogram is observed. This implies that if a null or near-null current is observed at the minimum, one immediately knows that the potential of the minimum is given by $(E_{d.c.})_{min} = E^{r}_{\frac{1}{2}}$ or $(E_{d.c.})_{min} = E^{rc}_{\frac{1}{2}}$. The symmetry of the current amplitude polarogram allows one to decide which of the two possibilities is applicable. The chances that one will encounter conditions where the minimum indicates the value of $E^{r}_{\frac{1}{2}}$ or $E^{rc}_{\frac{1}{2}}$ within the usable frequency spectrum is actually more favorable than implied by the limiting conditions, $k \ll \omega$ and $k \gg \omega$. Examination of the relevant equations and computational results shows that a more precise statement of the low frequency limit for the minimum is

$$(E_{d.c.})_{min} = E^{rc}_{\frac{1}{2}} \tag{44}$$

if

$$k/\omega > (10/K)^2 \tag{45}$$

The corresponding statement for the high frequency limit is

$$(E_{d.c.})_{min} = E^{r}_{\frac{1}{2}} \tag{46}$$

if

$$k/\omega < 0.2 \tag{47}$$

The origin of the null current minimum can be explained in the same manner as for the following reaction case[28].

From calculations of ω values appropriate to the high and low frequency limits for various combinations of K and k, it is evident that normally only one of these limiting cases will be observed within the presently accessible frequency spectrum. Nevertheless, the ability to determine either $E^{r}_{\frac{1}{2}}$ or $E^{rc}_{\frac{1}{2}}$ simply from the

minimum on the second harmonic current amplitude polarogram with nernstian systems has important implications. This possibly, by itself, will often represent sufficient stimulus to perform the second harmonic experiment because the acquisition of one of these important pseudo-thermodynamic parameters represents a very important step in the kinetic-mechanistic analysis of voltammetric data.

Phase angle polarograms depicted in Figs. 1 and 2 illustrate the marked sensitivity of this observable to the kinetic status of the preceding chemical reaction. Noteworthy features are the influence of the chemical reaction on the shape of the phase angle polarogram and on the limiting value of the phase angle at very cathodic potentials. Careful inspection of these results shows that whenever the second harmonic current amplitude polarogram exhibits a zero current minimum, the phase angle polarogram is essentially identical to the diffusion-controlled counterpart, even when the current amplitude is substantially influenced by the chemical reaction. In effect, this implies that the second harmonic phase angle is uninfluenced by the chemical reaction when the latter is kinetically unimportant in the a.c. sense—*i.e.* when $k \gg \omega$ or $k \ll \omega$. This behavior parallels that observed for the fundamental harmonic phase angle[10,11,24]. Under such circumstances, phase angle data are of little direct use in obtaining chemical rate parameters. Like the minimum on the current amplitude polarogram, the sharp discontinuity of the phase angle polarogram in the low and high frequency limits serves as an indicator for $E_{\frac{1}{2}}^{rc}$ and $E_{\frac{1}{2}}^{r}$.

The complex plane polarograms of Figs. 1 and 2 represent a composite of the current amplitude and phase angle responses discussed above. It is apparent that their shape in the frequency range intermediate between the high and low frequency limits is distinctive and sensitive to the variations in the kinetic parameters of the chemical reaction. The complex plane polarograms reveal an interesting point: the first quadrant and the adjacent one-half of the fourth quadrant are never traversed by the current vector, at least for the nernstian situation under consideration. This sector is shifted 180° from a similar sector predicted for the following chemical reaction mechanism[28].

Figure 3 illustrates some effects of the preceding chemical reaction on the frequency response of the second harmonic currents at the anodic and cathodic peaks for $K = 1.0, 0.1$ and 0.01. The largest k value in each plot represents the diffusion-controlled limit where $k \gg \omega$ at all frequencies and produces the expected linear response. At the other extreme where $k \ll \omega$ at all frequencies, *i.e.*, where the chemical reaction is kinetically inoperative in the a.c. sense, a linear response is also found and is illustrated by the smallest k value in each plot. Figure 3 shows that the frequency response can become decidedly non-linear with intermediate rate constants. As one would expect in light of the data shown in Figs. 1 and 2, the frequency response of the anodic peak shows more sensitivity to kinetic influences of the preceding chemical reaction than the cathodic peak, with the slight exception of the smallest k values. Although quite sensitive to the effects of the preceding chemical reaction, the current amplitude frequency response by itself is not particularly useful for mechanistic diagnosis, as other mechanisms yield results of a similar nature[16,19,28]. However, once the mechanism has been established with reasonable certainty, experimental frequency response behavior can be useful for establishing quantitatively the rate parameter k.

The predicted dependences of several observables as a function of the di-

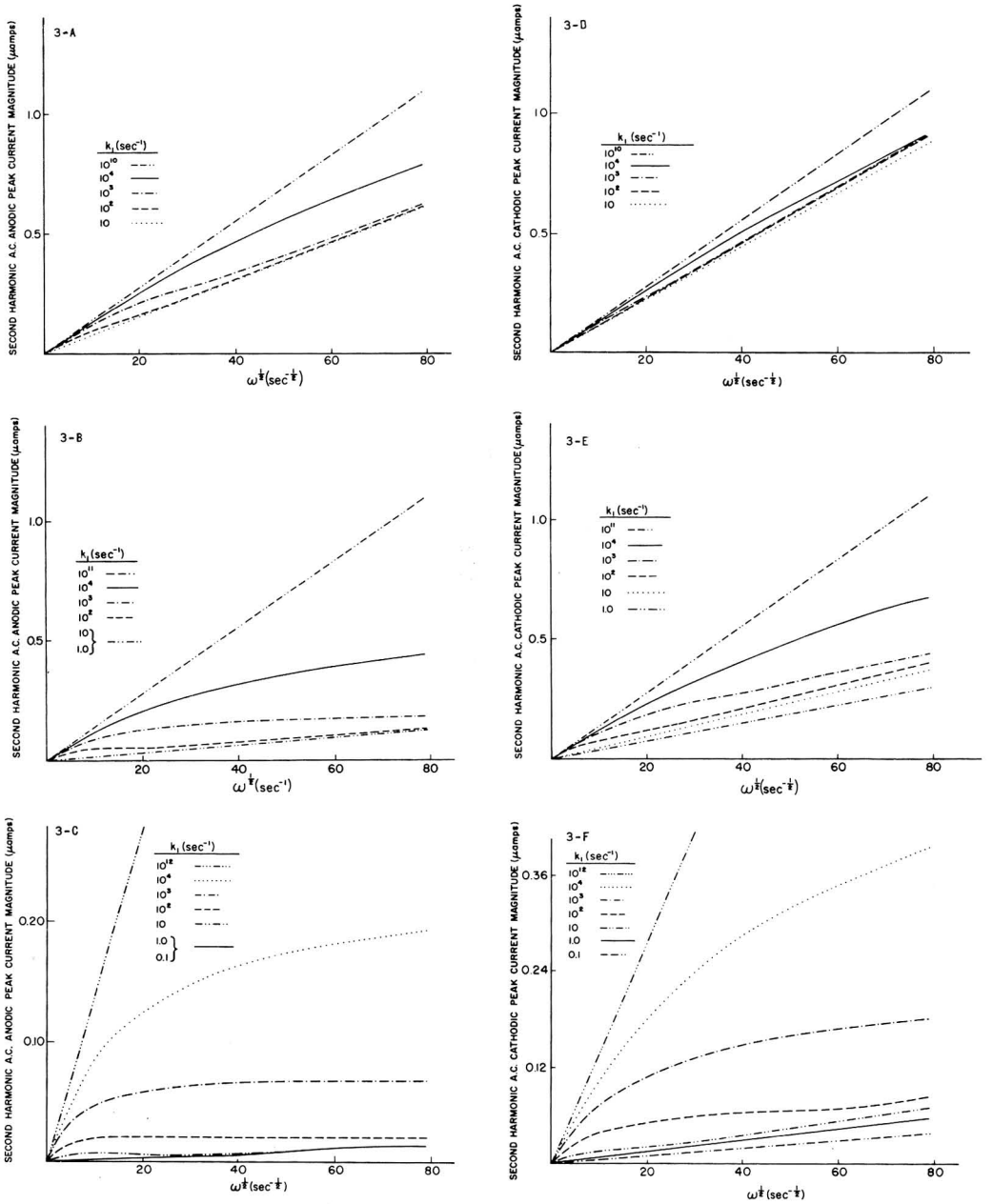

Fig. 3. Frequency dependence of second harmonic current amplitude at anodic and cathodic peaks with nernstian system: all parameters same as Fig. 1, except ω given by abscissa, k_1 values shown in figure, and (A, D) $K = 1.00$, $t = 12.0$ s; (B, E) $K = 0.100$, $t = 6.00$ s; (C, F) $K = 1.00 \times 10^{-2}$, $t = 6.00$ s.

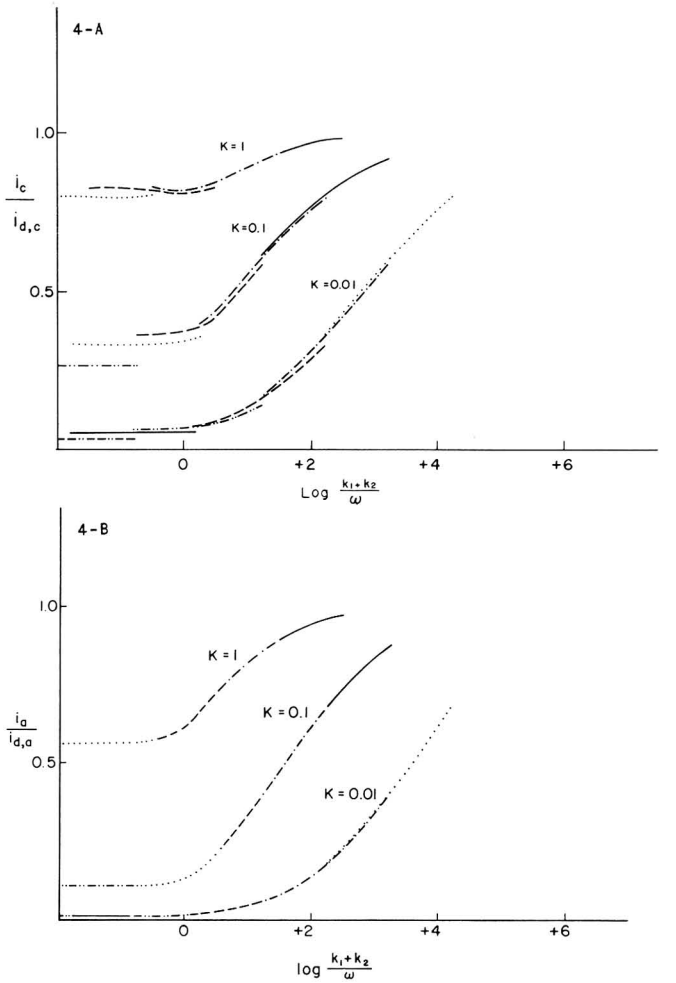

Fig. 4. Dependence of second harmonic cathodic and anodic peak current ratios ($i_c/i_{d,c}$ and $i_a/i_{d,a}$) on log (g) with nernstian behavior: all parameter values same as Fig. 1, except K values given in figure and key for k values corresponds to Fig. 3.

mensionless kinetic parameter g [$g = (k_1 + k_2)/\omega$] are shown in Figs. 4 and 5 for $K = 1.0$, 0.1, and 0.01. The curves were constructed from the theoretical equations by selecting a particular k value and varying ω. For each k value, only those values of k/ω corresponding to realistic ω values were considered. Thus, the relevant figures establish the general range where experimental data are likely to fall in such plots with particular k values. As expected, the characteristics of the various curves depend markedly on the equilibrium constant K. In addition, it is important to note that, even for a particular K value, the predicted variations of such observables in general do not lie on a single continuous curve, but depend on the k value in question unless k is sufficiently large. This effect arises from the previously mentioned duality in the time scale operative in the a.c. polarographic experiment. Unless the d.c. process is diffusion-controlled, g is not a unique kinetic parameter in determining the kinetic contribution

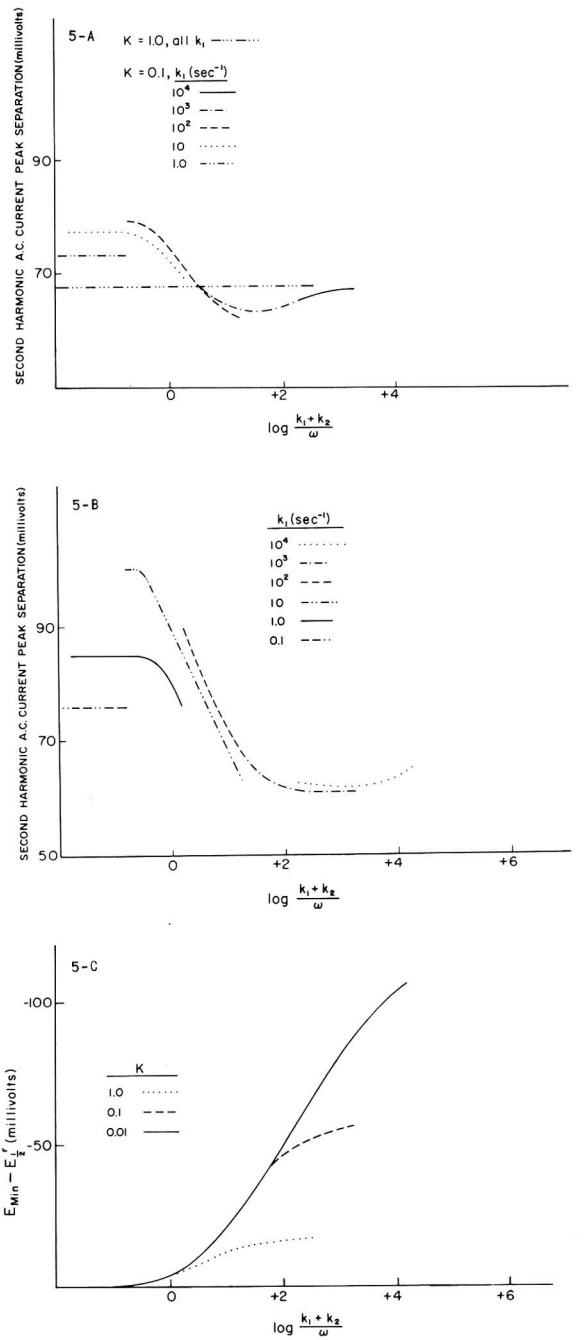

Fig. 5. Working curves of various second harmonic observables *vs.* log (g) with nernstian system: all parameters same as Fig. 1 except ω values in abscissa argument and (A) $K = 1.00$, $K = 0.100$; (B) $K = 1.00 \times 10^{-2}$; (C) K values given in figure.

of the coupled chemical reaction. Rather, it shares a role with the parameter which is a measure of the chemical kinetic contributions in the d.c. sense, $(1+e^{J})K(kt)^{\frac{1}{2}}$. Two notable exceptions are found in Figs. 4-B and 5-C where the observables in question are independent of the status of the d.c. process for essentially all values of k—*i.e.* g alone is the determining parameter. The fact that d.c. dependence is not observed in Fig. 4-B is due to the large value of J at potentials where the anodic peak occurs, *i.e.* the d.c. dependence of the preceding reaction is kinetically unimportant at these potentials. A corresponding situation is not found for the following chemical reaction mechanism[28]. However, the somewhat surprising d.c. independence of the

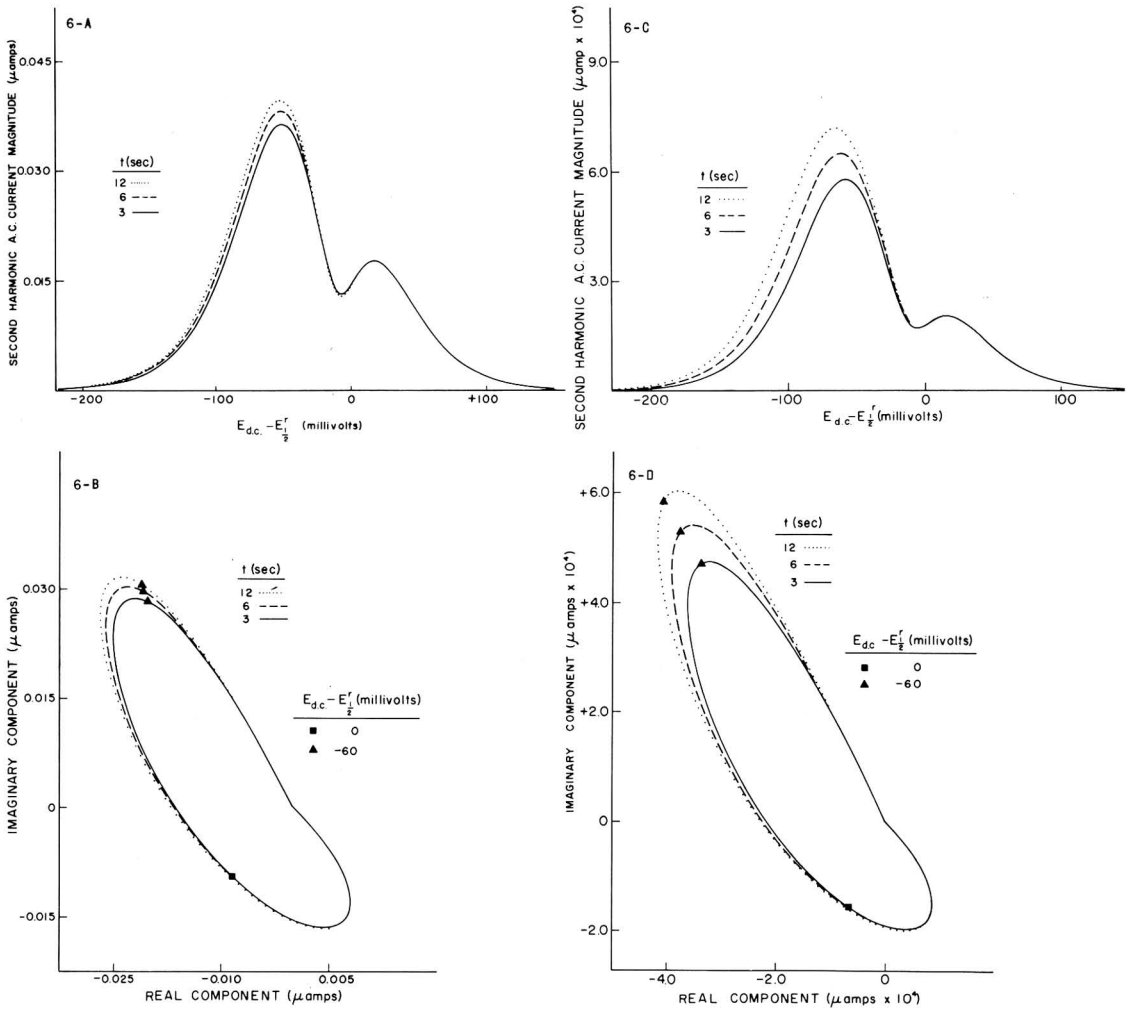

Fig. 6. Drop life dependence of second harmonic a.c. polarograms with nernstian system: (A, C) conventional second harmonic a.c. polarograms, (B, D) second harmonic complex plane polarograms.
All parameters same as Fig. 1 except t values shown in figure and (A, B) $K=0.100$, $k_1=1.00\ s^{-1}$; (C, D) $K=1.00\times10^{-3}$, $k_1=1.00\times10^{-2}\ s^{-1}$.

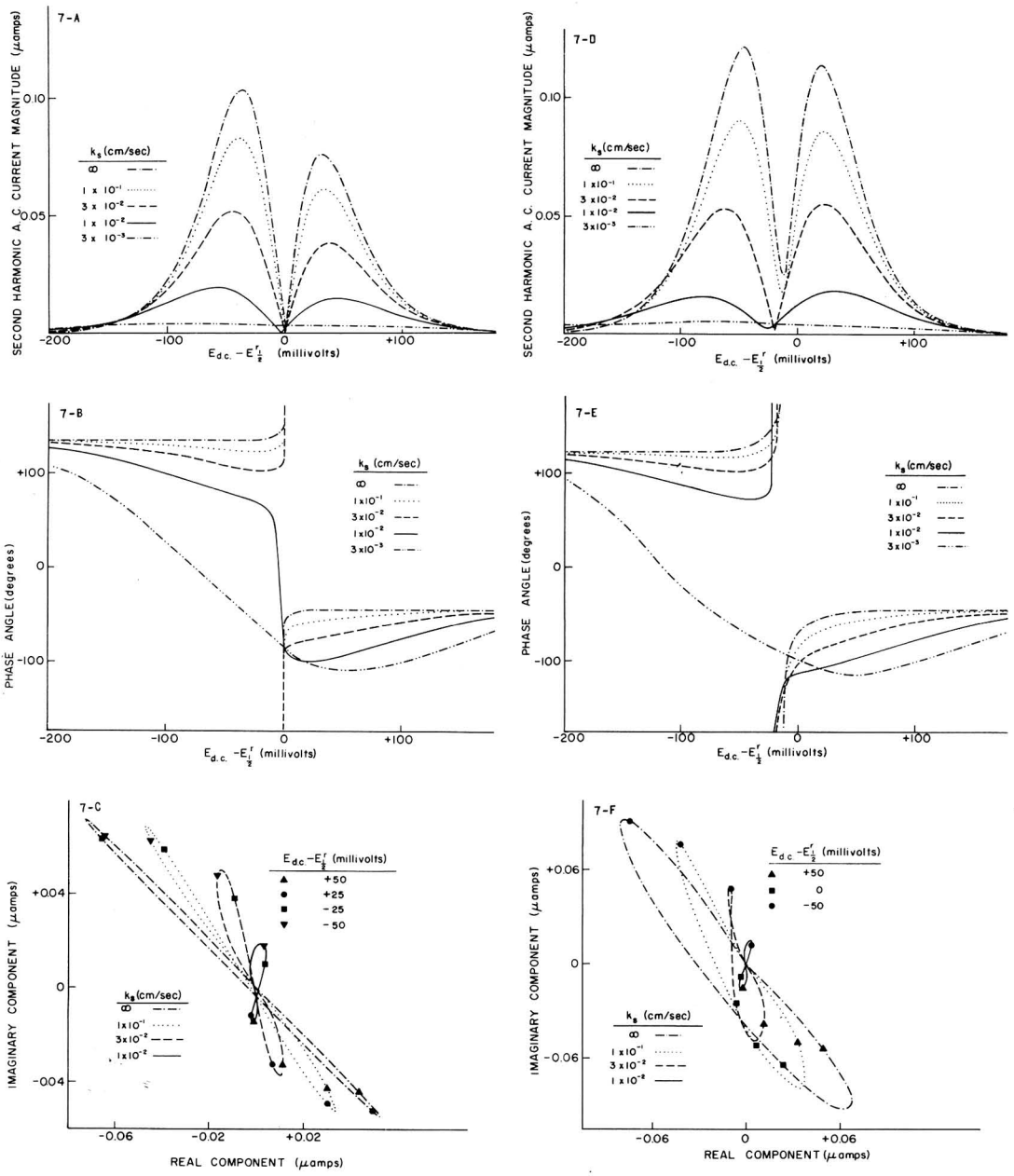

Fig. 7. Second harmonic a.c. polarographic response *vs.* d.c. potential with non-nernstian systems: all parameters and notation same as Fig. 1, except $\omega = 1.00 \times 10^2\ s^{-1}$, $K = 1.00$, $t = 3.00$ s, k_s values given on figure, $\alpha = 0.500$, and (A, B, C) $k_1 = 5.00\ s^{-1}$, (D, E, F) $k = 5.00 \times 10^2\ s^{-1}$.

potential of the minimum, Fig. 5-C, is also found in the following chemical reaction case. Clearly, of the working curves considered in Figs. 4 and 5, those represented by Figs. 4-B and 5-C are preferable for initial data analysis. In favorable circumstances one may obtain both k and K by comparing plots of any experimental quantity considered in Figs. 4 and 5 *versus* $\log \omega^{-1}$ with the appropriate theoretical working curve. The apparent K value of the system under investigation is the one whose theoretical working curve best matches the corresponding experimental plot in shape and magnitude of the experimental quantity. The separation of these matched and theoretical working curves on the abscissa yields the k value (separation $= \log k$). In many cases such an approach will provide only a fair estimate of the k and K values and further data refinement by detailed comparison of theoretical polarograms with experiment is advocated[21].

Kinetic influence of a following chemical reaction on the d.c. process gives rise to a dependence of the a.c. polarographic response on the mercury drop life (*i.e.* on the mercury column height)[13]. The magnitude of this effect on the second harmonic response with nernstian systems is depicted in Fig. 6. The results are rather similar to those predicted for the fundamental harmonic response[13]. The magnitude of the drop life dependence increases with decreasing K, although not as much as in the following chemical reaction mechanism, and the direction of the effect is positive—*i.e.* increasing drop life increases the current. The effect can be significant for small K values (Fig. 6-C) and must be considered in any quantitative analysis of experimental data. One should note that the drop life dependence of the complex plane polarograms of Fig. 6 reflects only a time dependence of the current amplitude, not the phase angle. The fact that the phase angle is independent of drop life is shown by the behavior of the d.c. potential markers on the complex plane polarograms. The markers for a particular d.c. potential with different drop lives describe a straight line through the origin, indicating constancy of phase angle. This type of behavior, which reflects the phase angle's independence of the kinetic status of the d.c. process, is predicted for the fundamental harmonic phase angle under all conditions with the mechanism in question. However, the second harmonic phase angle can become drop life dependent when non-nernstian conditions prevail (see below), a property which makes this observable useful for detecting the existence of non-nernstian behavior.

B. Non-nernstian conditions

The existence of kinetic influence by the heterogeneous charge transfer step, on top of that due to the preceding chemical reaction and diffusion is expected to complicate notably the second harmonic behavior. Our calculations have confirmed that the magnitude and nature of the predicted kinetic manifestations of the preceding chemical reaction are altered significantly by a slow heterogeneous charge transfer step. Figures 7–13 provide a sampling of calculational results which illustrate the most significant trends associated with the onset of kinetic influence by slow charge transfer.

Figures 7 and 8 illustrate some of the alterations on the second harmonic current amplitude, phase angle and complex plane polarograms induced by slow charge transfer. A wide range of k_s values is considered in combination with a single value of the charge transfer coefficient, α ($\alpha = 0.500$). Because theoretical expectations[29] and experimental evidence seem to suggest that charge transfer coefficient values

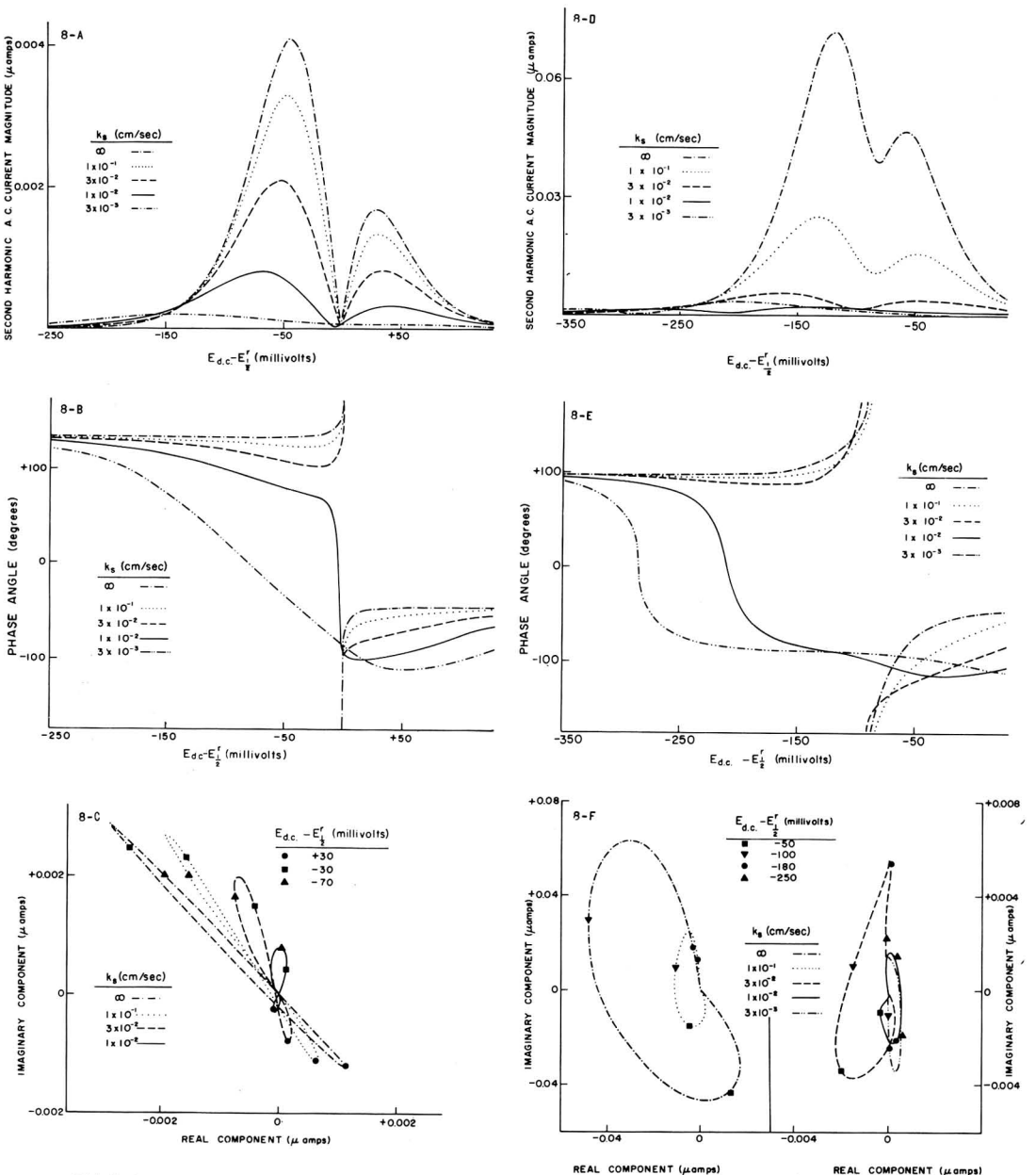

Fig. 8. Second harmonic a.c. polarographic response *vs.* d.c. potential with non-nernstian systems: all parameters and notation same as Fig. 7, except $K = 1.00 \times 10^{-2}$, k_s values given on figure and (A, B, C) $k_1 = 0.100\ s^{-1}$, (D, E, F) $k_1 = 1.00 \times 10^3\ s^{-1}$.

close to 0.5 will predominate, the presentation of results for this single α value is not unduly restrictive. For the chemical reaction, K values of 1.00 (Fig. 7), and 1.00×10^{-2} (Fig. 8) are considered.

A number of the illustrated effects of slow heterogeneous charge transfer are those one would anticipate from the behavior of the simple quasi-reversible system[19]

$$O + ne \overset{k_s, \alpha}{\rightleftharpoons} R \qquad \text{(R2)}$$

For example, accompanying reduction in k_s is a reduction of the current magnitude, a reduction of phase angles (ϕ becomes less positive), and a shift in current amplitude and phase angle waves to more cathodic potentials. One should note that in both figures under consideration, the contribution of charge transfer kinetics is significant even for k_s values as large as 10^{-1} cm s^{-1}, despite the relatively low frequency utilized in the calculations. While the presence of a large charge transfer rate, *e.g.* 10^{-1} cm s^{-1}, is not readily apparent experimentally from the current magnitude data, the approximate figure-eight appearance of the complex plane polarogram in Figs. 7-C and 8-C and the narrowness and pitch of the upper portion of the complex plane polarogram in Figs. 7-F and 8-F indicate its presence.

The expected types of kinetic interactions between the preceding chemical reaction and heterogeneous charge transfer become evident upon careful perusal of the figures. For example, a comparison of Figs. 8-A and 8-D (or Figs. 8-B and 8-E) clearly shows that the slower the preceding chemical reaction, the less important the contributions of heterogeneous charge transfer, and *vice versa*. For a given k_s ($\neq \infty$), the current amplitude polarograms of Fig. 8-D ($k_1 = 10^3$ s^{-1}) exhibit substantially greater influence of the charge transfer step than those of Figs. 8-A ($k_1 = 0.10$ s^{-1}). Actually, the effects of slow charge transfer are enhanced in the former case relative to what one finds with the simple quasi-reversible case[19]. This type of effect has been discussed at greater length elsewhere[13,24,28]. Just as the existence of the preceding chemical reaction influences the kinetic contribution of the heterogeneous charge transfer step, a reciprocal effect is also evident, as one would expect. A sufficiently slow charge transfer step tends to suppress the importance of the preceding chemical reaction as a factor controlling the second harmonic response. For sufficiently small k_s values (usually $k_s < 10^{-3}$ cm s^{-1}), manifestations of the preceding chemical reaction may be completely eliminated. For example, the current amplitude and phase angle responses with the smallest k_s values in Figs. 7 and 8 approach those predicted by the theory for a simple quasi-reversible process[19]. Most certainly these polarograms for small k_s do not remotely resemble their nernstian counterparts.

One of the second harmonic observables which tends to preserve its nernstian characteristic to smaller k_s values than most is the position of the current amplitude minimum on the d.c. potential coordinate, whose importance was described above. For the conditions in Figs. 7-A, 7-D, and 8-A it is evident that this parameter can remain unaltered for the case under consideration ($\alpha = 0.50$) to relatively small k_s values.

The effects of non-nernstian behavior on the peak current amplitude *vs.* frequency profiles are shown in Figs. 9 and 10. These results illustrate that the importance of slow charge transfer kinetics is enhanced as the frequency increases. The ultimate result is a frequency-independent limiting value at high frequencies, rather

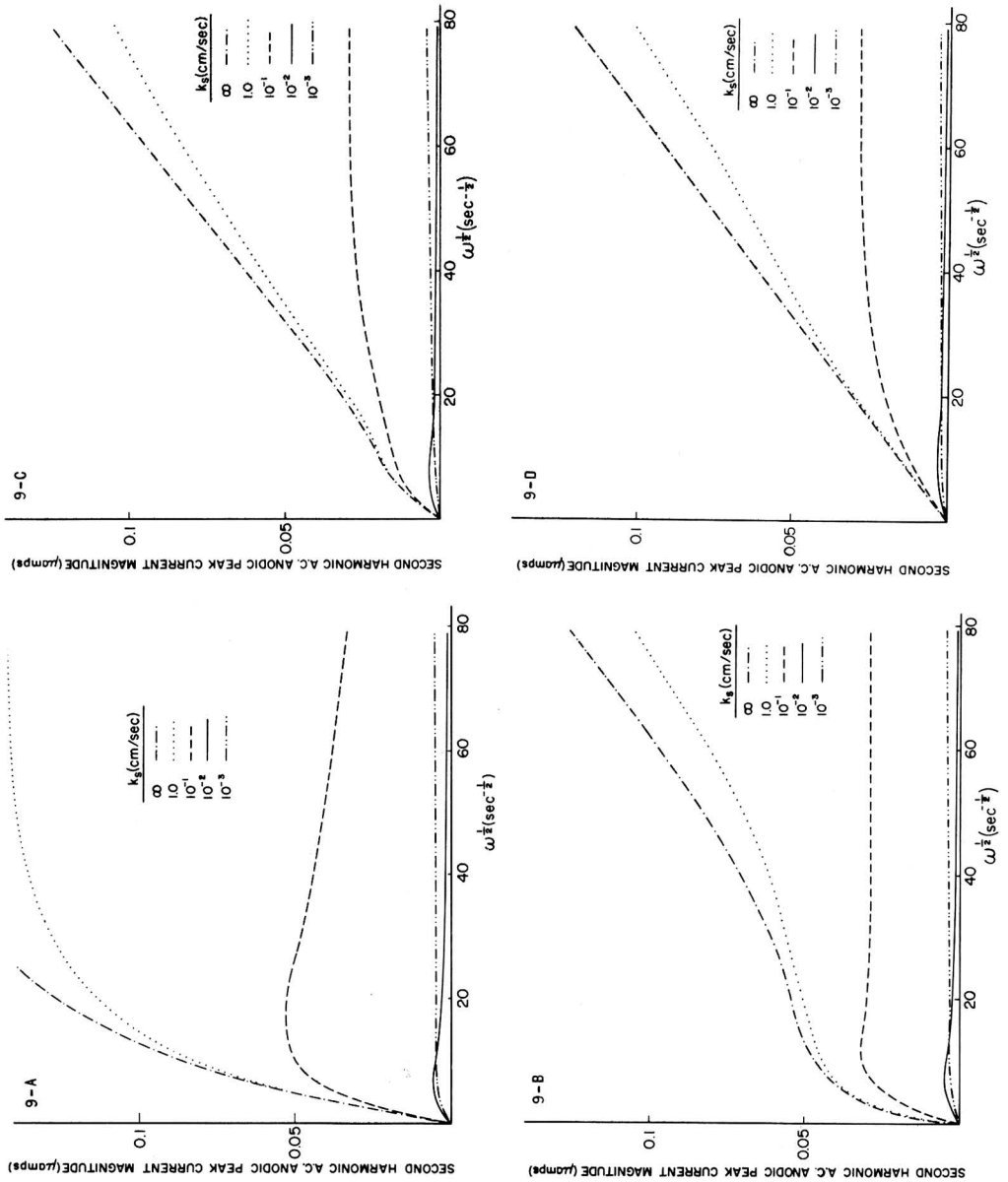

Fig. 9. Frequency dependence of second harmonic current amplitude at anodic peak with non-nernstian systems: all parameter values same as Fig. 1 except ω which is given by abscissa, $K=0.100$, $t=6.00$ s, $\alpha=0.500$, and $k_1=$(A) 1.00×10^3, (B) 1.00×10^2, (C) 1.00×10, (D) 1.00 s^{-1}.

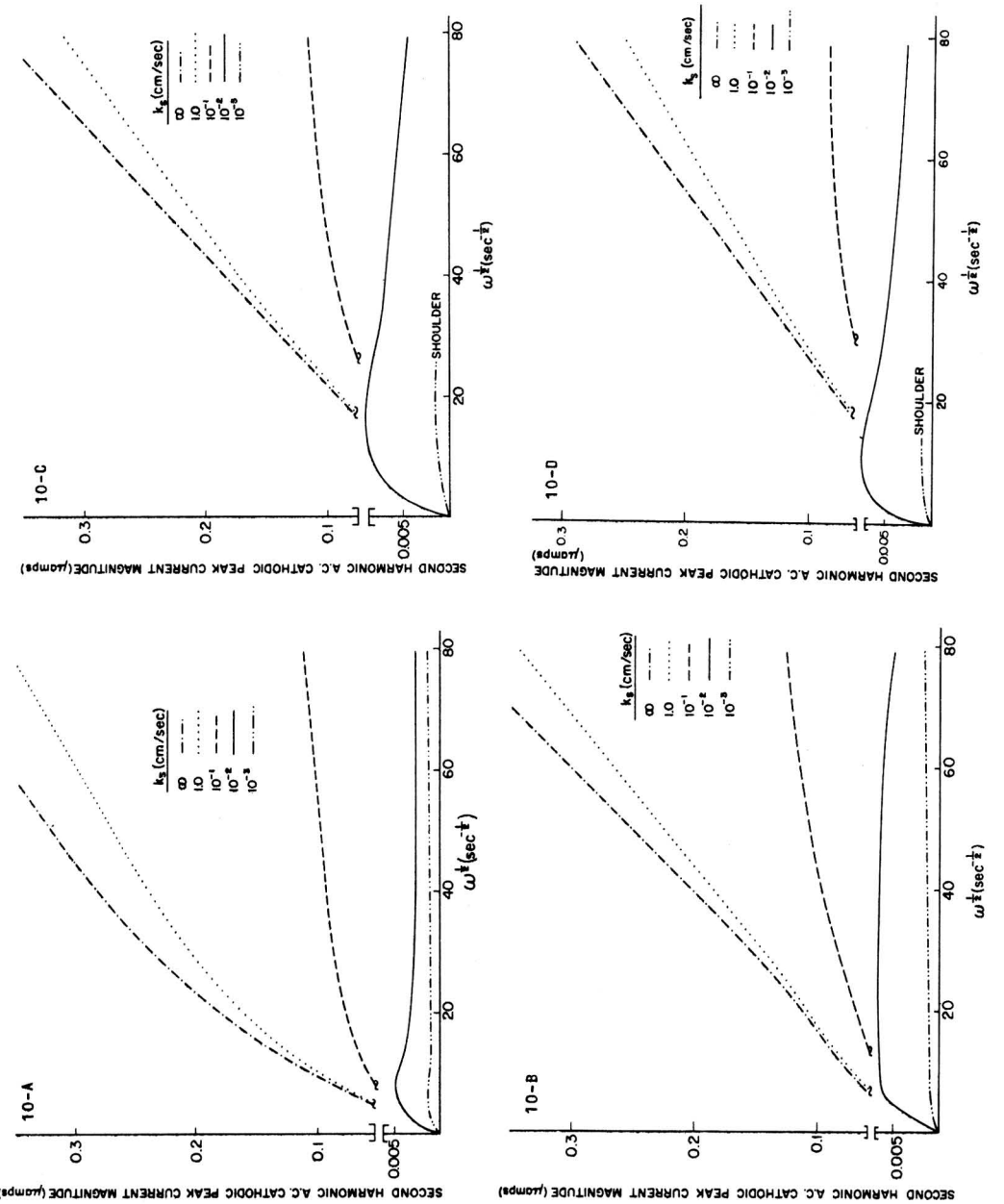

Fig. 10. Frequency dependence of second harmonic current amplitude at cathodic peak with non-nernstian systems: all parameters and notation same as Fig. 9.

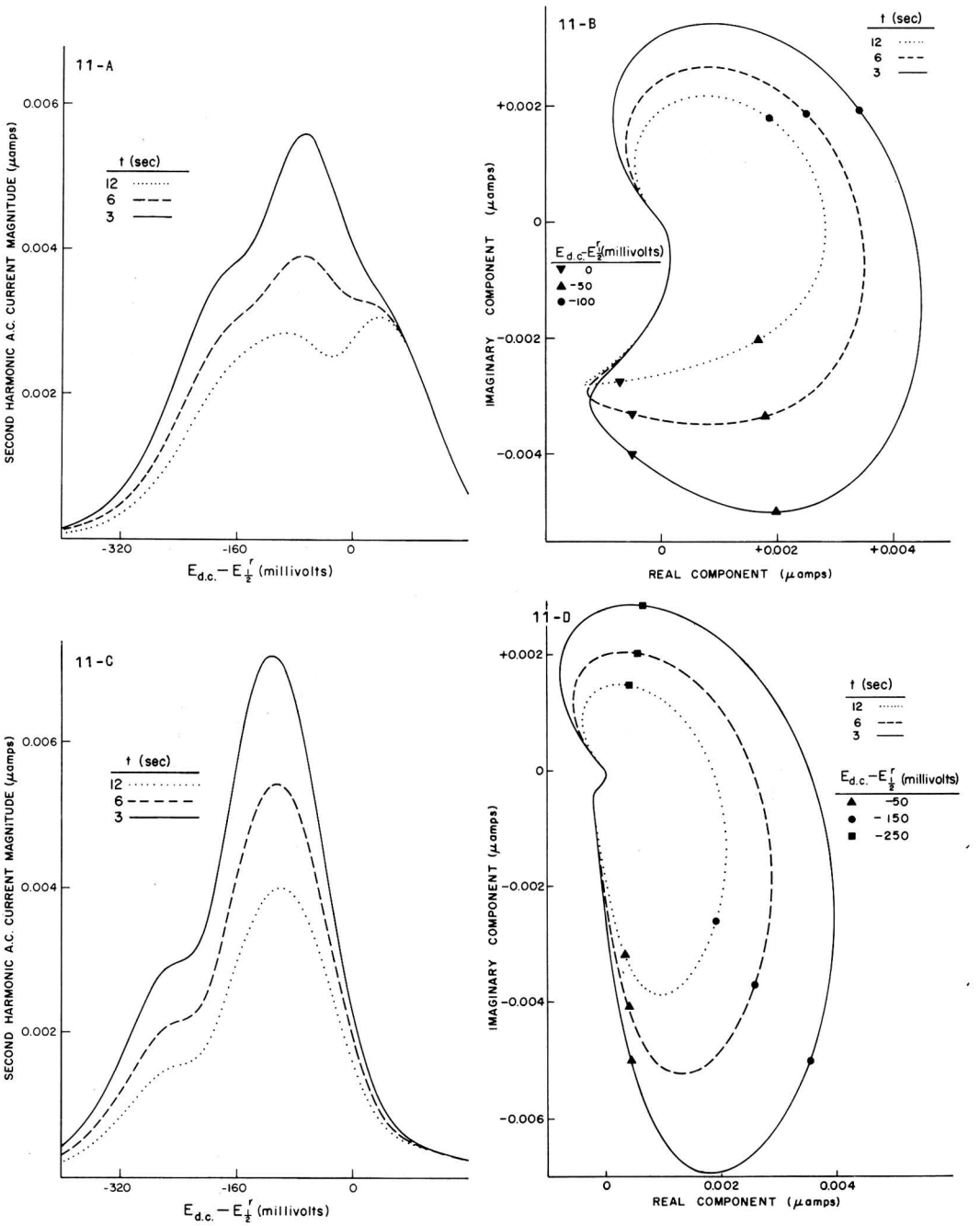

Fig. 11. Drop life dependence of second harmonic a.c. polarograms with non-nernstian systems: (A, C) conventional second harmonic a.c. polarograms, (B, D) second harmonic complex plane polarograms. All parameters and notation same as Fig. 1 except $\omega = 1.00 \times 10^2$ s^{-1}, $k_1 = 5.00 \times 10^5$ s^{-1}, $K = 1.00$, $\alpha = 0.500$, t values given in figure and (A, B) $k_s = 3.00 \times 10^{-3}$ cm s^{-1}, (C, D) $k_s = 1.00 \times 10^{-3}$ cm s^{-1}.

than the linear response of positive slope which is characteristic of high frequencies with the nernstian case (Fig. 3). The frequency response profiles also manifest the kinetic interactions between the charge transfer and preceding chemical reaction rate processes—*e.g.* note the enhancement of charge transfer kinetic contributions attending an increase in k.

The importance of the status of the d.c. process on the a.c. polarographic response (fundamental and higher harmonic) has been pointed out frequently[11,18,19,22,24,30-32]. Whenever a rate process in addition to diffusion is kinetically important in the d.c. sense, polarograms of rather anomalous shape often are predicted[11,19,33]. The appearance of a dependence of current amplitude on drop life also heralds this type of situation. The observation of a mercury drop life dependence allows one to use the a.c. polarographic response as a very sensitive probe into the status of the d.c. process. In Fig. 6, discussed above, were illustrated predictions for the case where the chemical reaction alone is responsible for deviations of the d.c. process from diffusion-control. Figures 11–13 show that the situation changes considerably when slow charge transfer together with the preceding chemical reaction are kinetically important in the d.c. sense. The prediction of polarograms of anomalous shape, together with a profound dependence of wave shape on drop life is found in this unusual kinetic realm. In addition, avoidance of the first quadrant is no longer a characteristic of the complex plane polarograms and phase angles are no longer insensitive to drop life (*i.e.* markers on complex plane polarograms for particular $E_{d.c.}$ values and varying drop life do not always describe a straight line through the origin). Figure 11 presents some predictions for a situation where the chemical reaction is sufficiently rapid that equilibrium conditions prevail with respect to the preceding chemical reaction on both the d.c. and a.c. time scales. Consequently, the relatively large drop life dependence illustrated in this figure originates solely from heterogeneous charge transfer kinetic influence of the d.c. process. The enhancement of charge transfer kinetic influence due to a preceding chemical reaction is demonstrated in Fig. 11-A which bears only slight resemblance to its counterpart in the absence of the chemical reaction as described in Fig. 5-A of ref. 19. Figures 12 and 13 present examples of the interaction between the kinetics of the preceding chemical reaction and kinetics of charge transfer for two equilibrium constants. In Figs. 12-A–12-E the chemical reaction is at equilibrium so that only the effects of charge transfer are evident while in Figs. 12-D–12-H mixed effects due to the slowness of the chemical reaction and charge transfer are present. Two unusual aspects in Fig. 13 are the sharp minimum in Fig. 13-C and 13-G, due to the fact that the real component of the current amplitude is small at all potentials, and the lack of drop life dependence at negative potentials in Figs. 13-D and 13-H.

The foregoing predictions regarding effects of non-nernstian behavior on the second harmonic response carry the following important implications: (*a*) care must be exercised before invoking the assumption of nernstian behavior when calculating chemical rate parameters from experimental second harmonic data; (*b*) one will often find it necessary to work with the relatively cumbersome general theoretical formulation (eqns. 1–26, unsimplified), which accounts for all relevant rate processes, when attempting quantitative data analysis; (*c*) calculation of chemical kinetic parameters will be precluded when very slow heterogeneous charge transfer steps are operative; (*d*) the possibility of obtaining by second harmonic measurements the rate

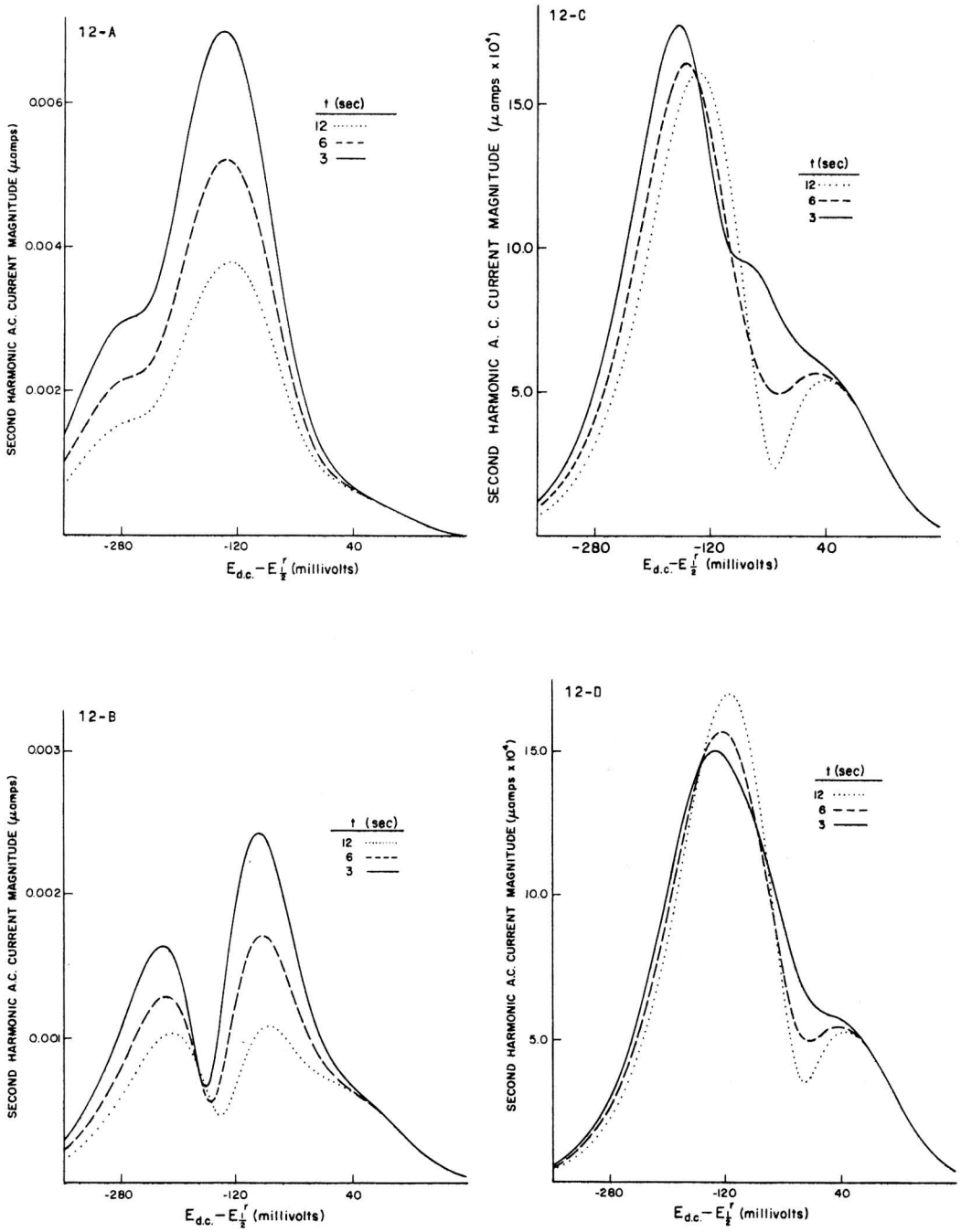

Fig. 12. Drop life dependence of second harmonic a.c. polarograms with non nernstian system: (A–D) conventional second harmonic a.c. polarograms, (E–H) second harmonic complex plane polarograms. All parameters and notation same as Fig. 11 except $K=0.100$, $k_s=3.00\times10^{-3}$ cm s^{-1}, and $k_1=$(A, E) 9.10×10^{6}, (B, F) 9.10×10, (C, G) 9.10, (D, H) 0.910 s^{-1}.

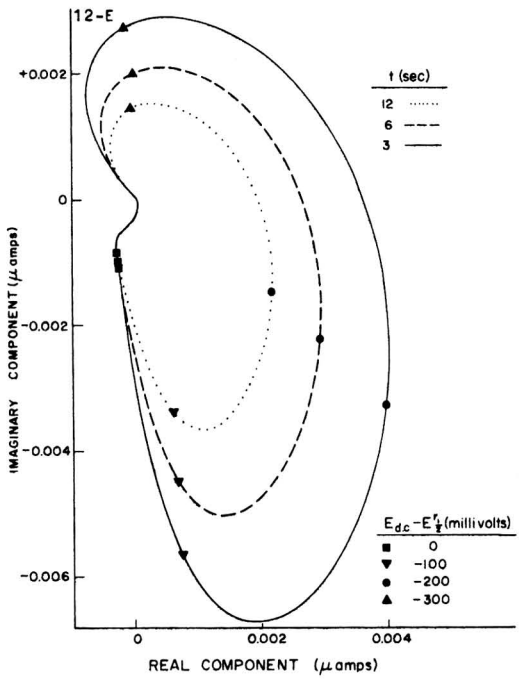
12-E
t (sec)
12
6
3
$E_{d.c.}-E^r_{\frac{1}{2}}$(millivolts)
0
-100
-200
-300
+0.002
0
-0.002
-0.004
-0.006
IMAGINARY COMPONENT (μamps)
0
0.002
0.004
REAL COMPONENT (μamps)

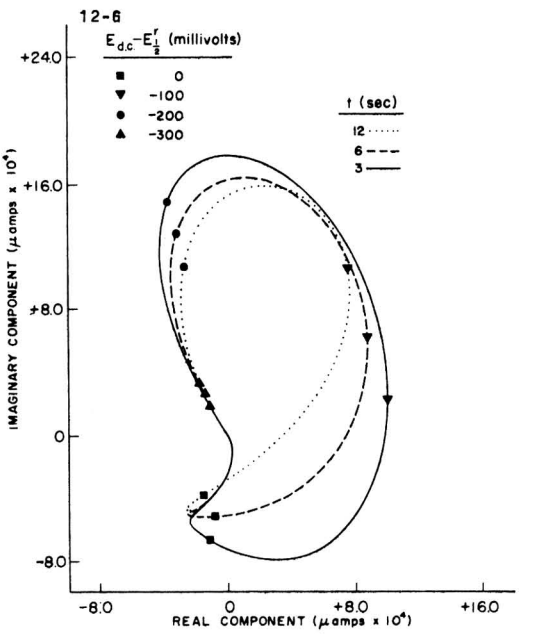
12-6
$E_{d.c.}-E^r_{\frac{1}{2}}$ (millivolts)
0
-100
-200
-300
t (sec)
12
6
3
+24.0
+16.0
+8.0
0
-8.0
IMAGINARY COMPONENT (μamps x 10^4)
-8.0
0
+8.0
+16.0
REAL COMPONENT (μamps x 10^4)

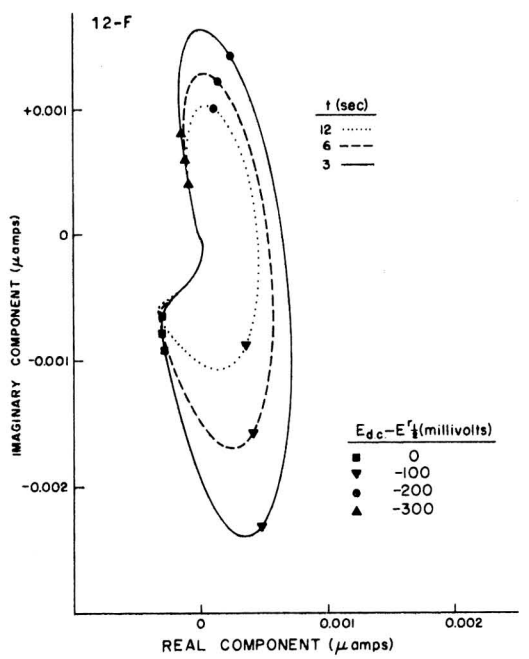
12-F
t (sec)
12
6
3
$E_{d.c.}-E^r_{\frac{1}{2}}$(millivolts)
0
-100
-200
-300
+0.001
0
-0.001
-0.002
IMAGINARY COMPONENT (μamps)
0
0.001
0.002
REAL COMPONENT (μamps)

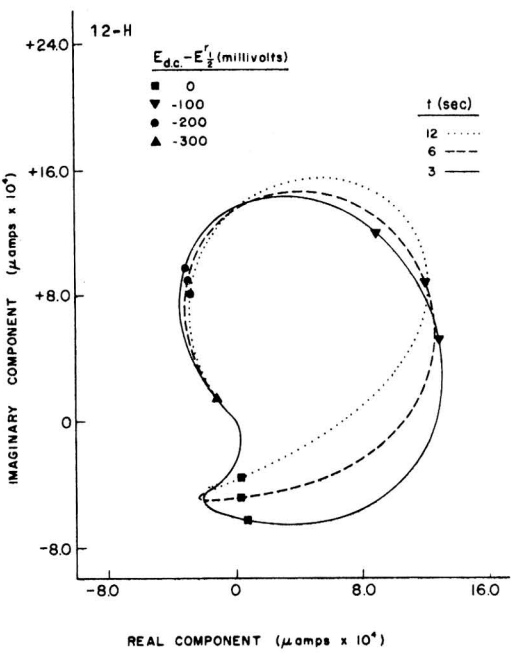
12-H
$E_{d.c.}-E^r_{\frac{1}{2}}$(millivolts)
0
-100
-200
-300
t (sec)
12
6
3
+24.0
+16.0
+8.0
0
-8.0
IMAGINARY COMPONENT (μamps x 10^4)
-8.0
0
8.0
16.0
REAL COMPONENT (μamps x 10^4)

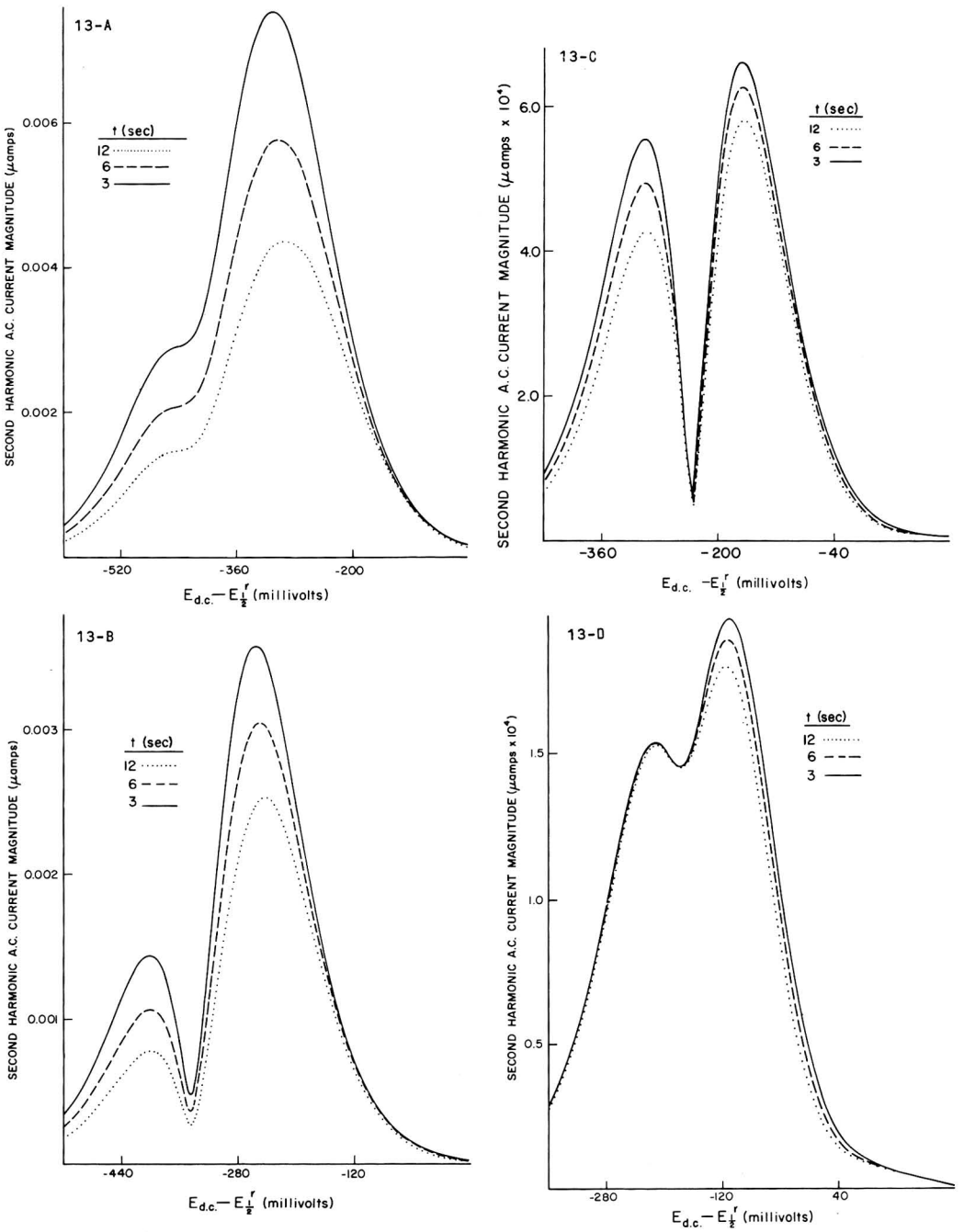

Fig. 13. Drop life dependence of second harmonic a.c. polarograms with non-nernstian system: (A–D) conventional second harmonic a.c. polarograms, (E–H) second harmonic complex plane polarograms. All parameters and notation same as Fig. 11 except $K = 1.00 \times 10^{-2}$, $k_s = 1.00 \times 10^{-3}$ cm s^{-1}, and $k_1 =$ (A, E) 1.00×10^8, (B, F) 1.00×10^3, (C, G) 1.00×10, (D, H) $0.100\ s^{-1}$.

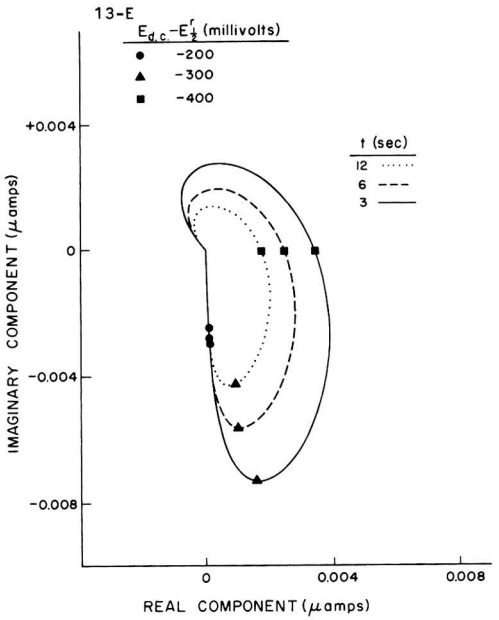
13-E
$E_{d.c.}-E^r_{\frac{1}{2}}$ (millivolts)
-200
-300
-400
t (sec)
12
6
3
+0.004
0
-0.004
-0.008
IMAGINARY COMPONENT (μamps)
0
0.004
0.008
REAL COMPONENT (μamps)

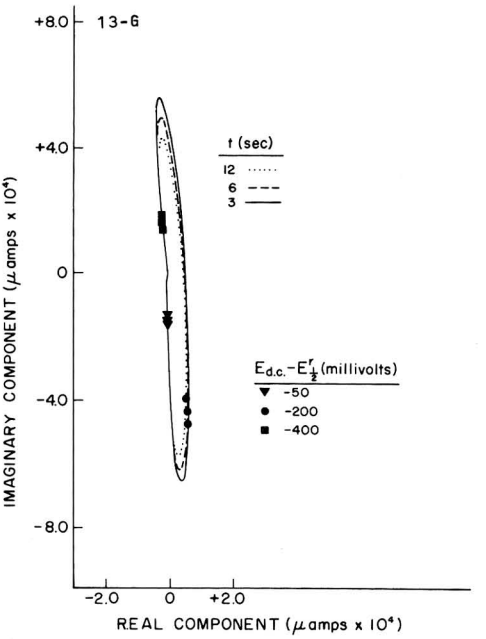
13-G
t (sec)
12
6
3
$E_{d.c.}-E^r_{\frac{1}{2}}$ (millivolts)
-50
-200
-400
+8.0
+4.0
0
-4.0
-8.0
IMAGINARY COMPONENT (μamps x 10⁴)
-2.0
0
+2.0
REAL COMPONENT (μamps x 10⁴)

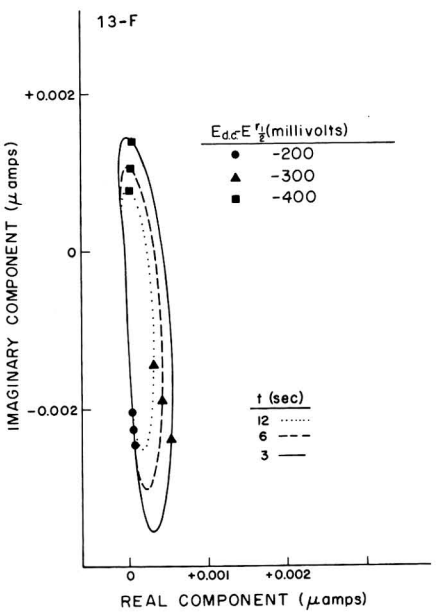
13-F
$E_{d.c.}-E^r_{\frac{1}{2}}$ (millivolts)
-200
-300
-400
t (sec)
12
6
3
+0.002
0
-0.002
IMAGINARY COMPONENT (μamps)
0
+0.001
+0.002
REAL COMPONENT (μamps)

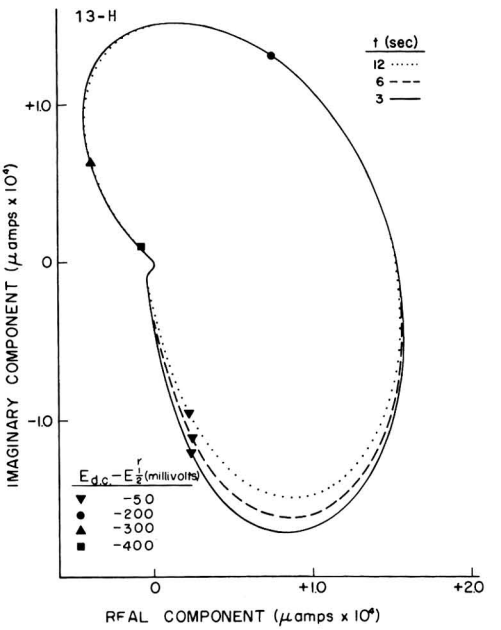
13-H
t (sec)
12
6
3
$E_{d.c.}-E^r_{\frac{1}{2}}$ (millivolts)
-50
-200
-300
-400
+1.0
0
-1.0
IMAGINARY COMPONENT (μamps x 10⁴)
0
+1.0
+2.0
REAL COMPONENT (μamps x 10⁴)

parameters for the heterogeneous charge transfer step in the presence of the preceding chemical reaction is excellent, comparing quite favorably with the situation encountered with the simple quasi-reversible case.

Some suggestions regarding data analysis were given above for the case of nernstian systems. All other approaches which might be suggested here, including those appropriate to the more complex situation where rate control by both the chemical reaction and heterogeneous charge transfer must be considered, are essentially identical or analogous to those discussed elsewhere[11,13,19,21,24,28,34]. A discussion of these ideas in the context of the mechanism and observables of concern in this work would be overly repetitious and will not be undertaken.

CONCLUSIONS

The results presented here provide theoretical evidence in support of the concept that second harmonic a.c. polarography can be profitably applied to the study of systems following mechanism R1. This view appears to be supported regardless of whether one's interest lies primarily in the heterogeneous charge transfer step or the preceding homogeneous chemical reaction (or both). Distinct features of the second harmonic response through which mechanism R1 can be recognized also are shown to exist. Unusual sensitivity of the second harmonic response to the electrode reaction's mechanistic identity and the magnitude of rate parameters appears to represent the chief advantage of this method. The most evident disadvantage is that attending the cumbersome nature of the relevant theory, a problem which is readily suppressed with computer-aided data analysis.

SUMMARY

Theoretical predictions for the second harmonic a.c. polarographic response of systems involving rate control by diffusion, a first-order preceding chemical reaction and/or heterogeneous charge transfer kinetics are presented and discussed. A rigorous solution of the expanding plane boundary value problem by the Matsuda method is the basis of the theoretical formulation employed. The predicted second harmonic behavior, including both amplitude and phase characteristics, is examined for a wide range of kinetic conditions encompassing both nernstian and non-nernstian behavoir. Properties of the second harmonic response which make its observation eminently useful in quantitatively characterizing kinetics of homogeneous chemical reactions preceding heterogeneous charge transfer are made apparent.

REFERENCES

1 P. DELAHAY, *New Instrumental Methods in Electrochemistry*, Interscience, New York, 1954, pp. 87–100.
2 P. DELAHAY in P. DELAHAY (Ed.), *Advances in Electrochemistry and Electrochemical Engineering*, Vol. 1, Interscience, New York, 1961, Chap. 5.
3 A. A. VLECK in F. A. COTTON (Ed.), *Progress in Inorganic Chemistry*, Vol. 5, Interscience, New York, 1963, pp. 258–296.
4 H. STREHLOW in S. L. FRIESS, E. S. LEWIS AND A. WEISSBERGER (Eds.), *Technique of Organic Chemistry*, Vol. 8, Part 2, Interscience, New York, 1963, Chap. 15.
5 J. HEYROVSKÝ AND J. KŮTA, *Principles of Polarography*, Academic Press, New York, 1966, pp. 341–380.
6 K. J. VETTER, *Electrochemical Kinetics*, Academic Press, New York, 1967, pp. 247–281.

7 H. GERISCHER, *Z. Physik. Chem. Leipzig*, 198 (1951) 286.
8 H. MATSUDA, P. DELAHAY AND M. KLEINERMAN, *J. Am. Chem. Soc.*, 81 (1959) 6379.
9 S. SATHYANARAYANA, A. K. N. REDDY AND K. S. G. DOSS, *Australian J. Chem.*, 13 (1960) 177.
10 D. E. SMITH, *Anal. Chem.*, 35 (1963) 602.
11 D. E. SMITH in A. J. BARD (Ed.), *Electroanalytical Chemistry*, Vol. 1, Marcel Dekker, New York, 1966, Chap. 1.
12 H. L. HUNG, Doctoral Thesis, Northwestern University, Evanston, Ill., 1967.
13 T. G. MCCORD AND D. E. SMITH, *Anal. Chem.*, 41 (1969) 116.
14 H. H. BAUER, *J. Electroanal. Chem.*, 1 (1960) 256.
15 D. E. SMITH AND W. H. REINMUTH, *Anal. Chem.*, 33 (1961) 482.
16 J. PAYNTER, Ph.D. Thesis, Columbia University, New York, 1964.
17 H. H. BAUER AND D. C. S. FOO, *Australian J, Chem.*, 19 (1966) 1103.
18 T. G. MCCORD, E. R. BROWN AND D. E. SMITH, *Anal. Chem.*, 38 (1966) 1615.
19 T. G. MCCORD AND D. E. SMITH, *Anal. Chem.*, 40 (1968) 289.
20 J. E. B. RANDLES AND D. R. WHITEHOUSE, *Trans. Faraday Soc.*, 64 (1968) 1376.
21 T. G. MCCORD AND D. E. SMITH, *Anal. Chem.*, 41 (1969) 131.
22 T. G. MCCORD AND D. E. SMITH, *Anal. Chem.*, 40 (1968) 1967.
23 J. HEYROVSKÝ AND J. KŮTA, *Principles of Polarography*, Academic Press, New York, 1966, pp. 77–83.
24 T. G. MCCORD, H. L. HUNG AND D. E. SMITH, *J. Electroanal. Chem.*, 21 (1969) 5.
25 D. E. SMITH, *Anal. Chem.*, 35 (1963) 1811.
26 D. E. SMITH, unpublished work. Northwestern University, Evanston, Illinois, 1968.
27 E. R. BROWN, D. E. SMITH AND G. L. BOOMAN, 40 (1968) 1411.
28 T. G. MCCORD AND D. E. SMITH, *Anal, Chem.*, 41 (1969) 1423.
29 R. A. MARCUS, *J. Chem. Phys.*, 43 (1965) 679.
30 H. L. HUNG AND D. E. SMITH, *Anal. Chem.*, 36 (1964) 922.
31 G. H. AYLWARD, J. W. HAYES, H. L. HUNG AND D. E. SMITH, *Anal. Chem.*, 36 (1964) 2218.
32 G. H. AYLWARD AND J. W. HAYES, *J. Electroanal. Chem.*, 8 (1964) 442.
33 H. MATSUDA, *Z. Elektrochem.*, 62 (1958) 977.
34 H. L. HUNG AND D. E. SMITH, *J. Electroanal. Chem.*, 11 (1966) 425.
35 E. R. BROWN, D. E. SMITH AND D. D. DEFORD, *Anal. Chem.*, 38 (1966) 1230.

ELECTROANALYTICAL CHEMISTRY AND INTERFACIAL ELECTROCHEMISTRY
Elsevier Sequoia S.A., Lausanne – Printed in The Netherlands

OSCILLOPOLAROGRAPHIC AND POLAROGRAPHIC INVESTIGATION OF THE ELECTRODE REACTION OF Pu AND U IONS IN CARBONATE SOLUTIONS

S. CASADIO AND F. ORLANDINI
Industrial Chemistry Laboratory of C.N.E.N., C.S.N. Casaccia, Rome (Italy)
(Received December 22nd, 1969)

INTRODUCTION

The aim of the present work is to investigate the possibility of determining the valence states of plutonium in mineral acid media by polarography. By using the carbonate ion as complexing agent it is possible to shift the half-wave potentials of plutonium ions to values compatible with the use of the DME.

While the polarographic behavior of U(IV), U(V) and U(VI) carbonate complexes is well known[1-3] only preliminary work has so far been carried out[4] on Pu(IV) electroreduction in carbonate media by cyclic voltammetry at the HMDE.

We have therefore investigated experimentally the behavior of the Pu(IV)/Pu(III) system in 1 *M* Na_2CO_3 by conventional polarographic and oscillopolarographic techniques. The same type of study has been repeated for the U(VI)/U(V) system. The electrode-kinetic parameters for these two systems have then been characterized.

EXPERIMENTAL

The Chemtrix SSP-2 oscillopolarograph was used in conjunction with a three-electrode cell assembly. Polarographic scans were made using a DME *vs.* SCE with a flux $m = 0.575$ mg Hg s^{-1} for a 70 cm column length and a drop time $t = 11.1$ s. The electrode potential scanning rate was varied from 0.025 to 20 V s^{-1}; the Tektronix C-12 oscilloscope camera system was used to record voltammetric curves.

Conventional polarograms were carried out with an Electroscan Beckman using dropping mercury electrodes; the values of $m^{\frac{2}{3}}t^{\frac{1}{6}}$ are reported in Table 1.

Inert gas (pure N_2) was bubbled through the supporting electrolyte before each measurement. Solutions were thermostatted at $(25 \pm 0.1)^\circ$C and $(22 \pm 0.1)^\circ$C for

TABLE 1

Process	$E_{\frac{1}{2}}$/*V vs. SCE*	i_d/C	$m^{\frac{2}{3}}t^{\frac{1}{6}}/mg^{\frac{2}{3}}\,s^{-\frac{1}{2}}$	*Ion*	$D/cm^2\,s^{-1}$	$T/^\circ C$	*Log* $(k_s/cm\,s^{-1})$
$Pu(IV)+e=Pu(III)$	−0.95	1.6	1.825	Pu(IV)	2.1×10^{-6}	25	−4.3
$Pu(III)=Pu(IV)+e$	−0.553	1.64		Pu(III)	2.2×10^{-6}		
$U(VI)+e=U(V)$	−0.915	2.0	1.725	U(VI)	3.6×10^{-6}	22	−4.0

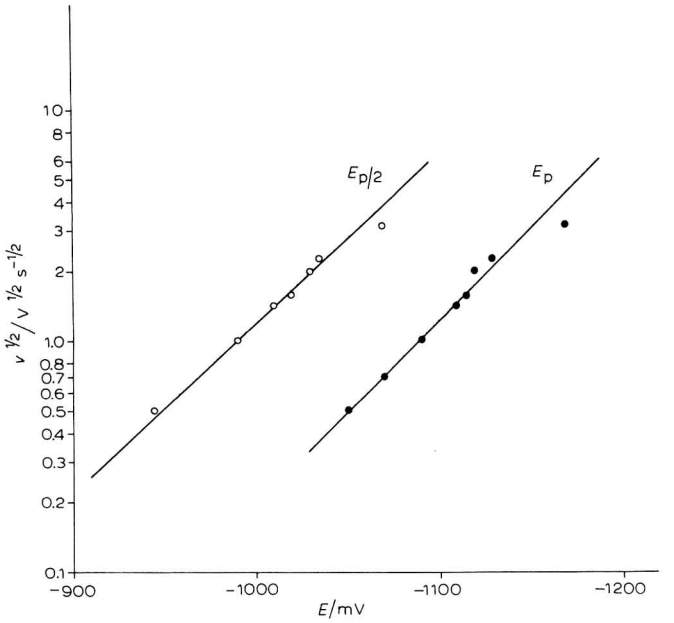

Fig. 1. E_p and $E_{p/2}$ *vs.* $v^{\frac{1}{2}}$ for the cathodic reduction of Pu(IV) to Pu(III) ions.

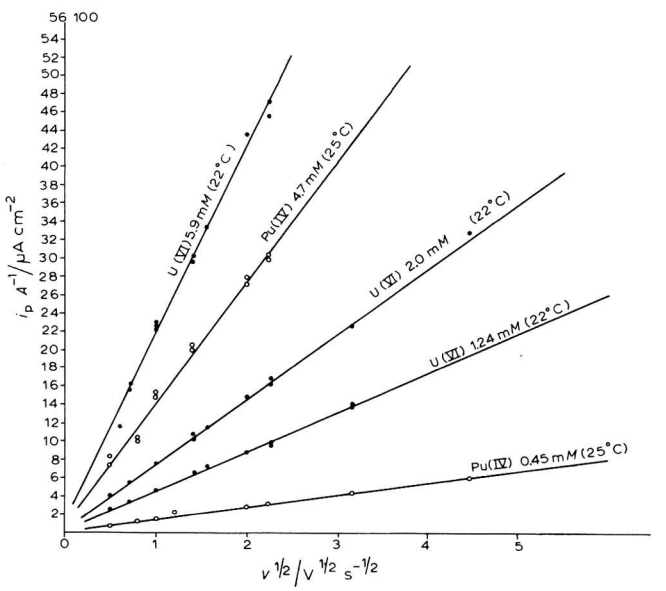

Fig. 2. i_p/A *vs.* $v^{\frac{1}{2}}$ for U(VI) and Pu(IV) monoelectronic irreversible reductions at various concentrations.

the Pu and U systems, respectively. Stock solutions of PuVI), Pu(IV) and Pu(III) in 3 *M* $HClO_4$ were obtained as in ref. 5. A standard solution of U(VI) was prepared from a weighed aliquot of U_3O_8, NBS 4950. All reagents used were AnalaR grade.

RESULTS AND DISCUSSION

Pu(IV)/Pu(III) system

No detailed information is available concerning the structure of the carbonate complexes of Pu in these valence states; evidence for the existence of the $[Pu(CO_3)(OH)_n(H_2O)_{6-n}]^{2-n}$ complex has been given[6] but polycarbonate anions also seem to be present[7].

We have obtained polarograms in 1 *M* Na_2CO_3 in the pH range 11.4–10.5 without any significant effects on the voltammetric behavior of the Pu(III) oxidation and Pu (IV) reduction steps.

Both processes follow the Ilkovic equation. In Table 1 the half-wave potentials for the cathodic and anodic processes and the diffusion coefficients for the Pu(III) and Pu(IV) carbonate complexes, are reported. The kinetic-parameters reported in Table 2 have been obtained from the theoretical solution of the boundary value problem for the case of totally irreversible reductions by voltammetry with linear (triangular) scan of potential on a spherical electrode (see ref. 8 for an extensive bibliographical review).

TABLE 2

Process	*Exptl. correlation*	αn_a	*Ion*	$D/cm^2\ s^{-1}$	$T/°C$	*Log* $(k_s/cm\ s^{-1})$
Pu(IV) + *e* = Pu(III)	Difference $E_p - E_{p/2}$	0.48			25	
	E_p *vs.* log $v^{\frac{1}{2}}$ slope	0.48				
	Intercept $(E_p)_{v=1}$					−4.6
	i_p/A *vs.* $v^{\frac{1}{2}}$ slope		Pu(IV)	2.1×10^{-6}		
U(VI) + *e* = U(V)	Difference $E_p - E_{p/2}$	0.43			22	
	E_p *vs.* log $v^{\frac{1}{2}}$ slope	0.45				
	Intercept $(E_p)_{v=1}$					−4.05
	i_p/A *vs.* $v^{\frac{1}{2}}$ slope		U(VI)	3.6×10^{-6}		

Peak and half-peak potentials for the cathodic process are plotted in Fig. 1 *vs.* the square-root values of the scan rate employed.

Peak current density *vs.* the scanning rate is reported in Fig. 2 for different uranium and plutonium concentrations.

A notable difference in the charge-transfer coefficient αn_a is evident on comparing our value with the value of 0.68 reported in ref. 4.

U(VI)/U(V) system

Conventional polarographic data, obtained at 22°C and reported in Table 1, are in agreement with the results of Branica and Pravdic[1]; the reduction of the $UO_2(CO_3)_3^{4-}$ complex follows the Ilkovic equation.

The oscillopolarograms obtained with single triangular scans show cathodic and anodic peaks (Fig. 3).

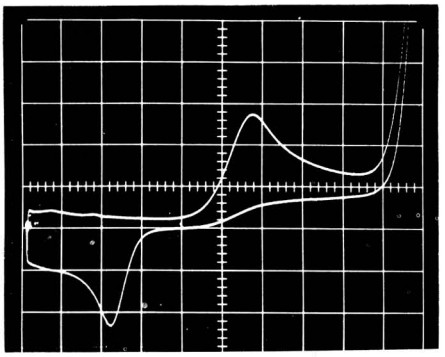

Fig. 3. Oscillopolarogram obtained from a solution of 4.76 m*M* U(VI) in 1 *M* Na_2CO_3. Scanning electrode potential at 20 V s^{-1} from 0 to −2 V; current scale, 1 μA $div.^{-1}$.

The kinetic parameters of the irreversible reduction of U(VI) obtained with the same criteria as used for the Pu(IV) reduction (Figs. 4 and 2) are shown in Table 2.

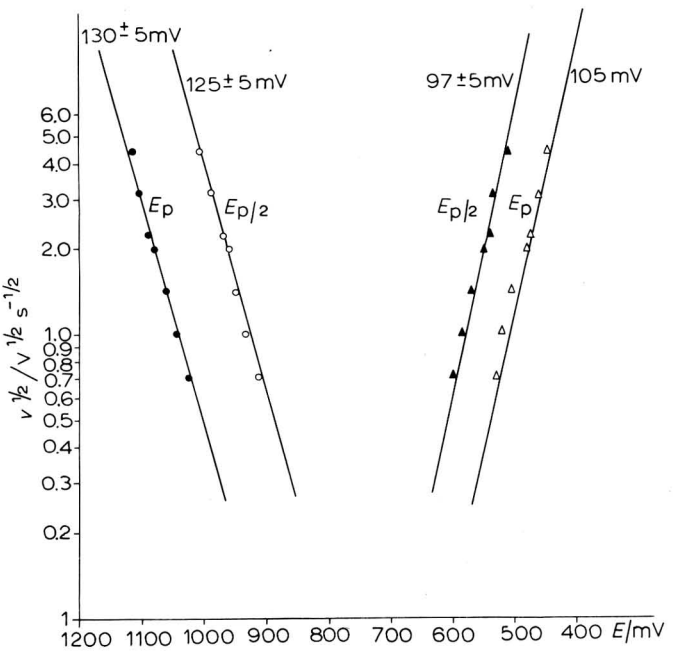

Fig. 4. E_p and $E_{p/2}$ *vs.* $v^{\frac{1}{2}}$ for the cathodic and anodic processes of the U(VI)/U(V) system.

Our values of the charge-transfer coefficient, uncorrected for double layer effect, are in agreement with those given in ref. 4. The value of 0.6 reported in ref. 2 is corrected for the diffuse layer effect.

The rate constants k_s for both systems are obtained by evaluating the formal redox potential from conventional polarography by the criterion of ref. 9.

Pu(VI) reduction

The carbonate ion does not shift (under our experimental conditions) the half-wave potential for the first step of the plutonyl ion reduction to such a value as to allow the use of the DME. The wave due to the irreversible reduction step:

$$Pu(VI) + 3e = Pu(III)$$

has $E_{\frac{1}{2}} = -1.03$ V, and is observed on the current plateau due to Pu(V) formation.

Analytical implications

The direct voltammetric analytical detection of the various valence states of plutonium in mineral acid media has the disadvantage of involving the use of a solid electrode (Pt). Good quantitative evaluations with a stationary working electrode are possible only when single ionic species are present in solution. On the other hand, by using carbonate as complexing ion, it is possible to shift the Pu(IV) reduction and Pu(III) oxidation waves to values compatible with the use of the DME. Such waves have the property of being analytically suitable for the simultaneous quantitative determination of Pu(III) and Pu(IV) ions also by oscillopolarography on a quasistationary mercury drop electrode using an adequate range of scan for each of the two ions. This is due to the good separation between the cathodic and the anodic process.

As an example, a conventional polarogram of a 3 *M* $HClO_4$ solution containing both Pu(III) and Pu(IV) in the ratio 9/1 to which solid Na_2CO_3 has been added, is shown in Fig. 5.

The Pu(VI) ion interferes because in carbonate media the Pu^{3+} species rapidly oxidizes and its second reduction step overlaps the Pu^{4+} reduction wave. This effect

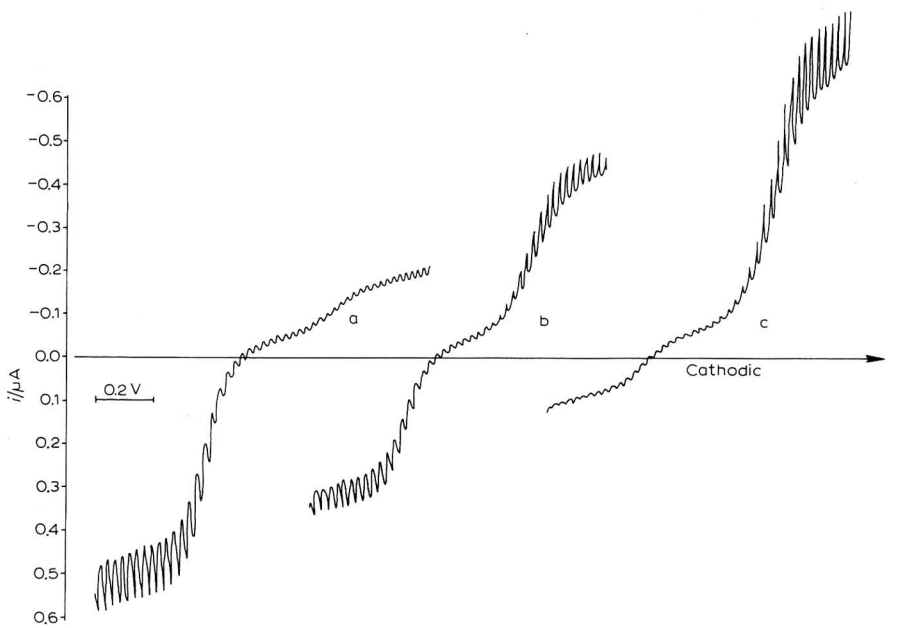

Fig. 5. (a) Polarogram of a carbonate solution containing 0.28 m*M* Pu(III) and 0.03 m*M* Pu(IV); (b) and (c) interference due to the addition of 0.12 and 0.24 m*M* Pu(VI), respectively, to the solution of polarogram (a).

is shown in Fig. 5 which gives three consecutive polarograms of Pu^{3+} and Pu^{4+} after the addition of aliquots of Pu^{6+} ion. This type of interference is not present in the simultaneous detection of all valence states of U[1].

SUMMARY

Electrode-kinetic parameters for the one-electron irreversible step of Pu(IV) reduction in 1 *M* Na_2CO_3 are obtained by an oscillopolarographic technique.

Conventional polarographic data (half-wave potentials and diffusion coefficients) are given for the Pu(IV)/Pu(III) system in carbonate medium.

Suggestions are made regarding the analytical determination of plutonium valence states in mineral acid media using the carbonate ion as complexing agent.

REFERENCES

1 M. BRANICA AND V. PRAVDIC, paper presented at the 3rd Intern. Congr. of Polarog., Southampton (U.K.), July, 1964.
2 L. GIERST, L. VANDENBERGHEN, E. NICOLAS AND A. FRABONI, *J. Electrochem. Soc.*, 113 (1966) 1025.
3 D. CUKMAN, J. CAJA AND V. PRAVDIC, *J. Electroanal. Chem.*, 19 (1967) 267.
4 L. JEFTIC, J. CAJA AND M. BRANICA, *Croat. Chem. Acta*, 39 (1967) 225.
5 D. PETERS AND W. D. SHULTS, *J. Electroanal. Chem.*, 8 (1964) 200.
6 A. J. MOSKOVIN AND A. D. GEL'MAN, *Russ. J. Inorg. Chem.*, 3 (1958) 962.
7 A. D. GEL'MAN AND L. M. ZAITSEV, *Zh. Neorgan. Khim.*, 4 (1959) 2688.
8 R. S. NICHOLSON AND I. SHAIN, *Anal. Chem.*, 36 (1964) 706.
9 J. M. HALE AND R. PARSONS, *Collection Czech. Chem. Commun.*, 27 (1962) 244.

ELECTROANALYTICAL CHEMISTRY AND INTERFACIAL ELECTROCHEMISTRY
Elsevier Sequoia S.A., Lausanne – Printed in The Netherlands

CATION EFFECT ON THE POLAROGRAPHIC REDUCTION OF NICKEL(II) PERCHLORATE IN ACETONITRILE

EIKI ITABASHI AND SHIGERO IKEDA
Department of Chemistry, Faculty of Science, Osaka University, Toyonaka, Osaka (Japan)
(Received October 22nd, 1968; in revised form September 26th, 1969)

The effect of supporting electrolyte in non-aqueous inorganic polarography has received less attention than that in aqueous media. Several reports dealing with coordination compounds in acetonitrile have noted changes in electrochemical behavior with change in supporting electrolyte[1,2].

In the previous paper[2], the polarographic behavior of acetatonickel(II) in acetonitrile was investigated and the electrode process of acetatonickel(II) was found to be affected by the nature of the cation and the concentration of supporting electrolyte.

An acetonitrile solution of nickel(II) gave a single irreversible wave in a $LiClO_4$, $NaClO_4$ or $(CH_3)_4NClO_4$ supporting electrolyte, and a double wave in other quaternary ammonium perchlorates. Polarographic studies of nickel(II) in various nitrile solvents have been carried out by several investigators[3-7]. Kolthoff and Coetzee[3] reported that nickel(II) in acetonitrile gave a single reversible wave with a half-wave potential of -0.33 V *vs.* SCE in 0.1 *M* $NaClO_4$.

Popov and Geske[5] obtained a double wave with a half-wave potential of -0.69 V and -1.22 V *vs.* the Ag–$AgNO_3$ electrode, and attributed the double wave to the presence of two reducible species of nickel(II) ion. Two reduction waves of nickel(II) were also investigated in benzonitrile solution containing 0.1 *M* $(C_2H_5)_4NClO_4$ by Larson and Iwamoto[6], and in acetonitrile containing the same electrolyte by Nelson and Iwamoto[7]. They concluded that the second step involved the reduction of the hydrated nickel(II) ion.

In the present paper are reported the results of a study of the effect of the nature and the concentration of supporting electrolyte on the polarographic reduction of nickel(II) in acetonitrile solvent.

The cation effect is discussed on the basis of the inhibition of the charge transfer process of nickel(II) by the relatively weak adsorption of quaternary ammonium ion at the DME.

EXPERIMENTAL

Reagents

Extra pure reagent acetonitrile purchased from Nakarai Chemicals Ltd. (Kyoto) was purified by a modification of the method of Forcier and Olver[8]. The purity was checked by both polarography and spectrophotometry[9]. The water content was approximately 2–4 m*M*.

Hexaaquonickel(II) perchlorate was prepared and recrystallized using the procedure given in the literature[10].

$Ni(H_2O)_6(ClO_4)_2$ was dried in a vacuum oven to constant weight at 110–120°C for 60 h, and $Ni(H_2O)_2(ClO_4)_2$ was obtained as reported by Hathway and Underhill[11]. The analysis of $Ni(H_2O)_2(ClO_4)_2$ gave the following result. Found: Ni, 19.0 ± 0.8; ClO_4, $65.8 \pm 1.4\%$. Calcd. for $Ni(H_2O)_2(ClO_4)_2$: Ni, 19.99; ClO_4, 67.74%.

Anhydrous lithium perchlorate, sodium perchlorate, tetramethylammonium perchlorate (Me_4NClO_4) and tetra-n-butylammonium perchlorate ($n\text{-}Bu_4NClO_4$) were prepared by the procedure previously reported[2].

Tetraethylammonium perchlorate (Et_4NClO_4) was prepared by neutralizing a 40% tetraethylammonium hydroxide solution (K & K) with 5 *M* perchloric acid. The salt was recrystallized several times from water and subsequently twice from purified acetonitrile and dried in a vacuum oven at 60–65°C for 60 h.

Benzyltrimethylammonium perchlorate, phenyltrimethylammonium perchlorate and cetyltrimethylammonium perchlorate were prepared by neutralizing the respective quaternary ammonium hydroxide solutions (Tokyo Kasei Kogyo Co. Ltd.) with 3 *M* perchloric acid. After evaporating at room temperature under reduced pressure in a desiccator containing calcium chloride, the salts were recrystallized three times from methyl alcohol and then twice from purified acetonitrile, and dried in a vacuum oven at 60–65°C for 60 h.

Procedure

Polarograms and current–time (*i–t*) curves during the life of a mercury drop at constant potential were obtained with a Underkofler and Shain type potentiostat[12], based on operational amplifiers K2-XA and stabilized amplifiers K2-P and K2-PA of Philbrick Researches Inc.

Polarograms were recorded with a Yokogawa X-Y recorder, PRO-11A type, and *i–t* curves were recorded with a Riken Denshi SP-G2 type recorder.

In the following section, the word "current" refers to the maximum current observed just before the fall of a mercury drop. Measurements were made at 25 ± 0.1°C. A beaker-type cell was used.

The potential of the DME was measured against a saturated calomel electrode (SCE) which was connected to the test solution through a Luggin capillary with a pair of sintered glass discs to prevent water contamination. A platinum spiral electrode which served as the counter electrode was placed in the glass tube with a disc of sintered glass, which was connected with the test solution. The dissolved oxygen in the solution was removed by bubbling pure nitrogen gas through the solution.

The dropping mercury electrode (DME) had an m value of 1.44_6 mg s^{-1} and a drop time, t_d, of 5.01 s in a deaerated 0.1 *M* lithium perchlorate acetonitrile solution at -0.70 V *vs.* SCE and 60 cm mercury height. After the measurements of the polarograms, the water content of the polarographic solution was determined to be 7–15 m*M* by Karl Fischer titration.

RESULTS

The polarograms of 0.5 m*M* nickel(II) in acetonitrile solution containing various supporting electrolytes are shown in Figs. 1-A and -B. Nickel(II) gave a

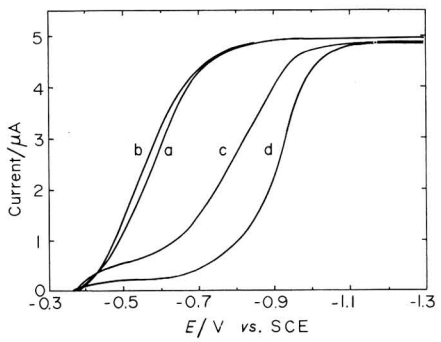

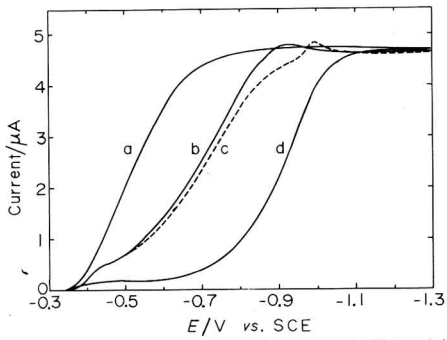

Fig. 1. A. Effect of electrolyte on the polarograms of Ni(II). $[Ni(II)] = 0.5 \times 10^{-3}$ *M*. (a) 0.1 *M* $LiClO_4$, (b) 0.1 *M* $NaClO_4$, (c) 0.1 *M* Et_4NClO_4, (d) 0.1 *M* n-Bu_4NClO_4.

Fig. 1. B. Effect of electrolyte on the polarograms of Ni(II).$[Ni(II)] = 0.5 \times 10^{-3}$ *M*. (a) 0.05 *M* Me_4NClO_4, (b) 0.1 *M* $C_6H_5(CH_3)_3NClO_4$, (c) 0.1 *M* $C_6H_5CH_2(CH_3)_3NClO_4$, (d) 0.1 *M* $CH_3(CH_2)_{15}(CH_3)_3NClO_4$.

single irreversible wave in $LiClO_4$, $NaClO_4$ and Me_4NClO_4 electrolyte solutions, and a double wave in the other quaternary ammonium perchlorate electrolyte solutions. The limiting current of the single irreversible wave was diffusion-controlled from the results of the measurement of the *i–t* curve of an individual drop and proportional to the concentration of nickel(II). Figure 2 demonstrates the dependence of the limiting currents obtained in a 0.1 *M* n-Bu_4NClO_4 electrolyte solution on the concentration of nickel(II). The total limiting current was diffusion-controlled and proportional to the concentration of depolarizer, while that of the first step was not proportional to the depolarizer concentration.

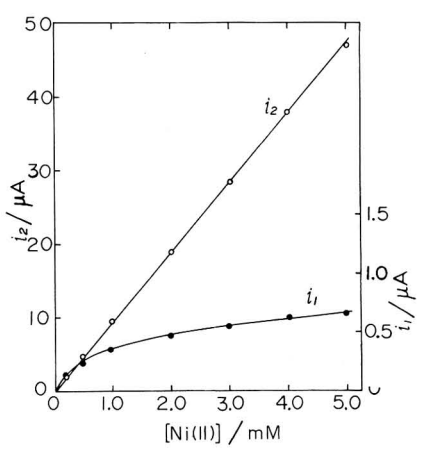

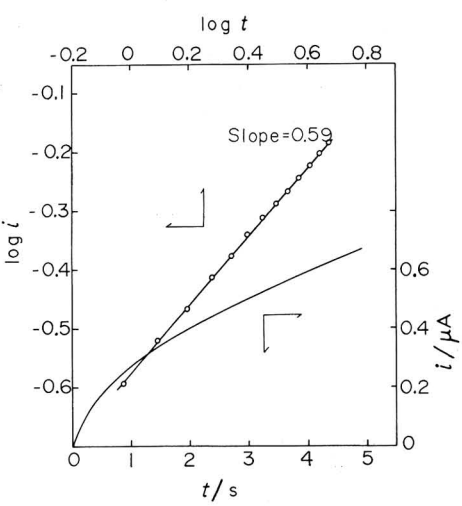

Fig. 2. Variation of the wave height with concn. of Ni(II). $[n\text{-}Bu_4NClO_4] = 0.1$ *M*.(i_1) 1st wave, (i_2) total wave.

Fig. 3. Current–time curve and log *i*–log *t* plot of 1st wave. $[Ni(II)] = 4 \times 10^{-3}$ *M*, $[n\text{-}Bu_4NClO_4] = 0.1$ *M*, applied potential = −0.60 V *vs.* SCE.

Figure 3 shows a typical *i–t* curve for the first step obtained in a 0.1 *M* n-Bu_4NClO_4 electrolyte solution. The slope of the log *i vs.* log *t* for the curve has a value of 0.59 which is well beyond the value of 0.17 expected for a diffusion-controlled mechanism.

Figures 4-A and -B show the effect of the concentration of $NaClO_4$ and Et_4NClO_4, respectively, on the polarograms of nickel(II). In both electrolyte solutions,

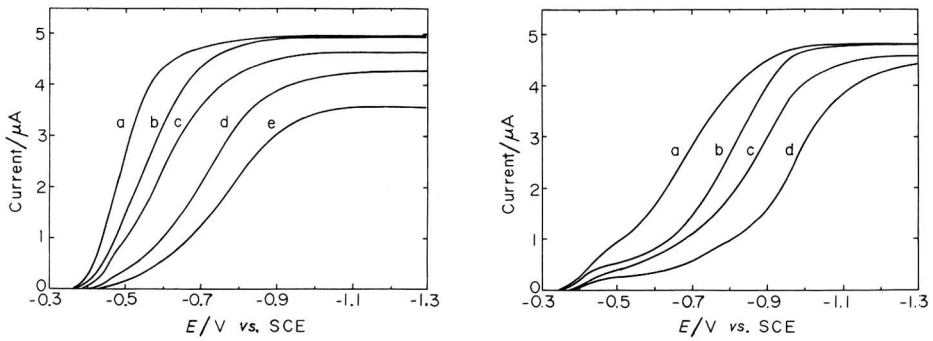

Fig. 4. A. Effect of concn. of $NaClO_4$ on the polarograms of Ni(II). $[Ni(II)] = 0.5 \times 10^{-3}$ *M*. $[NaClO_4]$: (a) 0.05, (b) 0.1, (c) 0.2, (d) 0.5, (e) 1.0 *M*.

Fig. 4. B. Effect of concn. of Et_4NClO_4 on the polarograms of Ni(II). $[Ni(II)] = 0.5 \times 10^{-3}$ *M*. $[Et_4NClO_4]$: (a) 0.05, (b) 0.1, (c) 0.2, (d) 0.5 *M*.

the reduction potential shifts to more negative values and the limiting current decreases with increasing concentration of electrolyte.

The polarograms of nickel(II) in $LiClO_4$–n-Bu_4NClO_4 (ionic strength 0.10) electrolyte mixtures are given in Fig. 5.

A single irreversible wave observed in 0.1 *M* $LiClO_4$ electrolyte alone was separated into a double wave by the addition of n-Bu_4NClO_4 electrolyte, and the reduction potential of the second step shifted to more negative values with increasing concentration of n-Bu_4NClO_4 up to about 25 m*M*. There was no appreciable change on the polarogram by further addition of n-Bu_4NClO_4.

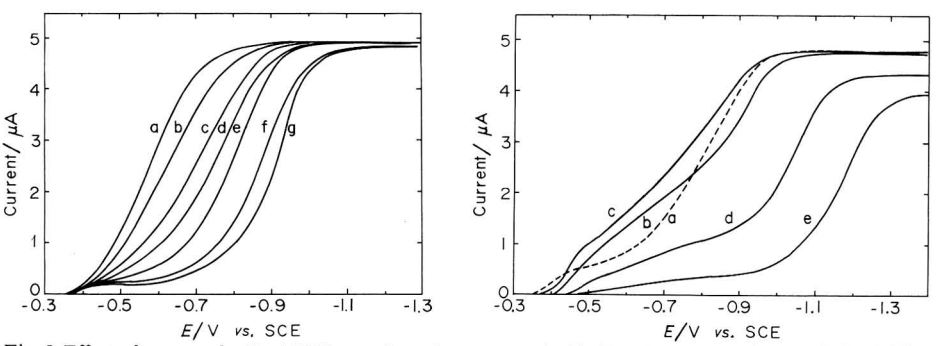

Fig. 5. Effect of concn. of n-Bu_4NClO_4 on the polarograms of Ni(II) in $LiClO_4$ soln. ($\mu = 0.10$). $[Ni(II)] = 0.5 \times 10^{-3}$ *M*. [n-Bu_4NClO_4]: (a) 0, (b) 1×10^{-3}, (c) 3×10^{-3}, (d) 5×10^{-3}, (e) 1×10^{-2}, (f) 2.5×10^{-2}, (g) 0.1 *M*.

Fig. 6. Effect of concn. of water on the polarograms of Ni(II). $[Ni(II)] = 0.5 \times 10^{-3}$ *M*, $[Et_4NClO_4] = 0.1$ *M*. $[H_2O]$: (a) 9×10^{-3}, (b) 0.18, (c) 0.41, (d) 0.96, (e) 2.01 *M*.

The contribution of water for the reduction wave was also investigated. Figure 6 shows the polarograms of nickel(II) in 0.1 *M* Et_4NClO_4 electrolyte solution containing various concentrations of water. The limiting current of the first step was enhanced by the addition of water up to 0.2 *M*, and reduced at concentrations of water above 0.4 *M*. An ill-defined wave was obtained in a 0.1 *M* Et_4NClO_4 electrolyte solution containing 2 *M* H_2O.

DISCUSSION

The distorted reduction wave of nickel(II) in acetonitrile solution containing a quaternary ammonium perchlorate as supporting electrolyte could be interpreted by the inhibition of the charge transfer process of nickel(II) by the relatively weak adsorption of the cation of the electrolyte, but not by the presence of two kinds of electroactive species, as has been pointed out by several investigators[5-7].

The limiting current of the first step observed in 0.1 *M* Et_4NClO_4 electrolyte solution is enhanced by the presence of small amounts of water and reduced at relatively higher concentrations of water. The enhancement of the limiting current of the first step by the presence of small amounts of water was observed in other quaternary ammonium perchlorates such as n-Bu_4NClO_4, $C_6H_5(CH_3)_3NClO_4$ and $C_6H_5CH_2$-$(CH_3)_3NClO_4$.

The reduction wave of nickel(II) observed in $LiClO_4$, $NaClO_4$ or Me_4NClO_4 electrolyte solution, however, is almost unaltered by the presence of water up to 0.12 *M*. At concentrations of water above 0.25 *M*, however, the reduction wave becomes drawn out and the reduction potential shifts to more negative values.

The enhancement of the limiting current of the first wave by the presence of small amounts of water may be caused by the partial desorption of the cation of the supporting electrolyte from the surface of mercury electrode. The presence of higher concentrations of water, on the other hand, causes the electroactive species to change from $Ni(CH_3CN)_n^{2+}$ to the hydrated nickel(II) ion[3].

The changes in the polarograms obtained in the mixed electrolyte of $LiClO_4$ and n-Bu_4NClO_4 at constant ionic strength suggest the adsorption of n-Bu_4N^+ at the electrode. The introduction of n-Bu_4NClO_4 causes the single wave observed in $LiClO_4$ electrolyte to split into a double wave. With increasing concentration of n-Bu_4NClO_4, the limiting current of the first step decreases and also becomes progressively independent of the height of mercury reservoir, and has the character of a kinetic current at concentrations of n-Bu_4NClO_4 above 25 m*M*. A single wave observed in a solution of $LiClO_4$ or $NaClO_4$ as supporting electrolyte also splits into a double wave by the step-wise addition of other quaternary ammonium perchlorates in place of n-Bu_4NClO_4.

These results may be explained on the basis of the inhibition of the charge transfer process of nickel(II) by the weak adsorption of quaternary ammonium ions at the DME.

Tetra-n-butylammonium ion is a relatively weak surface active substance in acetonitrile solution compared with aqueous medium[2]. The weakly surface active substance at considerably higher concentrations causes the limiting current to decrease and also the drop life dependence of the intantaneous current to change[13,14] from $t^{\frac{1}{6}}$ to $t^{\frac{2}{3}}$.

The reduction potential of the first step observed in quaternary ammonium perchlorate solution is almost independent on the nature of the cation of the supporting electrolyte; that of the second step, on the other hand, shifts to more negative values with increasing radius of cation and concentration of electrolyte. This may be due to the fact that the surface coverage of quaternary ammonium ion increases with increase of the radius and the concentration of the cation of the electrolyte.

The cation effects for the reduction of nickel(II) in propionitrile and benzonitrile solvents were also investigated and the results were found to be almost identical with the data obtained in acetonitrile solution.

SUMMARY

The effect of supporting electrolyte on the electrode reaction of nickel(II) in acetonitrile solution was investigated. An acetonitrile solution of nickel(II) gave a single irreversible wave in $LiClO_4$, $NaClO_4$ and $(CH_3)_4NClO_4$ supporting electrolytes, and a double wave in $(C_2H_5)_4NClO_4$, $(n\text{-}C_4H_9)_4NClO_4$, $C_6H_5(CH_3)_3NClO_4$, $C_6H_5CH_2(CH_3)_3NClO_4$ and $CH_3(CH_2)_{15}(CH_3)_3NClO_4$.

The effects of water and mixed electrolyte on the reduction wave were also investigated. A single wave observed in a solution containing alkali metal perchlorate splits into a double wave on the addition of small amounts of quaternary ammonium perchlorate. The limiting current of the first step of a double wave is a kinetic-controlled mechanism based on the result of the *i–t* curve measurement of an individual drop.

The double wave is due to the inhibition of the charge transfer process by the relatively weak adsorption of the quaternary ammonium ion and not to the presence of two electroactive species.

REFERENCES

1 R. W. MURRAY AND L. K. HILLER, JR., *Anal. Chem.*, 39 (1967) 1221.
2 S. IKEDA AND E. ITABASHI, *Bull. Chem. Soc. Japan*, 41 (1968) 1844.
3 I. M. KOLTHOFF AND J. F. COETZEE, *J. Am. Chem. Soc.*, 79 (1957) 1852.
4 J. F. COETZEE, D. K. MCGUIRE AND J. L. HEDRICK, *J. Phys. Chem.*, 67 (1963) 1814.
5 A. I. POPOV AND D. H. GESKE, *J. Am. Chem. Soc.*, 79 (1957) 2074.
6 R. C. LARSON AND R. T. IWAMOTO, *J. Am. Chem. Soc.*, 82 (1960) 3239.
7 I. V. NELSON AND R. T. IWAMOTO, *J. Electroanal. Chem.*, 6 (1963) 234.
8 G. A. FORCIER AND J. W. OLVER, *Anal. Chem.*, 37 (1965) 1447.
9 J. F. O'DONNEL, J. T. AYRES AND C. K. MANN, *Anal. Chem.*, 37 (1965) 1161.
10 A. E. WICKENDEN AND R. A. KRAUSE, *Inorg. Chem.*, 4 (1965) 404.
11 B. J. HATHWAY AND A. E. UNDERHILL, *J. Chem. Soc.*, (1961) 3091.
12 W. L. UNDERKOFLER AND I. SHAIN, *Anal. Chem.*, 35 (1963) 1778.
13 R. W. SCHMID AND C. N. REILLEY, *J. Am. Chem. Soc.*, 80 (1958) 2087.
14 H. MATSUDA, *Rev. Polarog. Kyoto*, 14 (1967) 87.

ELECTROANALYTICAL CHEMISTRY AND INTERFACIAL ELECTROCHEMISTRY
Elsevier Sequoia S.A., Lausanne – Printed in The Netherlands

SELECTIVE EFFECT OF SUPPORTING ELECTROLYTE ON THE POLAROGRAPHIC CATALYTIC CURRENT OF NICKEL(II) IN ACETONITRILE IN THE PRESENCE OF HALIDE IONS

EIKI ITABASHI AND SHIGERO IKEDA
Department of Chemistry, Faculty of Science, Osaka University, Toyonaka, Osaka (Japan)
(Received October 22nd, 1968; in revised form September 26th, 1969)

It has been shown by several groups of investigators[1-7] that aqueous solutions of nickel(II) in the presence of pyridine, *o*-phenylenediamine, ethylenediamine, triethylenetetramine, chloride ion, thiocyanate ion, etc. give a catalytic polarographic wave which occurs at less negative potentials than that for the usual hydrated nickel(II) reduction wave.

The polarographic studies of nickel(II) in the presence of chloride ion have been carried out in both aqueous and acetonitrile media.

In the presence of high concentrations of chloride ion, the reduction wave of nickel(II) shifts to less negative potentials and shows that the electrode reaction takes place with greater reversibility. This behavior has been attributed to the formation and reduction of tetrachloronickel(II) ion[8,9].

Nelson and Iwamoto[6] studied the polarographic behavior of nickel(II) in acetonitrile in the presence of chloride ion, and concluded that nickel(II) in a 0.1 *M* Et_4NClO_4 electrolyte solution containing small amounts of chloride ion gave a double wave; the first step involved the reversible reduction of the four nickel(II)–chloride complexes, $NiCl^+$, $NiCl_2$, $NiCl_3^-$ and $NiCl_4^{2-}$, and the second step involved the reduction of the hydrated nickel(II). The catalytic nature of the first step was also discussed.

During the study of the effect of the cation of the supporting electrolyte upon the electrode reaction of metal complexes in non-aqueous media[10,11], it was found that an acetonitrile solution of nickel(II) in the presence of small amounts of chloride, bromide and iodide ions gave a catalytic pre-wave; the activity of halide ions was dependent on the nature of the cation of the supporting electrolyte employed.

The present paper reports on the results of the study on the effect of cations on the catalytic pre-wave of nickel(II) in acetonitrile containing halide ion.

EXPERIMENTAL

Reagents

Purified acetonitrile was obtained by the procedure given in the previous report[11].

Lithium perchlorate, tetraethylammonium perchlorate (Et_4NClO_4) and tetra-n-butylammonium perchlorate (n-Bu_4NClO_4) were prepared by neutralizing the respective hydroxide solutions with dilute perchloric acid. The dried perchlorate

salts were obtained by the procedure described previously[11]. Guaranteed reagents, LiCl, LiBr, LiI, $(C_2H_5)_4NBr$, $(C_2H_5)_4NI$, $(n\text{-}C_4H_9)_4NBr$ and $(n\text{-}C_4H_9)_4NI$ were recrystallized several times from purified acetonitrile and were then dried in a vacuum oven at 80–85°C for 60 h. Nickel(II) perchlorate $Ni(H_2O)_2(ClO_4)_2$ was obtained as reported previously[11].

The water content of the polarographic solution containing the supporting electrolyte, halide ion and nickel(II) perchlorate was found to be 10–15 m*M* by Karl Fisher titration.

Procedure

Polarograms and the current–time (*i–t*) curve of an individual drop at constant potential were recorded with the same circuit as described previously[11].

The dropping mercury electrode had a value of 1.44_6 mg s^{-1} and a drop time of 5.01 s in a deaerated 0.1 *M* lithium perchlorate acetonitrile solution at −0.70 V *vs.* SCE and 60 cm mercury height. The potential of the DME was measured against a saturated calomel electrode (SCE).

The cell equipment has already been described[11]. The dissolved oxygen in the solution was removed by bubbling pure nitrogen gas through the solution.

Measurements were made at 25±0.1°C. In the following section, the word "current" in the Figures refers to the maximum current observed just before the fall of a mercury drop.

RESULTS

$LiClO_4$ system

The reduction waves of nickel(II) in a 0.1 *M* $LiClO_4$ electrolyte solution containing halide ions are shown in Fig. 1. Nickel(II) in the absence of halide ions gave an irreversible wave, and in the presence of halide ions gave a pre-wave, where it was reduced with greater reversibility. When the concentration of iodide ion was very small, the pre-wave exhibited a peak current.

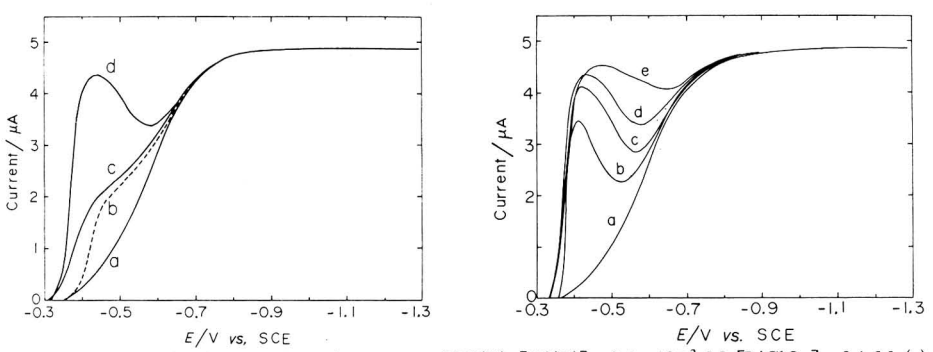

Fig. 1. Effect of halide ions on the polarograms of Ni(II). $[Ni(II)] = 0.5 \times 10^{-3}$ *M*, $[LiClO_4] = 0.1$ *M*. (a) absence of halide ion, (b) 0.1×10^{-3} *M* LiCl, (c) 0.1×10^{-3} *M* LiBr, (d) 0.1×10^{-3} *M* LiI.

Fig. 2. Effect of concn. of LiI on the polarograms of Ni(II). $[Ni(II)] = 0.5 \times 10^{-3}$ *M*, $[LiClO_4] = 0.1$ *M*. [LiI]: (a) 0, (b) 0.02×10^{-3}, (c) 0.05×10^{-3}, (d) 0.1×10^{-3}, (e) 0.5×10^{-3} *M*.

Figure 2 shows the polarograms of nickel(II) in a 0.1 *M* $LiClO_4$ electrolyte solution containing various concentrations of iodide ion.

The relations between the height of the pre-wave and the concentration of various halide ions are given in Fig. 3. The term i_c, was defined as

$$i_c = i_t - i_1$$

where i_t is the observed total height of the pre-wave and i_1 the current observed in the absence of halide ions at the same potential. The currents i_t and i_1 in the presence of

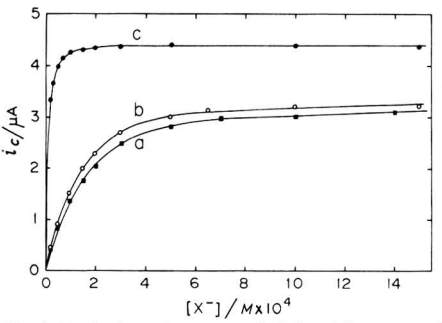

Fig. 3. Variation of pre-wave height with concn. of halide ion. $[Ni(II)] = 0.5 \times 10^{-3}$ *M*, $[LiClO_4] = 0.1$ *M*. (a) LiCl, (b) LiBr, (c) LiI.

chloride and bromide ions were measured at -0.50 V and -0.48 V *vs.* SCE, respectively; in the presence of iodide ion they were measured at the peak potential. The concentration of halide ions necessary to obtain the maximum height of the pre-wave increased in the following order: iodide, bromide, chloride ions.

The *i–t* curve of an individual drop for the pre-wave was investigated to determine if the electrode process was diffusion- or kinetic-controlled. The exponents of the *i–t* curves are shown in Table 1.

The normal *i–t* curves were obtained in the presence of chloride and bromide

TABLE 1

EFFECT OF CONCENTRATION OF HALIDE IONS ON THE EXPONENT OF CURRENT–TIME CURVES FOR THE PRE-WAVES OF Ni(II)

$[Ni(II)] = 0.5 \times 10^{-3}$ *M*, $[LiClO_4] = 0.1$ *M*

Concn. of halide ion/M	*LiCl*		*LiBr*		*LiI*	
	E/V vs. SCE	*x in* $i_1 = kt^x$	*E/V vs. SCE*	*x in* $i_1 = kt^x$	*E/V vs. SCE*	*x in* $i_1 = kt^x$
2×10^{-5}					−0.42	0.62 ~ 1.05*
5×10^{-5}	−0.54	0.45	−0.48	0.43	−0.42	0.28 ~ 0.43*
1×10^{-4}	−0.54	0.30	−0.48	0.35	−0.44	0.26
2×10^{-4}					−0.45	0.26
5×10^{-4}	−0.54	0.25	−0.48	0.23	−0.46	0.25
1×10^{-3}	−0.54	0.21	−0.48	0.20	−0.48	0.25

* The plot of log *i vs.* log *t* is not linear.

ions, but the plot of the log i–log t for the peak current observed in conditions where the concentration of iodide ion was less than 5×10^{-5} M, was not linear.

Et_4NClO_4 and n-Bu_4NClO_4 systems

The reduction waves of nickel(II) in 0.1 M Et_4NClO_4 and 0.1 M n-Bu_4NClO_4 electrolyte solutions containing various halide ions are shown in Figs. 4-A and -B.

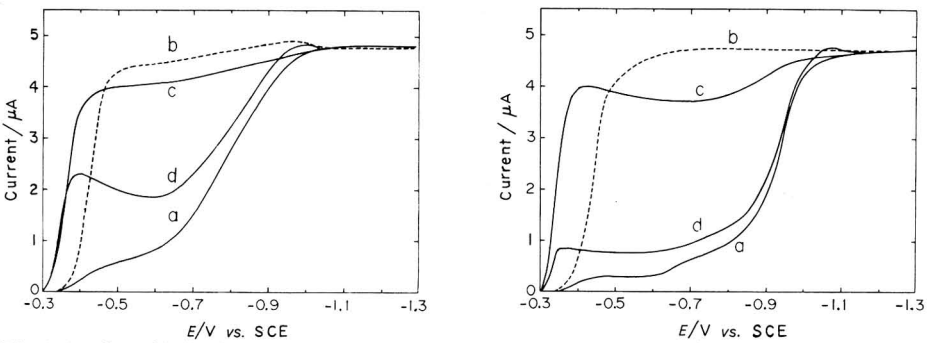

Fig. 4. A. Effect of halide ions on the polarograms of Ni(II). [Ni(II)] = 0.5×10^{-3} M, [Et_4NClO_4] = 0.1 M. (a) absence of halide ion, (b) 0.1×10^{-3} M LiCl, (c) 0.1×10^{-3} M Et_4NBr, (d) 0.1×10^{-3} M Et_4NI.

Fig. 4. B. Effect of halide ions on the polarograms of Ni(II). [Ni(II)] = 0.5×10^{-3} M, [n-Bu_4NClO_4] = 0.1 M. (a) absence of halide ion, (b) 0.1×10^{-3} M LiCl, (c) 0.1×10^{-3} M n-Bu_4NBr, (d) 0.1×10^{-3} M n-Bu_4NI.

Nickel(II) in the absence of halide ions gave a double wave, while in the presence of small amounts of halide ions, it gave a well-developed pre-wave of higher reversibility.

Figures 5-A and -B show typical polarograms obtained in 0.1 M Et_4NClO_4

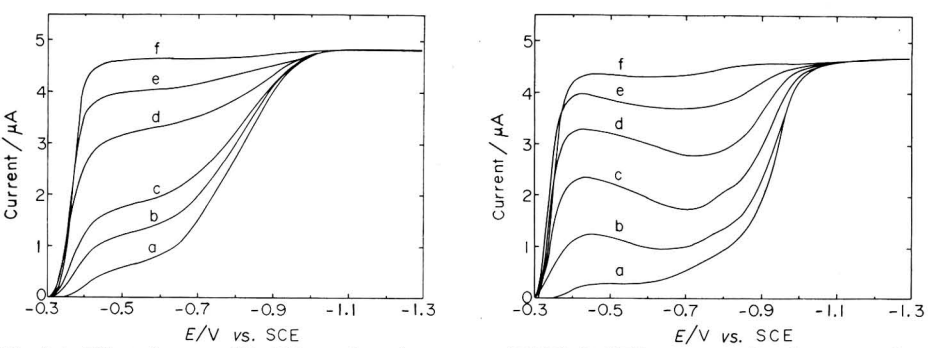

Fig. 5. A. Effect of concn. of Et_4NBr on the polarograms of Ni(II). [Ni(II)] = 0.5×10^{-3} M, [Et_4NClO_4] = 0.1 M. [Et_4NBr]: (a) 0, (b) 0.01×10^{-3}, (c) 0.02×10^{-3}, (d) 0.05×10^{-3}, (e) 0.1×10^{-3}, (f) 1.0×10^{-3} M.

Fig. 5. B. Effect of concn. of n-Bu_4NBr on the polarograms of Ni(II). [Ni(II)] = 0.5×10^{-3} M, [n-Bu_4NClO_4] = 0.1 M. [n-Bu_4NBr]: (a) 0, (b) 0.02×10^{-3}, (c) 0.05×10^{-3}, (d) 0.1×10^{-3}, (e) 0.2×10^{-3}, (f) 1.0×10^{-3} M.

and 0.1 M n-Bu_4NClO_4 electrolyte solutions, respectively. A peak current was observed in a 0.1 M Et_4NClO_4 electrolyte solution containing iodide ion, and in 0.1 M n-Bu_4NClO_4 solutions containing bromide and iodide ions, respectively.

The plots of i_c *vs.* the halide ion concentration for 0.1 *M* Et_4NClO_4 and 0.1 *M* n-Bu_4NClO_4 electrolyte solutions are shown in Figs. 6-A and -B. On the addition of small amounts of chloride or bromide ion, the double wave observed in the absence of halide ions changes to a single wave at the potential regions corresponding to the first step of the double wave.

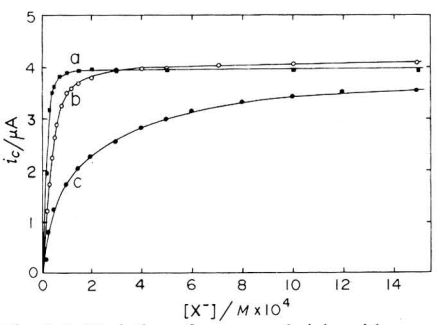

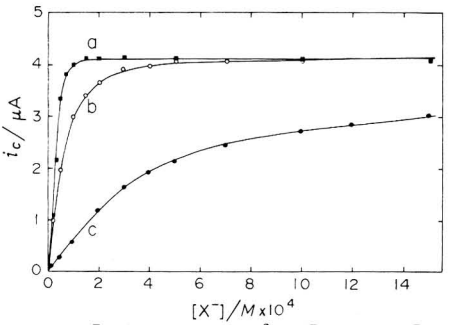

Fig. 6. A. Variation of pre-wave height with concn. of halide ion. $[Ni(II)] = 0.5 \times 10^{-3}$ *M*, $[Et_4NClO_4] =$ 0.1 *M*. (a) LiCl, (b) Et_4NBr, (c) Et_4NI.

Fig. 6. B. Variation of pre-wave height with concn. of halide ion. $[Ni(II)] = 0.5 \times 10^{-3}$ *M*, $[n\text{-}Bu_4NClO_4] =$ 0.1 *M*. (a) LiCl, (b) n-Bu_4NBr, (c) n-Bu_4NI.

A typical *i–t* curve and the log *i*–log *t* plot in the presence of iodide ion are shown in Fig. 7.

The exponents of the *i–t* curves for the pre-wave are represented in Tables 2 and 3. In both electrolyte solutions, the exponent of the *i–t* curve obtained at a relatively small concentration of iodide ion was above 0.67, which can be expected for a purely kinetic-controlled electrode mechanism.

The height of pre-wave i_c, measured at four different concentrations of nickel-(II) is shown in Fig. 8 as a function of bromide ion concentration; i_c does not vary

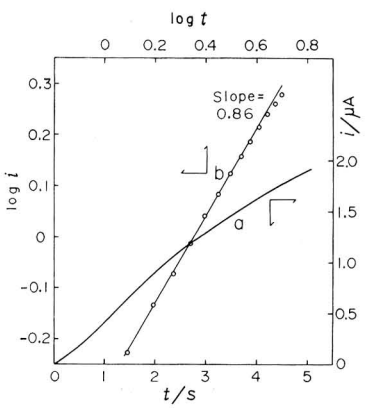

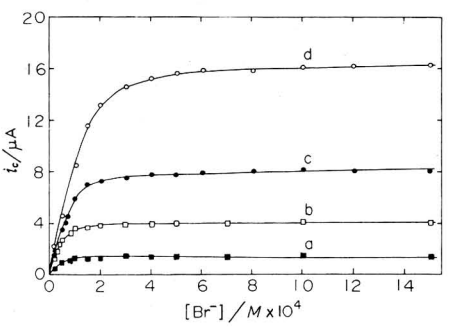

Fig. 7. Current–time curve (a) and log *i* – log *t* plot (b). $[Ni(II)] = 0.5 \times 10^{-3}$ *M*, $[Et_4NI] = 0.05 \times 10^{-3}$ *M*, $[Et_4NClO_4] = 0.1$ *M*. Applied potential = −0.40 V *vs.* SCE.

Fig. 8. Variation of pre-wave height with concn. of Et_4NBr. $[Et_4NClO_4] = 0.1$ *M*. [Ni(II)]: (a) 0.2×10^{-3}, (b) 0.5×10^{-3}, (c) 1.0×10^{-3}, (d) 2.0×10^{-3} *M*.

TABLE 2

EFFECT OF CONCENTRATION OF HALIDE IONS ON THE EXPONENT OF THE CURRENT–TIME CURVE FOR THE PRE-WAVE OF Ni(II)
$[Ni(II)] = 0.5 \times 10^{-3}$ *M*, $[Et_4NClO_4] = 0.1$ *M*

Concn. of halide ion/M	*LiCl*		*Et_4NBr*		*Et_4NI*	
	E/V vs. SCE	*x in $i_l = kt^x$*	*E/V vs. SCE*	*x in $i_l = kt^x$*	*E/V vs. SCE*	*x in $i_l = kt^x$*
1×10^{-5}	−0.54	0.57				
2×10^{-5}	−0.54	0.46	−0.50	0.59	−0.40	0.99
5×10^{-5}	−0.54	0.32	−0.50	0.44	−0.40	0.86
1×10^{-4}	−0.54	0.25	−0.50	0.33	−0.40	0.65
2×10^{-4}	−0.54	0.22	−0.50	0.27	−0.42	0.56
5×10^{-4}			−0.50	0.24	−0.60	0.45
1×10^{-3}			−0.50	0.21	−0.60	0.40

TABLE 3

EFFECT OF CONCENTRATION OF HALIDE IONS ON THE EXPONENT OF THE CURRENT–TIME CURVE FOR THE PRE-WAVES OF Ni(II)
$[Ni(II)] = 0.5 \times 10^{-3}$ *M*, $[n\text{-}Bu_4NClO_4] = 0.1$ *M*

Concn. of halide ion/M	*LiCl*		*n-Bu_4NBr*		*n-Bu_4NI*	
	E/V vs. SCE	*x in $i_l = kt^x$*	*E/V vs. SCE*	*x in $i_l = kt^x$*	*E/V vs. SCE*	*x in $i_l = kt^x$*
2×10^{-5}	−0.60	0.62	−0.46	0.61		
5×10^{-5}	−0.60	0.30	−0.44	0.52		
1×10^{-4}	−0.60	0.23	−0.44	0.41		
2×10^{-4}	−0.60	0.21	−0.44	0.31	−0.39	0.75
5×10^{-4}			−0.44	0.26	−0.39	0.56
1×10^{-3}			−0.47	0.22	−0.40	0.42

linearly with bromide ion concentration.

The concentration of halide ions necessary to obtain the maximum height of the pre-wave increased in the following order: chloride, bromide, iodide ions, in both 0.1 *M* Et_4NClO_4 and 0.1 *M* n-Bu_4NClO_4 electrolyte solutions. The pre-wave height i_c, at a constant concentration of halide ions did not vary linearly with the concentration of nickel(II) in various supporting electrolyte solutions.

DISCUSSION

The acetonitrile solution of nickel(II) in the absence of halide ions yields an irreversible wave in $LiClO_4$ and a double wave in Et_4NClO_4 and n-Bu_4NClO_4[11]. In the presence of small amounts of halide ions, nickel(II) exhibits a pre-wave which arises at less negative potentials than for the usual nickel(II) reduction wave.

The pre-wave height at a constant concentration of halide ions does not vary linearly with the concentration of nickel(II). This is a typical property of a catalytic

wave[12]. The catalytic nature of the pre-wave is also suggested by the measurement of the *i–t* curve of an individual drop for the pre-wave.

As the concentration of halide ions is increased, the pre-wave becomes a more appreciable portion of the total limiting current of the nickel(II) species, and the exponents of the *i–t* curve decrease. This indicates that the process has an appreciable contribution from a diffusion-controlled electrode mechanism, as shown in Tables 1, 2 and 3.

The catalytic pre-wave of nickel(II) in the presence of halide ions also involves an adsorbed species. The theoretical treatment of Mairanovskii predicts that the catalytic reaction involving an adsorbed species will exhibit a peak current[13].

The *i–t* curve measurements for the peak current observed in various supporting electrolyte solutions containing iodide ion show that the exponent of the *i–t* curve obtained at relatively small concentrations of iodide ion is well beyond the value of 0.67 expected for a purely kinetic-controlled electrode mechanism. This result also provides evidence of the adsorption of a catalyst at the electrode. As long as no concentration polarization occurs[14], the exponent of the *i–t* curve is 7/6.

The catalytic activity of halide ion depends on the nature of the cation of the supporting electrolyte. Chloride and bromide ions in a quaternary ammonium perchlorate solution are more active than those in a $LiClO_4$ electrolyte solution. In particular, the peak current height observed at a finite concentration of iodide ion decreases in the following order: $LiClO_4$, $NaClO_4$, Et_4NClO_4, n-Bu_4NClO_4. These results indicate that the cation of the supporting electrolyte plays an important role for the catalytic pre-wave. These properties of the pre-wave suggest that the mechanism involves very rapid adsorption equilibria of halide ions and of cations which control the reactive surface area of the electrode.

The maximum height of the pre-wave observed in a $LiClO_4$ electrolyte solution containing iodide ion and in a quaternary ammonium perchlorate containing chloride ion, is reached under conditions where the mole ratio of halide ion to nickel(II) is less than unity, and becomes nearly equal to the height of diffusion current of the main nickel(II) reduction wave. This indicates that an adsorbed halide ion reacts with nickel(II) to form a complex at the electrode surface prior to the electron transfer process; this complexation is relatively slow as the limiting current of the pre-wave is kinetic in nature.

The reaction mechanism of the catalytic pre-wave for the nickel(II)–halide ion systems in acetonitrile can be written as the following sequence[2,5]:

$$NiX_q(CH_3CN)_{n-q}^{(2-q)+} + q\,CH_3CN \overset{K_1}{\rightleftarrows} Ni(CH_3CN)_n^{2+} + q\,X^- \tag{1}$$

$$(X^-)_{bulk} \rightleftarrows (X^-)_{ads} \tag{2}$$

$$(R^+)_{bulk} \rightleftarrows (R^+)_{ads} \tag{3}$$

$$Ni(CH_3CN)_n^{2+} + p\,(X^-)_{ads} \xrightarrow[slow]{k_{chem}} \{NiX_p(CH_3CN)_{n-p}^{(2-p)+}\}_{ads} + p\,CH_3CN \tag{4}$$

$$\{NiX_p(CH_3CN)_{n-p}^{(2-p)+}\}_{ads} + 2\,e \xrightarrow[fast]{k_{el}} Ni(0) + p\,(X^-)_{ads} + (n-p)CH_3CN \tag{5}$$

where X^- refers to halide ion, R^+ is the cation of the supporting electrolyte, K_1 the

effective formation constant of the Ni(II)–halide complex in the bulk solution and k_{chem} and k_{el} are the rate constants of reactions (4) and (5), respectively.

Reactions (2) and (3) represent the adsorption equilibria of X^- and R^+, respectively. If R^+ is a quaternary ammonium ion, it is adsorbed at the electrode[11]. The cyclic regeneration of adsorbed halide ions in reactions (4) and (5) accounts for the catalytic enhancement.

Some spectrophotometric studies showed that appreciable amounts of nickel(II)–halide complexes were present in acetonitrile solution. The formation of nickel(II)–halide complexes has been reported by several investigators[15-18].

The effect of the cation of the supporting electrolyte on the catalytic wave is considered to be due to a selective passing of halide ion through holes in the adsorbed cation layer[19].

In a quaternary ammonium perchlorate solution, a comparatively large iodide ion cannot easily pass through a hole of an adsorbed layer of cation, so that reaction (4) would be inhibited. The activity of iodide ion for the enhancement of the pre-wave increases with decreasing radius of the cation of the supporting electrolyte. On the other hand, chloride ion will easily pass through a hole of an adsorbed layer of quaternary ammonium ion because of the small size of the chloride ion, and the adsorption of chloride ion participating in reaction (4) will not be affected.

The extent of electrode coverage of halide ion in $LiClO_4$ electrolyte solution is not limited by the presence of lithium ion because of the absence of marked specific adsorption of the cation, so that the catalytic activity of halide ion will be parallel to the extent of electrode coverage of halide ion. This assumption satisfactorily accounts for the height of pre-wave obtained in $LiClO_4$ electrolyte solution.

SUMMARY

An acetonitrile solution of nickel(II) in the presence of halide ion gives a catalytic pre-wave. The pre-wave height was studied as a function of the concentration of nickel(II) and halide ions. The catalytic activity of halide ion for the pre-wave in lithium perchlorate solution decreases in the following order: iodide, bromide, chloride ions; on the other hand, in a quaternary ammonium perchlorate solution it decreases in the order: chloride, bromide, iodide ions.

A mechanism which involves adsorption equilibria between bulk and adsorbed halide ion and the cation of the supporting electrolyte, and a complexation reaction of nickel(II) and adsorbed halide ions, is presented.

The cation effect on the catalytic polarographic current is discussed on the basis of the selective passing of halide ion through holes in the adsorbed layer of the cation of the supporting electrolyte.

REFERENCES

1 H. B. MARK, JR. AND C. N. REILLEY, *J. Electroanal. Chem.*, 4 (1962) 189; *Anal. Chem.*, 35 (1964).
2 H. B. MARK, JR., *Anal. Chem.*, 36 (1964) 940; *J. Electroanal. Chem.*, 7 (1964) 276; 8 (1964) 253.
3 H. B. MARK, JR. AND L. R. MCCOY, *Rev. Polarog. Kyoto*, 14 (1967) 122.
4 H. B. MARK, JR., *Rev. Polarog. Kyoto*, 15 (1968).
5 H. B. MARK, JR., L. R. MCCOY, E. KIROWA-EISNER AND H. C. MACDONALD, JR., *J. Phys. Chem.*, 72 (1968) 1083.

6 J. V. NELSON AND R. T. IWAMOTO, *J. Electroanal. Chem.*, 6 (1963) 234.
7 D. C. OLSON, *Anal. Chem.*, 39 (1967) 1785.
8 A. A. VLČEK, *Z. Elektrochem.*, 61 (1957) 1014.
9 N. TANAKA, R. TAMAMUSHI AND M. KODAMA, *Bull. Chem. Soc. Japan*, 33 (1960) 14.
10 S. IKEDA AND E. ITABASHI, *Bull. Chem. Soc. Japan*, 41 (1968) 1844.
11 E. ITABASHI AND S. IKEDA, *J. Electroanal. Chem.*, 26 (1970) 97.
12 L. MEITES, *Polarographic Techniques*, Interscience Publishers, Inc., New York, 1955, pp. 78–82.
13 S. G. MAIRANOVSKII, *J. Electroanal. Chem.*, 6 (1963) 77.
14 J. HEYROVSKÝ AND J. KŮTA, *Principles of Polarography*, Academic Press, New York, 1966, p. 304.
15 N. S. GILL AND R. S. NYHOLM, *J. Chem. Soc.*, (1959) 3997.
16 B. J. HATHWAY AND D. G. HOLAH, *J. Chem. Soc.*, (1964) 2400.
17 R. A. WALTON, *Quart. Rev.*, 19 (1965) 126.
18 R. K. SCARROW AND T. R. GRIFFITHS, *Chem. Commun.*, (1967) 425.
19 C. N. REILLEY AND W. STUMM in P. ZUMAN AND I. M. KOLTHOFF (Eds.) *Progress in Polarography*, Vol. I, Interscience Publishers, Inc., New York, 1962, pp. 81–121.

ELECTROANALYTICAL CHEMISTRY AND INTERFACIAL ELECTROCHEMISTRY
Elsevier Sequoia S.A., Lausanne – Printed in The Netherlands

POTENTIAL SWEEP VOLTAMMETRY OF METAL DEPOSITION AND DISSOLUTION

PART 2. EXPERIMENTAL

N. WHITE AND F. LAWSON
Department of Chemical Engineering, Clayton, Victoria (Australia)
(Received December 16th, 1969)

INTRODUCTION

It would seem that frozen mercury when used as an inert electrode in metal deposition and stripping has some advantages over platinum and other similar solid electrodes. The two most important advantages are the higher hydrogen overpotential and the absence of an oxide layer. In the case of platinum, the oxide layer necessitates electrode pretreatment if reproducible results are to be obtained.

Very few attempts have been made to study in detail electrode processes at a frozen mercury electrode, although some general work has been reported[1,2]. By choosing solvents which are liquid at the freezing temperature of mercury, it is possible to set up both spherical and planar electrodes of frozen mercury. The exciting function applied to the electrode in this work is a triangular wave voltage function. The current–potential responses are compared with those theoretically calculated for the various situations already presented[3].

EXPERIMENTAL

Choice of solvents

The results of work carried out on two solvents are reported. The solvents are anhydrous ammonia with 0.1 *M* NH_4Cl or KNO_3 as a base electrolyte and aqueous 30% (w/w) $CaCl_2$ (freezing point $-51°C$). Similar successful work has been carried out in DMF with 0.1 *M* $NaNO_3$ as a base electrolyte ($-60°C$) and 40% (w/w) H_2SO_4 ($-68°C$). For use with a solid mercury electrode, the solvent base–electrolyte system should (i) have a freezing point lower than $-40°C$, (ii) dissolve the depolariser of interest at room temperature and at $-40°C$, (iii) the depolariser should have a half-wave potential in the solution well away from the decomposition potential of the base electrolyte, and as well, not too close to the dissolution potential of mercury.

The behaviour of two solvents is described because they represent two extreme sets of conditions which might be encountered in such work. Merck AR grade $CaCl_2 \cdot 2H_2O$ was used for the preparation of the aqueous solutions and sodium dried ammonia (ICIANZ) was used to make up the ammonia base solutions.

Choice of depolarisers

In^{3+}, Cd^{2+} and Pb^{2+} all gave well developed anodic and cathodic peaks at a

frozen mercury electrode in the calcium chloride solution at $-48°C$. Only the first two were used for the quantitative work because the deposition of Pb^{2+} appeared to be slightly irreversible.

Since the diffusion coefficients of these depolarisers are quite low in the calcium chloride solution (*vide infra*) their concentrations must be sufficiently high so that the monolayer (or constant activity deposit) is formed well before the current begins to rise. After some experimentation it was found that the minimum concentration that could be used for sweep rates greater than 10^{-3} V s^{-1} was 10^{-2} *M*.

The polarographic data of Laitinen and his coworkers[4,5] leads one to believe that Cd^{2+}, Pb^{2+} and Tl^{+} give reversible waves in liquid ammonia. However, when cyclic voltammetry with a high voltage sweep rate (greater than 1 V s^{-1}) was applied to solutions of these ions in liquid ammonia with a dropping mercury electrode at $-36°C$, only the response for Tl^{+} still indicated a high degree for reversibility (based on the difference between the anodic and cathodic peaks). It was found that the presence of nitrate ions caused non-reproducibility of the responses for Tl^{+}, and the base electrolyte finally used was NH_4Cl at a concentration of 0.1 *M*. Despite the low solubility for TlCl that one might deduce from the data of Elliot and Yost[6], it was found that a concentration of 5×10^{-3} *M* of Tl^{+} was obtainable (this was ascertained by recording sweeps at an electrode of constant area for different concentrations, and observing the increase in peak current with concentration).

Cells and electrodes

The cell was designed for a three electrode system and incorporated a means whereby dry nitrogen could be flushed through the cell to prevent the ingress of air and moisture when the working electrode was being removed or inserted.

Two reference electrodes were used. A calomel microelectrode was filled with 30% (w/w) $CaCl_2$, and this permitted it to be used at low temperatures (as suggested by Head[7]). When high sweep rates were used with this electrode, potentiostat instability became a problem. Under these circumstances a platinum probe "quasi-reference" electrode was used (as recommended by Bewick[8]).

The spherical frozen electrodes may be prepared in two ways, either by freezing *in situ* or by freezing in a cryogenic liquid such as liquid nitrogen. In the latter case, the drop size is reproducible to within 5%, whereas when the drop is frozen slowly,

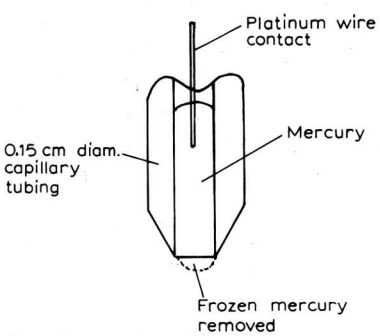

Fig. 1. Preparation of the planar frozen mercury electrode.

there is very little control on the absolute size. It was found only in the case of a liquid ammonia solvent that the responses obtained were independent of the method of frozen drop formation. In all experiments with the calcium chloride solvent, the spherical electrode was prepared by freezing *in situ*. At the completion of each experiment the drop was sliced from the syringe and weighed.

The planar frozen mercury electrode (used only in liquid ammonia) was prepared in a 0.15 cm capillary in which the edges had been ground as shown in Fig. 1. Mercury was taken up in the tubing and a drop of mercury allowed to protrude from the end. This drop was frozen in liquid nitrogen and the protruding portion sliced away. After wiping away any frost, the electrode was immediately inserted into the solution. Contact to the electrode was made by inserting a piece of platinum wire through the other end of the tube. Thermal equilibrium was established very rapidly as indicated by the reproducibility of the current potential response.

The cell was lowered into a "Colora" bath, which had been modified to reach a temperature of $-48°C$, by a vibration-free mounting system.

Potentiostat and readout systems

The potentiostat was of the Booman–Holbrook[9] design with some of the modifications suggested by Brown and others[10] incorporated. The readout for the fast sweep rates was a Tektronix storage oscilloscope with a polaroid camera attachment, whereas the slower sweeps were recorded on a Moseley model 135 X-Y-Recorder. The transient sequence shown in Fig. 2 was recorded using a Nikon-F camera with motor back attachment.

A full description of the experimental details is given elsewhere[11].

RESULTS AND DISCUSSION

Preliminary experiments

In all Figures given, cathodic currents are plotted vertically and cathodic potentials are plotted horizontally. All sweeps commence from a zero current position unless some other situation is indicated.

Figure 2 shows the changes in the current–potential response, for cyclic voltammetry, as an HME freezes. The liquid response is given at the top left hand corner, and the response from the solid is given at the bottom of the right hand corner. The base electrolyte was 30% (w/w) aqueous calcium chloride at $-48°C$ with 8.9×10^{-4} M Cd^{2+} as the depolariser. There is a shift in the cathodic and anodic peaks to more cathodic potentials as expected because no amalgamation of the deposited metal occurs. One would expect the cathodic peak for the deposition on the solid to be greater than that when the electrode is liquid since the cathodic peak current parameter I_p for amalgam formation is 0.446 but, for solid deposition, it is 0.610, all other factors being equal. On freezing, the shrinkage corresponds only to a 3% change in surface area as can be deduced from the data on mercury given by Mellor[12]. The apparent discrepancy can probably be attributed to the fact that the temperature of the liquid drop surface is close to $-39°C$ but after it freezes the surface rapidly reaches the solution temperature of $-48°C$.

The anodic peak at the solid electrode is much larger than any of the other peaks observed for either the solid or liquid electrode. This is in accord with the

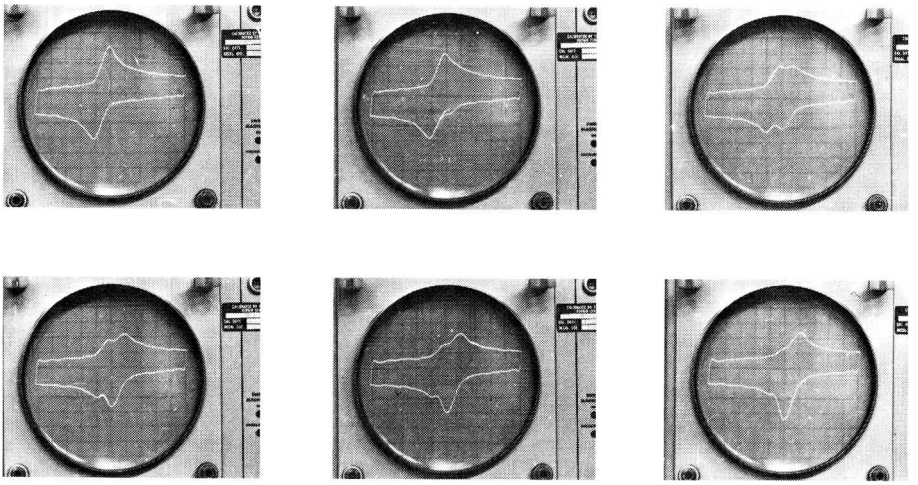

Fig. 2. Sequence showing the change in the current–potential response as the HME freezes from a liquid (top left-hand corner) to a solid (bottom right-hand corner). Solution: 8.9×10^{-4} *M* Cd^{2+} in 30% (w/w) $CaCl_2$ solution at $-48°C$.

results of the theoretical analysis for the anodic region. The anodic peak current drops to zero only when the deposit is depleted, unlike the anodic peak for amalgam dissolution which occurs at a potential independent of the amount deposited[13]. The experiment described below is offered as proof. An exciting function having a ramp increase followed by a plateau of duration τ and a ramp decrease, with varying values of the time plateau, τ, was applied to two systems, the first with a solid mercury electrode in a 5×10^{-3} *M* Tl^+–0.1 *M* NH_4Cl in anhydrous ammonia at $-48°C$, and the other an HME in an 8.9×10^{-4} *M* Cd^{2+} in a 30% (w/w) $CaCl_2$ solution at 17° C. The responses are given in Fig. 3 and confirm the statement above.

The lack of significance of the anodic peak potential from a thermodynamic

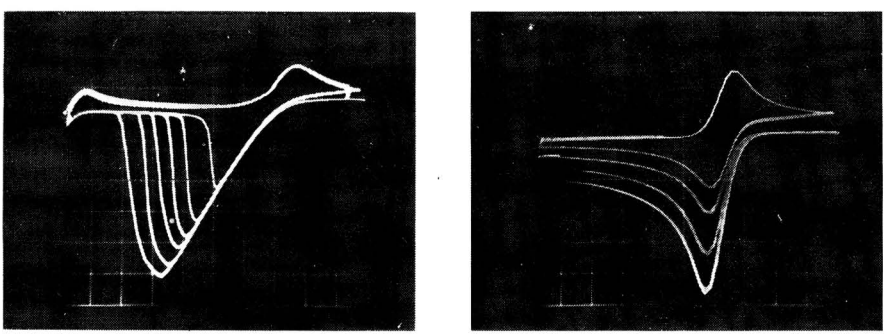

Fig. 3. Left: Voltammograms of 5×10^{-3} *M* Tl^+ in 0.1 *M* NH_4Cl–anhydrous NH_3 at $-48°C$. Frozen spherical electrode of area 0.072 cm^2, starting potential of sweep -0.17 V *vs.* Pt–quasi reference, with a vertical sensitivity of 100 $\mu A\ div^{-1}$, a horizontal sensitivity of 0.05 V div^{-1}, and a sweep rate of 0.1 V s^{-1}. Plateau times of 0, 5, 10, 15, 20, 25 s.
Right: Voltammograms of 8.9×10^{-4} *M* Cd^{2+} in a 30% (w/w) $CaCl_2$ solution at 17° C. Sweep commencing at -0.45 V *vs.* Pt–quasi reference, with a vertical sensitivity of 200 $\mu A\ div^{-1}$, a horizontal sensitivity of 0.05 V div^{-1} and a sweep rate of 0.5 V s^{-1}. Plateau times of 0, 1, 3 and 5 mins.

point of view should not therefore be overlooked in stripping voltammetry of metals (bulk-phase deposit) with an inert electrode. Furthermore, unlike the case where the reduced species is soluble, the voltage difference between the cathodic and anodic peak potentials cannot be used as a quantitative measure of the reversibility of the electrode reaction.

Responses using slow sweep rates

The aim of the work done with the slow sweep rates was to measure the ion diffusion coefficient. The results for the ammonia system are shown in Figs. 4 and 5 for

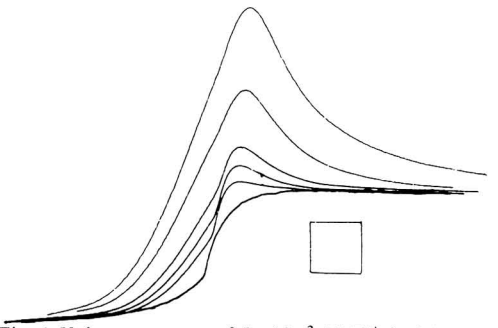

Fig. 4. Voltammograms of 5×10^{-3} *M* Tl^+ in 0.1 *M* NH_4Cl–anhydrous NH_3 at $-48°C$, using a frozen planar electrode of area 0.019 cm^2, sweep commencing at -0.32 V *vs.* Pt – quasi reference with a vertical sensitivity of 5 μA div^{-1}, a horizontal sensitivity of 0.05 V div^{-1} and sweep rates of 0.05, 0.025, 0.010, 0.0075, 0.005 and 0.001 V s^{-1}.

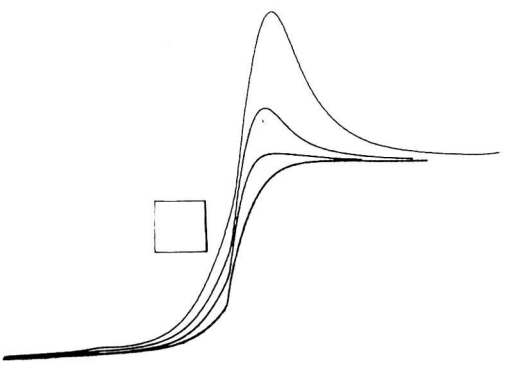

Fig. 5. Voltammograms of 5×10^{-3} *M* Tl^+ in 0.1 *M* NH_4Cl anhydrous NH_3 at $-48°$ C, using a frozen spherical electrode of area 0.064 cm^2, sweep commencing at -0.32 V *vs.* Pt – quasi reference with a vertical sensitivity of 10 μA div^{-1}, a horizontal sensitivity of 0.05 V div^{-1} and sweep rates of 0.025, 0.010, 0.005 and 0.001 V s^{-1}.

both the spherical and planar electrodes. It is apparent that with the lowest sweep rate, a convection or similar effect controls the current even at the planar electrode. Under these circumstances the diffusion coefficient can be measured by the difference between two current peaks for different sweep rates. This method also eliminates the necessity for accounting for sphericity effects. From the slowest two sweeps obtained with the planar electrode, the Tl^+ diffusion coefficient is calculated to be 6.7×10^{-6} cm^2 s^{-1}.

Using two identical (but slightly higher) sweep rates for both the planar and spherical electrodes, diffusion coefficients of 5.6 and 5.8×10^{-6} cm^2 s^{-1} are obtained, respectively. The apparent variation of diffusion coefficient with the sweep rate indicates either kinetic control of the electrode reaction and/or the presence of uncompensated cell resistance. This is discussed below.

By analogy with spherical current contributions, the convection current contribution, i_{CN}, to the total current would be of the form

$$i_{CN} = (c_0^* nFAD_0/\delta)(1-e^{-\lambda vt}) .$$

Taking the true diffusion coefficient as 6.7×10^{-6} cm^2 s^{-1} and the measured value of the limiting current, a value for δ of 5.0×10^{-3} cm is calculated for the planar electrode. Using these data, the curves shown in Fig. 6 can be drawn. Figure 6 shows the effect

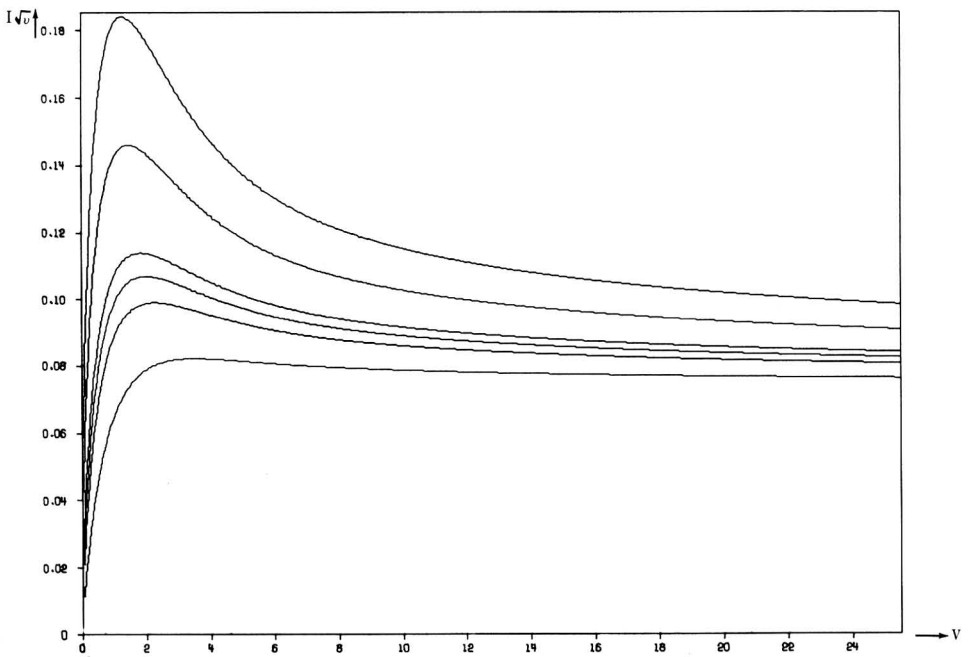

Fig. 6. Simulation of the system of Fig. 4, showing the effect of the convection contribution, with the same sweep rates as used for recording Fig. 4.

of convection current on the total current, the quantity $I\sqrt{v}$ is plotted against V, where

$$I\sqrt{v} = v^{\frac{1}{2}} 2\pi^{-\frac{1}{2}} F(\sqrt{V}) + D_0^{\frac{1}{2}} \lambda^{-\frac{1}{2}} \delta^{-1} (1-e^{-V})$$

for the same voltage sweep rates as those used to obtain Fig. 4. Each horizontal division in Fig. 4 corresponds to $0.050 \times 51 = 2.55$ units (for a one electron reduction at $-48°$C) of the horizontal scale of Fig. 6. The only portion of the responses in Fig. 4 not adequately accounted for by the curves in Fig. 6 is the region immediately before the commencement of the current rise. No explanation can be suggested as yet for this phenomenon. The limiting current at the planar electrode is reproducible to

within 2%, but despite the recording of over 200 runs on the spherical electrode, the limiting current at this electrode varied by as much as 50% from one run to the next.

Laitinen and Kolthoff[15] have shown that convection currents are most pronounced at spherical electrodes. Whilst it is generally held that horizontal planar electrodes do not give rise to natural convection currents[9,14] under some conditions heat transfer by natural convection to or from a horizontal surface is known to occur[16]. It is probable that in the system being studied the convection arises both from the concentration–density gradient effect and from thermal effects.

In contrast to the results described above, it was found that with 30% (w/w) calcium chloride solution even at the slowest sweep rates there was no apparent convection contribution. This can be seen from Fig. 7. Based on the difference between the

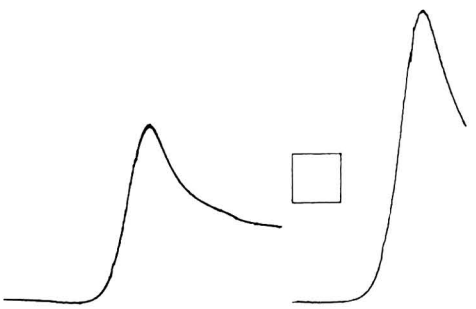

Fig. 7. Voltammograms of 10^{-2} *M* Cd^{2+} in a 30% (w/w) $CaCl_2$ solution at $-48°$C with a spherical frozen mercury electrode of area 0.078 cm^2. Sweep commences at -0.92 V *vs.* Pt–quasi reference, with a vertical sensitivity of 2 μA div^{-1}, a horizontal sensitivity of 0.05 V div^{-1}, and sweep rates of 0.0025 and 0.001 V s^{-1}.

two current peaks at different sweep rates, the diffusion coefficient for Cd^{2+} at $-48°$C in 30% (w/w) calcium chloride solution was found to be 7.3×10^{-8} cm^2 s^{-1}. Using this value and allowing for the spherical contribution, a peak current of 8.1×10^{-6} A is calculated for the scan and this compares very favourably with the measured value of 7.3×10^{-6} A.

The difference in the behaviour as far as the convection effect is concerned between the two base solutions is quite marked and a possible explanation is proposed. Referring to the heat transfer case, it is generally considered that when the product of the Grashof and Prandtl numbers reaches a critical value, it is then that heat transfer by natural convection commences. For mass transfer it is the product of Grashof and Schmidt numbers which is important. Whilst data are not available for calculating these dimensionless groups completely, the one quantity which will be most different in the two situations is viscosity. For liquid ammonia at $-48°$C, extrapolation of the data from Waddington's text[17] yields a viscosity of 0.36 cP, whereas from Perry's text[18] a viscosity of 16 cP is obtained for 30% $CaCl_2$ at $-48°$C, a 44-fold variation. Manning[19] has reported the presence of convection interference in some of his work.

It has been claimed[20] that the diffusion layer thickness is independent of the actual electrode process. This information was used in a further series of experiments aimed at obtaining data on diffusion coefficients. Runs were carried out on a solution containing equal concentrations of Tl^+ and Cd^{2+} in 0.1 *M* NH_4Cl in anhydrous ammonia with a frozen mercury spherical electrode at $-48°$C. Figure 8 shows the

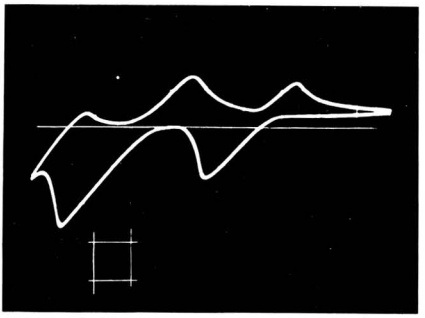

Fig. 8. Cyclic voltammogram of 5×10^{-3} *M* Tl^+ and Cd^{2+} in 0.1 *M* KNO_3–anhydrous NH_3 at $-48°C$, with a spherical frozen mercury electrode of area 0.035 cm^2. Sweep commencing at -0.16 V *vs.* 30% (w/w) $CaCl_2$ calomel electrode, with a vertical sensitivity of 200 μA div^{-1}, a horizontal sensitivity of 0.17 V div^{-1}, and a sweep rate of 32 V s^{-1}.
(Zero current line is the grid centre line.)

current–potential response of this system at a high sweep rate. At low sweep rates it was found that the limiting current for thallium deposition was within 5% of the cadmium deposition limiting current (measured relative to the thallium limiting current). Since the concentrations and electrode areas are the same, then

$$i_{L_1}/i_{L_2} = n_1(D_0)_1/n_2(D_0)_2 \quad (1)$$

At $-36°C$ the diffusion coefficient for Tl^+ in anhydrous ammonia is given by Laitinen and Shoemaker[4] as 3.30×10^{-5} cm^2 s^{-1}, and from the diffusion current constant given by McElroy and Laitinen[5] a value of 1.5×10^{-5} cm^2 s^{-1} is calculated for Cd^{2+} in the same solvent at the same temperature and it is likely that the ratio of the two diffusion constants is the same even at $-48°C$. When eqn. (1) is applied to the limiting currents, one would expect the diffusion coefficient of Cd^{2+} to be about half that of Tl^+ in 0.1 *M* NH_4Cl anhydrous ammonia and this agrees with the values calculated.

It is also of interest to point out the absence of any intermetallic compound formation at the electrode in the system used to obtain Fig. 8. This conclusion is based on the fact that the shape of the compound response was found to be the sum of the individual responses for Cd^{2+} and Tl^+. There is also no multiple peaking of either the anodic or cathodic peaks, which phenomena are symptomatic of intermetallic compound formation, such as are observed with platinum[21].

Responses using fast sweep rates

No attempt was made to determine the kinetic parameters for the calcium chloride solutions because of the large capacity currents which are encountered in this system when high sweep rates are used. These high capacity currents are evident in Fig. 2.

Even with some of the slow sweeps carried out in the ammonia system, Fig. 5, the forward movement of the peak is discernible. When a comparatively high sweep rate is used (1 V s^{-1}) as in Figs. 9 and 10, a value of $I_p = 0.575$ is calculated from the peak current (for the planar electrode) after deducting the convection current. A value of 134 mV is measured for $E_{p-p/2}$, which corresponds to 6.8 for the voltage shift parameter $V_{p-p/2}$. Referring to Fig. 5 of ref. 3 it is seen that these values do not coincide

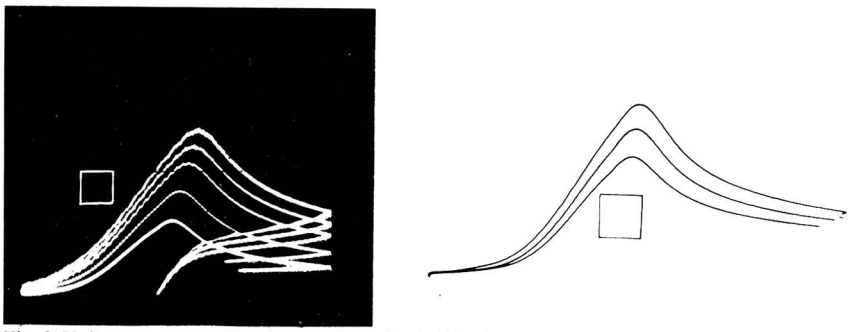

Fig. 9. Voltammograms of system used to obtain Fig. 4.
Left: Vertical sensitivity 20 μA div^{-1}, sweep rates of 1.0, 0.75, 0.50, 0.25 and 0.10 V s^{-1}.
Right: Vertical sensitivity of 10 μA div^{-1}, and sweep rates of 0.100, 0.075 and 0.050 V s^{-1}.

Fig. 10. Voltammograms of system used to obtain Fig. 5 (prepeaking due to some untraceable impurity).
Left: Vertical sensitivity of 50 μA div^{-1}, and sweep rates of 1.0, 0.75, 0.5, 0.25, and 0.1 V s^{-1}.
Right: Vertical sensitivity of 20 μA div^{-1}, and sweep rates of 0.10, 0.075, 0.05 V s^{-1}.

with an uncompensated resistance or kinetic effect. In fact, all of the points obtained at high sweep rates for both the planar and spherical electrodes gave peak minus half peak potentials very much greater than expected from their peak current parameters. The uncompensated cell resistance for the system from which the above results were obtained was found to be approximately 200 Ω. For a sweep rate of 1 V s^{-1}, this corresponds to an RH value of 5, and does not account for the large value of $V_{p-p/2}$. The problem was traced to the fact that a monolayer of deposit is not formed until the current reaches an appreciable fraction of the peak current. This particular point is discussed in detail below.

Monolayer deposition

To evaluate the charge required to form a monolayer for a square centimetre of geometric surface area, Nicholson[22] suggested that one should assume a square packing on the surface. For a metal ion M^{n+} which deposits with a free metal radius of r_M Angstrom units, the charge required per unit area is

$$q/A = Fn/(2r_M \times 10^{-8})^2 N_A$$
$$= (4.01 \times 10^{-4})n/r_M^2 \text{ C cm}^{-2}$$

where N_A is Avogadro's Number.

Using the value of r_M given by Wells[23], Table 1 can be set up.

TABLE 1

DATA FOR EVALUATING MONOLAYER COVERAGE

Metal	$r_M/\text{Å}$	$10^4 q\ A^{-1}/C\ cm^{-2}$
Pb	1.75	2.62
Cd	1.52	3.55
In	1.67	4.32
Tl	1.71	1.38

These values are identical with the corresponding values which can be calculated from similar data given by Nicholson[22]. Berzins and Delahay[24] however claim that for an electrode of area 0.107 cm^2, the deposition of a complete monolayer of cadmium requires only 2.21×10^{-6} C! If indeed the data in Table 1 are valid, it would appear that these latter authors did not form a monolayer on their electrode until they had reached their peak current.

Referring to the conditions under which Fig. 4 was obtained, one grid square is equivalent to 250×10^{-6} C for the slowest sweep, but the charge required to form a monolayer is 3.7×10^{-6} C. Hence the sudden break observed in the curves in Fig. 4 cannot be explained as being a result of monolayer formation. On the other hand, in the curves recorded for the calcium chloride solution, a discontinuity is always observed at about the point at which the monolayer formation is expected (one of these breaks is arrowed in Fig. 11). There is also a slight variation in the position of the peak potential.

This latter effect can be explained in terms of the parameter H, which is given by

$$H = \left(\frac{ms}{A}\right)\left(\frac{\lambda v}{\pi D_0}\right)^{\frac{1}{2}} e^{-\lambda(E_i - E_0)} = \left(\frac{ms}{A}\right)\frac{a^*}{c_0^*}\left(\frac{\lambda v}{\pi D_0}\right)^{\frac{1}{2}}$$

Because, experimentally, one always arranges for E_i to be appreciably anodic of E_0, a^* is likely to be small and its value is unlikely to equal the fractional coverage. It is also probably influenced by microscopic impurities and any localised disturbances from

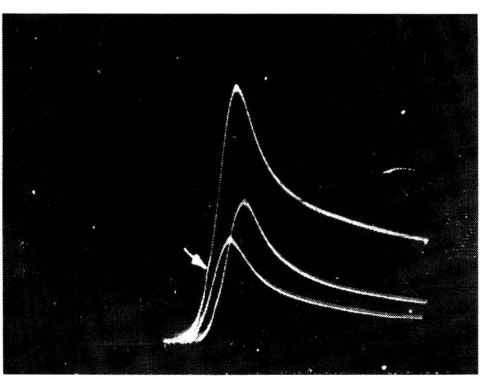

Fig. 11. Voltammograms of system used to obtain Fig. 7. Vertical sensitivity 5 μA div^{-1}, with sweep rates 0.05, 0.03 and 0.01 V s^{-1}.

equilibrium. This results in uncertainties in H which, in turn, governs how fast the monolayer is formed. In addition, there will be an uncertainty in E_i where E_i is now assumed to be the potential at which current begins to flow once the deposit activity is unity. Ultimately the small shift in the peak potentials from one run to the next is a reflection on how accurately a^* is reproduced at the commencement of each sweep. From the analysis given previously[3], it is possible to show

$$a(t) = a^* + (a^*/H)\int_0^y \psi(y)\mathrm{d}y\,,$$

or, using the appropriate dimensionless current and potential, and substituting for H,

$$a(t) = a^* + (A/ms)c_0^*(D_0/v)^{\frac{1}{2}}\int_0^{V_f} I(V)\mathrm{d}V \tag{2}$$

where the symbols have been previously defined and V_f is the value of V at which $a(t)$ will be unity.

Taking the conditions under which the slowest sweep ($v = 0.01$ V s^{-1}) of Fig. 11 was recorded and substituting these data into eqn. (2) gives

$$a(t) = a^* + 46.9\int_0^{V_f} I(V)\mathrm{d}V$$

Calling the integral term IN, values of IN are tabulated below for $V_f = 5$ (for the case being considered this corresponds to a potential 5 mV cathodic of the point at which current begins to rise).

TABLE 2

EVALUATION OF INTEGRAL TERM IN EQUATION (2)

H	IN
1	0.237
3	0.225
5	0.222
7	0.221
10	0.221
100	0.219

It is apparent that the monolayer is formed very early in the response. No explanation can be offered as to why the monolayer formation in the case of the liquid ammonia solutions is more drawn out than for the calcium chloride solutions. Whatever the reason, it is still possible to conclude that the effect of monolayer formation is to elevate the peak current, particularly at high sweep rates. Because as v increases, from eqn. (2), it can be seen that V_f must increase before $a(t)$ will reach unity. Furthermore if V is very large and/or c_0^* sufficiently small, $a(t)$ may not reach unity until V_f has exceeded 0.9, in which case the monolayer will not form until after a peak has been reached. Figure 4 shows that peaks which form in the sub-monolayer region are less sharp than for the unit activity case and do not drop away as rapidly. This is confirmed in Fig. 12, where sweeps have been carried out in a 30% w/w calcium chloride solution

with 5×10^{-4} *M* In^{3+} as a depolariser. In each case the monolayer is formed well after the peak. No quantitative information could be obtained from these responses because of the non-reproducibility of the curves. An important conclusion that can be drawn from the results in Fig. 12 is that where the activity of the sub-monolayer deposit is

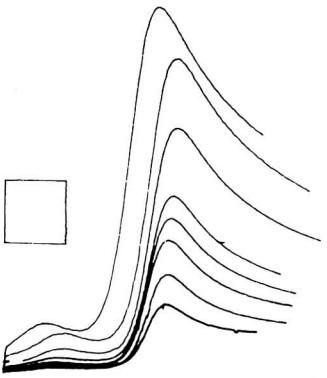

Fig. 12. Voltammograms of 5×10^{-4} *M* In^{3+} in a 30% (w/w) $CaCl_2$ solution at $-48°$ C, with a frozen mercury electrode of area 0.080 cm^2. Sweep commences at -0.75 V *vs.* Pt – quasi reference with a vertical sensitivity of 0.5 μA div^{-1}, a horizontal sensitivity of 0.05 V div^{-1}, and sweep rates of 0.075, 0.05, 0.025, 0.01, 0.0075, 0.005, 0.0025, and 0.001 V s^{-1}.

assumed to be equal to the fractional coverage, only one peak is observed. Hence this model for representing the activity of the deposit cannot be used to fit the prepeaking curves which are observed at platinum electrodes for a number of systems (these prepeaks have been attributed to the formation of a monolayer "phase"). The deposition of lead at a platinum electrode by linear sweep voltammetry is a good example of such a system.

In conclusion, it may be said that frozen mercury is a most suitable (if not an extremely convenient) inert electrode for studying metal deposition as a bulkphase or monolayer deposit.

ACKNOWLEDGEMENT

One of us (N.W.) is grateful to Monash University, for the provision of a Monash Research Scholarship.

SUMMARY

Voltammetric current potential responses to the deposition and dissolution of a metal on to or from a solid electrode, have been studied. The differentiation of the uncompensated cell resistance and kinetic effect has been put on a quantitative basis. Deposition of a sub-monolayer deposit has been investigated but difficulties arising from the establishment of the initial surface condition preclude any quantitative analysis of the results. The shapes of the voltammetric responses agreed with those calculated theoretically when a frozen mercury electrode was used. At slow sweep rates, convection interference occurs but this can be accounted for. At higher sweep

rates, capacity currents begin to interfere or insufficient current is passed to form the monolayer. The latter effect, broadens the response and elevates the peak current.

REFERENCES

1 B. BRUNS, A. FRUNKIN, S. JOFA, L. VANJUKOVA AND S. ZOLOLARENSKAJA, *Acta Physiochim. U.R.S.S.* IX (2) (1938) 359.
2 H. GERISCHER, *Anal. Chem.*, 31 (1959) 33.
3 N. WHITE AND F. LAWSON, *J. Electroanal. Chem.*, 25 (1970) 409.
4 H. A. LAITINEN AND C. E. SHOEMAKER, *J. Am. Chem. Soc.*, 72 (1950) 663, 4975.
5 A. D. MCELROY AND H. A. LAITINEN, *J. Phys. Chem.*, 57 (1953) 564.
6 N. ELLIOT AND D. N. YOST, *J. Am. Chem. Soc.*, 56 (1934) 1058.
7 R. A. HEAD, Ph.D. Thesis (1964) University Microfilms Inc. Dissertation No. 64-13, 383.
8 A. BEWICK, *Electrochim. Acta*, 13 (1968) 825.
9 G. L. BOOMAN AND W. V. HOLBROOK, *Anal. Chem.*, 35 (1963) 1793; 37 (1965) 795.
10 E. R. BROWN, T. G. MCCORD, D. E. SMITH AND D. DE FORD, *Anal. Chem.*, 38 (1966) 1119.
11 N. WHITE, Ph.D. Thesis (1969) Monash University, Victoria, Australia.
12 J. W. MELLOR, *A Comprehensive Treatise on Inorganic Chemistry*, Vol. 4, Longmans, London, 1961.
13 E. BARENDRECHT in A. J. BARD (Ed.), *Electroanalytical Chemistry*, Vol. II, Marcel Dekker, New York, 1966, p. 53.
14 N. IBL in P. DELAHAY AND C. W. TOBIAS (Eds.), *Advances in Electrochemistry and Electrochemical Engineering*, Vol. 2, Interscience, New York, 1961.
15 H. A. LAITINEN AND J. M. KOLTHOFF, *J. Am. Chem. Soc.*, 61 (1939) 3344.
16 E. R. G. ECKERT AND R. M. DRAKE JNR., *Heat and Mass Transfer*, McGraw-Hill, New York, 1959, p. 331.
17 T. C. WADDINGTON (Ed.), *Non-Aqueous Solvent Systems*, Academic Press, New York, 1965, p. 4.
18 J. H. PERRY (Ed.), *Chemical Engineers' Handbook*, McGraw-Hill, New York, 3rd ed. 1950, p. 1696.
19 D. L. MANNING, *J. Electroanal. Chem.*, 7 (1964) 302.
20 I. M. KOLTHOFF AND J. J. LINGANE, *Polarography* Interscience New York, 1952, p. 401.
21 E. SCHMIDT AND H. R. GYGAX, *J. Electroanal. Chem.*, 12 (1966) 300; 13 (1967) 378; 14 (1967) 126.
22 M. M. NICHOLSON, *J. Am. Chem. Soc.*, 79 (1957) 7.
23 A. F. WELLS, *Structural Inorganic Chemistry*, Oxford University Press, 2nd ed., 1950.
24 P. DELAHAY AND T. BERZINS, *J. Am. Chem. Soc.*, 75 (1953) 155.

ELECTROANALYTICAL CHEMISTRY AND INTERFACIAL ELECTROCHEMISTRY
Elsevier Sequoia S.A., Lausanne – Printed in The Netherlands

MECHANISM OF ANODIC DISSOLUTION OF TIN IN SODIUM HYDROXIDE SOLUTIONS

S. A. AWAD AND A. KASSAB
Chemistry Department, University College for Women, Ain Shams University, Heliopols, Cairo (U.A.R.)
(Received April 1st, 1969; in revised form December 5th, 1969)

INTRODUCTION

A limited amount of work has been concerned with the study of the anodic behaviour of tin in alkaline solutions, and the published results are somewhat conflicting. Thus, Foerster and Dolch[1] found that tin anodes passed into sodium hydroxide solutions as divalent ions until a definite concentration was attained. At this point the potential changed almost instantaneously to a more positive value, the dissolved tin was oxidised to the tetravalent state and oxygen was liberated at the anode which had become passive. Valessi[2], on the other hand, found that tin anodes in sodium hydroxide solutions dissolved directly as sodium stannite and sodium stannate, and the electrode became covered with powdery black tin metal.

In addition to this contradiction, it was observed that no mention is made in the literature of the kinetics of the anodic reactions of tin. In the present investigation the mechanism of its anodic dissolution in alkaline solutions is examined.

EXPERIMENTAL

Polarisation measurements on the tin anode were carried out in a cell (constructed from the arsenic-free hard borosilicate glass, Hysil) which permitted the rigorous purification of the solutions under investigation through anodic pre-electrolysis[3]. For this purpose a platinum anode (2 cm^2 platinum sheet welded to a platinum wire sealed to glass) was used.

The electrodes were prepared from extra pure tin rods 3 mm in diameter (Schering–Kahlbaum Company). The electrode area was 1 cm^2. Each run was carried out with a new electrode. All solutions were prepared from A.R. materials.

Before each run, the cell was cleaned with a mixture of nitric and sulphuric acids (A.R.), and thoroughly washed with conductance water. The test solution was then introduced into the pre-electrolysis compartment of the cell and pre-electrolysis was conducted at 10^{-3}–10^{-1} A cm^{-2} for 30 h. The tin electrode was then introduced into the anode compartment of the cell and adjusted to touch the Luggin capillary which led, *via* a salt bridge, to a saturated calomel electrode. Some of the pre-electrolysed solution was then transferred to the anode compartment, and the Tafel line was determined from low to high current densities and then downwards again. After each overpotential run, the concentration of the electrolyte was determined analytically.

All measurements were carried out in an air thermostat, the temperature of

which was kept constant within $\pm 0.5°C$. The current density was calculated using the apparent surface area. All potentials are recorded on the normal hydrogen scale.

RESULTS AND DISCUSSION

The potential of the tin anode was measured at 30°C in 0.1–10 *N* NaOH as a function of the current density within the range 10^{-6}–10^{-1} A cm^{-2}. At any current density the potential was constant within few minutes. In each solution, six potential–current density relations (on six new electrodes and solutions) were measured; the results were reproducible to ± 5 mV. At very low anodic polarisation the anode potential did not change with current, and a stationary potential was measured in each of these solutions. These stationary potentials are given in Table 1 together with the pH values of the different solutions.

TABLE 1

STATIONARY POTENTIALS AND PARAMETERS OF OVERPOTENTIAL FOR TIN ANODES IN DIFFERENT SOLUTIONS AT 30°C

$[NaOH]$/ $mol\ l^{-1}$	*pH*	*Stationary potential/V NHE*	*Tafel slope/mV*	$10^4\ i_0/A\ cm^{-2}$	$(\partial\eta/\partial i)_{\eta\to 0}/VA^{-1}\ cm^{-2}$	λ	*η/mV at* 10^{-3} *A* cm^{-2} *Pure soln.*	*Soln. containing 1 M* Na_2SO_4
0.1	12.89	−0.863	34	1.00	62.5	4.19	33	34
0.3	13.32	−0.897	33	1.20	57.5	3.78	29	31
0.5	13.54	−0.908	32	1.26	50.0	4.13	28	
1	13.83	−0.920	32	1.20	55.0	3.95	29	
2	14.15	−0.939	32	1.26	50.0	4.13	28	
5	14.68	−0.975	29	1.51	45.0	3.84	24	
10	15.04	−1.000	28	1.48	42.5	4.15	23	

1. *Nature of anode reaction*

The stationary potentials represent, or at least closely approach, the reversible potentials for the reaction taking place at the anode. We can, therefore, define the nature of this reaction by comparing the experimentally observed stationary potentials with the theoretical values for all possible reactions involving tin in alkaline solutions. The following oxidation reactions have been suggested as being the most probable to occur on the surface of the tin anode,

	E_B^0 *(at pH 14 and 25°C) V(NHE)*	
$Sn + 2\ OH^- \rightarrow Sn(OH)_2 + 2e$	−0.920	(1)
$Sn + 2\ OH^- \rightarrow SnO + H_2O + 2e$	−0.932	(2)
$Sn + 3\ OH^- \rightarrow HSnO_2^- + H_2O + 2e$	−0.909	(3)
$Sn + 4\ OH^- \rightarrow Sn(OH)_4 + 4e$	−0.836	(4)
$Sn + 4\ OH^- \rightarrow SnO_2 + 2\ H_2O + 4e$	−0.945	(5)
$Sn + 6\ OH^- \rightarrow Sn(OH)_6^{2-} + 4e$	−0.921	(6)

The standard potentials E_B^0 for the above reactions, at unit hydroxyl ion activity, are calculated from the standard free energy of formation[4] of the different products, OH^- and H_2O.

Since the standard potentials are little affected by temperature[5], the above

values may be taken as the standard potentials at 30°C. In Fig. 1 the observed potentials are plotted as a function of the pH value of the solution. The dotted lines represent the theoretical potential/pH relations of the oxidation reactions suggested above. These are drawn on the basis that the potential varies with pH by the same gradient as that for the hydrogen electrode (60 mV at 30°C), except in the case of tin/stannite and tin/stannate systems, for which the gradient is 90 mV. It is clear from Fig. 1 that the experimental potential/pH relation coincides with that of the Sn/SnO couple, indicating that the anode reaction is represented by eqn. (2). The oxide dissolves as stannite through the action of OH^- ions, with the result that the electrode surface remains active.

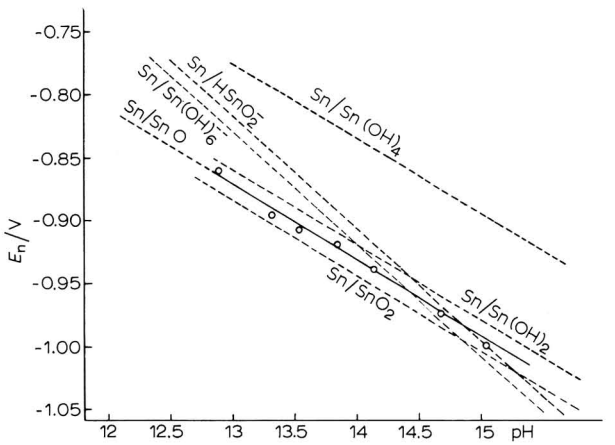

Fig. 1. Effect of pH on the reversible potential of tin anodes.

2. *Mechanism of anode reaction*

The discussion made so far indicates that the overpotential (difference between the potential measured at a given current density and the stationary potential) at the tin anode is associated with the formation of SnO. The mechanism of the reaction can be elucidated from the observed parameters and characteristics of overpotential. These are summarized below.

(*a*) *Slope of overpotential–log current density relations.* The mean values of overpotential, η, were plotted against the logarithm of the current density; some representative relations (which are usually called Tafel lines) are given in Fig. 2. It is clear that the Tafel lines exhibit a linear logarithmic part. The mean values of the slopes of these parts amount to 28–34 mV (see Table 1).

(*b*) *The electron number.* This is the number of electrons required to complete one act of the rate-determining step. This parameter is calculated from the exchange current of the Tafel line, i_0, and the slope of the overpotential–current density relation at low values of η; the expression for the electron number, λ, is:

$$\lambda = (RT/i_0F)(\partial i/\partial \eta)_{\eta \to 0}$$

Examples of the relations between η and current density at low anodic polarisation

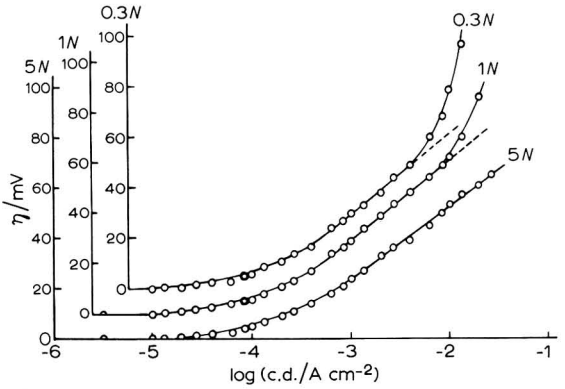

Fig. 2. Tafel lines for tin anodes in NaOH solns. at 30°C.

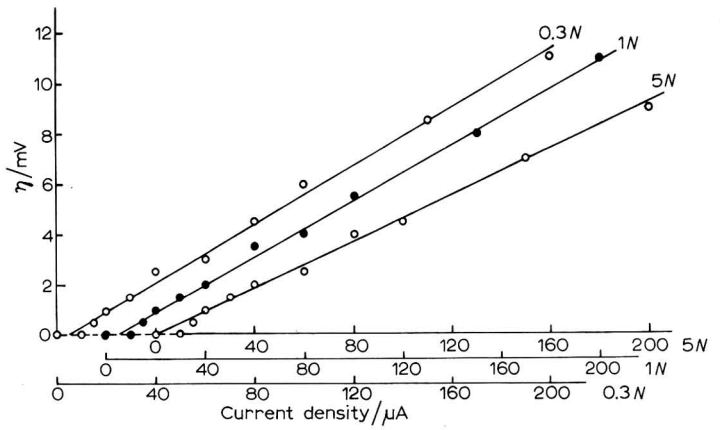

Fig. 3. Relation between current density and overpotential at low anodic polarisation of tin.

are shown in Fig. 3. The slopes of such relations, together with the exchange currents for the different Tafel lines and the calculated values for the electron number, are given in Table 1.

It is obvious from Table 1 that the experimental values of λ are very near to 4. This result may indicate that tin is oxidised to SnO_2. From the thermodynamic point of view, further oxidation of SnO according to:

$$SnO + 2\,OH^- \rightarrow SnO_2 + H_2O + 2e \qquad (7)$$

is possible, since the standard redox potential of SnO/SnO_2 (-0.958 V) is lower than that of the Sn/SnO system. It is, thus, possible that SnO undergoes 2 alternative reactions, namely the chemical dissolution into stannite, and the further oxidation to SnO_2 which dissolves as stannate. The fact that the electron number is 4 means that the rate of oxidation to SnO_2 is far larger than the rate of dissolution of SnO, and hence tin dissolves mainly as stannate. This is not actually true.

Reconciliation between the dissolution of tin as stannite and the doubled value of the electron number can be made by assuming that the surface tin atoms exist (or at least participate in electrochemical reactions) as diatomic molecules, Sn_2.

An analogous assumption has accounted satisfactorily for the cathodic[6] and anodic[7] behaviour of the tellurium electrode. As will be described below, a suboxide (Sn_2O) is first formed, which is then oxidised to the normal stannous oxide.

(*c*) *Effect of pH on overpotential.* One of the important means which help to distinguish between the different possible mechanisms is the dependence of overpotential, at a constant current density and temperature, on the pH of the solution. The overpotential at tin anodes was found to be almost independent of the alkali concentration, as is clear from Table 1, in which the values of η at 10^{-3} A cm^{-2} are given. This behaviour will give an indication as to whether the suboxide is oxidised anodically

$$Sn_2O + 2\,OH^- \rightarrow 2\,SnO + H_2O + 2\,e \tag{8}$$

or undergoes a self-oxidation process

$$2\,Sn_2O \rightarrow 2\,SnO + Sn_2 \tag{9}$$

(*d*) *Effect of neutral salts on overpotential.* Neutral salts affect the structure of the double layer at the anode–solution interface, and hence they affect the concentration of OH^- at that interface. It follows that they affect the velocity of the anode reaction. The effect of neutral salts can thus assist in elucidating the proper reaction mechanism. The overpotential was measured in 0.1 and 0.3 *N* solutions which contain excess (1 *M*) Na_2SO_4. The results indicated that the Tafel line is not affected by neutral salts; for instance, the overpotentials at 10^{-3} A cm^{-2} are the same as for the corresponding pure solutions (see Table 1). We concluded that the expression for η does not include the zeta potential (ζ).

On the basis of the above mentioned features of overpotential, the mechanism of anodic dissolution of tin in alkaline solutions was formulated as follows;

$$\text{Step I:} \quad Sn_2 + OH^- \underset{V_1'}{\overset{V_1}{\rightleftarrows}} Sn_2OH + e \tag{10}$$

$$\text{Step II:} \quad Sn_2OH + OH^- \underset{V_2'}{\overset{V_2}{\rightleftarrows}} Sn_2O + H_2O + e \tag{11}$$

$$\text{Step III:} \quad 2\,Sn_2O \overset{V_3}{\rightarrow} Sn_2 + 2\,SnO \tag{12}$$

Reaction (12) is the rate-determining step, since it requires 4 electrons. To confirm this mechanism, the Tafel line slope is theoretically deduced and compared with the experimentally observed values. The velocities of the different steps in the anodic direction are referred to as V_1, V_2 and V_3, and V_1' and V_2' represent the velocities of the first two steps in the cathodic direction. Since the velocity of the reverse of reaction (12) is negligible, the general expression for the overall rate is:

$$V_1 - V_1' = V_2 - V_2' = V_3 \tag{13}$$

It is assumed that in the anodic direction, step II is faster than step I, and hence, reaction (11) is governed by reaction (10). It follows that:

$$V_2 = V_1 \tag{i}$$

On the other hand, step II is assumed to be slower than step I in the cathodic direction.

Thus, reaction (10) is governed by reaction (11), and accordingly:

$$V_1' = V_2' \tag{ii}$$

Substituting V_1' by V_2' (*cf.* condition ii), or V_2 by V_1 (*cf.* condition i), eqn. (13) reduces to:

$$V_1 - V_2' - V_3 = 0 \tag{14}$$

It is important to mention that if reaction (11) is sufficiently fast in the anodic direction, Sn_2OH is rapidly converted into Sn_2O, with the result that the surface concentration of Sn_2OH is neglected. On the basis of a symmetrical energy barrier, the rate V_1, which represents the rate of the anodic formation of Sn_2O, is given by:

$$V_1 = k_1(1-x)[OH^-]_{d.l.} \exp(\Delta\phi F/2RT) = a_1(1-x) \tag{15}$$

where k_1 is the specific reaction rate, a_1 is the electrochemical rate constant, x is the fraction of the surface covered with Sn_2O, and $(1-x)$ is the bare fraction of the metal surface, $[OH^-]_{d.l.}$ is the activity of hydroxyl ions in the outer Helmholtz double layer, and $\Delta\phi$ is the potential difference between the electrode and this Helmholtz layer. The rate V_2', which represents the rate of cathodic reduction of Sn_2O, is given by:

$$V_2' = k_2' x \exp(-\Delta\phi F/2RT) = a_2' x \tag{16}$$

The rate of the self-oxidation process (reaction 12) is:

$$V_3 = k_3 x^2 = a_3 x^2 \tag{17}$$

The steady state corresponding to a constant coverage, current and potential is represented by eqn. (14). The self-oxidation process governs the dissolution of tin under the condition[8]:

$$(a_1 + a_2') > 10a_3 \tag{18}$$

From eqns. (14)–(18), the total surface coverage becomes:

$$x = a_1/(a_1 + a_2') \tag{19}$$

Under conditions when a_1 is much smaller than a_2',

$$x = a_1/a_2' = k_1/k_2'[OH^-]_{d.l.} \exp(\Delta\phi F/RT) \tag{20}$$

The net anodic current is given by:

$$i = 4FV_3 = 4Fk_3(k_1/k_2')^2 [OH^-]_{d.l.}^2 \exp(2\Delta\phi F/RT) \tag{21}$$

The Tafel line slope according to eqn. (21) is 0.03 V at 30°C, in agreement with the experimental values.

Equation (21) satisfies also the requirement that the overpotential is independent of the alkali concentration. This is revealed by substituting $[OH^-]_{d.l.}$ by $[OH^-]$ $\exp(\zeta F/RT)$, (where $[OH^-]$ is the OH^- concentration in the bulk of solution), and $\Delta\phi$ by $(\Delta\phi_r + \eta - \zeta)$, (where $\Delta\phi_r$ is the reversible potential in the given solution). Thus:

$$i = k[OH^-]^2 \exp(2\zeta F/RT) \exp(2(\Delta\phi_r + \eta - \zeta)F/RT) \tag{22}$$

and hence,

$$\eta = \text{const.} + (RT/2F) \ln i - (RT/F) \ln [OH^-] - \Delta\phi_r \tag{23}$$

Since $\Delta\phi_r = E_B^0 - (RT/F) \ln [OH^-]$, it is clear that at a constant current density,

$$\eta = \text{const.}$$

The absence of ζ from eqn. (23) accounts also for the fact that addition of neutral salts brings about no effect on the overpotential.

Derivation of the rate equation on the basis that the suboxide is oxidised anodically (reaction (8)), leads to the expression:

$$\eta = \text{const.} + (RT/2F) \ln i - (1.5\ RT/F) \ln [OH^-] - \Delta\phi_r - \zeta/2$$

This relationship requires that addition of excess neutral salt (which causes ζ to approach zero), leads to the change of overpotential in a given solution by half ζ. According to Quintin and Hagymas[9], the zero charge potential of tin is very close to -0.34 V. Such a value is shifted far from the potential of the metal in NaOH solutions (*ca.* -0.9 V), and hence ζ is expected to be of a considerable magnitude. The fact that addition of 1 *M* Na_2SO_4 does not affect the overpotential values (*cf.* Table 1), supports the self-oxidation mechanism.

It is curious that tin does not dissolve as stannate although the standard potential for the oxidation of SnO to SnO_2 (-0.958 V) is lower than that of the Sn/SnO system. This may be interpreted by the diatomic nature of the metal, which most probably leads to the formation of stannous oxide in the dimeric form, Sn_2O_2. This form is more stable, *i.e.*, its free energy of formation is relatively more negative than that of the monomer. This requires that the Sn/Sn_2O_2 potential is more negative than that of the Sn/SnO system. If the difference between the potentials of these two systems is not appreciable, the observed coincidence between the two systems may be due to an experimental error. On the other hand, the redox potential for Sn_2O_2/SnO_2 will be less negative than the corresponding value for SnO/SnO_2. The non-oxidation of tin anodes to the tetravalent state is thus explained on the basis that the diatomicity of the metal leads to a reversed sequence of redox potentials in comparison to the sequence deduced from thermal data.

3. *Heat of activation*

The heat of activation, ΔH^*, of the anode reaction at the reversible potential can be evaluated from the effect of temperature on the exchange current; the expression being:

$$\mathrm{d} \log i_0 / \mathrm{d}(T^{-1}) = -\Delta H^*/2.303\ R \qquad (24)$$

The overpotential was, therefore, measured at 20 and 40°C in 0.5, 5 and 10 *N* solutions. Figure 4 shows the Tafel lines at different temperatures for the 10 *N* solution. The values of $\log i_0$ for the different solutions are plotted against T^{-1} in Fig. 5. It is obvious that in case of the 0.5 *N* solution, the exchange current is almost unaffected by temperature. The reason for such anomalous behaviour is not fully understood. With increase of the alkali concentration, the usual temperature effect was observed, since the exchange current increased exponentially with temperature. The heat of activation at the reversible potential was computed as 8.3 and 11.7 kcal in the 5 and 10 *N* solutions, respectively.

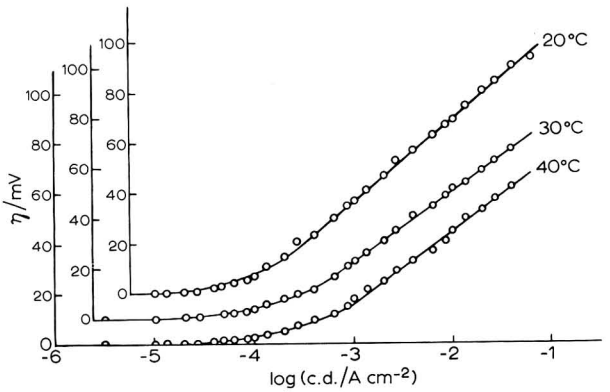

Fig. 4. Tafel lines for tin anodes in 10 *N* NaOH at different temperatures.

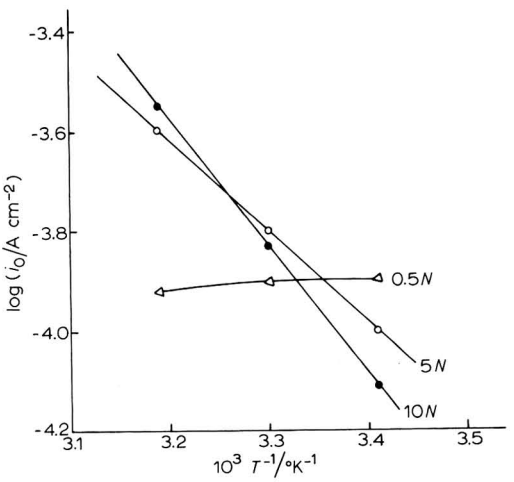

Fig. 5. Effect of temperature on the exchange current for tin anodes in different NaOH solns.

4. *Passivity of tin*

When the current density is such that the rate of formation of stannous oxide exceeds the rate of its chemical dissolution, the potential was found to rise rapidly to 2.2–3 V, the electrode became passive and oxygen was evolved. The current density at which passivity occurred, increased as the concentration of the alkali hydroxide was increased. No passivity was observed in 5 and 10 *N* solutions at the applied current densities (Figs. 2 and 4).

The decay of potential on switching off the current after oxygen was evolved showed a potential arrest, the so-called Flade potential. The value of the Flade potential was found to increase with the duration of polarising the electrode in the passive state; the lowest value was *ca.* −0.3 V. After several hours the passive layer dissolves and the electrode regains its active state.

SUMMARY

The potential of the tin anode was measured as a function of current density in 0.1–10 *N* NaOH solutions at 20–40°C. The results indicated the oxidation of tin to stannous oxide. The overpotential is independent of pH in pure solutions as well as in solutions containing excess neutral salts. From the electron number value (4), it was suggested that the surface tin atoms exist as diatomic molecules. A suboxide (Sn_2O) is first formed, which undergoes self-oxidation to stannous oxide. This latter step governs the overall reaction rate. The diatomic nature of tin allows for the formation of stannous oxide in the dimeric form, Sn_2O_2, and hence explains why tin does not dissolve at low current densities into stannate as required by the thermal data of the monomeric form.

The heat of activation at the reversible potential was found to be 8.3 and 11.7 kcal in the 5 and 10 *N* solutions, respectively. In dilute solutions the reaction rate was not affected by temperature.

At a given current density, that increases with the alkali concentration, the metal becomes passive and oxygen is evolved. A Flade potential of *ca.* −0.3 V was observed; but its value was found to increase as the time of polarisation in the passive state was prolonged.

REFERENCES

1 F. FOERSTER AND M. DOLCH, *Z. Elektrochem.*, 16 (1909) 559.
2 E. VALESSI, *Boll. Soc. Eustachiana Ist. Sci. Univ. Camerino*, 31 (1933) 1; *Chem. Zentr.*, II (1933) 2318.
3 S. A. AWAD, *Electrochim. Acta*, 7 (1962) 677.
4 W. M. LATIMER, *Oxidation Potentials*, Prentice-Hall, Englewood Cliffs, N.J., 2nd ed., 1952, p. 39 and 149.
5 A. J. DE BETHUNE, T. S. LICHT AND N. SWENDEMAN, *J. Electrochem. Soc.*, 106 (1959) 616.
6 S. A. AWAD, *J. Electrochem. Soc.*, 109 (1962) 865.
7 S. A. AWAD, *Electrochim. Acta*, 13 (1968) 925.
8 J. O'M. BOCKRIS AND E. C. POTTER, *J. Electrochem. Soc.*, 99 (1952) 169.
9 M. QUINTIN AND G. HAGYMAS, *J. Chim. Phys.*, 61 (1964) 541.

ELECTROANALYTICAL CHEMISTRY AND INTERFACIAL ELECTROCHEMISTRY
Elsevier Sequoia S.A., Lausanne – Printed in The Netherlands

EVALUATION OF STABILITY CONSTANTS OF METAL ION–FLUORIDE COMPLEXES BY THE SPECIFIC FLUORIDE ION ELECTRODE

A. M. BOND AND T. A. O'DONNELL
Department of Inorganic Chemistry, University of Melbourne, Parkville, Victoria, 3052 (Australia)
(Received December 9th, 1968)

INTRODUCTION

Since the development of the specific fluoride ion electrode (fluoride ion activity electrode) by Frant and Ross[1], with its high specificity towards fluoride ion and its ease of use, several applications have been reported in the literature.

The most obvious and widespread use has been in purely analytical applications, where the electrode has been used as a means for determining fluoride ion concentrations. The principles and practice of analytical uses have been well evaluated and established in several papers[1-6]. Lingane[7] has used the electrode to indicate the end point in titration of fluoride ion with thorium, lanthanum and calcium and has subsequently[8] used the electrode to measure solubility products of lanthanum(III) fluoride and europium(III) fluoride. Srinivasan and Rechnitz[9] have used the electrode to measure directly the concentration of free fluoride ion in acidic media and have been able to explain their results in terms of the species F^-, HF and HF_2^-. In a later communication[10] they have investigated, by means of the specific fluoride ion electrode, the kinetics of fluoride complex formation of aluminium(III) and iron(III). Recently, Hall and Slater[11] have used the fluoride electrode, in conjunction with a tin-amalgam electrode, to study the fluoride complexes of Sn(II).

In view of the fact that the fluoride ion activity electrode enables the direct and simple evaluation of free uncomplexed fluoride ion with high specificity, sensitivity and accuracy, the electrode should obviously be extremely useful and valuable as a means of measuring stability constants of fluoride ion complexes as is the pH, glass-membrane electrode in the evaluation of acidity or basicity constants of various compounds. So far, however, very little use has been made of the fluoride electrode for the purpose of measuring stability constants and the only complexes at present which have been examined by the fluoride electrode appear to be[9-11] those of H^+, Al(III), Fe(III) and Sn(II).

To date, most analytical measurements of metal ion–fluoride complexes have used indirect methods in which the fluoride ion activity or concentration has been measured by its effect on the redox potentials of metal ion couples such as cerium(III)–cerium(IV) or iron(II)–iron(III), *via* unequal complexation of the two conjugate oxidation states. This lack, until the recent development of the fluoride ion electrode, of a simple direct means of measuring fluoride ion activity is no doubt the reason why there is such a shortage of specific information on the thermodynamic properties of fluoride salts and complex compounds[7,12] in comparison with the other halides,

which have in general been thoroughly studied[12].

Indirect analytical methods and other common methods for determination of stability constants such as potentiometry, solubility, etc., are satisfactory in some cases for strongly complexing species. Consequently, some data are available on the fluoride stability constants of metal ion species of oxidation states (III), and higher, which in most cases form strong fluoride complexes, *e.g.* Al(III), Fe(III), Zr(IV), Ti(IV), Ta(V), U(VI). On the other hand, relatively little information, and in some cases none, is available on the weak fluoride complexes which are generally formed by metal ions of the (I) or (II) state. The fluoride complexes formed by such metal ions, are often too weak, or difficult, to detect with any precision by the usual methods for determination of stability constants, such as potentiometry, polarography, spectrophotometry, anion or cation exchange, solubility, etc. The possibility of evaluating the weak fluoride complexes of some of these $+1$ or $+2$ metal ions using the fluoride ion electrode was therefore investigated with a view to obtaining a simple, convenient and reliable method of measurement. In this paper the theory, experimental conditions, scope and reliability for one particular approach to the problem of determination of stability constants of some weak fluoride complexes by the specific ion electrode, are reported and results are given for the fluoride complexes of Cd(II), Mg(II), Ni(II), Zn(II), Tl(I) and Ag(I).

EXPERIMENTAL

All chemicals used were of reagent grade purity. Solutions of nickel(II), cadmium(II), silver(I) and thallium(I) were prepared from the nitrate salts. Zinc(II) solutions were prepared by the addition of appropriate amounts of nitric acid to zinc oxide, and magnesium(II) solutions were prepared from the perchlorate salt. Fluoride was added as sodium fluoride. The pH of all solutions was adjusted to the desired value by either nitric acid or sodium hydroxide except for the magnesium system where perchloric acid was used in place of nitric acid. The ionic strength was maintained constant in all systems by sodium nitrate except for the magnesium system where sodium perchlorate was used.

The concentrations of all species used were determined by conventional analytical methods, except for those materials which are accepted as primary standards for which concentrations can be calculated from weighed quantities of the salt.

To avoid contact with glass, standard fluoride solutions were prepared and maintained in polyethylene bottles, and a Teflon beaker was used as the test cell in which measurements were carried out. All measurements were made at a temperature of (16 ± 1)°C and with a total volume of solution of 25 ml.

A Specific Fluoride Ion Electrode (Model 94-09, Orion Research Incorporated, Cambridge, Massachusetts, U.S.A.) was used in conjunction with a saturated calomel reference electrode and a potentiometer (Phillips PR 9400 pH meter).

PRINCIPLES AND THEORY OF METHOD USED IN DETERMINATION OF STABILITY CONSTANTS BY THE SPECIFIC FLUORIDE ION ELECTRODE

The observed cell potential, E, of a solution in contact with a fluoride specific ion electrode and a reference electrode is

$$E = E_c - A \log a_{F^-} \quad (1)$$

where E_c = a constant of potential with respect to the particular indicating and reference electrode used; A = a constant, ideally given by the Nernst slope RT/F and a_{F^-} = the activity of the free fluoride ion in solution.

From eqn. (1) it can be seen that a graphical plot of the cell potential *versus* the logarithm of the activity of the free fluoride ion in solution should give a straight line of slope $-A$ and intercept E_c. However, in many cases it is more convenient and easier to work in terms of concentration of fluoride ion rather than activity.

In terms of concentration of free fluoride ion, C_{F^-}, eqn. (1) becomes

$$E = E_c - A \log \gamma_{F^-} \cdot C_{F^-} \quad (2)$$

where γ_{F^-} is the activity coefficient of the fluoride ion.

For a series of cell potential readings made at constant ionic strength, I, the γ_{F^-} essentially remains constant. Incorporating this term into the constant, E_c, to give a new constant E'_c leads to eqn. (3).

$$E = E'_c - A \log C_{F^-} \quad (3)$$

Consequently, a graphical plot of cell potential *versus* the logarithm of the free fluoride ion concentration, all values being made at constant I, should be a straight line.

Since, the fluoride ion electrode has a high degree of specificity towards fluoride ion, E should be independent of all species other than fluoride. In practice, this has been shown to be so to a high degree except for hydroxyl ion, so that measurements need to be made at a reasonably low hydroxyl ion concentrations. In this work, hydroxyl ion concentrations used were always less than 10^{-8} M, so that no interference was encountered from this species. E is also a function of the ionic strength, I, and the contribution to I from all ionic species present in solution other than and as well as fluoride needs to be considered in this regard. I is given by an expression $\frac{1}{2}\sum_i C_i z_i^2$, where C_i is the concentration of the ith ionic species, with charge z_i, and thus a suitable electrolyte can be simply used to maintain the ionic strength constant at the desired value I.

Hydrogen ion, H^+, forms fairly strong complexes with fluoride ion, to give the species HF and HF_2^- [9]. However, calculations can be made which show that at pH 5 or higher, formation of those hydrogen–fluoride complex species can be neglected. As previously mentioned, hydroxide interference to the electrode occurs at high pH, so that a convenient pH in which to work to study complex ion formation is between 5 and 6, over which range all measured effects on the fluoride electrode can be attributed to complex formation of $MF_n^{(x-n)+}$.

In accordance with the above, if a series of standard fluoride solutions is prepared, each at the same ionic strength, the same pH between 5 and 6, but with no complex ion species present, then as under these conditions the total fluoride ion concentration, C_{TF^-}, equals the free uncomplexed fluoride ion concentration, C_{F^-}, a calibration graph of E *versus* log C_{F^-} can be set up. If subsequently, solutions with the same C_{TF^-} as above are prepared and with the same ionic strength and at the same pH, but with added complexing species, M^{x+}, then due to complex formation to give $MF_n^{(x-n)+}$ it will be found that under these conditions C_{F^-} and C_{TF^-} will not be equal. However, C_{F^-} can be experimentally calculated by measuring E and referring the

value to the calibration graph prepared previously. Enough information is then available to calculate the stability constants β_n of $MF_n^{(x-n)+}$ in a slight modification of the standard manner[13,24]. If the experimental conditions are arranged such that the analytical or total concentration of M^{x+}, C_{TM}, is very much greater than that of the total fluoride ion concentration, C_{TF^-}, then the approximation that $[M^{x+}] = C_{TM}$ can be made. Under these conditions eqn. (4) is obtained

$$F_1(X) = \left(\frac{C_{TF^-} - C_{F^-}}{C_{F^-}}\right)\frac{1}{C_{TM}} = \beta_1 + 2\beta_2 C_{F^-} + \ldots + n\beta_n C_F^{n-1} \quad (4)$$

where the symbol $F_1(X)$ has the usual definition[24]. The usual type of graphical plot[24] can be used to determine the complex constants. In this work, all complex systems were weak, and within the limit of experimental error, only one complex, $MF^{(x-1)+}$, was found so that $F_1(X)$ was found to be a constant equal to β_1.

RESULTS AND DISCUSSION

A. Evaluation of some metal ion–fluoride complex systems

(1) *The cadmium(II)–fluoride system.* Fluoride solutions 0.1 *M* in cadmium(II) were prepared at pH 5.0 and the ionic strength was raised to 0.5, by addition of sodium nitrate. Reference to a calibration graph of fluoride solutions prepared at the same ionic strength and pH, and using the method described previously enabled $F_n(X)$ functions to be calculated. The results are given in Table 1. Within the limits of experimental error it can be seen that $F_1(X)$ is a constant which gives a value of

TABLE 1

THE CADMIUM–FLUORIDE SYSTEM AT IONIC STRENGTH 0.5

Concentration of cadmium(II) = 0.1 *M*, $T = (16 \pm 1)°C$

$C_{TF^-}/M \times 10^4$	$C_{F^-}/M \times 10^4$	$\left(\frac{C_{TF^-} - C_{F^-}}{C_{F^-}}\right)$	$F_1(X)$
1	0.737(9)	0.355	3.55
2	1.52(4)	0.312	3.12
3	2.23(4)	0.343	3.43
4	2.89(1)	0.384	3.84
5	3.71(5)	0.346	3.46
6	4.50(8)	0.331	3.31
7	5.03(5)	0.390	3.90
8	5.95(7)	0.343	3.43
10	7.32(8)	0.364	3.64

$\beta_1 = 3.5 \pm 0.4$ l mol^{-1} for the complex CdF^+. This value compares with $\beta_1 = 2.9$ l mol^{-1} (25°C) obtained potentiometrically with a cadmium amalgam electrode[13] at an ionic strength of 1.0 maintained by sodium perchlorate and $\beta_1 = 6.4$ l mol^{-1} ($T = 25°C$, $I = 2.0$-$NaClO_4$), $\beta_1 = 5.8$ l mol^{-1} ($T = 30°C$, $I = 1.0$-$NaClO_4$) obtained polarographically[14,15]. In view of the different methods of measurement, temperatures and ionic strengths used it is rather difficult to make quantitative comparison between results obtained in the work with the specific ion electrode and the literature

values[13-15], however, it can be seen that the orders of magnitude at least of all values are in agreement.

To examine the expected effect of ionic strength on the results, the measurement of β_1 was repeated at an ionic strength of 0.05 and using a cadmium(II) ion concentration of 0.01 M. Results at this ionic strength are given in Table 2. Again $F_1(X)$

TABLE 2

THE CADMIUM–FLUORIDE SYSTEM AT IONIC STRENGTH 0.05

Concentration of cadmium(II) = 0.01 M, $T = (16 \pm 1)$°C

$C_{TF^-}/M \times 10^5$	$C_{F^-}/M \times 10^5$	$\left(\frac{C_{TF^-} - C_{F^-}}{C_{F^-}}\right)$	$F_1(X)$
3	2.72(3)	0.102	10.2
4	3.57(6)	0.118	11.8
5	4.34(5)	0.151	15.1
6	5.40(8)	0.110	11.0
7	6.10(9)	0.146	14.6
8	7.01(5)	0.140	14.0
10	8.77(0)	0.140	14.0

is found to be constant, giving a value of $\beta_1 = 13 \pm 2$ l mol^{-1}.

The previous studies which have indicated the existence of a second very weak complex of cadmium, CdF_2[13,15], were carried out under conditions in which the fluoride ion concentration was several powers of 10 higher than in this work, so that it is not surprising that in the present study only the first complex was detected. Furthermore, in this work the metal ion concentration used is in excess of the fluoride ion so that unless higher complexes are fairly strong only β_1 will be detected.

(2) *The magnesium(II)–fluoride system.* Fluoride solutions 0.1 M in magnesium(II) perchlorate were prepared at pH 6 and the ionic strength was raised to 0.5 by addition of sodium perchlorate. Reference to a calibration graph prepared in 0.5 M sodium perchlorate at pH 6 and the method of calculation described previously gave a value of $\beta_1 = 18 \pm 3$ l mol^{-1}.

Connick and Tsao[16] have examined the complexing of Mg^{2+} indirectly by studying its effect on the fluoride complexing of Fe(III) as measured potentiometrically *via* the Fe(III)–Fe(II) couple and found a value for β_1 of 16 l mol^{-1} ($T = 15$°C, $I =$ 0.5-$NaClO_4$). Hence agreement between results obtained by both the fluoride ion electrode and potentiometrically for the magnesium–fluoride system is satisfactory.

Due to the insolubility of magnesium fluoride, results for β_1 were obtained at very low fluoride ion concentrations (5×10^{-5}–5×10^{-4} M), and additional errors in working at these very low concentrations are introduced. However, results obtained still appear to be satisfactory and the detection of only one complex, MgF^+, is in agreement with Connick and Tsao[16].

(3) *The zinc(II)–fluoride system.* At an ionic strength of 0.5 ($NaNO_3$) using a zinc concentration of 0.1 M at pH 5.3 only one complex with a value of $\beta_1 = 2.8 \pm 0.4$ l mol^{-1} was obtained.

This value of 2.8 l mol^{-1} is somewhat lower than values obtained potentiometrically with a quinhydrone electrode[17], $\beta_1 = 5.9$ l mol^{-1} ($T = 20°C$, $I = 1.0$-$NaClO_4$)[18,19] or $\beta_1 = 5.4$ l mol^{-1} with the Fe(III)–Fe(II) couple ($T = 15°C$, $I = 0.5$-$NaClO_4$), although all values are obviously of the same order of magnitude and in all cases only one complex, ZnF^+, has been detected.

4. *The nickel(II)–fluoride system.* For this system at an ionic strength of 0.5 ($NaNO_3$) and using a nickel concentration of 0.1 *M* at pH 5.0 a value of $\beta_1 = 1.5 \pm 0.4$ l mol^{-1} was obtained.

In what appears to have been the only other study of the nickel–fluoride system, Ahrland and Rosengren[17] also detected only one complex, NiF^+, with $\beta_1 = 4.6$ l mol^{-1} ($T = 20°C$, $I = 1.0$-$NaClO_4$).

5. *The silver(I)–fluoride system.* Only very weak complex formation was found to occur between silver and fluoride ions with a value for the complex, AgF, of $\beta_1 = 0.4 \pm 0.2$ l mol^{-1}. This value was obtained from solutions 0.1 *M* in silver ion, at pH 5.5 and at an ionic strength of 0.5 maintained by sodium nitrate.

Other workers in potentiometric studies, using a silver–silver chloride electrode[20], have measured a value of $\beta_1 = 0.5$ l mol^{-1} ($T = 25°C$, $I = 1.0$-$NaClO_4$), and with the Fe(III)–Fe(II) couple[19] $\beta_1 = 0.8$ l mol^{-1} ($T = 15°C$, $I = 0.5$-$NaClO_4$).

The value obtained in this work for β_1 by the specific ion electrode was too low to be measured with high precision as the $F_n(X)$ values for very weak complexes contain large errors which result from the very small difference in the experimentally measured term ($C_{TF^-} - C_{F^-}$). Consequently, the real significance of the value $\beta_1 = 0.4 \pm 0.2$ l mol^{-1} should be taken to mean that very weak complex formation occurs between silver and fluoride ions and no real quantitative emphasis should be placed on the magnitude of the β_1 value.

6. *The thallium(I)–fluoride system.* No evidence could be found for the formation of any fluoride complex of thallium(I) for measurements made at ionic strengths of 0.5 or 0.05 maintained by sodium nitrate and in the presence of 0.1 or 0.01 *M* Tl^+ at pH 6 or when fluoride concentrations were varied over the range 10^{-6}–5×10^{-3} *M*. Any complex, if formed, is presumably too weak to be detected by the fluoride ion electrode.

In agreement with this result, no fluoride complex formation of thallium(I) was found either in potentiometric studies[21] using an amalgam electrode ($T = 25°C$, $I = 1.0$-$NaClO_4$) or in polarographic studies[22] ($T = 30°C$, $I = 1.0$-$NaClO_4$). Hence results in this work as well as in others, show that little or no complex formation occurs in the thallium(I)–fluoride system.

B. Reliability, sources of error and precision of method

Comparison of results obtained in this work by the specific ion electrode with those obtained by other techniques is difficult because of the generally different conditions of temperature, ionic strength, and supporting electrolyte used in the various studies as well as the difficulty involved in estimating the likely errors of measurement present with each particular technique, as is necessary for a valid comparison of results. However, it has been found at least that good qualitative agreement is reached between results made by the specific ion electrode and other studies so that the reliability of results has been verified satisfactorily in this sense.

The quantitative reliability and usefulness of results obtained by the method

proposed in this paper need to be considered in terms of experimental errors and the approximations and assumptions made to calculate values of stability constants.

In Tables 1 and 2 it can be seen that fluoride ion concentrations are quoted to four significant figures; however in practice only three significant figures are reliable, the fourth figure has only been included as a result of averaging of several experimental results obtained on the same solution. Calculation of $F_n(X)$ functions requires a subtraction $(C_{TF^-} - C_{F^-})$ of two quantities of similar magnitude and this process leads to a loss of a further significant figure, so that the $F_n(X)$ function should be reliable to only two significant figures. In experimental results this is verified; for instance in the cadmium–fluoride system, it can be seen in Tables 1 and 2 that results for β_1 can only sensibly be quoted to two significant figures.

In experimentally evaluating the concentration of free uncomplexed fluoride ion, C_{F^-}, by relation of results to a calibration graph, it has to be assumed that junction potentials present in measurements made for the calibration graph are the same as those in the different ionic environments present when metal ions are added. It must also be assumed that with the different ionic environments between calibration and experimental solutions, the activity coefficients of the fluoride ion are still the same. Under the experimental conditions used in this work the bulk concentrations of both calibration and experimental solutions were made up from the electrolyte used to maintain the ionic strength. Consequently, variations in junction potential or activity coefficient would not be expected to be very significant.

The major source of error of $F_n(X)$ functions will arise from the use of the electrolyte to maintain the ionic strength. In all cases, except for the magnesium–fluoride system, the electrolyte used for this purpose was nitrate and this has been assumed to be non-complexing. However, the concentration of nitrate used was two to four powers of ten greater than that of the fluoride, so that neglect of any nitrate complexing could introduce significant errors. For instance, the nitrate complex of cadmium $CdNO_3^+$ has been measured[23] as $\beta_1 = 1.3$ l mol^{-1} ($T = 25°C$, $I = 3.0$-NaClO_4). If a correction is to be applied for this effect, then the value of metal ion, which in calculations made in this work was assumed to be the analytical or total metal ion concentration, must be lowered by an extent equivalent to that complexed as the nitrate. For instance, if a value of $\beta_1 = 1$ l mol^{-1} is assumed for the nitrate complex of the metal ion M^{x+} at an ionic strength of 0.5 maintained by sodium nitrate, then the correction to be applied would be as follows:

For $[M^{x+}] = 0.1\ M$ and $x = 1$, *e.g.* the Ag^+ or Tl^+ case

$$\beta_1 = \frac{[M^+][NO_3]}{[MNO_3]}$$

or

$$\beta_1 = \frac{(0.1-\alpha)(0.5-\alpha)}{\alpha}$$

where $\alpha = [MNO_3]$. By solving the equation above, a value of $\alpha = 0.032\ M$ is obtained. Hence the value which should be used for $[M^+]$ is 0.068 M rather than 0.1 M. This correction would obviously make β_n values larger than calculated by neglect of the nitrate complexing and this may well explain why results obtained for say the zinc–fluoride system and other systems appear to be slightly lower than those calculated

by other methods.

Because of the lack of suitable data on nitrate complexing for the systems studied[12] it has not been possible to correct β_n values for this effect and nitrate complexing has had to be neglected, leading to slightly lower values of β_n being reported than should be the case. The alternative approach, to use perchlorate medium, which in general would be considerably less complexing than nitrate, was not possible except with magnesium, because only the metal nitrate salts were available.

C. Application of method to other systems

The particular method proposed in this paper for study of fluoride complexes by the specific ion electrode is limited in some respects in that it will only be applicable to certain systems. For instance, the stability constants of very strong fluoride complexes would not be measurable. For these systems, under conditions in which the added fluoride ion, C_{TF^-}, is considerably less than that of the metal ion, M^{x+}, then the experimentally measured quantity, the free uncomplexed fluoride ion C_{F^-}, would be too low to measure. Also species with very insoluble hydroxides would not be suitable for study by the method proposed as the pH must be in the region 5–6 for this treatment to be applied. Mercury(II) and copper(II) systems, for instance, were examined for possible evaluation by the method given in this paper, but were not found to be suitable because of insolubility of the hydroxides even at pH 5. Obviously, however, alternative methods which would be expected to be applicable to strongly fluoride complexing species or to insoluble hydroxides could well be available, and other ways and approaches to the use of the fluoride ion electrode in the study of the complexing of fluorides are at present being investigated. On the whole therefore, it is anticipated that the fluoride ion electrode should be very widely applicable and should find an extensive use for studies on fluoride complexes of metal ions, in aqueous solutions. It should be also readily applicable to studies in non-aqueous media. Thus, the simplicity and ease with which direct experimental results are obtained should provide a method for obtaining a considerable amount of thermodynamic data on fluoride complexes which currently, as mentioned previously, is not available or experimentally easily accessible by other methods.

ACKNOWLEDGEMENTS

Grateful acknowledgement is given for assistance received from Mr. R. J. Taylor in obtaining some of the experimental results reported in this work and also to the Australian Atomic Energy Commission for financial assistance in the purchase of equipment.

SUMMARY

A method is given for calculation of the stability constants of some fluoride complexes using the fluoride specific ion electrode. Results are given for the fluoride complexes of Cd^{2+}, Mg^{2+}, Zn^{2+}, Ni^{2+}, Ag^+ and Tl^+, and they are found to be in good agreement with those obtained by other methods. Methods and experimental techniques of measurement of stability constants of fluoride complexes using this fluoride electrode are very simple and should allow a considerable amount of thermo-

dynamic data on fluoride complexes in solution to be obtained which is not available or easily accessible experimentally at present.

REFERENCES

1 M. S. FRANT AND J. W. ROSS, JR., *Science*, 154 (1966) 1553.
2 M. S. FRANT AND J. W. ROSS, JR., *Anal. Chem.*, 40 (1968) 1169.
3 R. A. DURST AND J. K. TAYLOR, *Anal. Chem.*, 39 (1967) 1483.
4 R. E. MESMER, *Anal. Chem.*, 40 (1968) 443.
5 R. BOCK AND S. STRECKER, *Z. Anal. Chem.*, 235 (1968) 322.
6 E. W. BAUMANN, *Anal. Chim. Acta*, 42 (1968) 127.
7 J. J. LINGANE, *Anal. Chem.*, 39 (1967) 881.
8 J. J. LINGANE, *Anal. Chem.*, 40 (1968) 935.
9 K. SRINIVASAN AND G. A. RECHNITZ, *Anal. Chem.*, 40 (1968) 509.
10 K. SRINIVASAN AND G. A. RECHNITZ, *Anal. Chem.*, 40 (1968) 1818.
11 F. M. HALL AND S. J. SLATER, *Australian J. Chem.*, 21 (1968) 2663.
12 *Stability Constants of Metal Ion Complexes, Chem. Soc. (London), Spec. Publ.*, 17 (1964).
13 I. LEDEN, Dissertation, Lund, 1943, p. 49.
14 S. S. MESARIC AND D. N. HUME, *Inorg. Chem.*, 2 (1963) 1063.
15 A. M. BOND, *J. Electroanal. Chem.*, 20 (1969) 223.
16 R. E. CONNICK AND M. S. TSAO, *J. Am. Chem. Soc.*, 76 (1954) 5311.
17 S. AHRLAND AND K. ROSENGREN, *Acta Chem. Scand.*, 10 (1956) 727.
18 R. E. CONNICK AND A. D. PAUL, *J. Am. Chem. Soc.*, 80 (1958) 2069.
19 A. D. PAUL, Thesis, University of California, Berkeley, 1955 (UCRL-2926).
20 I. LEDEN AND L. E. MARTHEN, *Acta Chem. Scand.*, 6 (1952) 1125.
21 R. O. NILSSON, *Arkiv Kemi*, 10 (1957) 363.
22 A. M. BOND, unpublished work, University of Melbourne, 1968.
23 I. LEDEN, (a) *Z. Physik. Chem.*, 188 A (1941) 160; (b) Dissertation, Lund, 1943, p. 48.
24 F. J. C. ROSSOTTI AND H. ROSSOTTI, The Determination of Stability Constants, McGraw-Hill, New York, 1961, p. 108.

ELECTROANALYTICAL CHEMISTRY AND INTERFACIAL ELECTROCHEMISTRY
Elsevier Sequoia S.A., Lausanne – Printed in The Netherlands

ELECTRODIMERIZATION

1. ONE-ELECTRON IRREVERSIBLE DIMERIZATION. DIAGNOSTIC CRITERIA AND RATE DETERMINATION PROCEDURES FOR VOLTAMMETRIC STUDIES

C. P. ANDRIEUX, L. NADJO AND J. M. SAVÉANT**
Laboratoire de Chimie de l'Ecole Normale Supérieure, Paris (France)
(Reçu le 22 décembre 1969)

Formally every oxido–reductive process can be considered as a combination of three kinds of reactions: (i) electron transfer reactions, (ii) dimerization–monomerization reactions in which no change in the oxidation degree of the reacting species occurs, and (iii) acid–base type reactions for which the same condition is also valid. Indeed, the terms "acid" and "base" have here to be interpreted in a very broad sense. For example, the decomposition of a halogenated radical, with the halogen anion as the group eliminated must be considered, within this conception, as an acid–base reaction.

In the particular case of *electrochemical* oxido–reductive processes this way of resolving the overall reaction in elementary steps has not only a formal character, *i.e.* uniquely concerned with thermodynamical equivalencies, but can also assume an actual mechanistic significance. In other words, the overall process may actually proceed through the various steps indicated above. It follows, as far as kinetic analysis of mechanisms is concerned, that the kinetics of every one of these individual steps has to be determined as a component of the overall kinetics. Other kinds of reactions representing a formal combination of the preceding reaction types are also to be considered eventually as actual reaction paths. This is the case of radical reactions involving atom abstraction from the solvent or atom expulsion from an intermediate species (the transferred atom being hydrogen in most cases). Omitting the eventual reactions between the metal of the electrode and the reacting particles as well as their possible adsorption at the interface, the various reaction paths can thus be summarized as follows:

—Electron transfer reactions at the electrode.
—Electron transfer reactions in solution.
—Dimerization–monomerization reactions.
—Acid–base reactions.
—Atom (hydrogen) exchange reactions.

In the kinetic analysis of such complex reaction schemes by an electrochemical method, diffusion has to be taken into account as a possible supplementary rate determining factor. For this reason the mechanism determinations in the field of electrochemistry are generally restricted to reaction schemes where, apart from diffu-

** To whom correspondence should be addressed: 24, rue Lhomond, 75 Paris 5, France.

sion, only one rate determining step is taken into consideration. For example the case of a reduction involving two fast electron transfer steps coupled with disproportionation reactions and with first-order acid–base reactions has been systematically investigated[1], considering either the disproportionation or the acid–base reaction as the rate determining step.

The aim of the present paper is similarly to present a systematic kinetic analysis of reaction schemes involving dimerization reactions coupled with electron transfer steps. Oxidative and reductive coupling is one of the most common reactions in the field of organic electrochemistry and one of the most valuable for synthetical purposes (*cf.* the Kolbe synthesis). Interest in this type of reaction has been recently renewed by the series of electroreductive coupling synthesis by Baizer *et al.* especially the synthesis of adiponitrile starting from acrylonitrile (see for example refs. 2–4).

In order that the kinetic analysis of a dimerization reaction scheme be systematic, restrictive assumptions must be made. Among all the possible reaction steps listed above, dimerization reactions will be retained, apart from diffusion, as the only possible rate determining ones. This means that the other reactions are either neglected or considered to reach equilibrium instantaneously. More precisely:

—Only one electron transfer at the surface of the electrode will be taken into account and it will be considered as fast.

—Possible electron transfer reactions in solution between the monomeric and the dimeric redox couples will be disregarded in the present analysis, *i.e.* these reactions will be considered as slow. Although it could be important in practice, the occurrence of this type of reaction parallel with other possible reaction paths has seldom been considered in the polarographic literature. Recently, the coupling of such reactions with first-order e.c.e. mechanism has been studied[1,5,6]. In the general case, the kinetic analysis is rather complex since rate determination is by the chemical reaction as well as by the redox reaction itself[1]. If the redox reaction is fast enough for the thermodynamical equilibrium to be considered as achieved, the complexity of the kinetic analysis is the same as when the reaction is disregarded[5]. Owing to the possible practical significance of such reactions, their interference in the overall reaction mechanism will be considered in a further paper.

—Acid–base reactions will be completely disregarded. This assumption represents the most severe limitation of the present analysis. Indeed, considering the usual solvents, it is rather difficult to define a medium whose acidity would be without any effect on each member of the usual redox couples. The same considerations are valid for oxidation processes, the basicity of the solvent being taken into consideration instead of acidity. Such systems are nevertheless available, as it will be shown in another part of this series. Moreover the consideration of such a simplified reaction scheme is a necessary stage in the general study of electrochemical coupling reactions for which acid–base reactions have to be taken into account.

—Atom-exchange reactions will also be disregarded. In most cases these reactions are an alternative pathway to a radical dimerization process.

—Adsorption of the reacting species at the electrode as well as surface reactions with the metal of the electrode will be neglected.

—Among the various dimerization processes themselves that may act simultaneously only one will be considered at a time as the rate determining step.

Formal electrochemical kinetics will be considered for two methods: *polaro-*

graphy and *linear sweep voltammetry*. The reason for considering the polarographic conditions is the reliability of this technique even though it suffers some practical limitations. One of these is caused by depletion effects arising after the first drop that cannot be taken into account in the mathematical analysis. For diffusion controlled currents the theoretical values calculated without consideration of depletion effects are inaccurate by about 20%[7]. Depletion effects can be avoided by using a horizontal or an inclined capillary, but owing to the fairly long duration of electrolysis involved in polarographic conditions, the sphericity of the electrode must be taken into account in addition to its expansion with time when deriving the exact solution of the polarization problem. Moreover, the drop time cannot be varied over very broad limits, say by a maximum of one order of magnitude, thus hindering an easy characterization of the mechanism and particularly an accurate determination of the rate constant. Thus, in practice, polarography would be used chiefly for obtaining the first elements of the mechanism diagnosis. It follows that precise mathematical analysis of the dimerization polarization problem is of little use in practice. For this reason the variations of the characteristic quantities of the polarograms with the various experimental parameters will be given only, and in approximate form, for the simplest polarization cases. For the other cases only the qualitative trends will be outlined. Results obtained in this approximate way are also valid for *rotating electrode voltammetry* as used qualitatively with no special care about the electrode geometry and with moderate rotation speeds.

Linear sweep voltammetry has been chosen as an example of a relaxation method. The advantages of the method over conventional polarography are two-fold: (i) shorter times of electrolysis, and hence higher diffusion rates, can be reached, allowing faster reactions to be characterized; (ii) the direction of the net redox process at the electrode can be reversed during the same micro-electrolysis allowing an easier and more accurate study of follow-up reactions. Single linear scan provides the means for precise mechanistic diagnosis and therefore the mathematical analysis of the polarization problems will be treated rigorously. Symmetrical triangular scanning is a convenient way of testing qualitatively the reversibility of the electrochemical system but is rather difficult to use for rate constant determination since the polarization pattern is dependent upon the value of the switching potential. Results for this technique will thus be reported qualitatively from the point of view of evaluating the reversibility of the system. Asymmetrical triangular sweep, or any other double-scanning techniques with largely different durations for each part of the scan, as for example a trapezoidal scanning, allows a more convenient rate determination procedure as shown earlier for first and second orders[8]. Under these conditions, numerical computation of theoretical working curves is moreover greatly simplified. This technique will be thus considered here as providing a means for accurate rate constant measurement. Analysis of the polarization problems for other relaxation methods such as potential-step chronoamperometry (or chronocoulometry) and current-step chronopotentiometry follows the same lines, for single-step as well as for double-step techniques. Diagnostic criteria and rate determination procedures can thus be transposed from the case of linear sweep voltammetry to the other relaxation techniques.

A preliminary thermodynamical analysis of the whole system is necessary in order to define the limits within which the rate determining step may interfere.

Reasonings are for a reduction process. Transposition to oxidation is obvious.

The system is represented as follows:

$$\begin{array}{ll} A^+ + e \rightleftarrows A & (E_1) \\ 2A \rightleftarrows A\text{–}A & (K_1) \\ A + A^+ \rightleftarrows A\text{–}A^+ & (K_2) \\ A\text{–}A^+ + e \rightleftarrows A\text{–}A & (E_2) \end{array} \qquad (1) \qquad (2)$$

Charges carried by the various species indicated possess only a formal character. The analysis is then not restricted to a positively charged reactant but applies also to a neutral reactant. E_1 and E_2 are the normal potentials of the two redox couples, K_1 and K_2 are the equilibrium constants of the coupling reactions defined as:

$$K_1 = \frac{[A]^2}{[A\text{–}A]} \qquad K_2 = \frac{[A^+][A]}{[A\text{–}A^+]}$$

The thermodynamical properties of the system are conveniently represented in an E–pC diagram, E being the electrode equilibrium potential and pC the cologarithm of the total concentration of A^+ initially introduced. Consequently the equilibrium constants K_1 and K_2 are better introduced through their cologarithms pK_1 and pK_2. Two cases are to be distinguished according to the relative values of the normal potentials or, equivalently according to the relative values of the pK's since the E's and the pK's are related as follows:

$$E_2 - E_1 = 0.0591\ (pK_1 - pK_2), \quad \text{at } 25°C$$

In the first case $E_1 > E_2$ (pK_1 < pK_2); in the second the opposite condition is assumed. The corresponding diagrams are given in Fig. 1. These diagrams provide a rough representation of the half-wave potentials, for polarography, and of peak potential for linear sweep voltammetry, as functions of pC under conditions of fast equilibrium for the dimerization reactions.

In order to characterize the most typical voltammetric patterns as reflecting the kinetics of the overall process it will be assumed that the pC values are largely

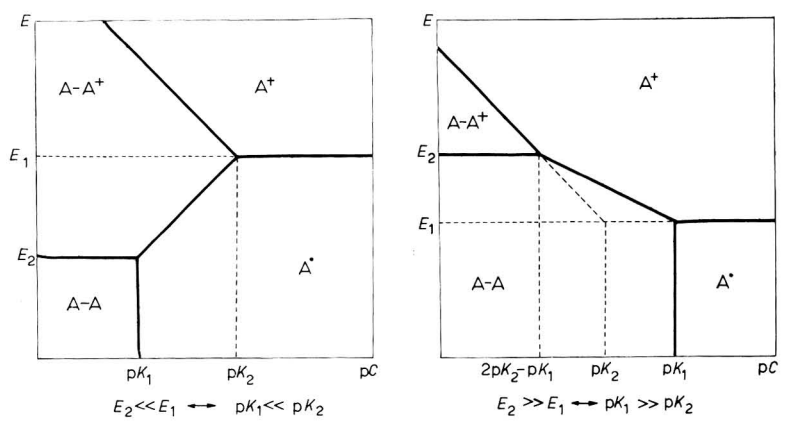

Fig. 1. Thermodynamical analysis of one-electron electrodimerization. Equilibrium potential E *vs.* cologarithm of monomeric depolarizer initial concn. pC.

different from pK_1, pK_2 and $2pK_2 - pK_1$. In particular, this means that dimerization equilibria are considered as very much in favour of either the dimer or the monomer. Considering the transition between A^+ and A–A, four different thermodynamical situations arise:

—case I: $pC \ll pK_1 \ll pK_2$ $(E_2 \ll E_1)$
—case II: $pC \ll 2pK_2 - pK_1$ $(E_2 \gg E_1)$
—case III: $2pK_2 - pK_1 \ll pC \ll pK_2$ $(E_2 \gg E_1)$
—case IV: $pK_2 \ll pC \ll pK_1$ $(E_2 \gg E_1)$

In the first three cases the *radical dimerization* reaction (reaction 1) as well as the *radical-ionic dimerization* reaction (reaction 2) are very much displaced toward the dimeric form. These two kinds of dimerization processes may thus control the overall kinetics simultaneously. For the sake of simplicity each one will be considered separately. In other words, for the first three cases, the radical coupling process (DIM 1) and the radical-ionic coupling process (DIM 2) will be analyzed successively. In the fourth case the radical reaction acts as a coupling process (DIM 1) whereas the radical-ionic reaction acts as a fission process (monomerization: MON 2); the reaction scheme to be considered in these conditions can thus be termed: DIM 1–MON 2.

Qualitative as well as quantitative kinetic analysis of the mechanism by polarography and linear sweep voltammetry is based on the experimental observation of a departure from equilibrium conditions. In order to characterize the degree of irreversibility for the whole system we use the concept of kinetic zones. This concept has been proposed first for a first-order chemical reaction preceding the electron transfer process in the case of linear sweep voltammetry[9], and then extended to other reaction schemes and to conventional polarography[10]. Its applicability could be extended to the other electrochemical techniques as well. The polarization patterns depend on two parameters. The first one describes the equilibrium conditions. For a dimerization reaction, the initial depolarizer concentration C^0 as well as the equilibrium constant K both define the equilibrium parameter: $\chi = K/C^0$. The second parameter describes competition between diffusion, or more generally mass transfer, and chemical reaction. If k is the rate constant of the dimerization reaction, this kinetic parameter λ is given by the following expressions: $\lambda = (RT/F)(kC^0/v)$ for linear sweep voltammetry and $\lambda = kC^0\theta$ for polarography where v is the sweep rate and θ the drop time.

Each point of the $\log \chi$–$\log \lambda$ plane defines the state of the whole electrochemical system as to mass transfer and chemical reaction. The general form of the kinetic zone diagram is given in Fig. 2. The limiting lines are vertical for small values of λ since the system does not depend on the equilibrium constant in this region. The limiting lines for high values of λ have a slope of $-\frac{2}{3}$ as already shown in the case of a DIM 1 reaction scheme[19] and will be shown later for the other possible mechanisms[11]. For peak potential measurements at 25°C (accuracy being 2 mV) the diagram has been drawn for the DIM 1 reaction scheme as an example. Values for the limiting lines will be given in a subsequent section for the other possible mechanisms. In the left region DO of the plane, the chemical reaction is slow in comparison with the mass transfer process. Kinetics and thus polarization curves are controlled by the mass transfer rate. On the extreme right of the plane, DE, the dimerization reaction is much faster than the mass transfer process. As soon as the concentrations in solution are

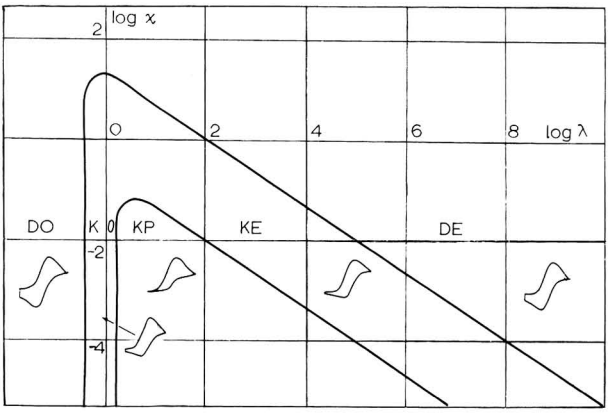

Fig. 2. Kinetic zone diagram. (DO) pure diffusion control, dimerization reaction slow; (KO) mixed reaction–diffusion control; (KP) pure chemical reaction kinetic control; (DE) pure diffusion control, fast equilibration of the dimerization reaction.

modified by diffusion of the electroactive species, the dimerization equilibrium instantaneously shifts in favour of the monomer. It follows that mass transfer occurs for the dimer in exactly the same way as for the electroactive species. Thus zone DE is also representative of purely diffusion-controlled processes. For large values of the equilibrium parameter χ, zone DO and zone DE merge. This means that the dimerization reaction has to be in favour of the dimeric form for a significant kinetic influence to be observed. In these conditions, when χ is large and λ small, a stationary state is reached by mutual compensation of chemical reaction and mass transfer process. This is the exact equivalent of the stationary state assumption for homogeneous kinetics where, however, compensation occurs between two different chemical reactions. These particular polarization conditions correspond to the "pure kinetic currents" for reaction schemes involving a chemical reaction that precedes the electron transfer process. An important feature of this polarization situation is that the mathematical analysis is much simpler than in the general case owing to (i) the existence of a stationary state from which it follows that the partial derivative equations can be replaced by differential equations with respect to the space coordinate and (ii) the fact that the reverse reaction can be neglected. Indeed, much of the Prague school's work dealing with secondary chemical reactions in polarography has been made under these simplifying assumptions (see for example refs. 12 and 13). Similarly, the first analysis of a dimerization reaction scheme under conditions of linear potential sweep has been derived by assuming a stationary state in the electrode vicinity[14]. But the most distinctive feature of this "pure kinetic" zone KP is that the chemical reaction has its largest influence on the overall electrochemical kinetics. KO and KE are transition zones between the pure kinetic situation and the pure diffusion ones. The various limiting zones DO, DE and KP are reached, strictly speaking, for infinitely small or infinitely large values of the parameters. In practice, however, measurements of the characteristic quantities such as limiting current, half-wave potential, peak current, peak potential... are made with a given finite uncertainty. Given the measured quantity and the error on its measurement, the lines

separating the various zones can be defined by giving to the limiting zones, DO, DE, KP, their maximum extension. On the zone diagram (Fig. 2) the degree of reversibility of each zone is indicated by the schematic representation of the polarization patterns obtained for a symmetrical triangular scan. Reversibility is complete for the diffusion zones DO and DE. There is total irreversibility for zone KP and partial reversibility for the intermediate zones KO and KE. Although not strictly specified, the order of magnitude of the extension of the intermediate zones (dependent upon the reaction scheme, the quantity measured and the experimental uncertainty) is represented in Fig. 2. On the other hand, the sweep rate of the linear scan cannot be varied by more than 4 or 5 orders of magnitude. For the other relaxation techniques possible variations of the electrolysis duration are nearly the same and for conventional polarography hardly a one order of magnitude variation in drop time is available. For dimerization processes largely in favour of the dimeric form at equilibrium, it is thus not possible to shift the point representing the system from one diffusion zone to the other. The kinetic analysis is practically restricted to a shift from one of the diffusion zones toward the pure kinetic zone. These present experimental limitations lead to a classification of the dimerization systems:

—irreversible dimerization processes, where zones DO, KO and KP are concerned,

—reversible dimerization processes, where zones DE, KE, and KP are concerned.

Only the first case will be treated here, the second will be the object of a subsequent paper, where, in particular, voltammetric patterns corresponding to equilibrium will be presented. Thermodynamical equilibrium for the dimerization reaction will thus be considered now only to establish the framework within which chemical polarization occurs.

GENERAL FEATURES OF VOLTAMMETRIC WAVE SYSTEM

The number of waves and qualitative characteristics of the polarization patterns obtained by polarography and by linear sweep voltammetry are now examined. The degree of reversibility is given by the qualitative description of the current–potential curves corresponding to symmetrical triangular potential scan. For this purpose it is of no use to separate DIM 1 and DIM 2 reaction schemes. As to the number of waves obtained with polarography three cases arise (see Fig. 3):

1. $E_1 \gg E_2$, $pC \ll 2pK_2 - pK_1$

Two successive waves are observed as soon as chemical polarization appears. When the dimerization reaction is slow compared to diffusion (zone DO), a one-electron wave in the E_1 potential region is obtained, as for all the other possible cases. For a fast equilibrated dimerization (zone DE), two equal half-electron diffusion-controlled waves are observed, the second one in the E_2 potential region and the first in a potential region defined according to the first thermodynamical diagram of Fig. 1. For pure kinetic conditions (zone KP), a similar polarization pattern is obtained. The second wave is still in the E_2 potential region, but the first is less anodic than previously and its half-wave potential will depend on initial concentration and drop time. For mixed chemical reaction–diffusion control (zone KO), the first wave is

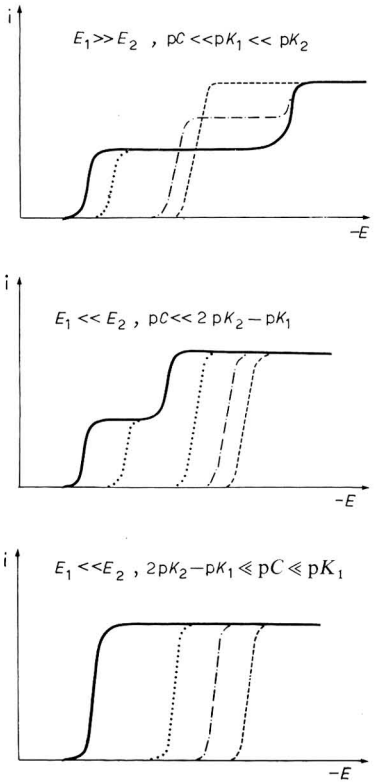

Fig. 3. Schematic representation of the polarographic wave system. (-----) pure diffusion control (DO), (·····) pure kinetic control (KP), (——) pure diffusion control (DE), (-·-·-) mixed reaction–diffusion control (KO).

higher than the second, their sum still corresponding to a one-electron exchange, according to the relative importance of chemical reaction and diffusion kinetic control. The half-wave potential of the first wave is still less anodic tending toward the E_1 region as kinetic control of the chemical reaction weakens.

2. $E_1 \ll E_2$, $pC \ll 2pK_2 - pK_1$

Two successive half-electron waves are again observed for a fast equilibrated dimerization, but the second wave (situated in the E_2 region) is anodic to the one-electron wave corresponding to a very slow dimerization (situated in the E_1 region). For pure kinetic conditions two situations may thus arise. For one of them the polarization pattern shows two equal half-electron waves as in the preceding case. For the other, a unique one-electron wave is observed as in the following case. The occurrence of either one situation or the other depends on the relative values of the potential separation $E_2 - E_1$ and the kinetic parameter λ. For a fast dimerization (as compared to diffusion) and a small potential separation, the first situation is obtained, and conversely for the second. Observation of either one or two waves is not an intrinsic property of the electrochemical–chemical system since the diffusion rate interferes in the practical distinction between the two situations. In the KO zone, one

wave is obtained in the near vicinity of the pure diffusion pattern (DO). This wave may split as the kinetic control increases. However the splitting would require rather small potential separation values to be effectively observed. Since we are interested here in irreversible dimerizations, the most common situation will thus be a one-electron pattern. In these conditions the general features of the polarographic wave system are the same as in the following case.

3. $E_1 \ll E_2$, $2pK_2 - pK_1 \ll pC \ll pK_1$

A unique one-electron wave is to be observed whatever the magnitude of the kinetic control by the dimerization reaction. For a very slow dimerization, a diffusion-controlled one-electron wave is observed as previously (zone DO). For a fast equilibrated dimerization (zone DE) the same polarization pattern arises, located in a more anodic potential region according to the thermodynamical diagram of Fig. 1. Pure kinetic conditions are also characterized by a similar wave, located between the previous ones, but depending, particularly through its half-wave potential, on initial concentration and drop time. The same general features are observed whatever the value of pC as compared to pK_2.

For *linear sweep voltammetry* a very similar qualitative analysis can be performed as to the number of waves, their height and potential localisation. Results are nearly the same as for polarography. However, the peak height for the pure kinetic conditions are slightly higher than for pure diffusion-controlled waves. Moreover in the case of a double-wave system and mixed reaction–diffusion control the height of the small second wave depends on the potential difference between the two waves and on sweep rate. The exact expression of this second wave is thus rather complex, depending on numerous factors. The problem is in fact very similar to that of the anodic trace with a symmetrical triangular scan. Similarly, straightforward expressions are better obtained by using a double scan, as shown later. The various polarization patterns for linear sweep conditions are represented schematically on Fig. 4. The same diagram also gives the current–potential curves for a triangular potential scan showing the reversibility of the system in various conditions. Four cases instead of three have been distinguished for this representation, since the third previous case has to be divided according to the value of pC as compared to pK_2.

1. $E_1 \gg E_2$, $pC \ll pK_1 \ll pK_2$

For a very slow dimerization process (zone DO) a reversible diffusion-controlled one-electron wave is obtained. For opposite diffusion conditions (zone DE), two successive reversible diffusion-controlled half-electron waves arise. When pure kinetic control is achieved (zone KP), the first wave is completely irreversible whereas the second one, located in the E_2 potential region, is reversible. In the intermediate zone KO, the first wave is partially reversible, its degree of reversibility depending on sweep rate and switching potential. The small second wave is reversible, its height depending on the potential separation between the two waves and on sweep rate.

2. $E_1 \ll E_2$, $pC \ll 2pK_2 - pK_1$

The polarization pattern in the DE zone, is exactly the same as in the previous case. The current–potential curves obtained for the other polarization conditions are as for the following case.

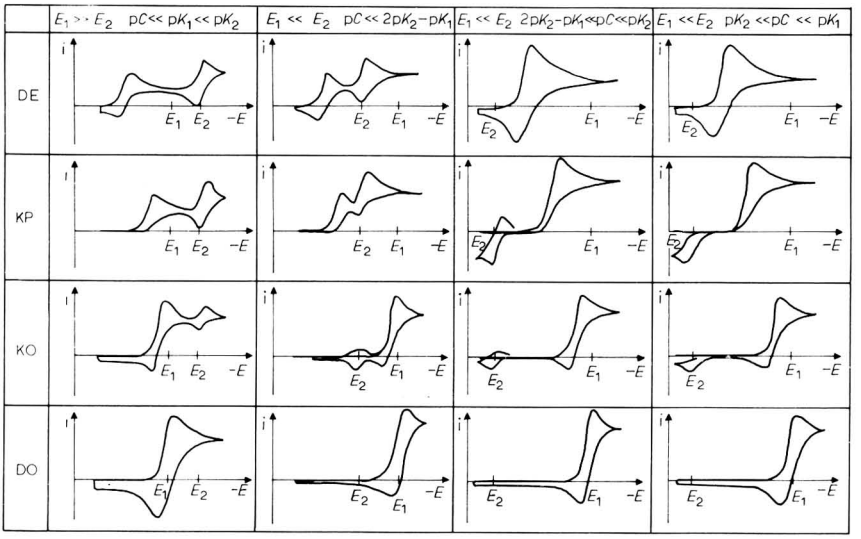

Fig. 4. Schematic representation of linear and triangular sweep voltammograms.

3. $E_1 \ll E_2$, $2pK_2 - pK_1 \ll pC \ll pK_2$

Pure diffusion conditions prevailing in the DO and DE zones give rise to one-electron reversible waves, the second being anodic to the first. For pure kinetic control, the cathodic trace is located between the preceding waves and is slightly higher. The anodic trace shows the complete irreversibility of the process, but, proceeding toward more anodic potentials, a purely diffusion-controlled wave arises in the E_2 potential region. This wave is a reversible one as shown by the cathodic trace obtained when scanning again the potential cathodically by adding to the symmetrical triangular sweep a third branch parallel to the first one. Mixed reaction–diffusion control (zone KO) gives rise to a partially reversible wave. In the anodic range a small reversible wave appears in the E_2 region. The height of this wave depends on the time elapsed between the main wave and the reoxidation wave. The anodic second wave is the largest, the smallest is the first one. Reversibility of the anodic wave in the E_2 region corresponds to the reoxidation of A–A leading to $A–A^+$.

4. $E_1 \ll E_2$, $pK_2 \ll pC \ll pK_1$

The situation is the same as in the previous case for the main wave in the various polarization conditions defined by each zone. The difference concerns the anodic wave in the E_2 potential region which is now irreversible or quasi-reversible if the rate of the fission reaction MON 2 is of the same magnitude as the rate of the dimerization process DIM 1. This is an important feature allowing a qualitative characterization of the DIM 1–MON 2 mechanism.

CHARACTERISTIC POTENTIALS AND WAVE HEIGHTS

The exact expression for the voltammetric waves is now given in the case of a single linear cathodic sweep. Waves are characterized in a quantitative way by the

values of the peak current, the peak potential and the peak width. This last factor is defined as the potential difference between the half-peak potential and the peak potential. For polarography, approximate expressions are given concerning the limiting current and the half-wave potential. The cases to be distinguished according to the thermodynamical properties of the system are the same as in the beginning of the preceding section. No operative distinction can be made for the DIM 1–MON 2 reaction scheme which is characterized by the observation of the anodic trace. As seen above the number of cases to be considered finally can be reduced to two, a single-wave system and a double-wave system. Within each of these cases another distinction must be made between the DIM 1 and DIM 2 reaction schemes. On the whole, four possibilities will thus be discussed:

I. Single-wave system–DIM 1 reaction scheme
II. Single-wave system–DIM 2 reaction scheme
III. Double-wave system–DIM 1 reaction scheme
IV. Double-wave system–DIM 2 reaction scheme

The mathematical formulation of the polarization problem is given in Table 1 for the DIM 1 and the DIM 2 reaction schemes, in the cases of linear and semi-infinite diffusion. The partial derivative equation systems are different for each

TABLE 1

PARTIAL DERIVATIVE EQUATION SYSTEM WITH INITIAL AND BOUNDARY CONDITIONS

DIM 1	*DIM 2*
$\frac{\partial C_{A^+}}{\partial t} = D_M \frac{\partial^2 C_{A^+}}{\partial x^2}$	$\frac{\partial C_{A^+}}{\partial t} = D_M \frac{\partial^2 C_{A^+}}{\partial x^2} - kC_A C_{A^+}$
$\frac{\partial C_A}{\partial t} = D_M \frac{\partial^2 C_A}{\partial x^2} - kC_A^2$	$\frac{\partial C_A}{\partial t} = D_M \frac{\partial^2 C_A}{\partial x^2} - kC_A C_{A^+}$
$\frac{\partial C_{A-A^+}}{\partial t} = D_D \frac{\partial^2 C_{A-A^+}}{\partial x^2}$	$\frac{\partial C_{A-A^+}}{\partial t} = D_D \frac{\partial^2 C_{A-A^+}}{\partial x^2} + kC_A C_{A^+}$
$\frac{\partial C_{A-A}}{\partial t} = D_D \frac{\partial^2 C_{A-A}}{\partial x^2} + \frac{k}{2} C_A^2$	$\frac{\partial C_{A-A}}{\partial t} = D_D \frac{\partial^2 C_{A-A}}{\partial x^2}$

Initial conditions $t = 0 \quad x \geqq 0$

$$C_{A^+} = C^0; \quad C_A = C_{A-A^+} = C_{A-A} = 0$$

Boundary conditions $x = \infty \quad t \geqq 0$

$$C_{A^+} = C^0; \quad C_A = C_{A-A^+} = C_{A-A} = 0$$

$$x = 0 \quad t \geqq 0$$

$\frac{\partial C_{A^+}}{\partial x} + \frac{\partial C_A}{\partial x} = 0$;	$\frac{\partial C_{A-A^+}}{\partial x} + \frac{\partial C_{A-A}}{\partial x} = 0$
$\frac{C_{A^+}}{C_A} = \exp \frac{F}{RT}(E - E_1)$;	$\frac{C_{A-A^+}}{C_{A-A}} = \exp \frac{F}{RT}(E - E_2)$

$$i = FS\left[D_M\left(\frac{\partial C_{A^+}}{\partial x}\right)_{x=0} + D_D\left(\frac{\partial C_{A-A^+}}{\partial x}\right)_{x=0}\right]$$

Polarography: E = constant

Linear sweep voltammetry: $E = E_i - vt$ (E_i: initial potential, v: sweep rate).

reaction scheme but the set of initial and boundary conditions is the same. Activities and concentrations are assumed to be equal.

C^0 is the initial concentration, t the time and x the distance to the electrode, n the number of electrons exchanged in the charge transfer reaction, and k the rate constant of the dimerization reaction. The diffusion coefficients are assumed to be the same for each monomeric form (D_M) and for each dimeric form (D_D) but to be unequal for monomers and dimers.

The boundary conditions in Table 1 are to be supplemented by the condition defining the variation of the electrode potential E with time. For polarography this condition is the constancy of E with time. For linear and triangular sweep voltammetry E is considered as varying linearly with time in the appropriate intervals.

In the expression defining the current intensity, the area of the working electrode S is considered as independent of time for linear sweep voltammetry and as varying with time for polarography according to the following expression:

$$S = A(mt)^{\frac{2}{3}}$$

A being a constant depending on the units employed, and m the mass of mercury flowing per unit of time.

In order to solve the polarization problem defined by the formulation given in Table 1, it appears convenient to use an adimensional formulation. The various variables and parameters to be introduced in this respect are given in Table 2 for polarography and for linear sweep voltammetry beside the resulting forms of the partial differential equations system for each mechanism and of the set of initial and boundary conditions. The relative influence on the polarization curves of the diffusion process and of the dimerization reaction is precisely expressed by the value of the parameter λ.

1. For a dimerization process very slow as compared to diffusion, *i.e.* for small values of λ, a purely diffusion-controlled one-electron wave is obtained in every case. The exact expression of the wave and the values of the characteristic potentials and currents are well known for linear sweep voltammetry[15,18]:

$$\psi_p = 0.446 \quad \xi_p = 1.11 \quad \xi_p - \xi_{p/2} = 2.20$$

Thus

$$j_p = 0.446\, F D_M^{\frac{1}{2}} C^0 (Fv/RT)^{\frac{1}{2}}$$
$$E_p = E_1 - 1.11\, RT/F$$
$$E_{p/2} - E_p = 2.20\, RT/F$$

at 25°C

$$j_p = 0.268\, D_M^{\frac{1}{2}} C^0 v^{\frac{1}{2}}$$
$$E_p = E_1 - 0.0283$$
$$E_{p/2} - E_p = 0.0565$$

j_p, the current density is in A cm^{-2}, D in cm^2 s^{-1}, C^0 in mmol l^{-1}, v in V s^{-1}, E_p and $E_{p/2}$ in V. These units will be used in the following without further mention.

For a very fast equilibrated dimerization a diffusion-controlled wave is also obtained, but its expression is not the same as the preceding one, owing to the non-linearity of the Nernst law for a second-order process. The exact expression for such

TABLE 2

DEFINITION OF ADIMENSIONAL VARIABLES

Adimensional variables and parameters

time: $T = t/\theta$; potential: $\xi = -(F/RT)(E-E_1)$ (1)

—for polarography θ is the drop time and ξ is a constant.
—for linear sweep voltammetry the initial potential E_i is compared to the normal potential E_1 through the parameter:

$$u=(F/RT)(E_i-E_n)\,. \quad \text{Thus } T=\xi+u \quad \text{and} \quad \theta=RT/Fv \tag{2}$$

space: $y = x/(D_M\theta)^{\frac{1}{2}}$

concentrations: $a^+ = C_{A^+}/C^0$; $a = C_A/C^0$; $aa^+ = C_{A-A^+}/C^0$; $aa = C_{A-A}/C^0$ (3)

kinetic parameter: $\lambda = k\theta$ (4)

diffusion factor: $d = D_D/D_M$ (5)

Partial derivative equation system

DIM 1

$$\frac{\partial a^+}{\partial T} = \frac{\partial^2 a^+}{\partial y^2} \tag{6}$$

$$\frac{\partial a}{\partial T} = \frac{\partial^2 a}{\partial y^2} - \lambda a^2 \tag{7}$$

$$\frac{\partial aa^+}{\partial T} = d\frac{\partial^2 aa^+}{\partial y^2} \tag{8}$$

$$\frac{\partial aa}{\partial T} = d\frac{\partial^2 aa}{\partial y^2} + \frac{\lambda}{2}a^2 \tag{9}$$

DIM 2

$$\frac{\partial a^+}{\partial T} = \frac{\partial^2 a^+}{\partial y^2} - \lambda a^+ a \tag{10}$$

$$\frac{\partial a}{\partial T} = \frac{\partial^2 a}{\partial y^2} - \lambda a^+ a \tag{11}$$

$$\frac{\partial aa^+}{\partial T} = d\frac{\partial^2 aa^+}{\partial y^2} + \lambda aa^+ \tag{12}$$

$$\frac{\partial aa}{\partial T} = d\frac{\partial^2 aa}{\partial y^2} \tag{13}$$

Initial and boundary conditions

$T = 0 \quad y \geqq 0 \qquad a^+ = 1; \quad a = aa^+ = aa = 0$ (14)

$y = \infty \quad T \geqq 0 \qquad$ idem

$y = 0 \quad T \geqq 0 \qquad \frac{\partial a^+}{\partial y} = -\frac{\partial a}{\partial y} = \psi_1; \quad \frac{\partial aa^+}{\partial y} = -\frac{\partial aa}{\partial y} = \psi_2$ (16)

$$\frac{a^+}{a} = \exp(-\xi)\,; \quad \frac{aa^+}{aa} = \exp(-\xi)\exp\frac{F}{RT}(E_1-E_2) \tag{17}$$

Quantity to be calculated

$$\psi = \psi_1 + d\psi_2; \quad i = FSC^0 D_M^{\frac{1}{2}}\theta^{-\frac{1}{2}}\psi \tag{18}$$

a wave has been derived for an n-electron transfer[19]*, and can be used here for the single one-electron case as well as for the double half-electron case. Explicit recalling of these results is of little use here as we are mainly interested in quasi-irreversible dimerization processes.

* This expression has been recently re-derived by Shuman[20] who states that no closed form can be obtained for the current function. This statement may be true for reaction orders higher than 2 (the problem is then to solve an algebraic equation of degree larger than two, as shown earlier[21]), but not for a second-order process for which a closed form is readily derivable and has already been derived[19]. Discrepancies between our results[19] and those of Shuman[20] are only apparent and arise from a different definition of the electron number n. Normalizing factors have thus to be introduced: $\sqrt{2}$ on the current expression and 2 on the potential scale.

2. For pure kinetic conditions (zone KP), the influence of the dimerization reaction on the overall kinetics reaches its maximum. The best conditions are thus achieved for making an experimental distinction between the DIM 1 and DIM 2 reaction schemes. As shown above, four different cases arise:

I. Single wave system–DIM 1 reaction scheme

The corresponding polarization problem has already been solved for *linear sweep voltammetry*[14,19,22]. The equation of the voltammetric wave in adimensional form is as follows:

$$\psi^{\frac{2}{3}} \exp(-\xi_1^+) = 1 - \frac{1}{\pi^{\frac{1}{2}}} \int_{-u_i^+}^{\xi_1^+} \frac{\psi(\eta)}{(\xi_1^+ - \eta)^{\frac{1}{2}}} d\eta$$

The adimensional current function ψ is the same as has been defined in Table 2. The adimensional potential scale is now:

$$\xi_1^+ = \xi + \tfrac{1}{3} \ln \tfrac{2}{3}\lambda .$$
$$u_1^+ = u - \tfrac{1}{3} \ln \tfrac{2}{3}\lambda$$

characterizes the position of the initial potential. In the usual practice of linear sweep voltammetry the initial potential is made sufficiently anodic to the wave in order that the peak be independent of it within experimental error. From the mathe-

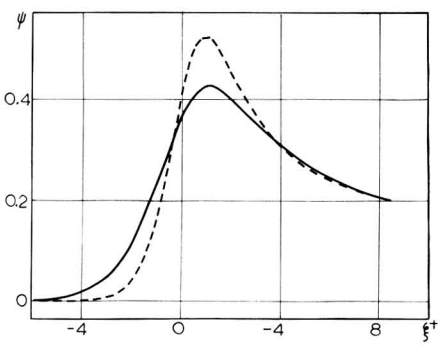

Fig. 5. Adimensional current function featuring DIM 1 (------) and DIM 2 (———) for a singlewave system. Symbols defined in the text.

matical point of view this means that u is considered as infinite. These conditions will be considered as achieved for every polarization curve dealt with in this paper, without further mention. For the present case it follows that the peak-characteristic values are:

$$\psi_p = 0.527 \quad \xi_{p,1}^+ = 0.903 \quad \xi_{p,1} - \xi_{p/2,1} = 1.51$$

The shape of the ψ function is set out in Fig. 5*. Peak current density, peak potential and wave width parameters are thus

$$j_p = 0.527\, F D_M^{\frac{1}{2}} C^0 (Fv/RT)^{\frac{1}{2}}$$

* The corresponding ψ values are available in tabular form on request for every graphical representation in this paper.

$$E_p = E_1 - 0.902\ RT/F + (RT/F)\ln \tfrac{2}{3}(RT/F) + (RT/3F)\ln k - (RT/3F)\ln v + (RT/3F)\ln C^0$$

$$E_{p/2} - E_p = 1.51\ RT/F$$

at 25°C

$$j_p = 0.317\ D_M^{\frac{1}{2}} C^0 v^{\frac{1}{2}}$$

$$E_p = E_1 - 0.058 + 0.0197 \log k - 0.0197 \log v + 0.0197 \log C^0$$

$$E_{p/2} - E_p = 0.0388$$

Peak height is very close to the value corresponding to a purely diffusion-controlled one-electron wave and is still proportional to the initial concentration and to the square root of the sweep-rate. The peak width is somewhat smaller but the most significant feature is the linear variation of the peak potential with the logarithm of initial concentration and sweep rate, by 19.7 mV per decade at 25°C, anodically for an increase of the first factor and cathodically for an increase of the second.

For *polarography* the wave characteristics[23,24] are similar: the wave height is exactly the same as for a purely diffusion-controlled one-electron wave, but the wave shape is different and the half-wave potential varies linearly with the logarithm of initial concentration and drop time by 19.7 mV per decade at 25°C, anodically for an increase of the first factor and cathodically for an increase of the second.

II. Single wave system–DIM 2 reaction scheme

Pure kinetic conditions involve, as above, a stationary A concentration. Moreover, λ being considered as very large, the reaction layer is very thin so that $C_{A^+} + C_A$ is approximately constant in this layer. There follows a noteworthy simplification of the mathematical treatment and the adimensional expression can be deduced from the corresponding expression in the DIM 1 case without further numerical computation (see appendix A). Keeping the same definition of ψ and the adimensional potential scale being defined by:

$$\xi_2^+ = \xi + \tfrac{1}{2}\ln\lambda + \ln 2\,, \quad u_2^+ = u - \tfrac{1}{2}\ln\lambda - \ln 2$$

the wave expression is

$$\psi^{\frac{2}{3}} \exp(-\tfrac{2}{3}\xi_2^+) = 1 - \frac{1}{\pi^{\frac{1}{2}}} \int_{-u_2^+}^{\xi_2^+} \frac{\psi(\eta)}{(\xi_2^+ - \eta)^{\frac{1}{2}}} d\eta$$

and the peak characteristic values for the *linear sweep voltammetric wave* are:

$$\psi_p = 0.430 \quad \xi_{p,2}^+ = 1.15 \quad \xi_{p,2}^+ - \xi_{p/2,2}^+ = 2.27$$

The shape of the $\psi(\xi_2^+)$ function is shown in Fig. 5. Peak current density, peak potential and wave width parameters are then:

$$j_p = 0.430\ F D_M^{\frac{1}{2}} C^0 (Fv/RT)^{\frac{1}{2}}$$

$$E_p = E_1 - 0.457(RT/F) + (RT/2F)\ln RT/F + (RT/2F)\ln k + (RT/2F)\ln v + (RT/2F)\ln C^0$$

$$E_{p/2} - E_p = 2.27\ RT/F$$

at 25°C.

$$j_p = 0.259\, D_M^{\frac{1}{2}} C^0 v^{\frac{1}{2}}$$

$$E_p = E_1 - 0.059 + 0.0296 \log k - 0.0296 \log v + 0.0296 \log C^0$$

$$E_{p/2} - E_p = 0.0583$$

The peak current is still proportional to the initial concentration and the square root of the sweep rate and not very different from the peak height corresponding to a purely diffusion-controlled one-electron exchange. For comparable conditions, the peak current is about 20% lower than in the DIM 1 case. Accordingly the peak width is now larger than for the DIM 1 reaction scheme. The most distinct feature of the polarization curve is the variation of the peak potential with the initial concentration and the sweep rate. This variation is still logarithmic and in the same direction as above, but the rate of variation is different: 29.6 mV instead of 19.7 mV per decade at 25°C.

For *polarography* the wave characteristics are similar: the limiting current is purely diffusion-controlled, but the wave shape is different. The half-wave potential varies linearly with the logarithm of initial concentration and of sweep rate in the same direction as above but with a different rate: 29.6 mV instead of 19.7 mV per decade at 25°C. These results are consistent with the brief indications given by Cizek *et al.* concerning this polarization scheme[25].

III. Double wave system–DIM 1 reaction scheme

The two successive waves are assumed to be largely separated. In the potential region of the first one an irreversible reduction of A^+ occurs leading to the dimer A–A which reoxidizes immediately to $A\text{–}A^+$. The second wave, located in the E_2 potential region corresponds to the reversible reduction of $A\text{–}A^+$ to A–A. Thus *the first wave is half the wave obtained in case I* for linear sweep voltammetry as well as for polarography. The peak potential and peak width is exactly the same as for the single wave system with a DIM 1 reaction scheme (for demonstration of these statements see appendix B) and likewise for the polarographic half-wave potential.

The *second wave*, as measured to the extension of the first as a base line, is purely diffusion-controlled and is half a normal diffusion wave, its peak potential being related to the normal potential E_2 in the usual way:

$$E_{p,2} = E_2 - 1.11\, RT/F$$

Peak current densities for the first and the second waves are thus:

$$j_{p,1} = 0.264\, F D_M^{\frac{1}{2}} C^0 (F/RT)^{\frac{1}{2}}$$

$$j_{p,2} = 0.223\, F D_M^{\frac{1}{2}} C^0 (F/RT)^{\frac{1}{2}}$$

at 25°C:

$$j_{p,1} = 0.159\, D_M^{\frac{1}{2}} C^0 v^{\frac{1}{2}}$$

$$j_{p,2} = 0.134\, D_M^{\frac{1}{2}} C^0 v^{\frac{1}{2}}$$

The ratio of the first to the second peak height is thus 1.18. The most distinct feature of the first wave remains the logarithmic variation of the peak potential (or half-wave potential for polarography) with the initial concentration and sweep rate (or drop time for polarography) by 19.7 mV per decade at 25°C.

IV. Double wave system–DIM 2 reaction scheme

In the potential region of the first wave, a direct and irreversible reduction of A^+ to $A–A^+$ occurs, whereas the second wave corresponds to the reversible reduction of $A–A^+$ to A–A.

The *second wave* is thus purely diffusion-controlled and possesses exactly the same characteristics as in the preceding case.

The *first wave is half the wave obtained in case II* and is mainly characterized by the logarithmic variation of the peak potential with the initial concentration and sweep rate (or drop time in the case of the polarographic half-wave potential) by 28.6 mV per decade (for demonstration see appendix B). The ratio of the first to the second peak is now 0.96.

3. For mixed reaction–diffusion control (zone KO) an intermediate behaviour is obtained. For single-wave as well as for double-wave systems the variation of peak potential with the various experimental factors is intermediate between a logarithmic variation with initial concentration and sweep rate and complete independence of these quantities. The peak heights do not change markedly in the KO zone for both single-wave systems: 18% on the whole for the DIM 1 reaction scheme and 4% for the DIM 2 reaction scheme. Peak current values exhibit much larger variation for the double-wave systems since they change approximately by a factor 2 from the KP to the DO zone. The same considerations are valid for polarography, replacing the sweep rate by the drop time, the peak height by the plateau current and the peak potential by the half-wave potential.

The A concentration is no longer stationary and at least one of the partial derivative equations possesses a quadratic term. A finite difference method has therefore to be used for solving the polarization problem. We employed, for the DIM 1 case, the same computational procedure as we did previously for the disproportionation reaction scheme[1], *i.e.* a combination of the Crank–Nicholson finite difference method and the usual integral equation computation method (for pertinent details on the method see appendix in ref. 1). As stated before[1], this computational procedure is applicable to the other electrochemical methods. Indeed, a similar finite difference approach has already been applied to potentiostatic chronoamperometry for second order processes[26,27]. The procedure we used here as well as for the disproportionation reaction scheme differs from the latter by a simpler way of linearizing the quadratic term avoiding an iterative calculation (see appendix in ref. 1). Another feature of our method is specifically related to linear sweep voltammetry: since the boundary condition on the electrode surface is an integral relation owing to the linear dependence of potential with time, the computation procedure usually employed to solve this kind of relation has been combined with the finite difference method (see appendix in ref. 1).*

For the DIM 2 reaction scheme the numerical solution of the polarization problem is somewhat more complex since the first two partial derivative equations possess quadratic terms. The method we used in this connection is a *simultaneous*

* Recently, Olmstead and co-workers[28] have discussed in great detail a computation procedure very similar to the one we used previously for the disproportionation reaction scheme[1]. The only difference is in the expression of the quadratic term for which these authors employed the iterative procedure of Booman and Pence[26].

finite difference resolution of the two partial derivative equations. A unique resolution matrix is obtained for the two equations and is resolved by a Gaussian-like method. The calculation technique is described in appendix C which also provides some further details on the technique used for the DIM 1 case (the corresponding programs in Fortran language are available on request).

The general expression of the dimensionless current function deals with the diffusion gradient of the monomer as well as the diffusion gradient of the dimer:

$$\frac{j}{FD_M^{\frac{1}{2}}C^0(Fv/RT)^{\frac{1}{2}}} = \psi = \psi_1 + d\psi_2 = \left(\frac{\partial a^+}{\partial y}\right)_{y=0} + d\left(\frac{\partial aa^+}{\partial y}\right)_{y=0}$$

$$= -\left(\frac{\partial a}{\partial y}\right)_{y=0} - d\left(\frac{\partial aa}{\partial y}\right)_{y=0}$$

Generally speaking, the diffusion coefficient ratio $d = D_D/D_M$ thus interferes in the numerical expression of the current function. However, in the case of a single-wave system and a DIM 1 reaction scheme (case I) as well as for a double-wave system with a DIM 2 reaction scheme in the region of the first wave (case IV), the gradient of dimer concentration at the electrode surface is equal to zero. For case I this is the consequence of two facts: (i) the dimeric form A–A$^+$ is involved in purely diffusive process (see eqn. (8) in Table 2), (ii) its concentration at the electrode surface is practically zero owing to the large separation between the potentials E_1 and E_2. For case IV the same considerations apply to the dimeric form A–A leading to the same result.

For case II (single-wave system–DIM 2 reaction scheme) and case III (double-wave system–DIM 1 reaction scheme) the current function does depend on the diffusion coefficients ratio. In case II, for instance, the dimeric form initially formed is A–A$^+$. Its formation occurs in solution owing to the relative slowness of the dimerization reaction. In the potential region of the wave every molecule of A–A$^+$ present at the electrode is immediately reduced to A–A. The total current flowing through the electrode surface is therefore a function of A–A$^+$ diffusion. In case III the initially formed dimer is A–A which has to re-oxidise at the potential of the first wave to give A–A$^+$ through an interposed diffusion process.

In other words, cases II and III correspond to e.c.e. reaction schemes (e.c.e. 1 for case II and e.c.e. 2 for case III according to the conventions already introduced[1]) whereas case I and IV are simple e.c. mechanisms, at least in the potential regions of the first waves.

If the diffusion coefficient of the monomeric and dimeric forms were identical, the numerical calculations concerning case II and III would be deducible from those corresponding to case I and IV by resolution of an integral relation resulting from the linear combination of the partial derivative equations and integration. Since the diffusion coefficients must be considered as different, the foregoing procedure is not applicable and an additional finite difference resolution concerning one of the dimeric forms must be performed. These calculations have been restricted here to one value of the diffusion parameter d which has been chosen according to the Stokes–Einstein relation[29]. The ratio of the dimer and monomer molecular weights being equal to 2, it follows that the selected value for d is

$$d = (0.5)^{\frac{1}{3}}$$

The results of the numerical calculations are given for the peak characteristics: peak height, peak potential and peak width in their adimensional form as functions of the kinetic parameter log λ. Figure 6 presents these three quantities for the single-wave systems (full line for DIM 2 and dashed line for DIM 1)*.

The corresponding quantities for the first wave in the case of double-wave systems (full line for DIM 2, dashed line for DIM 1) are represented on the same figure.

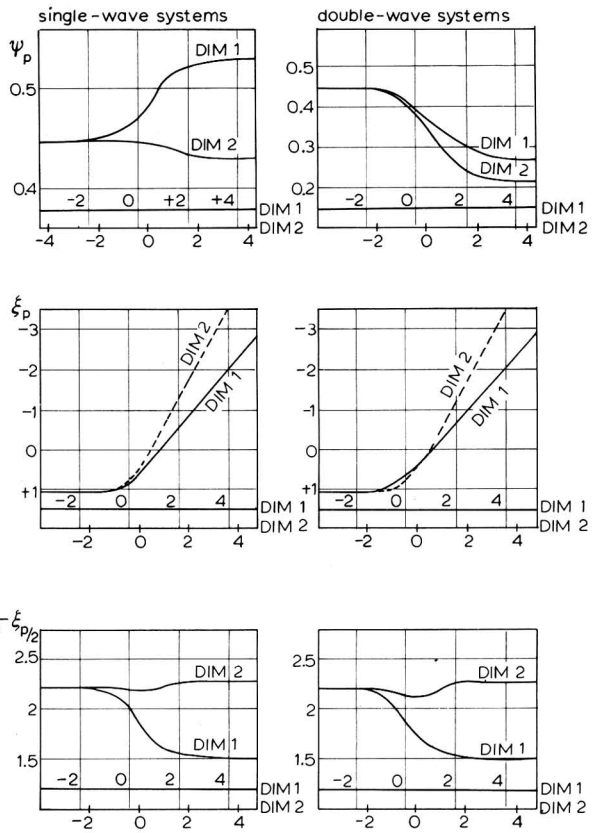

Fig. 6. Peak height, peak potential and peak width adimensional functions (for definitions see the text) featuring the DIM 1 and DIM 2 reaction schemes for single-wave and double-wave systems.

Although detailed calculations have not been performed for conventional polarography, it can be stated that the trends in the variations of limiting currents and half-wave potentials with initial concentration and drop time are the same as for the peak in linear sweep voltammetry, substituting drop time for sweep rate.

In the case of double-wave systems the second wave varies according to the λ values between a purely diffusion-controlled wave (zone KP) and zero (zone DO). In the region of the second wave it can be considered that an e.c.e. 2 mechanism is acting

* Peak heights and peak potentials have already been calculated for the single-wave system with a DIM 1 reaction scheme[28].

for the DIM 1 case as well as for the DIM 2 case. In the last case the second wave corresponds to the reduction of $A\text{–}A^+$ to A–A with mixed kinetic and diffusion control. In the DIM 1 case the overall process in the potential region of the second wave is a simple e.c. process and a reoxidation process occurs in the region of the first wave, so that the behaviour of the second wave is analogous to that of the DIM 2 case. Such e.c.e. 2 reaction schemes have already been studied when the chemical reaction is first-order. It has been shown that for linear sweep voltammetry the magnitude and characteristics of the second wave depend not only on the sweep rate but also on the potential separation between the first and the second wave[30]. This potential separation being given, the variation of the peak height of the second wave with sweep rate is quite unusual for small values of this peak height, *i.e.* for high values of the sweep rate, since the peak height decreases as the sweep rate is raised (as $v^{-\frac{1}{2}}$). The same trend is to be observed in the present cases. A strong similarity thus exists between these processes and the study of a follow-up reaction by observing the anodic trace on inverting the sweep direction. This analogy has suggested the use of a double-scan technique for the e.c.e. 2 mechanisms, both parts of the scan being in the same direction and the second one being faster than the first[30]. Use of such a technique for the double-wave systems will be discussed in the section dedicated to double-scan methods. For polarography, when the second wave is small, the variation of the limiting current with the mercury height is a decrease of the current value as the mercury height is raised. Such unusual behaviour has already been experimentally observed in the reduction of α-substituted aliphatic aldehydes[31] and theoretically justified as featuring an e.c.e. 2 reaction scheme[30,10]. For the present double-wave system similar behaviour is to be expected.

4. The above calculations allow the limiting lines of zone KO to be evaluated. When the peak potential is the quantity to be measured, assuming an accuracy of 2 mV at 25°C, the limiting values of log λ for the various cases are as follows:

—single-wave system–DIM 1 reaction scheme:
DO/KO: $\log \lambda = -0.44$ KO/KP: $\log \lambda = 0.11$
—single-wave system–DIM 2 reaction scheme:
DO/KO: $\log \lambda = -1.18$ KO/KP: $\log \lambda = 1.62$
—double-wave system–DIM 1 reaction scheme:
DO/KO: $\log \lambda = -1.07$ KO/KP: $\log \lambda = 2.65$
—double-wave system–DIM 2 reaction scheme:
DO/KO: $\log \lambda = -1.32$ KO/KP: $\log \lambda = 2.27$

The peak current variation is very small for the single-wave systems so that a zone diagram using it as measured quantity would be of little value. This is not the case for the double-wave systems where the peak current exhibits a significant variation (by about a factor of 2) from the pure kinetic zone to the pure diffusion zone. Assuming an accuracy of 4% in peak current measurements, the limiting lines of the KO zone are defined as follows:

—double-wave system–DIM 1 reaction scheme:
DO/KO: $\log \lambda = -0.55$ KO/KP: $\log \lambda = 3.86$
—double-wave system–DIM 2 reaction scheme:
DO/KO: $\log \lambda = -1.10$ KO/KP: $\log \lambda = 2.50$

DOUBLE-SCAN TECHNIQUES

As shown above, symmetrical triangular sweep voltammetry provides a convenient means for testing the degree of reversibility of the electrochemical system. For a quantitative analysis of the dimerization kinetics as well as for other reaction schemes, this method has the disadvantage that the anodic trace depends, among other factors, on the value of the switching potential. This is the reason why a double-scan technique with the second part of the scan shorter than the first, has been proposed[8]. Triangular as well as trapezoidal wave forms may be employed in this connection. As originally devised, the principle of the method is as follows: in the first part of the scan the representative point of the system is located in the KP zone whereas in the second part it is shifted in the DO zone. The anodic wave is then purely diffusion-controlled and corresponds to a depolarizer concentration which is equal to the concentration of the reduction product in the electrode plane at the end of the first scan segment. The anodic current is measured by taking the current value at the switching time as zero current. The switching potential value is selected cathodic enough for the concentration of the depolarizer at the electrode surface to be zero. Under these conditions, the ratio between the anodic peak current and the cathodic peak current obtained with the same sweep rate as the anodic trace, *i.e.* in pure diffusion conditions, is the exact measure of the adimensional concentration of the reduction product at the end of the slow cathodic part of the scan, at the electrode surface. This adimensional concentration depends only on the kinetic factor characterizing the cathodic process. This factor contains the electrolysis time of the cathodic stage, the rate constant of the chemical reaction and the initial depolarizer concentration if the chemical process is second-order. The peak current ratio measurement is therefore a simple route to rate constant determination. When the cathodic stage is concerned with pure kinetic conditions (zone KP), the expression of the peak current ratio as a function of the kinetic parameter featuring the cathodic process is rather simple even for second-order inactivating chemical reactions as shown earlier[8]. The method has already been successfully applied to the e.c.e.–disproportionation mechanism occurring in the reduction of the uranyl cation in strongly acidic media[32]. In this case and during the study of the dimerization processes occurring in the reduction of immonium cations[33], the measuring procedure has been improved, mainly in two directions:

(i) As originally devised the double-scan method requires pure kinetic conditions in the first part of the scan. The advantage of such conditions is the simplicity of the mathematical analysis. However, these conditions involve rather small anodic currents that may be difficult to measure accurately with current electrochemical instrumentation. It appears interesting therefore in practice to supplement these determinations by measurements corresponding to higher values of the peak current ratio. In this last case pure kinetic conditions are no longer achieved during the cathodic process and are replaced by polarization conditions involving a mixed reaction–diffusion control (*i.e.* corresponding to zone KO). A finite difference calculation is thus necessary in order to obtain the adimensional concentration of the reduction product on the electrode surface, at the end of the cathodic stage, as a function of the kinetic parameter. For mixed reaction–diffusion control as well as for pure kinetic conditions, the duration of the second potential segment has to be

sufficiently lower than for the first segment in order that the evolution of the dimerization reaction be inappreciable during the reoxidation step. In the first situation error arising from the use of an insufficiently asymmetrical scan is more likely to occur than in the second. θ_f being the switching time and θ'_f the time elapsed from the switching potential to the reoxidation peak, an upper limit of the error is given by

$$\Delta k/k = \theta'_f/\theta_f$$

measuring the anodic peak current to the extension of the cathodic curve as a base line. The experimental measurement leads then to too large a value for k. This evaluation of the error is however pessimistic, since the measuring procedure implies that the current at time θ_f is taken as base line for the determination of the anodic peak current[8]. A partial compensation of the precedingly evaluated error thus occurs. It will be shown that the resulting uncertainty in k can be neglected in current practice.

(ii) For a trapezoidal scan, determination of the time θ_f to be considered in the kinetic parameter λ characterizing the cathodic process ($\lambda = kC^0\theta_f$) is straightforward since it is simply the duration of the cathodic step itself. In the case of a triangular scan, the same definition is valid provided the switching potential is sufficiently cathodic for the depolarizer concentration to be equal to zero at the electrode surface. In the first case this condition is fulfilled from the very beginning of the cathodic process whereas in the second case, this condition tends to be achieved asymptotically as the switching potential, and thus the switching time, shift. This situation may be of little convenience in experimental practice, particularly if the potential region following the wave under examination is concerned with a successive charge transfer process, or with the discharge of the supporting electrolyte. The best approximate procedure is then to define the electrolysis duration of the cathodic sweep as the time elapsed from the middle of the interval between half peak and peak to the switching potential as will be shown later.

For the DIM 1 and DIM 2 reaction schemes the expression of the adimensional concentration of the reduction product (A) on the electrode surface and at the end of the cathodic stage is the same whatever the number of waves on the polarization pattern. The result of calculations for the quantity $(a)_{y=0}$ which is equal to the peak-current ratio as defined above, is shown in Fig. 7. The definition of the kinetic factor coordinate is slightly different for the two cases DIM 1 and DIM 2 in order to ensure the coincidence of the working curves for large values of the kinetic factor, *i.e.* in pure kinetic conditions.

Using these working curves, the order of magnitude of the errors caused by the approximations defined above can be evaluated for current measuring procedures.

We consider as a typical example a triangular sweep experiment performed at 25°C with a switching potential separated from the peak by 250 mV, the ratio of anodic to cathodic sweep rates being 10. The error arising from the use of an insufficiently asymmetrical scan has been evaluated for peak currents ratios of 0.75 and 0.5. The error resulting from an approximate choice of θ_f has been estimated for pure kinetic conditions by noting that

$$\frac{\Delta[(i_a)_p/(i_d)_p]}{(i_a)_p/(i_d)_p} = \frac{2}{3}\frac{\Delta\psi}{\psi}$$

where $\Delta\psi/\psi$ is the relative difference between the linear sweep cathodic current–time

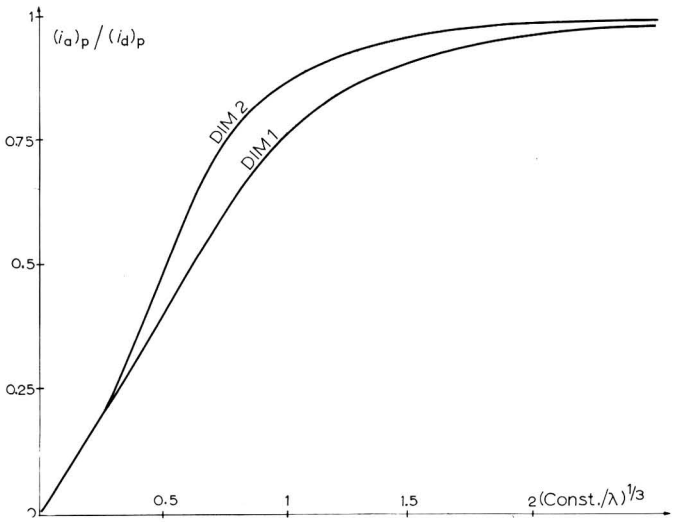

Fig. 7. Asymmetrical potential scan. Peak current ratio as a function of the kinetic parameter $\lambda = kC^0\theta_f$. (θ_f time elapsed in the cathodic stage). DIM 1: const. = 1.0, Dim 2: const. = 0.5.

curve and the potentiostatic current pattern at time θ_f, when initiation of the potential step occurs in the middle of the peak/half-peak interval. The relative error on k has been then deduced and considered to be the same for mixed reaction–diffusion control. These estimations of $\Delta k/k$ are given in Table 3 where they are compared to the experimental uncertainty in k resulting from a 10% error on peak currents ratio. Results in Table 3 show that the errors arising from the above approximations are negligible in practice.

TABLE 3

EVALUATION OF THE SYSTEMATIC ERRORS IN ASYMMETRIC TRIANGULAR SCAN VOLTAMMETRY

Reaction scheme	*Peak current ratio*	*Error due to lack of asymmetry in scan* /%	*Error due to approx. determination of the anodic stage duration* /%	*Total relative error* /%	*Exptl. uncertainty* /%
DIM 1	0.75	+6	−2	4	±45
	0.50	+2.4	−2	0.4	±30
DIM 2	0.75	+6	−4	2	±45
	0.50	+0.7	−4	−3.3	±26

As indicated above, the second wave in double-wave systems can be studied using double-scan techniques in which both parts of the scan are cathodic. The possible forms of such potential scans are presented in Fig. 8, together with the trapezoidal or triangular potential scans studied before. The first part of the scan in the present case may be either a step or a linear sweep. In each case, the second part of the potential scan is much shorter than the first. Under these conditions, the second

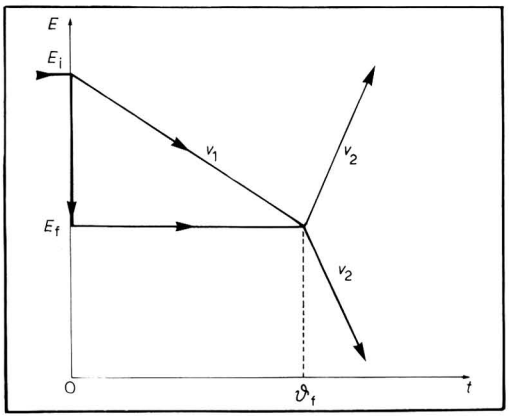

Fig. 8. Various forms of the working electrode potential for double-scan techniques.

cathodic wave and the anodic wave obtained by reversing the potential sweep are complementary. When the cathodic wave increases, the anodic one decreases and *vice versa*. For purely kinetic conditions, *i.e.* for a small anodic wave, the second cathodic peak expression can be derived from the anodic peak expression using the following relation between the adimensional concentrations of monomer and dimer in the electrode plane and at the end of the first part of the scan:

$$(a)_{y=0} + 2d(aa^+)_{y=0} = d^{\frac{1}{2}}$$

For mixed reaction–diffusion control, the trend of variation is the same. The exact expression for the second cathodic wave would require numerical calculations of the same complexity as for the expression of the first wave in cases II and III.

The second anodic wave in single wave systems is exactly the same as the second cathodic wave in the preceding conditions, representing now an oxidation of the dimer A–A.

EFFECT OF OHMIC DROP

The main problem to solve here is the effect of ohmic drop on the single scan polarization curves and particularly on the peak potential. For the double-scan procedures described above, the eventual ohmic drop effect is only on the anodic trace which is a diffusion-controlled wave. Although the effect of ohmic drop can be taken into account knowing the corresponding theoretical behaviour as a function of the uncompensated resistance, it must be noted that experimental conditions involving only a small ohmic drop are to be preferred using compensation devices if necessary. Under these conditions the voltammetric results can be used, after a correction for ohmic drop, to analyse the mechanism and determine the rate constant with good accuracy since the kinetic effect and not the ohmic drop effect governs mainly the shape and characteristics of the polarization patterns. In the case of double-scan procedures the eventual correction to be performed is only on the anodic peak height since the cathodic part of the scan can be set up in such a way that the condition:

$(C_{A^+})_{y=0}=0$ is still fulfilled. The correction on the peak height will thus be quite small and negligible in practice as can be shown using the previously reported results concerning a diffusion-controlled nernstian wave[29,34].

For the cathodic wave corresponding to a simple linear sweep, derivation of the ohmic drop effect is on the same lines as for the cases already treated which concern pure diffusion[22,34] and mixed diffusion–change transfer[35] kinetic control. The treatment is restricted here to chemical reaction pure kinetic control for which the most significant behaviour is to be expected. We introduce the ohmic adimensional parameter:

$$\rho=(F/RT)FSC^0 D_M^{\frac{1}{2}}(Fv/RT)^{\frac{1}{2}}R_u$$

(note the slight difference between ρ and the parameter H in ref. 22: $H=\rho\pi^{\frac{1}{2}}$). R_u is the uncompensated resistance and S is the working electrode surface area, the other symbols have their usual meaning.

For *the single-wave systems*, the adimensional current functions are expressed by the following integral equations:

DIM 1 case:

$$\psi^{\frac{2}{3}}\exp(-\xi_1^+)\exp\rho\psi=1-\frac{1}{\pi^{\frac{1}{2}}}\int_{-u_1^+}^{\xi_1^+}\frac{\psi_{(\eta)}}{(\xi_1^+-\eta)^{\frac{1}{2}}}\,d\eta$$

DIM 2 case:

$$\psi^{\frac{2}{3}}\exp(-\tfrac{2}{3}\xi_2^+)\exp\tfrac{2}{3}\rho\psi=1-\frac{1}{\pi^{\frac{1}{2}}}\int_{-u_2^+}^{\xi_2^+}\frac{\psi_{(\eta)}}{(\xi_2^+-\eta)^{\frac{1}{2}}}\,d\eta$$

The result of computing these equations (for the calculation procedure see appendix C) are presented, together with the corresponding quantity pertaining to the pure diffusion nernstian case, in Fig. 9a (adimensional peak potential shift *vs* parameter ρ), in Fig. 9b (adimensional peak potential shift *vs.* i_pR_u which is the formal ohmic drop corresponding to the observed peak current), in Fig. 9c (which represents the percentage decrease of the peak height *vs.* i_pR_u) and in Fig. 9d (adimensional peak width factor *vs.* i_pR_u).

The peak potential shift is nearly the same for the DIM 1 electrodimerization as for a one-electron pure diffusion-controlled wave (the largest deviation from this identity is about 1 mV for a temperature of 25°C). For DIM 2 the peak potential shift is different although not by a large amount.

The shift of the peak potential starting from a zero value of the resistance parameter ρ is nearly proportional to the formal ohmic drop for the peak current, in the case of DIM 1, DIM 2 as well as for the diffusion wave, and is about 20% larger.

For the percentage decrease of the peak current as well as for the peak width, the behaviour is very similar in the case of DIM 1 and pure diffusion but quite different for DIM 2.

The first wave in *double-wave systems* is affected by ohmic drop in a way that is readily derivable from the preceding results. The integral equations for the single-wave system can be used, as shown above, for the double-wave system by considering that the ψ function in these equations is twice the actual ψ function. It follows that the double-wave system is the same as for the single wave for half the resistance.

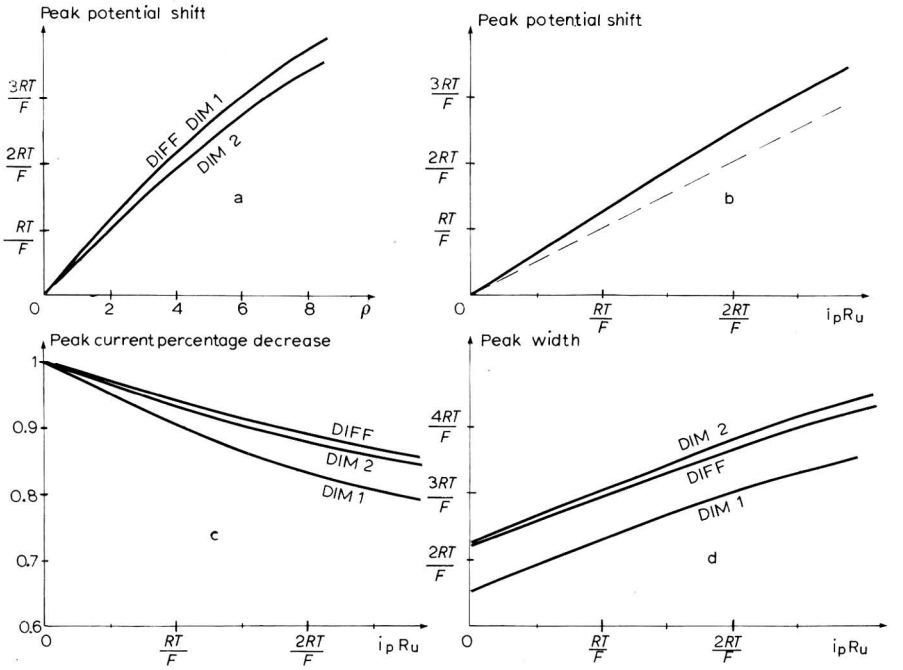

Fig. 9. Effect of ohmic drop on the voltammograms for a simple linear sweep for DIM 1 and DIM 2 electrodimerizations and for pure diffusion control (a) Peak potential shift as a function of the adimensional resistance parameter, (b) peak potential shift as a function of the formal ohmic drop corresponding to the peak current, (c) percentage decrease of the peak current as a function of the formal ohmic drop corresponding to the peak current, (d) peak width as a function of the formal ohmic drop corresponding to the peak current.

PURELY IONIC ELECTRODIMERIZATIONS (DIM 3)

DIM 1 and DIM 2 represent, respectively, purely radical and radical-ionic electrodimerizations. Another possible reaction scheme is the reactions between the product of a two-electron transfer and the reactant itself. With our notation:

$$A^+ + A^- \rightarrow A\text{–}A$$

This kind of purely ionic mechanism (DIM 3) will not be studied in detail here, particularly the thermodynamics of the system and the various possibilities concerning the number of waves. However for a single-wave system corresponding to a DIM 3 reaction scheme, the main features of the polarographic and voltammetric behaviours are readily deducible from the results obtained in the DIM 2 case by considering that two electrons are exchanged instead of one. It is to be emphasized that the *half-wave potential*, for polarography, and the *peak potential* for linear sweep voltammetry *shift by* 14.8 *mV* (at 25°C) *per decade of the initial concentration and sweep rate* (or drop time) instead of 19.7 mV for DIM 1 and 29.6 mV for DIM 2. This variation has already been taken into consideration as a diagnostic criterion in the case of linear sweep voltammetry[36].

DIAGNOSTIC CRITERIA AND RATE CONSTANT DETERMINATION

From the results of the previous analysis, diagnostic criteria and rate constant determination procedures can be summarized as follows:

1. The number of waves exhibited by the polarographic or the linear sweep polarization patterns provides some information on the thermodynamical properties of the dimerizing system:

—if two successive half-electron waves are observed the thermodynamics of the system are characterized either by

$$E_1 \gg E_2, \quad pC \ll pK_1 \ll pK_2$$

or by

$$E_1 \ll E_2, \quad pC \ll 2pK_2 - pK_1$$

—if only one single one-electron wave is observed the system is characterized either by

$$E_1 \ll E_2, \quad pC \ll 2pK_2 - pK_1$$

or by

$$E_1 \ll E_2, \quad 2pK_2 - pK_1 \ll pC \ll pK_2 \ll pK_1$$

This thermodynamical characterization is indeed incomplete since the diffusion rate cannot be varied over a very large range even for linear sweep voltammetry so that scanning the whole kinetic diagram is very unlikely. Complete thermodynamical analysis would involve polarization conditions corresponding to the DE zone and the possibility of varying the initial concentration in a large range in order to determine experimentally the E–pC diagram. Such conditions are very unlikely to occur for the quasi-irreversible dimerization processes as considered here. Nevertheless, even the incomplete characterization derived from the number of waves is of much value.

2. Reversibility of waves obtained with symmetrical triangular potential scan confirms the information gained using the number of waves. Observation of the changes in the degree of reversibility according to sweep rate variations allows the kinetic control by the dimerization process and by the diffusion process to be qualitatively characterized. In the case of the DIM 1–MON 2 mechanism the polarization pattern is featured by an, at least partial, irreversibility of the anodic reoxidation wave. In this case, three linear segments of equal slopes will be used as input signal.

3. Operative distinction between the DIM 1, DIM 2 and DIM 3 reaction schemes is provided by the experimental determination of the peak potentials of the first cathodic wave as a function of the logarithm of the sweep rate. The dimerization reaction has to be fast enough for pure kinetic conditions to be achieved in a sufficient range of sweep rate values. This is not a very big problem in practice since for slower dimerization processes the course of reaction may be followed by homogeneous kinetic techniques checking the decay of the monomer or the appearance of the dimer. A straight line is then drawn through the experimental points using, for instance, a least squares method. Comparison of its slope with the theoretical values: 19.7 mV (DIM 1), 29.6 mV (DIM 2), 14.6 mV (DIM 3) at 25°C allows a distinction to be made between these possible three mechanisms.

The determination of mechanism can be similarly performed through the variation of the peak potential with the initial concentration. Polarography can be also employed in the same manner measuring the variations of the half-wave potential with initial concentration and drop time. However the variation range of these factors hardly exceeds one order of magnitude, leading to a less accurate mechanism determination since four or five orders of magnitude are available for sweep rate with linear sweep voltammetry. In all cases correction for ohmic drop must be performed, especially for high values of sweep rate. The most convenient procedure is to perform this correction using as reference for the uncompensated cell resistance the peak potential measurements obtained with a similar substance which reduces reversibly in the same medium.

Theoretically, the distinction between the DIM 1 and DIM 2 reaction schemes could be performed with a double-scan technique using the different behaviour of the peak currents ratio as a function of the pre-electrolysis duration as shown on Fig. 7. In this way, however, no distinction can be made when purely kinetic conditions are achieved in the first part of the scan. Moreover, even for mixed chemical reaction–diffusion kinetic control, the behaviour corresponding to DIM 1 and DIM 2 are not largely different preventing an unambiguous characterization of the mechanism. Peak potential measurements varying the sweep rate are therefore to be preferred to mechanism analysis.

4. For rate constant determination of the dimerization reaction two different procedures may be applied, one employing peak potential determination as function of the sweep rate with a single linear scan and the other one employing peak currents ratio measurements with a double-scan technique varying the pre-electrolysis duration. For both procedures, the dimerization reaction must not be too fast since on raising the sweep rate, pure diffusion control (zone DO) has to be reached for the determination of the rate constant to be feasible.

—With the first procedure, measurements of peak potential are made, raising the sweep rate until the variation with the logarithm of this last quantity ceases. Pure diffusion conditions are then reached and the normal potential of the monomeric redox system is readily derivable from the peak potential value. Both quantities characterizing the electrodimerizing system, *i.e.* normal potential and dimerization rate constant can then be separated. The abscissa λ_i of intersection of the two linear parts of the peak potential *vs.* $\log \lambda$ diagram does not depend on the normal potential (see Fig. 6). The theoretical values for λ_i are:

$$\lambda_i = 0.8 \text{ for DIM 1} \quad \text{and} \quad \lambda_i = 0.27 \text{ for DIM 2}$$

In other words:

$$k = 0.8\, Fv_i/RTC^0 \text{ for DIM 1} \quad \text{and} \quad k = 0.27\, Fv_i/RTC^0 \text{ for DIM 2}$$

v_i is the value of the sweep rate corresponding to the intersection, v_i is readily measured on the experimental diagram of peak potential *vs.* sweep rate. The value of the rate constant is then calculated using one or the other of the foregoing relations.

—The second procedure is as follows.

A range of sweep rate values, where the reduction is diffusion-controlled, is determined, using as criterion either the independence of the peak potential of the

sweep rate or with a symmetrical triangular scan the equality between the cathodic peak current and the anodic peak current as measured to the extension of the cathodic trace as a base line. A value for the sweep rate of the second part of the scan can thus be selected in this range. Moreover these experiments provide the value of the diffusion-controlled peak current $(i_d)_p$.

The second term of the peak current ratio $(i_a)_p$ is measured for various values of the time elapsed in the first part of the scan. A set of values for the peak currents ratio is thus obtained. Using the theoretical working curves of Fig. 7 a corresponding set of λ values is deduced. For each value of λ the pre-electrolysis time θ and the initial concentration C^0 are known and one value for the rate constant k is thus obtained. A mean value for k is finally calculated from the set of k values. A similar procedure varying the initial concentration can also been applied.

In both procedures rather high sweep rates may be used giving rise to an important double-layer charging current. If adsorption of the reactants can be neglected, the capacitive component will be eliminated by subtracting the curve obtained in a blank experiment performed at the same sweep rate.

It will be shown using an experimental example[33] that the accuracy for the second procedure is better than for the first one as foreseen earlier[14]. The peak potential procedure leads to an accuracy of k of about 50%, whereas the peak current ratio procedure give an accuracy of about 30%. The difference in accuracy between the two methods although significant is not dramatic and is to be paralleled with the greater simplicity of the peak potential procedure. The superiority of cyclic voltammetry over simple linear sweep voltammetry for the study of follow-up chemical reactions must not therefore be considered as a rigid dogma. Moreover, data treatment procedures for linear sweep voltammetry can be improved leading to a better accuracy in mechanism diagnosis and rate constant determination. Possible future trends in this field can be foreseen as follows[37]:

For follow-up reactions the modification of the peak height due to the presence of the reaction is quite inappreciable. This is why the measuring procedure deals with peak potential variations. However, in restricting the observations to peak characteristics all the experimental information available in a single polarization curve is not fully employed even if it is true that measurements of current intensity, for example, are the most accurate in the peak region. Measurement of the peak width factor in addition to peak potential and/or peak current would increase the information gained but also the tedium in handling data. One can even think of using the entire polarization curve by comparing it to its formal model for all the attainable values of the experimental parameters *i.e.* mainly sweep rate, initial concentration and acidity of the medium (pH). Using manual procedures, handling of data then rapidly becomes a formidable problem. These difficulties can be overcome by converting the output analogue signal in a digital form. Apart from the accuracy improvement resulting from an easy application of time-averaging techniques, digitalization of the polarization curves allows mathematical transformations of the experimental data to be performed conveniently on computers. Consequently, the comparison of the experimental system with the model can be performed automatically. Use of all the information contained in the polarization curve can thus be faced reasonably in these conditions. These considerations apply not only for electrodimerization problems but for all mechanistic analysis as performed using linear sweep voltammetry. Among the

mathematical transformations to be performed on the digitalized current–potential curves, it seems particularly interesting to calculate the convolution integrals corresponding to the diffusion process. Experimental quantities proportional to the values of the reactant concentrations at the electrode surface are obtained in this way. If it is born in mind that pure chemical reaction kinetic control or pure diffusion control are the most common situations to be met in practice (*i.e.* mixed chemical reaction–diffusion control occurs in very restricted ranges of experimental parameter values, see for example zone KO on Fig. 2) it appears that the theoretical relations between the concentrations of the reactants at the electrode surface are mathematically simple. The comparison of the transformed experimental data with the model may thus be satisfactorily effected at this stage automatically. Application of such a procedure for data processing would cancel a severe limitation in the use of linear sweep voltammetry for the study of charge transfer kinetics, *i.e.* the necessity of knowing *a priori* the form of the kinetic law in order to make the model mathematically explicit and then to compare it to the experimental data. Automatic computation of the convolution integrals would thus allow the form of the kinetic law to be established as a result of experiment and data processing. In other words, Tafel lines corresponding to various values of sweep rate could be drawn in this way.

Turning back to electrodimerization, maximal values of the dimerization rate constant measurable by the above-mentioned procedures can be evaluated as follows. For the peak potential procedure, the minimal value of λ that must be reached in order for the rate constant to be determined is the limiting value which defines the separation between zone KO and zone DO.

However, selecting these values to get an estimation of the greatest rate constant attainable would lead to very inaccurate determination in the range of high rate constant since too little space is available in order to verify the constancy of the peak potential *vs.* sweep rate and to determine a reasonably accurate value for it. It can be estimated that the minimal value for λ has to be distant by about 1 in logarithmic scale from the intersection of the linear part of the diagram (Fig. 6) in order for a reasonably accurate measurement of the rate constant to be performed. The minimal λ values are therefore:

0.08 for DIM 1 and 0.03 for DIM 2

The greatest values of sweep rate attainable in the present state of instrumentation and data handling procedures is about 5 kV s^{-1}. Thus the greatest values of the dimerization rate constant that are to be expected at the present time are of the order of magnitude of:

1.5×10^7 mol^{-1} l s^{-1} for DIM 1 and 0.5×10^7 mol^{-1} l s^{-1} for DIM 2

at 25°C for a depolarizer concentration of 10^{-3} *M*.

For the peak currents ratio method the same orders of magnitude are to be expected. In practice, slightly lower values of rate constants are however attainable which correspond to the fact that for the same values of sweep rate a little more time elapses in the double-scan technique than in the single-scan one.

ACKNOWLEDGEMENT

The work was supported in part by the CNRS (Laboratoire associé no. 32, mécanismes reactionnels). Numerical calculations were performed on the CDC 3600 digital computer of the Blaise Pascal Institute (CNRS, Paris, France).

SUMMARY

Formal kinetics for an irreversible dimerization reaction coupled with a nernstian charge transfer process is analysed under conditions of linear and semi-infinite diffusion. It is shown that three kinds of dimerization reaction schemes must be considered: purely radical, radical ionic and purely ionic. Diagnostic criteria permitting the distinction between these reaction paths are presented for polarography, single-scan sweep voltammetry and symmetrical triangular sweep voltammetry. Procedures for the determination of the dimerization rate constant are described, using either peak potential measurements with a single linear potential scan or an anodic to cathodic peak currents ratio technique with a double-scan polarization. Both methods are compared as to accuracy and maximal rate constants attainable. The effect of ohmic drop is studied and correction procedures are suggested.

APPENDIX A

DIM 2–single wave systems: derivation of the current function for linear sweep voltammetry

The polarization problem (non-dimensional formulation) is as follows:

$$\frac{\partial a^+}{\partial \mathrm{T}} = \frac{\partial^2 a^+}{\partial y^2} - \lambda a a^+ \tag{A1}$$

$$0 = \frac{\partial^2 a}{\partial y^2} - \lambda a a^+ \tag{A2}$$

$$\frac{\partial a a^+}{\partial \mathrm{T}} = d\frac{\partial^2 a a^+}{\partial y^2} + \lambda a a^+ \tag{A3}$$

$\mathrm{T} = 0, y \geqq 0 \quad a^+ = 1; \quad a = a a^+ = 0$

$y = \infty, \mathrm{T} \geqq 0 \quad$ idem

$$y = 0, \mathrm{T} \geqq 0 \quad a^+ = a \exp(F/RT)(E - E_1) \tag{A4}$$

$$\frac{\partial a^+}{\partial y} + \frac{\partial a}{\partial y} = 0 \tag{A5}$$

$$a a^+ = 0$$

The quantity to be calculated is

$\psi = \psi_1 + d\psi_2$, ψ_1 and ψ_2

being defined by:

$$\psi_1 = \left(\frac{\partial a^+}{\partial y}\right)_{y=0} = -\left(\frac{\partial a}{\partial y}\right)_{y=0}; \quad \psi_2 = \left(\frac{\partial a a^+}{\partial y}\right)_{y=0}$$

The second partial derivative eqn. (2) can be integrated by noting that, $a^+ + a$ is a constant throughout the reaction layer:

$$a^+ + a = a^+_{y=0} + a_{y=0}$$

λ has been assumed to be very large so that $a_{y=0}$ is negligible in comparison to $a^+_{y=0}$. Thus,

$$\psi_1^2 = \lambda a^2_{y=0} a^+_{y=0} \tag{A6}$$

The following linear combination of (2) and (3):

$$\frac{\partial(aa^+ + a/d)}{\partial \mathrm{T}} = d\,\frac{\partial^2(aa^+ + a/d)}{\partial y^2}$$

leads, after integration in the Laplace space to:

$$\overline{aa}^+_{y=0} + \frac{1}{d}\bar{a}_{y=0} + \frac{\sqrt{d}}{\sqrt{s}}\left(\bar{\psi}_2 - \frac{\bar{\psi}_1}{d}\right) = 0 \tag{A7}$$

Taking (5) into account as well as the smallness of a_0 we obtain:

$$\psi_1 = d\psi_2$$

and then

$$\psi = 2\psi_1 \tag{A8}$$

By subtracting (A2) from (A1) and integrating it follows that:

$$\bar{a}^+_{y=0} + 2\frac{\bar{\psi}_1}{\sqrt{s}} - \frac{1}{s} = 0 \tag{A9}$$

In linear potential sweep conditions, the dimensionless potential and time scale is cenveniently defined by:

$$\xi = -(F/RT)(E - E_1) = (F/RT)vt - u$$

where

$$u = (F/RT)(E_i - E_1)$$

Then eqn. (A9) becomes in the original space:

$$a^+_{y=0} = 1 - \frac{2}{\pi^{\frac{1}{2}}}\int_{-u}^{\xi} \frac{\psi_1(\eta)}{(\xi - \eta)^{\frac{1}{2}}}\,\mathrm{d}\eta$$

Equation (A6) leads to:

$$a^+_{y=0} = \psi_1^{\frac{2}{3}} \exp(-\tfrac{2}{3}\xi)\lambda^{-\frac{1}{3}} \tag{A10}$$

Thus:

$$\psi_1^{\frac{2}{3}} \exp(-\tfrac{2}{3}\xi)\lambda^{-\frac{1}{3}} = 1 - \frac{2}{\pi^{\frac{1}{2}}}\int_{-u}^{\xi} \frac{\psi_1(\eta)}{(\xi - \eta)^{\frac{1}{2}}}\,\mathrm{d}\eta \tag{A11}$$

Considering (18) and introducing

$$\xi_2^+ = \xi + \tfrac{1}{2}\ln\lambda + \ln 2 \tag{A12}$$

$$u_2^+ = u - \tfrac{1}{2}\ln\lambda - \ln 2 \tag{A13}$$

the integral equation becomes:

$$\psi^{\frac{2}{3}} \exp(-\tfrac{2}{3}\xi_2^+) = 1 - \frac{1}{\pi^{\frac{1}{2}}} \int_{-u_2^+}^{\xi_2^+} \frac{\psi\ (\eta)}{(\xi_2^+ - \eta)} \, d\eta \tag{A14}$$

Changing the ξ scale and the ψ scale through:

$$\xi' = \tfrac{2}{3}\xi_2^+ - \tfrac{1}{3} \ln \tfrac{2}{3} \tag{A15}$$

$$u' = \tfrac{2}{3}u_2^+ + \tfrac{1}{3} \ln \tfrac{2}{3}$$

$$\psi' = \tfrac{3}{2}\psi \tag{A16}$$

the integral equation becomes:

$$\psi'^{\frac{2}{3}} \exp(-\xi) = 1 - \frac{1}{\pi^{\frac{1}{2}}} \int_{-u'}^{\xi'} \frac{\psi'(\eta)}{(\xi' - \eta)^{\frac{1}{2}}} \, d\eta \tag{A17}$$

i.e. the expression corresponding to the DIM 1 case. Thus, using (A15) and (A16) the peak characteristics for the DIM 2 case can be deduced without any further calculation:

$$\psi_1 = 0.430; \quad \xi_{p,2}^+ = 1.15; \quad \xi_{p,2}^+ - \xi_{p/2,2}^+ = 2.27$$

APPENDIX B

For *case III* (double-wave system–DIM 1 reaction scheme) the adimensional formulation of the polarization problem is given in Table 2. Since pure kinetic conditions are assumed to be achieved, eqn. (7) can be simplified:

$$0 = \frac{\partial^2 a}{\partial y^2} - \lambda a^2 \tag{B1}$$

and then

$$\psi_1^2 = \tfrac{2}{3}\lambda (a)_{y=0}^3 \tag{B2}$$

In the *first wave* region

$$(aa)_{y=0} = 0 \tag{B3}$$

By linear combination of (B1) and (9) and integration in the Laplace space (the symbol $\bar{}$ designates the Laplace transform function and s is the Laplace variable) it follows that:

$$(\bar{a})_{y=0} + 2d(\overline{aa})_{y=0} - \frac{d^{\frac{1}{2}}}{s^{\frac{1}{2}}} (\bar{\psi}_1 + 2d\bar{\psi}_2) = 0 \tag{B4}$$

since λ is very large, $(a)_{y=0}$ is small (eqn. (B2)) and the first two terms in eqn. (B4) can be neglected. Thus the total current function becomes

$$\psi = \psi_1 + d\psi_2 = \tfrac{1}{2}\psi_1$$

The expression of ψ_1 as a function of ξ_1^+:

$$\xi_1^+ = \xi + \tfrac{1}{3} \ln \tfrac{2}{3}\lambda$$

is the same as in case I. Thus the adimensional expression of the polarization curves is

exactly half the expression corresponding to case I.

In the *second wave* region, the extension of the first wave is expressed by

$$1/2(\pi T)^{\frac{1}{2}}$$

Thus considering the second wave to the extension of the first one as a base line, the expression to be calculated is:

$$\psi' = \psi - 1/2(\pi T)^{\frac{1}{2}} = \psi_1 + d\psi_2 - 1/2(\pi T)^{\frac{1}{2}}$$

the second wave being assumed very distant from the first one, in the second wave region:

$$\psi_1 = 1/(\pi T)^{\frac{1}{2}} \tag{B5}$$

and thus

$$\psi' = d\psi_2 + 1/2(\pi T)^{\frac{1}{2}} \tag{B6}$$

On the other hand, neglecting $(\bar{a})_{y=0}$ in eqn. (B4) but not $(\overline{aa})_{y=0}$ and turning back into the original space taking due account of (B5) we obtain:

$$aa_0 = \frac{1}{2d^{\frac{1}{2}}} + \int_0^T \frac{d\psi_2}{(T-\tau)^{\frac{1}{2}}} d\tau \tag{B7}$$

Integration of eqn. (8) taking (17) into account leads to

$$aa_0 = \frac{1}{d^{\frac{1}{2}}} \frac{\exp -(F/RT)(E-E_2)}{\pi^{\frac{1}{2}}} \int_0^T \frac{d\psi_2}{(T-\tau)^{\frac{1}{2}}} d\tau \tag{B8}$$

From (B6), (B7) and (B8) it follows that

$$\frac{1}{\pi^{\frac{1}{2}}} \int_0^T \frac{\psi'(\tau)}{(T-\tau)^{\frac{1}{2}}} d\tau = \tfrac{1}{2} \frac{1}{1+\exp(F/RT)(E-E_2)} \tag{B9}$$

Defining a new adimensional potential scale:

$$\xi_2 = -(F/RT)(E-E_2); \quad u_2 = (F/RT)(E_i - E_2) \tag{B10}$$

and considering u_2 as infinite

$$\psi'(\xi_2) = \tfrac{1}{2}\psi_d(\xi_2) \tag{B11}$$

where ψ_d is the usual expression of a purely diffusion-controlled nernstian wave. Thus:

$$\psi'_p = 0.223; \quad \xi_{p,2} = 1.11; \quad \xi_{p,2} - \xi_{p/2,2} = 2.20 \tag{B12}$$

For *case IV* (double-wave system–DIM 2 reaction scheme) the resolution of the polarization problem follows the same lines as in appendix A for the single-wave system

In the *first wave* region:

$$(aa)_{y=0} = 0 \tag{B13}$$

Thus integrating eqn. (13) (Table 2):

$$\psi_2 = 0$$

and then

$$\psi = \psi_1 \tag{B14}$$

The derivation leading to eqn. (A11) for the single-wave system is still valid. Then, taking (B14) into account it follows that:

$$\psi^{\frac{2}{3}} \exp\left(-\tfrac{2}{3}\xi\right)\lambda^{-\frac{1}{3}} = 1 - \frac{2}{\pi^{\frac{1}{2}}}\int_{-u}^{\xi} \frac{\psi(\eta)}{(\xi-\eta)^{\frac{1}{2}}}\,\mathrm{d}\eta \tag{B15}$$

With the same scale definition as in case II (eqns. (A12), (A13)):

$$(2\psi)^{\frac{2}{3}} \exp\left(-\tfrac{2}{3}\xi_2^+\right) = 1 - \frac{1}{\pi^{\frac{1}{2}}}\int_{-u_2^+}^{\xi_2^+} \frac{2\psi(\eta)}{(\xi_2^+-\eta)^{\frac{1}{2}}}\,\mathrm{d}\eta \tag{B16}$$

Comparison between (A14) and (B16) shows that the adimensional expression of the wave is now exactly the half the expression corresponding to the single-wave system. Thus

$$\psi_p = 0.215; \quad \xi_{p,2}^+ = 1.15; \quad \xi_{p,2}^+ - \xi_{p/2,2}^+ = 2.27$$

For the second wave the result and its proof are the same as in the DIM 1 case.

APPENDIX C

Procedures for numerical calculations

1. For purely kinetic conditions, the polarization problem can be reduced to a boundary value formulation which involves the solving of an integral equation. In the present case these integral equations are not linear. The calculation procedure is based on the transformation of the integrals in series by dividing the integration interval in elementary intervals of equal length. For this transformation we used rectangles positioned at the midpoint of the interval according to the method of Matsuda and Ayabe[18] originally devised for similar calculations. More refined procedures may be used[38] which allow the saving of some computer time for a given accuracy. Since this type of calculation does not require much computer time, such an optimization, although useful, is not strictly necessary. For this reason and owing to the simplicity of the rectangle method we continued to use it. When the above transformation has been effected the value of the adimensional current function ψ for a given value of the potential variable ξ is the solution of a non-linear algebraic equation of the form:

$$\psi^{\frac{2}{3}} + A\psi = B$$

where B depends on the previously computed values of the ψ function. These equations have been resolved by the "chord" iteration method, noting that the solution sought is unique in the interval 0–B/A, so that these quantities can be taken as starting values for the iteration. The principle of the "chord" iteration method is recalled in Fig. 10 for the resolution of an equation of the type:

$$F(\psi) = 0$$

ψ_1 and ψ_2 are two values of ψ selected in such a way that only one solution of the equation is comprised between ψ_1 and ψ_2. In these conditions an elementary interval

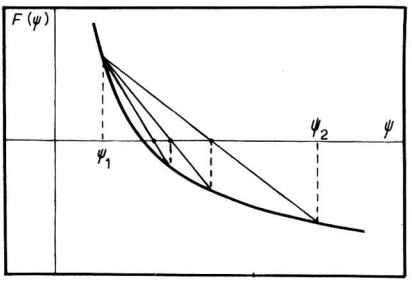

Fig. 10. The "chord iteration method".

of 0.1 leads to an accuracy of about 0.2% for the ψ function.

2. In the case of a single-wave system and a DIM 1 reaction scheme, application of the finite difference method of Crank–Nicholson is particularly simple since ψ_2 is equal to zero, only the partial derivative equation corresponding to a has to be solved by this technique. The boundary condition on the electrode surface is:

$$(a)_{y=0} \exp(-\xi) = 1 - \frac{1}{\pi^{\frac{1}{2}}} \int_{-u}^{\xi} \frac{\psi_1(\eta)}{(\xi-\eta)^{\frac{1}{2}}} \, d\eta$$

This integral equation is transformed into an algebraic equation relating the values of the function a on the electrode surface, at the first space interval and at the second one for each value of the time variable ξ. The partial derivative equation to be solved is linearized by replacing the term a^2 by the product of the a values corresponding to the ξ value for which the calculation is performed and to the immediately preceding ξ value. This is exactly the same procedure we have already used for the numerical analysis of the disproportionation reaction scheme[1]. The accuracy and stability of the numerical calculation depends on three factors: the length of the elementary interval for the time variable ξ, the adimensional distance δ from the electrode for which the boundary condition for $y=\infty$, *i.e.* $a=0$, can be considered as fulfilled and, finally, the number N of elementary intervals in which the length δ is divided. The elementary interval F for the space variable y is then defined by:

$$F = \delta/N$$

The procedure for selecting the value of δ has been as follows: δ is considered as m times the "reaction-diffusion layer". Let μ be defined by the distance from the electrode where the concentration gradient of a meets the space coordinate axis (see Fig. 11), then

$$\delta = m\mu$$

The value of μ is, of course, unknown in the range of λ values for which the calculation is performed, *i.e.* for mixed reaction–diffusion control, but is readily calculable for pure diffusion control as well as for purely kinetic conditions:

$$\mu_{diff} = \pi^{\frac{1}{2}}(\xi+u)^{\frac{1}{2}} \; ; \quad \mu_{kin} = \pi^{\frac{1}{6}}(\xi+u)^{\frac{1}{6}}(\tfrac{2}{3}\lambda)^{-\frac{1}{3}}$$

when considering ξ values close to the end of the polarization curve. This estimation of both concentration layers is also approximately valid for all the ψ values that differ significantly from zero. The value of μ as a function of the kinetic parameter has the

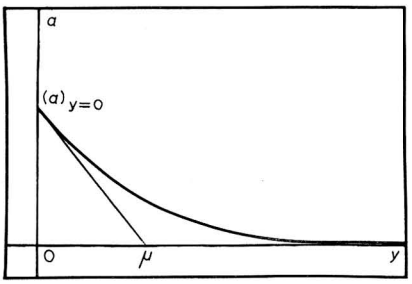

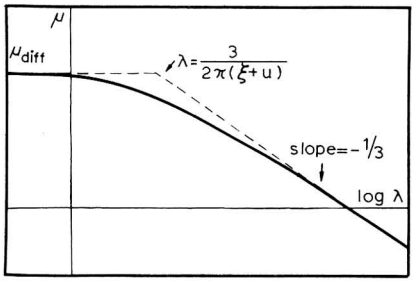

Fig. 11. Concn. profile of the species A and definition of the "reaction-diffusion" layer thickness μ.

Fig. 12. "Reaction-diffusion" layer thickness μ as a function of the kinetic parameter λ.

general form shown on Fig. 12, for which only the asymptotes are precisely known. These asymptotes meet each other when $\lambda = 3/2\pi(\xi+u)$. The value of μ in the calculation zone is then approximated as follows:

—if $\lambda < 3/2\pi(\xi+u)$, then $\mu = \mu_{\text{diff}}$
—if $\lambda > 3/2\pi(\xi+u)$, then $\mu = \mu_{\text{kin}}$

The value of $\xi+u$ has been chosen equal to 30 which represents the entire range of time values scanned, in order to get a good definition of the peak characteristics. The calculation then depends on the parameters h, m and N. Tests have been made for various values of these parameters and have shown that the values $h=0.1$, $m=5$ and $N=300$ lead to an accuracy of about 0.2% on the ψ function in a region of λ where the ψ values differ significantly from 0.

3. For a double-wave system and a DIM 2 reaction scheme, the application of the Crank–Nicholson method is still rather simple since $\psi_2 = 0$. The partial derivative equations concerning the monomeric forms are thus the only ones to be treated by the finite difference approach. The problem is nevertheless more complicated as in the preceding case since two equations instead of one are involved in this procedure. One could have thought to calculate the difference $a^+ - a$ as solution of the equation:

$$\frac{\partial(a^+ - a)}{\partial \mathrm{T}} = \frac{\partial^2(a^+ - a)}{\partial y^2}$$

(difference between eqn. (10) and eqn. (11)), which is the simple equation of diffusion, and to solve eqn. (11) by the finite difference method using values of $a^+ - a$ for each point of the network T–y.

The mathematical expression of this difference is

$$a^+ - a = 1 - 2\pi^{-\frac{1}{2}} \int_{-u}^{\xi} \psi_1(\eta) \exp[-y^2/4(\xi-\eta)](\xi-\eta)^{-\frac{1}{2}} \, \mathrm{d}\eta$$

Two reasons render this approach unworkable: (i) the number of convolution integrals to be solved numerically is extremely large and equal to the number of points on the T–y network, *i.e.* about 10,000. (ii) Each convolution integral depends on ψ_1 and then on the first three values of a on each horizontal line, complicating the resolution of eqn. (11) after the substitution of a^+ by its expression as function of a. The procedure we chose was thus a double application of the Crank–Nicholson

method, to eqn. (10) as well as to eqn. (11). In these conditions, on each horizontal line of the T–y network, the partial derivative equations are replaced by a set of linear algebraic equations since linearization can be performed by replacing in the product $a^+ \cdot a$, a^+ by its value for the line under consideration and a by its value for the preceding line, in eqn. (10), and performing the inverted operation for eqn. (11). The set of linear equations corresponding to one partial derivative equation is independent from the other except for the boundary conditions on the electrode surface:

$$a^+ = a \exp(-\xi) \; ; \quad \frac{\partial a^+}{\partial y} + \frac{\partial a}{\partial y} = 0$$

which lead to two linear relations between the first three values of a^+ and a. From this fact derives the necessity of using a unique matrix for the coefficients of the entire set of linear equations. This matrix has been worked out by using a Gaussian-like procedure.

For the determination of the reaction-diffusion layer thickness and then the range of y values inside which the finite difference calculation has to be performed, a procedure similar to the preceding case has been employed. The results are the following:

—if $\lambda < 6/\pi(\xi + u)$, then $\mu = \mu_{\text{diff}}$

—if $\lambda > 6/\pi(\xi + u)$, then $\mu = \mu_{\text{kin}} = 2 \cdot (\frac{3}{4})^{\frac{1}{3}} \pi^{\frac{1}{6}} (\xi + u)^{\frac{1}{6}} \lambda^{-\frac{1}{3}}$

A slight modification has however been introduced owing to the fact that the distance from the electrode where a is nearly zero, which defines the reaction-diffusion layer, can be, according to the values of λ, quite different from the distance where a^+ is nearly equal to 1. This difficulty has been overcome by considering that, at the external boundary of the reaction diffusion layer, a^+ is not equal to 1 and that the boundary condition to be used instead is:

$$a_\mu^+ = 1 - \frac{1}{\pi^{\frac{1}{2}}} \int_{-\mu}^{\xi} \left(\frac{\partial a^+}{\partial \eta}\right)_\mu \frac{\mathrm{d}\eta}{(\xi - \eta)^{\frac{1}{2}}}$$

where the subscript μ indicates that the functions are considered for $y = \mu$. This condition expresses that the dimerization reaction no longer influences the distribution of the a^+ concentrations on the external side of the reaction-diffusion layer corresponding to a.

Performing the finite difference calculation along these lines, instability and lack of accuracy are nevertheless encountered for large values of λ, before the purely kinetic conditions are reached. In order to avoid the finite difference calculation in this range of λ values it has been shown that "quasi"-pure kinetic conditions prevail in this region. As shown in appendix A, the purely kinetic conditions are featured by (i) the constancy of a ($\partial a/\partial \mathrm{T} = 0$), (ii) the relation $a^+ + a = a^+_{y=0} + a_{y=0}$, (iii) the assumption that a is negligible in comparison to a^+ even at the electrode surface. The "quasi"-pure kinetic conditions are the same except for the third one. Then integration of eqn. (A1) leads to:

$$\psi_1^2 = \lambda a_{y=0}^2 (\tfrac{1}{3} a_{y=0} + a^+_{y=0})$$

and thus

$$a_{y=0} = \psi_1^{\frac{3}{2}} / \lambda^{\frac{1}{2}} [\exp(-\xi) + \tfrac{1}{3}]^{\frac{1}{2}}$$

On the other hand, integrating the partial derivative equations obtained by difference of eqns. (A1) and (A2) gives:

$$a^{+}_{y=0} - a_{y=0} = 1 - \frac{2}{\pi^{\frac{1}{2}}} \int_{-u}^{\xi} \frac{\psi_1(\eta)}{(\xi-\eta)^{\frac{1}{2}}} \, d\eta$$

and thus:

$$a_{y=0}[\exp(-\xi)-1] = 1 - \frac{2}{\pi^{\frac{1}{2}}} \int_{-u}^{\xi} \frac{\psi_1(\eta)}{(\xi-\eta)^{\frac{1}{2}}} \, d\eta$$

The current function ψ_1 is thus solution of the following integral equation:

$$\frac{\psi_1^{\frac{2}{3}}}{\lambda^{\frac{1}{3}}} \frac{\exp(-\xi)-1}{[\exp(-\xi)+\frac{1}{3}]^{\frac{1}{3}}} = 1 - \frac{2}{\pi^{\frac{1}{2}}} \int_{-u}^{\xi} \frac{\psi_1(\eta)}{(\xi-\eta)^{\frac{1}{2}}} \, d\eta$$

This equation is then solved numerically according to the procedure described in the first section of this appendix, either on the form given above or on the form obtained after the transformation of the ξ scale defined in appendix A (A 12, A13).

The results of this calculation are in agreement with the results corresponding to purely kinetic conditions, for large values of λ and to those obtained by the finite difference method, for smaller values of λ.

The finite difference approach has been used for $\lambda < 100$. For the range of λ values comprised between this limit and the pure diffusion conditions the number N of elementary intervals on the y-scale has been varied from 300 to 2000, according to the increase of λ.

4. In the case of the single–wave system and the DIM 2 reaction scheme the procedure for calculating ψ_1 is exactly the same as above, but now ψ_2 also has to be calculated. As shown in the text this last calculation requires another application of the Crank–Nicholson method since the diffusion coefficients of the monomeric and dimeric forms cannot be considered as equal. The partial derivative equation to be numerically solved by the finite difference method is eqn. (12) (Table 2). The numerical resolution of eqn. (12) must follow the combined resolution of eqns. (10 and (11) since the values of a^{+} and a have to be introduced in the kinetic term of (12) for each point of the T–y network. The boundary condition on the electrode surface for the finite difference resolution of eqn. (12) is $(aa^{+})_{y=0} = 0$.

5. For the double-wave system with a DIM 1 reaction scheme the calculation procedure for the first wave is two-fold. The calculation of ψ_1 is exactly the same as in section 1 of the present Appendix. The calculation of ψ_2 is on the same lines as in section 4, *i.e.* eqn. (9) is solved by the finite difference method after the resolution of (7) taking into account the boundary condition $(aa)_{y=0} = 0$. However for large values of λ, the reaction-diffusion layers corresponding to a and to aa become quite different leading to erroneous results if the technique described above (implying the consideration of only one reaction-diffusion layer) is still used. To overcome this difficulty without employing a double reaction-diffusion layer technique, the following assumption has been made. For large values of λ, it can be stated that the concentration of a is stationary in the linear combination $a + 2d\,aa$, even if λ is not yet large enough for considering this condition to be fulfilled in the resolution of the partial derivative equation relative to a (eqn. 7). In these conditions, ψ_2 can be deduced

from ψ_1, knowing $(a)_{y=0}$ for each value of ξ through the following integral relation:

$$(a)_{y=0} = \frac{d^{\frac{1}{2}}}{\pi^{\frac{1}{2}}} \int_{-u}^{\xi} (\psi_1 + d\psi_2)(\xi - \eta)^{-\frac{1}{2}} d\eta$$

The results of the numerical calculation are evidence that this assumption is valid since they are in accordance with both those obtained for the purely kinetic conditions and those obtained by the Crank–Nicholson method.

6. The preceding calculations provide not only the values of the function for the various cases but also the value of the *a* concentration at the electrode surface for the end of the linear scan. The working curves for the double-scan techniques are thus obtained together with the results pertaining to single linear scan.

REFERENCES

1 M. MASTRAGOSTINO, L. NADJO AND J. M. SAVÉANT, *Electrochim. Acta*, 13 (1968) 721.
2 M. M. BAIZER, *J. Electrochem. Soc.*, 111 (1964) 215.
3 M. M. BAIZER, *J. Org. Chem.*, 29 (1964) 1670.
4 J. P. PETROVICH, J. D. ANDERSON AND M. M. BAIZER, *J. Org. Chem.*, 31 (1966) 3897.
5 M. D. HAWLEY AND S. W. FELDBERG, *J. Phys. Chem.*, 70 (1968) 3459.
6 S. W. FELDBERG, *J. Phys. Chem.*, 73 (1969) 1238.
7 J. KUTA AND I. SMOLER in P. ZUMAN AND I. M. KOLTHOFF (Eds.), *Progress in Polarography*, Interscience, New York, 1962, p. 43.
8 J. M. SAVÉANT, *Electrochim. Acta*, 12 (1967) 999.
9 J. M. SAVÉANT AND E. VIANELLO, *Electrochim. Acta*, 8 (1963) 905.
10 J. M. SAVÉANT, *Bull. Soc. Chim. France*, (1967) 471.
11 C. P. ANDRIEUX AND J. M. SAVÉANT, unpublished results.
12 J. KOUTECKY AND J. KORYTA, *Electrochim. Acta*, 3 (1961) 318.
13 R. BRIDCKA, V. HANUS AND J. KOUTECKY, in P. ZUMAN AND I. M. KOLTHOFF (Eds.), *Progress in Polarography*, Interscience, New York, 1962, p. 145.
14 J. M. SAVÉANT AND E. VIANELLO, *Compt. Rend.*, 256 (1963) 2597.
15 J. E. B. RANDLES, *Trans. Faraday Soc.*, 44 (1948) 322.
16 A. SEVCIK, *Collection Czech. Chem. Commun.*, 13 (1948) 349.
17 P. DELAHAY, *New Instrumental Methods in Electrochemistry*, Interscience, New York, 1954, pp. 119–120.
18 H. MATSUDA AND Y. AYABE, *Z. Elektrochem.*, 59 (1955) 494.
19 J. M. SAVÉANT AND E. VIANELLO, *Electrochim. Acta*, 12 (1967) 1545.
20 M. S. SHUMAN, *Anal. Chem.*, 41 (1969) 142.
21 J. M. SAVÉANT AND E. VIANELLO, *Electrochim. Acta*, 12 (1967) 629.
22 R. S. NICHOLSON, *Anal. Chem.*, 37 (1965) 667.
23 J. KOUTECKY AND V. HANUS, *Collection Czech. Chem. Commun.*, 20 (1955) 124.
24 S. G. MAIRANOVSKII, *Izv. Akad. Nauk SSSR, Otd. Khim. Nauk*, (1961) 2140.
25 J. CIZEK, J. KORYTA AND J. KOUTECKY, *Collection Czech. Chem. Commun.*, 24 (1959) 663.
26 G. L. BOOMAN AND D. T. PENCE, *Anal. Chem.*, 37 (1965) 1366.
27 D. T. PENCE, J. R. DELMASTRO AND G. L. BOOMAN, *Anal. Chem.*, 41 (1969) 737.
28 M. L. OLMSTEAD, R. G. HAMILTON AND R. S. NICHOLSON, *Anal. Chem.*, 41 (1969) 260.
29 I. M. KOLTHOFF AND J. J. LINGANE, *Polarography*, Interscience, New York, 1951, p. 57.
30 J. M. SAVÉANT, *Electrochim. Acta*, 12 (1967) 753.
31 J. M. SAVÉANT, *Bull. Soc. Chim. France*, (1967) 486, 493.
32 L. NADJO AND J. M. SAVÉANT, submitted.
33 C. P. ANDRIEUX AND J. M. SAVÉANT, in press.
34 W. T. DE VRIES AND E. VAN DALEN, *J. Electroanal. Chem.*, 10 (1965) 183.
35 S. ROFFIA AND M. LAVACHIELLI, *J. Electroanal. Chem.*, 22 (1969) 117.
36 A. M. KHOPIN AND S. I. ZHDANOV, *Electrokhimiya*, 4 (1968) 228 *English Transl.: Soviet Electrochem.*, 4 (1968) 200.
37 J. M. SAVÉANT, unpublished results.
38 M. L. OLMSTEAD AND R. S. NICHOLSON, *J. Electroanal. Chem.*, 16 (1968) 145.

Elsevier Sequoia S.A., Lausanne – Printed in The Netherlands

BOOK REVIEW

Electroanalytical Chemistry, Vol. 3, edited by Allen J. Bard, Marcel Dekker Inc., New York, 1969, xii + 311 pages, $15.75.

As the editor remarks in his preface, this series is designed to cover "modern electroanalytical chemistry in its broadest sense". As such the series takes its place beside the longer established *Modern Aspects* and *Advances* in covering the field which more or less coincides with that of this Journal. The other series have been established longer but *Electroanalytical Chemistry* shows signs of outstripping them. This volume like its predecessors has four articles and contains the titles for 10 future articles which suggests that the (almost) annual rate will be maintained.

If the four articles in the current volume have anything in common it is in the emphasis on techniques, which is the bias one might expect from the title of the series. The first and last articles (*Application of Controlled-Current Coulometry to Reaction Kinetics* by J. Janata and H. B. Mark Jr.; *Digital Simulation: A General Method for Solving Electrochemical Diffusion-Kinetic Problems* by S. W. Feldberg) are strongly oriented towards computers. Janata and Mark spend 20 of their 55 pages on the application of analog computers to the solution of rate equations, while Feldberg's chapter is of course entirely about the use of digital computers. Both of these are useful techniques and are clearly described (though some knowledge of Fortran is necessary to read Feldberg's article). The articles provide useful introductions so that anyone having a problem which might be soluble using these techniques could easily learn to use them.

The third article by N. A. Balashova and V. E. Kazarinov (*Use of the Radioactive-Tracer Method for the Investigation of the Electric Double Layer Structure*) is also nominally about a technique, but the description of experimental methods is rather brief and there are few practical details. The great value of this article is that it summarizes recent Soviet work on adsorption of ions or solid metals (particularly platinum) by this technique and discusses its implications. Work by other schools is mentioned but not discussed in detail. It is not always easy reading and although there are many diagrams of results given, some of the qualitative statements in the text would be helped by illustrations.

The second article (*Nonaqueous Solvents for Electrochemical Use* by C. K. Mann) is an attempt to survey an enormous field in the space of 75 pages. 38 solvents are discussed in terms of four properties: (a) Supporting electrolytes; (b) Reference electrodes; (c) Accessible potential range; (d) Solvent purification. There is also a table giving ten other properties. Inevitably such an article cannot be comprehensive —omissions noted include: the use of the Ag/AgCl electrode in formamide and in methanol (perhaps the excellent review of amide solvents (Reid and Vincent, this Journal 18 (1968) 427) appeared too recently for inclusion). Nevertheless such a survey serves a useful purpose for the electrochemist (or electroanalytical chemist) looking

for a solvent suitable to carry out a particular process. The many references will lead him on to further information.

In conclusion, this volume carries on the series in a worthy manner. It will be used with profit by many.

Roger Parsons, University of Bristol

J. Electroanal. Chem., 26 (1970) 187–188

ANNOUNCEMENT

A CONFERENCE on
The Electrical Double Layer and its Influence on Electrode Processes
will take place at the University of Kentucky in september 1970.

Speakers: Drs. F. C. Anson, J. O'M. Bockris, M. Bonnemay, D. Inman, R. De Levie, D. M. Mohilner, R. Payne and J. E. B. Randles.

Place: University of Kentucky, Lexington, Kentucky, U.S.A.

Dates: September 10, 11, 12, 1970.

Fees: nominal charge for three meals and social hour.

Further information: Please write to Dr. Gary D. Christian, Chemistry Department, University of Kentucky, Lexington, Kentucky 40506, U.S.A.

J. Electroanal. Chem., 26 (1970) 188

Preliminary note

Chemisorption of hydrogen on platinum electrodes in sulphuric acid

T. LOUČKA and J. WEBER

The J. Heyrovský Institute of Polarography, Czechoslovak Academy of Sciences, Prague (Czechoslovakia)

On voltammetric current–voltage curves obtained with polycrystalline platinum electrode in 0.5 *M* H_2SO_4 two maxima of current can be observed in the region of potentials corresponding to the formation and oxidation of chemisorbed hydrogen. According to Breiter these maxima correspond respectively to less and more strongly chemisorbed hydrogen.

In the course of our studies of electrochemical processes on platinum electrodes in sulphuric acid of higher concentration than 1 *M* we found a third, less marked hydrogen maximum at a potential of about +0.31 V *vs.* hydrogen electrode in the same solution. The *i*–*E* curve showing the chemisorption of hydrogen is represented in Fig.1. This curve was obtained by polarizing a smooth platinum electrode in 5 *M* H_2SO_4 at 25°C by periodic triangular voltage impulses of the rate of 30 V sec^{-1}. The measurement was carried out with an apparatus already described[1].

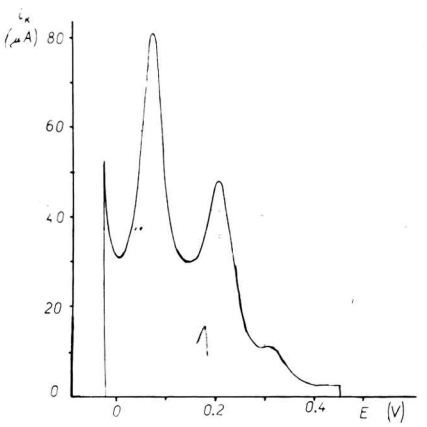

Fig. 1. Voltammetric *i*–*E* curve in 5 *M* H_2SO_4 showing the chemisorption of hydrogen. Periodic triangular polarization impulses between potentials of +0.45 V and -0.05 V; rate 30 V sec^{-1}. Potentials *vs.* hydrogen electrode in the same solution.

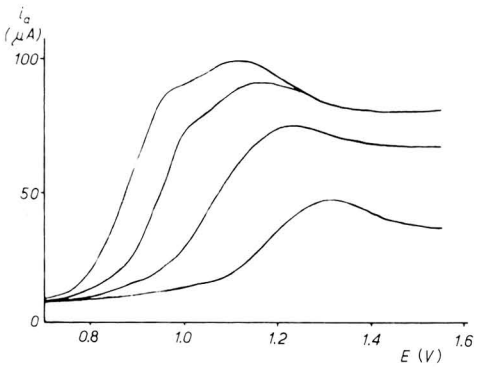

Fig. 2. Part of voltammetric i–E curves showing the formation of an oxide at a smooth Pt electrode in H_2SO_4 of different concentrations. Periodic triangular polarization impulses between potentials of 0 V and +1.55 V; rate 30 V sec^{-1}. Concentration of H_2SO_4: (1) 0.5, (2) 5, (3) 10, (4) 15 *M*. Potentials are referred to the hydrogen electrode in solutions of H_2SO_4 of the respective concentrations in which the i–E curves were observed.

A similar third maximum appears also with 10 *M* and 15 *M* H_2SO_4 and even when platinized platinum is used. An analogous maximum at +0.31 V was observed on the curve of the anodic current due to oxidation of the chemisorbed hydrogen. The change of the shape of i–E curves of chemisorption of hydrogen and the appearance of the third maximum of the current did not change, however, the total charge, which passed through the electrode during the formation of the layer of chemisorbed hydrogen. The value of this charge was within the limit of the experimental error the same in 1 *N* H_2SO_4 solution as in more concentrated solutions of sulphuric acid.

After changing the solution of 5 *M* H_2SO_4 for 0.5 *M* H_2SO_4 the third maximum stays on the curves for several minutes before it disappears. On introducing sulphur dioxide into the solution of 0.5 *M* or 5 *M* H_2SO_4 in no case the above described third maximum on the i–E curves was produced. Therefore, the possibility that this maximum might be caused by the presence of SO_2 in the more concentrated solutions of H_2SO_4 can be excluded.

A third maximum due to chemisorption of hydrogen at the potential of +0.31 V has been already observed by Will[2] at the crystal plane (100) of a platinum single crystal electrode in 4 *M* H_2SO_4. A similar maximum was observed at the Pt electrode in 0.5 *M* $HClO_4$ or 0.5 *M* H_2SO_4 after addition of Cl^- ions[3,4]. Chloride ions change the shape of i–E curves of chemisorption of hydrogen without changing the charge corresponding to a monolayer of chemisorbed hydrogen. In that case the third maximum was ascribed to the effect of the adsorbed chloride ions.

The addition of Cl^- ions also shifts the beginning of oxidation of the surface of the Pt electrode towards more positive potentials. When following the formation of platinum oxide by anodic reaction in sulphuric acid of different concentrations we found a similar effect. The voltammetric current–potential curves showing the formation of an oxide or an adsorbed oxygen are given in Fig.2.

Since in our experiments a contamination of the electrolyte by chloride ions was carefully avoided it appears that sulphate ions in higher concentrations act in a similar way as chloride ions. Hence it can be assumed that in sulphuric acid of a concentration of 5 *M* and higher a relatively strong adsorption of sulphate ions takes place which affects the shape of *i*–*E* curves of chemisorption of hydrogen, and which shifts the beginning of the surface oxidation of the platinum electrode to more positive potentials.

The adsorption of sulphate ions in 0.5 *M* and more dilute sulphuric acid has been already measured by radiometric[5] and ellipsometric[6] methods. In these solutions the relative degree of coverage of the platinum electrode did not exceed the value of 0.1. It is probable, however, that for higher concentrations of sulphuric acid used in the present work the adsorption of sulphate ions will be markedly higher.

REFERENCES

1 T. Loučka and J. Weber, *J. Electroanal. Chem.*, 21 (1969) 329.
2 F.G. Will, *J. Electrochem. Soc.*, 112 (1965) 451.
3 M.W. Breiter, *Electrochim. Acta*, 8 (1963) 925.
4 J. Weber, J.B. Vasil'ev and V.S. Bagotskii, *Elektrokhimiya*, 5 (1969) 323.
5 V.E. Kazarinov and N.A. Balashova, *Collection CZech. Chem. Commun.*, 30 (1965) 4184.
6 Ying-Chech Chiu and M.A. Genshaw, *J. Phys. Chem.*, 11 (1969) 3571.

Vol. 26 No. 1 JOURNAL OF ELECTROANALYTICAL CHEMISTRY AND INTERFACIAL ELECTROCHEMISTRY JUNE 1970

CONTENTS

A New Important Encyclopaedic Work of Reference

COMPREHENSIVE CHEMICAL KINETICS

edited by C.H. BAMFORD F.R.S., and C.F.H. TIPPER

The aim of this series is to cover in a critical way the practice and theory of kinetics and the kinetics of inorganic and organic reactions in the gas and condensed phases or at interfaces.
Each chapter is written by an expert in the field so that the series as a whole will serve as a direct source of reference and information over the whole range of kinetics.
The vast amount of material scattered through the literature has never before been gathered together and presented in this accessible form.

Elsevier

P.O. BOX 211,
AMSTERDAM - THE NETHERLANDS

Volume 1. The Practice of Kinetics

1. Experimental methods for the study of slow reactions (L. Batt)
2. Experimental methods for the study of fast reactions (D.N. Hague)
3. Experimental methods for the study of heterogeneous reactions (D. Shooter)
4. The detection and estimation of intermediates (R.P. Wayne)
5. The treatment of experimental data (D. Margerison)

7 x 10″, xiii + 450 pages, 32 tables, 161 illus., 1174 lit. refs., 1969, Dfl. 95.00, £11.5.0
SBN 444-40673-5

Volume 2. The Theory of Kinetics

1. Kinetic characterization of complex reaction systems (Z.G. Szabó)
2. Chain reactions (V.N. Kondratiev)
3. Theory of the kinetics of elementary gas phase reactions (R.P. Wayne)
4. Theory of elementary reactions in solution (I.D. Clark and R.P. Wayne)
5. Theory of solid phase kinetics (L.G. Harrison)

7 x 10″, xiii + 486 pages, 13 tables, 77 illus., 794 lit. refs., 1969, Dfl. 100.00, £11.10.0
SBN 444-40674-3

Volume 3. The Formation and Decay of Excited Species

1. Effect of low energy radiation (C.S. Burton and W.A. Noyes, Jr.)
2. Effect of high energy radiation (G. Hughes)
3. The chemical production of excited states (T. Carrington and D. Garvin)
4. The transfer of energy between chemical species (A.B. Callear and J.D. Lambert)

7 x 10″, xii + 300 pages, 30 tables, 53 illus., 1969, Dfl. 70.00, £8.5.0
SBN 444-40802-9

The series as a whole will comprise about 25 volumes divided into a number of sections:

Section 1. The practice and theory of kinetics (3 volumes)
Section 2. Decomposition and isomerisation reactions (2 volumes)
Section 3. Inorganic reactions (2 volumes)
Section 4. Organic reactions (6 volumes)
Section 5. Polymerization reactions (2 volumes)
Section 6. Oxidation and combustion reactions (2 volumes)
Section 7. Selected elementary reactions (2 volumes)

Other sections are planned on heterogeneous reactions, solid state reactions, and kinetics and technological processes.